SOME EXPERIMENTAL INVESTIGATIONS CONCERNING FRACTURE MECHANICS OF SHORT FIBRE COMPOSITES

By

GOVINDER SINGH GIARE

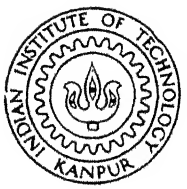

DEPARTMENT OF MECHANICAL ENGINEERING

INDIAN INSTITUTE OF TECHNOLOGY KANPUR

MAY, 1980

SOME EXPERIMENTAL INVESTIGATIONS CONCERNING FRACTURE MECHANICS OF SHORT FIBRE COMPOSITES

A Thesis Submitted
in Partial Fulfilment of the Requirements
for the Degree of
DOCTOR OF PHILOSOPHY

By

GOVINDER SINGH GIARE

to the

DEPARTMENT OF MECHANICAL ENGINEERING
INDIAN INSTITUTE OF TECHNOLOGY KANPUR
MAY, 1980

ME-1980-D-GIA-SOM

DEDICATED

TO

MY FATHER

Late Shri Kishan Lal Giare

and

MY UNCLE

Late Shri Jagadishwar Singh

CERTIFICATE

This is to certify that this thesis entitled "SOME EXPERIMENTAL INVESTIGATIONS CONCERNING FRACTURE MECHANICS OF SHORT FIBRE COMPOSITES", by GOVINDER SINGH GIARE is a record of work carried out under my supervision and has not been submitted elsewhere for a degree.

B.D. Agarwal
Assistant Professor
Department of Mechanical Engineering
Indian Institute of Technology Kanpur
Kanpur, 208 016

May, 1980

ACKNOWLEDGEMENT

I wish to express my deep sense of gratitude and appreciation to my advisor, Professor B.D. Agarwal, for his valuable guidance and constructive criticism, throughout the present work. His generous attitude has been a constant source of inspiration, encouragement to complete the work in a very short time.

I am also thankful to Professor Prashant Kumar for his numerous suggestions in setting up of the experiments and help in many other ways.

Professors M.M. Oberai and P.N. Murthy have guided and helped me throughout my stay at I.I.T. Kanpur. I am also thankful to Professors B.L. Dhoopar, G.S. Murthy, N.G.R. Iyengar, B. Sahay, S.N. Bandyopadhyay, S.G. Dhande, and D.C. Agarwal for the interest they have taken in my work.

I highly value the discussions and helpful comments of my friends Messrs. G.T. Kochar, P.A. Saini, S.K. Joneja and R.C. Gupta.

I am thankful for the cooperation and help of the technical staff of Mechanical Engineering Department, in particular that of Messieurs S.L. Srivastava, S.N. Yadava, O.R. Shukla, D.R. Tiwari, B.L. Sharma, P.P. Singh, B.P. Vishwakarma, Jcginder Singh, R.M. Jha, B.P. Bhartiya, Munna Singh, M.M. Singh, Lalta Prasad and Ajodhya Prasad.

Help rendered by Messieurs T.A. Ansari, H.N. Sharma, K.K. Mittal, F.B. Nigam, J.C. Srivastava, V.K. Srivastava and Shri R.S. Verma is gratefully acknowledged. I am also thankful to Mr. Jain of A.C.M.S.

I am thankful to Mr. B.L. Arora and S.S. Kushwaha for their sincere efforts in preparing illustrations without any delay and to Mr. D.K. Sarkar for preparing photographs. I highly appreciate the careful typing of the thesis by Mr. J.D. Verma.

Last, but not the least, I must thank to my wife Anjali and children Rano, Mannu and Bhanu for their patience and the hardship to which they were subjected while this work was beeing carried out.

This research work has been partially supported by Structural Panel of Aeronautical Research and Development Board.

GOVINDER SINGH GIARE

TABLE OF CONTENTS

LIST OF TABLES

LIST OF FIGURES

NOMENCLATURE

a	:	Crack length
a_o	:	Initial crack length
C	:	Compliance for Mode I, Mode II, Mode III
C_o	:	Non-dimensional compliance $(\frac{E\ t\delta}{S})$ in Mode II
C'_o	:	Non-dimensional compliance $(\frac{G\ t\delta}{F})$ in Mode III
c_o	:	Characteristic length (Eq. 4)
d_o	:	Characteristic length (Eq. 3)
DBP	:	Dibutyl-phathalate
E_c	:	Modulus of composite
E_m	:	Modulus of matrix
F	:	Out-of-plane shear load (Mode III)
G	:	Shear modulus of composite
G_I	:	Strain energy release rate for Mode I
G_{II}	:	Strain energy release rate for Mode II
G_{III}	:	Strain energy release rate for Mode III
G_{IC}	:	Critical strain energy release rate for Mode I
G_{IIC}	:	Critical strain energy release rate for Mode II
G_{IIIC}	:	Critical strain energy release rate for Mode III
K_I	:	Stress intensity factor for Mode I
K_R	:	Crack growth resistance for Mode I
$K_{R(ins)}$	:	Stress intensity at instability for Mode I
K_Q	:	Candidate stress intensity factor

K_{IIR} : Crack growth resistance for Mode II

K_{IIIR} : Crack growth resistance for Mode III

$K_{IIR(ins)}$: Stress intensity at instability for Mode II

$K_{IIIR(ins)}$ Stress intensity at instability for Mode III

L : Length of specimen between the grips

P : Tensile Load (Mode I)

S : Forward shear load (Mode II)

T : Temperature

t : Thickness of specimen

V_f : Fibre volume fraction

W : Width of specimen

X : Calibration factor for Mode II

Y : Calibration factor for Mode I

Z : Calibration factor for Mode III

τ : Shear stress in Mode II and Mode III

ϵ : Strain

θ : Crack angle

ν : Poisson's ratio

σ_N : Notched stress

σ_o : Normal tensile stress without crack

σ_{mu} : Ultimate tensile stress of matrix

σ_{cu} : Ultimate stress of composite

SYNOPSIS

SOME EXPERIMENTAL INVESTIGATIONS CONCERNING FRACTURE MECHANICS OF SHORT FIBRE COMPOSITES

A Thesis Submitted in Partial Fulfilment
of the Requirements for the Degree of

DOCTOR OF PHILOSOPHY

by

GOVINDER SINGH GIARE

to the

Department of Mechanical Engineering
Indian Institute of Technology Kanpur

Kanpur, May, 1980

Short glass fibre reinforced plastic composites are being increasingly used in many applications such as automobile bodies, safety helmets, house hold furnitures etc. For an efficient use of the material it is desirable to establish criteria which will accurately predict failure loads. Fracture mechanics is the discipline concerned with failure by crack initiation and propogation. Application of fracture mechanics approach has provided useful information on the flaw sensitivity of isotropic materials and for establishing the inspection requirements concerning criticality of cracks. The present studies are a part of considerable efforts being directed by the composite materials community to study the relevance and applicability of the fracture mechanics approach to composite materials.

The present investigations have been performed on short-glass-fibre-mat reinforced epoxy composites. The composite material plates were fabricated in the laboratory using chopped strand mat of glass fibres having a weight of 0.6 kg/m^2 and an average fibres length of 50 mm. The volume fraction of fibres was varied between 20 and 52 percent by placing different number of layers of mat in the composite material plate. The matrix material was generally an epoxy which is commercially designated LY 553 and is recommended for structural applications. However, tests have also been performed on some other grades of epoxy. The fracture toughness tests have been performed on the testing system designed, fabricated and instrumented in the laboratory. The load is measured by a 20 KN Instron load cell. The crack opening displacement is measured by a clip gauge developed in the laboratory. The material and test parameters include the initial crack length, fibre concentration, specimen thickness, width, test temperature and matrix materials. Most of the fracture toughness tests have been performed in the crack extension mode (Mode I). Since the practical structures are subjected to tensile as well as shear loads and the fact that the fibrous composites generally have a low shear strength, the fracture toughness tests have been performed in shear modes (Modes II and III) as well. For each parameter four to five specimens have been tested. Thus the results described in this thesis pertain to tests on nearly 400 specimens.

In the short fibre composites investigated here, considerable amount of damage is observed to occur at the crack tip prior to final unstable fracture. Although there are a number of microcracks in the damage zone, the progress of damage zone is not a crack extension in the conventional sense. However, the crack tip damage does increase the compliance as crack extension does in metallic materials. The size of the damage zone can be represented by an effective crack length determined through compliance matching. This effective crack length has been used to obtain the crack growth resistance curves (R - curves). The R - curve approach has been found useful in comparing the fracture behaviour of composite materials. The present results, however, indicate that at room temperature and at -1.1 ^{o}C, the crack growth resistance at instability, $K_{R(ins)}$, depends upon the initial crack length. The $K_{R(ins)}$ also depends upon the volume fraction of fibres. At elevated temperatures of 43.3 and 60 ^{o}C the $K_{R(ins)}$ is nearly independent of initial crack length. The material also exhibits notch insensitivity at these temperatures, because the matrix becomes very ductile. The results with different matrix materials also indicate that the $K_{R(ins)}$ may be independent of initial crack length when the matrix is very ductile. The candidate stress intensity factor shows a slight increase with the specimen thickness, where as it decreases with increase in specimen width. The notched strength of these composites has been found to be

in reasonable agreement with some theoretical predictions provided the overall failure is brittle. At elevated temperatures the criteria predicting notched strength are no more applicable because of the material behaving in a ductile manner.

Fracture toughness tests in Mode II and Mode III have also been performed in the same testing system through special fixtures to apply appropriate loading. For the analysis of results, the compliance calibration factor is first obtained through the compliance curve in each case. It appears that the linear elastic fracture mechanics concepts can be better applied to the short fibre composites when tested in Mode II and Mode III.

CHAPTER 1

INTRODUCTION

1.1 INTRODUCTION TO FRACTURE OF COMPOSITES

Fibre reinforced composites are certainly one of the oldest and most widely used form of composite materials. Their study and development have been largely carried out due to their vast structural applications. The two outstanding features of oriented fibrous composites are their specific strength and stiffness and controlled anisotropy. High specific strength and stiffness make them attractive structural materials where weight saving is at a premium. Controlled anisotropy means that the desired ratio of its property values in different directions can be easily obtained. Other advantages of fibrous composites include ease of processing and structural forms otherwise inconvenient or impossible to manufacture. Their utilization, therefore,in aerospace and transportation industries is continuously increasing.

Most of the structural elements or laminate made of fibrous composites consist of several distinct layers of unidirectional laminae, properties and orientation of the laminae are chosen to meet the laminate design requirements. The laminates constructed from

unidirectional laminae have one disadvantage: although the overall composite has requisite strength in all directions, the surface layers, where the failure is quite often initiated, are very weak in the transverse direction. In applications where protection from a corrosive environment is an important factor, such as storage tanks in the chemical industry and in many applications in the automobile industries, the weakness of surface layers in the transverse direction is a serious limitation. In many other applications, where the state of stress may not be predictable or where it is known that the stresses are approximately equal in all directions, unidirectional composites or laminae may not be required or cost effective. Thus, in many applications it is advantageous to have each layer or laminae isotropic. Randomly oriented short fibre composites are commonly used to provide such isotropic layers. Short fibre composites are also widely used in producing components by injection or compression moulding such as in safety helmets, household furnitures and other appliances. The present studies are carried out on short fibre composites.

A continuum analysis of anisotropic materials is employed to formulate the stress strain relations for composite materials. The predictions of continuum analysis regarding deformational response of composites have proven to be accurate, because the deformation is an average

property and is not influenced by local heterogeneity. The applicability of a continuum approach can not be taken for granted in a process like failure that is initiated by localised conditions. The strengths of composites are evaluated by conducting tests on geometrically smooth specimens in which no sharp stress gradients are present. However, experience with fracture of metals suggests that the occurrence of failure in the presence of sharp stress gradients (or flaws) is different from that in a relatively slow varying stress field. Moreover, in practical structures, macroscopic cracks, which produce sharp stress gradients, can accrue during the various manufacturing processes as well as in service. The study of quasi static crack growth can, therefore, provide useful information on the flaw sensitivity of the materials and for establishment of inspection requirement concerning criticality of the cracks.

The subject of fracture mechanics is concerned with the study of fracture of materials by crack propogation. The fracture mechanics approach has been found very useful in predicting the strength of homogeneous isotropic materials in the presence of flaws or cracks and also in developing the techniques for their quality control and service inspection. Fracture mechanics applied to composite materials is more complicated because self similar crack growth which occurs in homogeneous materials, usually

does not occur in composite materials. Fracture behaviour of composite materials has been studied, both theoretically and experimentally, by a number of research workers. However, the concepts of fracture mechanics as applied to composite materials are still in the developing stage and require further theoretical and experimental investigations. The work reported here is an experimental investigation concerning fracture mechanics of short fibre composites.

1.2 LITERATURE SURVEY

Preliminary results of Sih et al [1] with glass and graphite fibre reinforced epoxy indicate that there exists an optimum fibres volume fraction for which the composites achieve maximum fracture toughness. The tests were performed on unidirectional composites with the crack running parallel to the fibres. Zweben [2] theoretically studied different approaches to the study of fracture behaviour of composites and showed that with the use of relatively simple models, it is possible to predict many of the unusual fracture phenomena that are observed. Atluri, Kobayashi and Nakagaki [3] have a finite element procedure to solve two dimensional problems in fracture mechanics involving anisotropic, nonhomogeneous but linearly elastic materials. They further developed a hybrid finite element procedure for treating a general

class of problems involving mixed mode behaviour of cracks to solve the problems involving rectilinear, anisotropic materials [4].

Beaumont [5] presented a review of the fracture processes which occur in brittle thermosetting resins containing long strong fibres of carbon, boron and glass and indicated that fibre strength and strength of fibre matrix interface play an important roll in the fracture behaviour of fibrous composites. Other parameters which must be considered include, component geometry, environment and loading mode. Mandell, Wang and McGarry [6] investigated the size and character of damage zone at the tip of sharp notches in fibre reinforced plastic laminates. The damage zone was found to increase in extent approximately in proportion to K_I^2. Using the crack tip analysis Wu [7] has formulated phenomenological failure criterion and established that the unstable crack propogation can be characterized by failure within critical volume.

Whitney and Nuismer [8, 9] have developed two stress fracture criteria for laminated composites, containing stress concentrations. The criteria results in two parameters (unnotched tensile strength and a characteristic dimension) models which are capable of predicting observed discontinuity size effects without resorting to classical concepts of linear fracture mechanics. They examined the

effect of changes in the material system, laminate fibre orientations, and the notch shape and size through experiments on two material systems, glass/epoxy and graphite/epoxy, in conjunction with two orientations of fibre dominated laminates containing through the thickness, circular holes and sharp tipped cracks of several sizes. Their experimental results show reasonable agreement with the theoretical developments. Nuismer and Labor [10, 11] investigated applications of the average stress failure criterion to the tensile and compressive fracture strength of several graphite/epoxy laminates and showed that the criterion leads to acceptable strength predictions.

Brinson et al [12, 13] investigated the fracture behaviour of graphite/epoxy laminates containing single edge notches, double edge notches, centrally located circular or square holes with various aspect ratio. They compared their experimental results with the theoretical predictions of Whitney and Nuismer. The results tend to show that use of only isotropic correction factors allow good correlation between theory and experiment. Morris and Hahn [14, 15] have applied the resistance method to characterise fracture resistance of graphite/epoxy laminates through a compliance matching procedure to model a self similar crack extension. Experimental datas for central cracked tension specimens reveal a linear relationship between crack growth resistance and initial crack length.

Daniel [16 - 18] used experimental stress analysis techniques to study the deformation and failure of axially and biaxially loaded graphite/epoxy plates with cracks and holes. Barrett and Foschi [19] studied the Mode II (Forward shear) fracture of wood, a highly oriented natural composite. Bunnsell [20] studied the failure of asbesto cement, boron aluminium and carbon reinforced epoxy resin and concluded that in the case of asbesto cement in which the cement matrix controls the failure of composite, crack propogation occurs in a similar manner to that which is found in more homogeneous materials. The failure of boron aluminium and carbon reinforced epoxy resin is found to be controlled by the fibres.

Kanninen, Raybicki and Brinson [21] presented a critical look at the applications of fracture mechanics to the failure of fibre reinforced composites. They found that, these are generally empirical extension of linear elastic fracture mechanics that are not capable of coping with the complexity of the crack extension processes, as seen from the micromechanical point of view and concluded that innovative fracture mechanic techniques are required. They suggested that the material, treated as heterogeneous, where microstructural effects are predominant and as a homogeneous anisotropic continuum, where they are not.

Fracture toughness studies cited in the preceding paragraphs are mostly concerned with the oriented

materials, such as continuous fibre reinforced unidirectional or laminated composites. Due to the vast industrial application of continuous fibre reinforced composites, fracture toughness tests are performed on them, even though they can not be well interpreted. Fracture toughness tests can be more effectively used for randomly oriented short fibre composites that are isotropic in the plane of the composite. Gaggar and Broutman [22 - 27] have extensively studied fracture mechanics of short fibre reinforced epoxy and polyester resins. They have applied the concepts of linear elastic fracture mechanics (LEFM) by assuming that the damage growth at the crack tip can be modelled as a self similar crack extension through compliance matching. They observed that substantial slow crack growth occurs prior to unstable fracture and pointed out that the total fracture behaviour of the materials may be studied by applying the concept of crack growth resistance curves (R - curve). However, further theoretical and experimental investigations are necessary before the R - curves concepts can be applied with confidence to the composite materials. The present studies are a step in the same direction.

1.3 SCOPE OF PRESENT WORK

The present studies are a part of considerable efforts being directed by the composite material community to study the relevance and applicability of fracture mechanics approach to composite materials. It was decided

to carry out investigations on short fibre reinforced composites for two reasons. One, short fibre composites have become important material for the manufacture of many moulded components and structuresand also for producing an isotropic layer on the surface of laminates made from unidirectional laminae. Two, the short fibre composites are isotropic in the plane of the plate and thus, the fracture toughness tests can be better interpreted. It is expected that the results of the tests on short fibre composites would lead to an insight into the fracture behaviour of oriented composites.

The present investigations have been performed on short glass fibre mat reinforced epoxy composites. The composite material plates were fabricated in the laboratory using chopped strand mate of glass fibres and different grades of epoxy resins. The fracture toughness tests have been performed on the testing system, fabricated and instrumented in the laboratory. The details concerning material preparation and the testing system are given in Chapter 2. The material and tests parameters studied include the initial crack length, fibre concentration, specimen thickness and width, test temperature and matrix material, Most of the fracture toughness tests have been performed in the crack extension mode (Mode I) using notched tension specimens. Since the practical structures are subjected to tensile as well as shear loads and the

fact that fibrous composites generally have a low shear strength, the fracture toughness tests have been performed in shear modes (Modes II and III) as well. The fixtures used for performing tests in Mode II and Mode III are also discussed in Chapter 2. The results of fracture toughness tests in Mode I have been discussed in Chapter 3 and those in Modes II and III in Chapter 4. Important conclusions and some suggestions for future work are described in Chapter 5.

CHAPTER 2

TESTING SYSTEM AND MATERIALS PREPARATION

2.1 TESTING SYSTEM

The fracture toughness tests were performed on a testing system designed, fabricated and instrumented in the laboratory. The testing system is essentially a tension testing machine. The Mode I tests were all performed in tension. For fracture toughness tests in Mode II and Mode III additional fixtures were designed so that the desired shear loads would be applied through the same testing system. The only reason behind the decision to have a separate testing system in the laboratory rather to use a commercial testing system available elsewhere in the Institute was the desired to have an uninterrupted access to the testing system.

2.1.1 Basic Testing System

The basic testing system is schematically shown in Fig. 1. In this system the specimen is mounted between two 25 mm thick mild steel plates. The lower plate is fixed and is bolted to three 50 mm diameter 600 mm long solid mild steel columns whose lower ends are fixed to the heavy cast iron base of the testing system. The upper plate is connected to another identical plate through three 50 mm diameter and 500 mm long solid mild steel columns. This assembly of two plates is movable and its

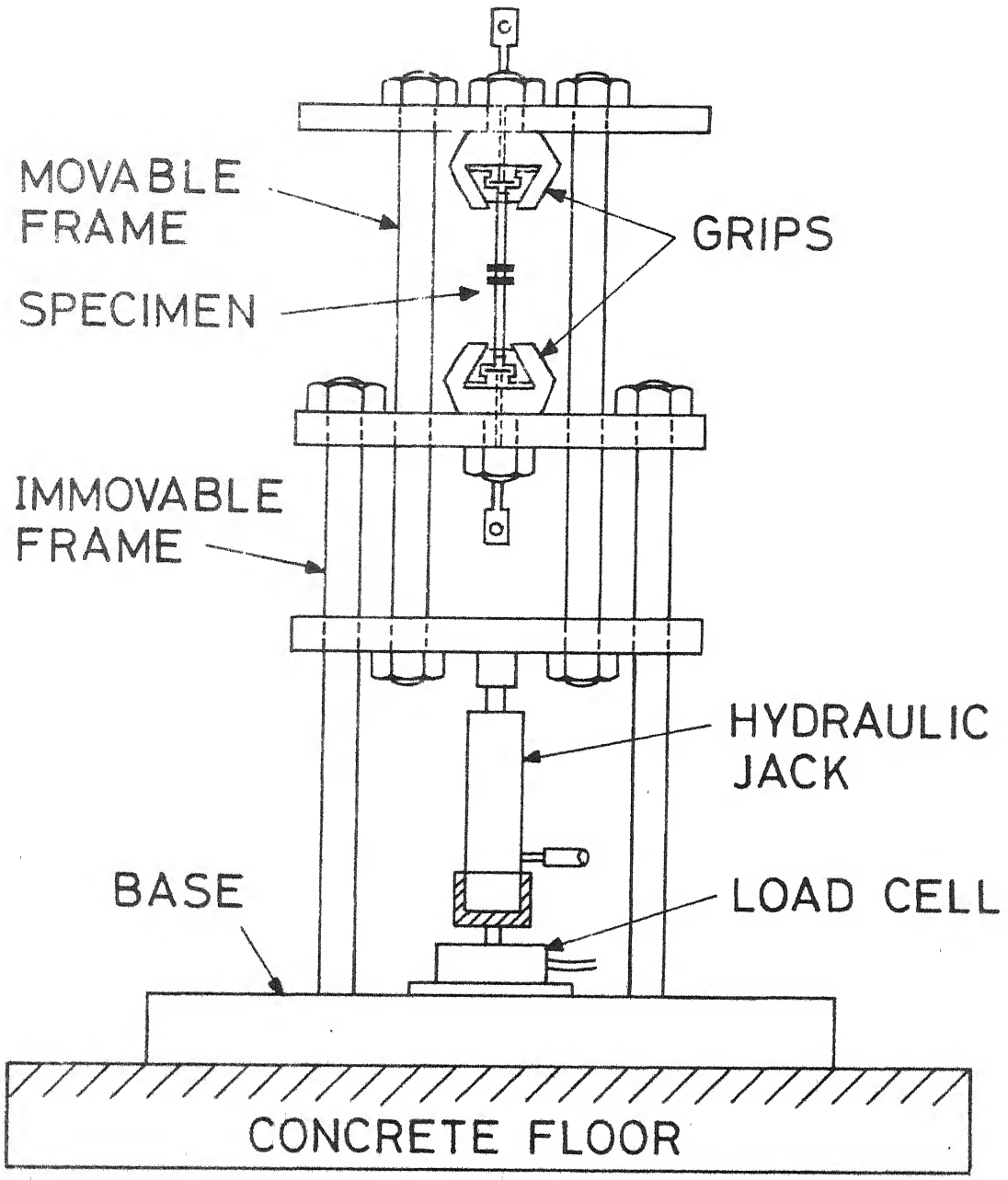

FIG. I SCHEMATIC DIAGRAM OF TESTING SYSTEM

movement is guided by the fixed columns, that supports the lower plate. These fixed columns pass through the lower plate of the movable assembly. The assembly is moved by a hand operated hydraulic jack. The applied load is measured by a 20 KN Instron load cell connected in series with the jack and resting on the base of the machine. A photograph of the machine along with the measuring instruments is shown in Fig. 2.

2.1.2 Clamps For Mode I

The tension tests (required for fracture toughness testing for Mode I) are performed by placing the central longitudinal axis of the specimen along the load axis of the testing system. The specimen ends are gripped in the wedge type serrated jaws which can move in the body of the clamp for self tightening during application of loads. The clamps are mounted on the mild steel plates of the testing system. Schematic diagram of a clamp is shown in Fig. 3. The self tightening occurs due to the taper provided in the clamp body and the jaws. Movement of the jaws is controlled by a screw passing through the body of clamp and connected to the back of jaws through a simple mechanism. This simple arrangement helps to provide initial grip to the specimen to hold it in position and also to release the specimen after the test. Figure 4 shows a photograph of the clamps.

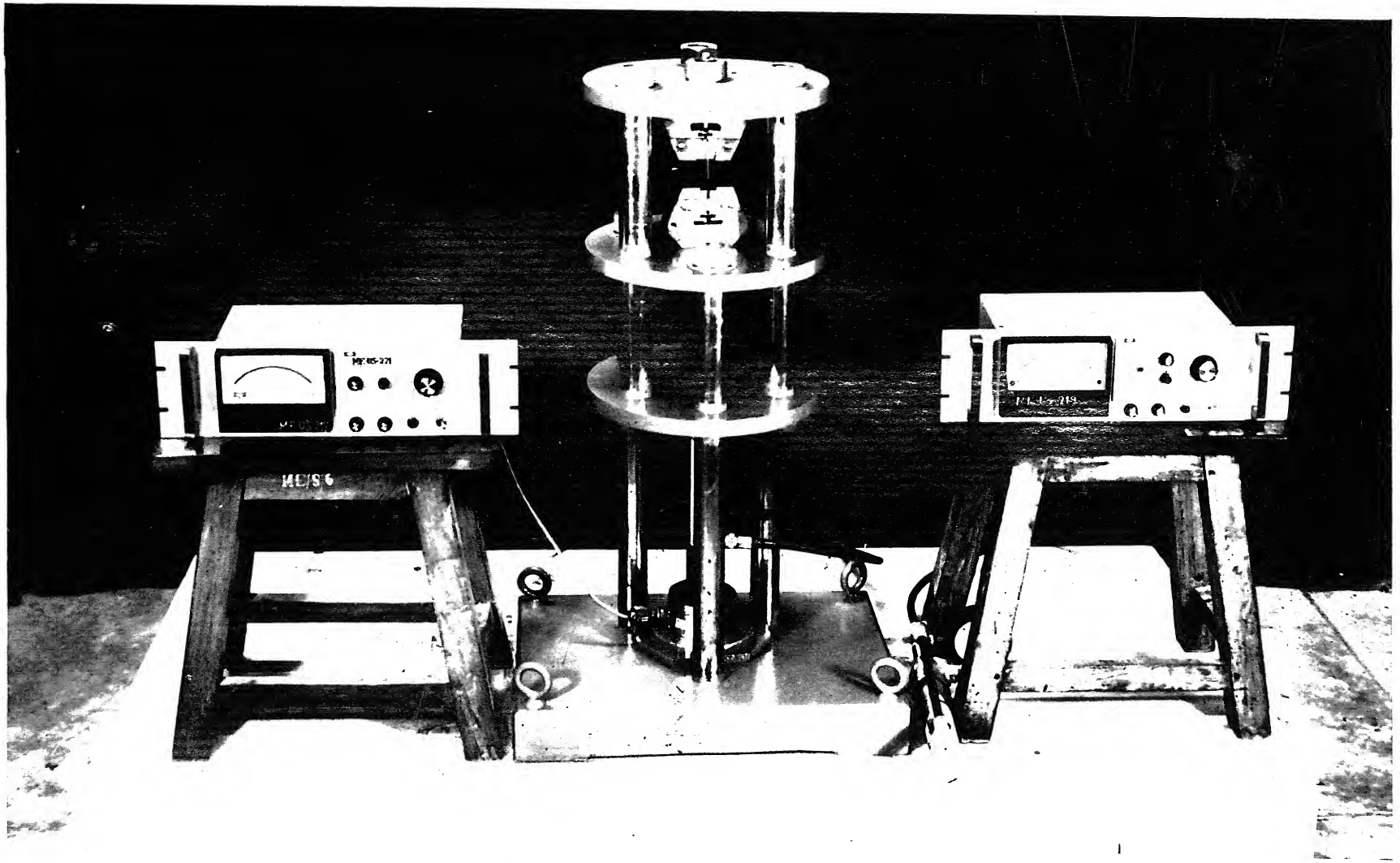

FIG.2 TESTING SYSTEM

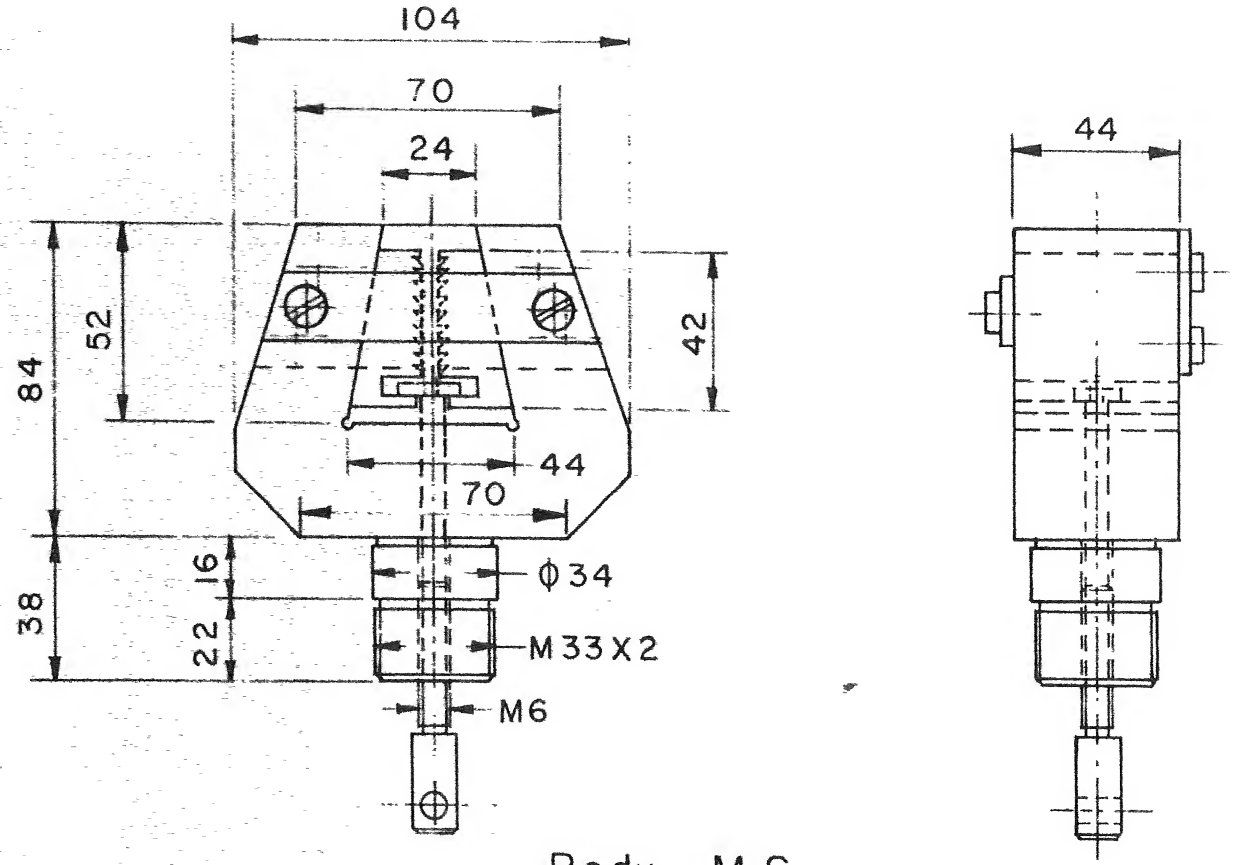

FIG. 3 DESIGN OF CLAMPS FOR TESTS IN MODE I

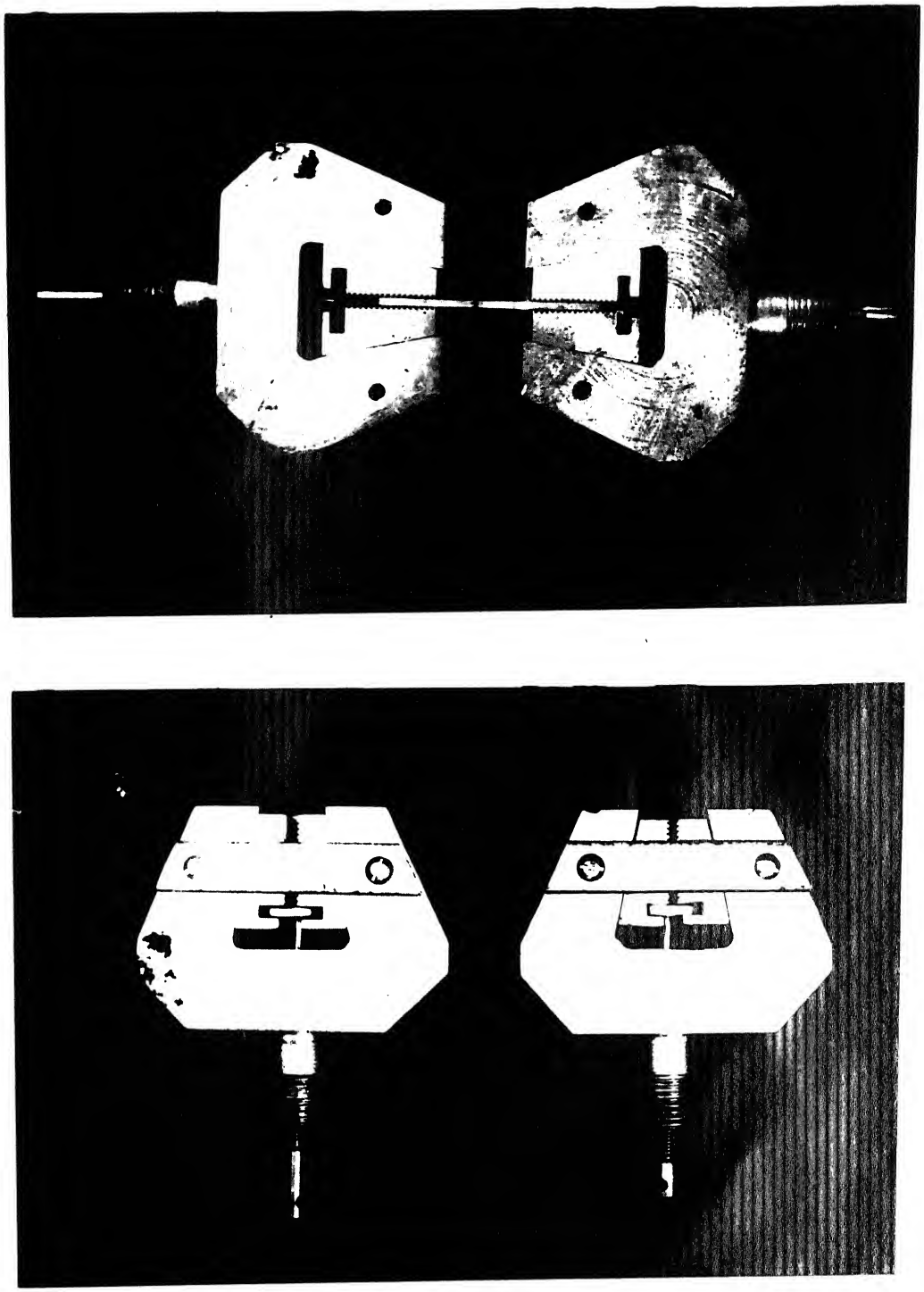

FIG. 4 PHOTOGRAPHS OF CLAMPS

2.1.3 Fixture for Mode II Loading

In the forward shear mode (Mode II) fracture toughness tests, it is desired to apply equal and opposite loads parallel to the plane of the crack. In practice, it is desired to obtain the loading condition of the specimen as shown in Fig. 5. The specimen is gripped on the edge over a small area near the mouth of the crack (the shaded area in Fig. 5). The large gripping area will give rise to an undesired bending moment on the specimen and too small an area will cause crushing of the specimen. One of the two identical parts of the fixture used for loading in Mode II is shown in schematically in Fig. 6. Photograph of the fixture is shown in Fig. 7. Two aluminium strips, one of each of the two parts are bonded to the fixture. The clip gauge described later is slipped on these strips to measure the differential movement of the two parts which is taken to be relative lip displacement of the crack.

2.1.4 Fixture for Mode III Loading

The fracture toughness tests in Mode III (anti-plane shear mode) require that equal and opposite forces be applied on the specimen edge parallel to the crack front (perpendicular to the plane of the thin specimen). The loading condition on the specimen is represented in Fig. 8. It has been observed that the extent of gripping area does not have much influence on the loading condition. However, the gripping area is kept small so that load is

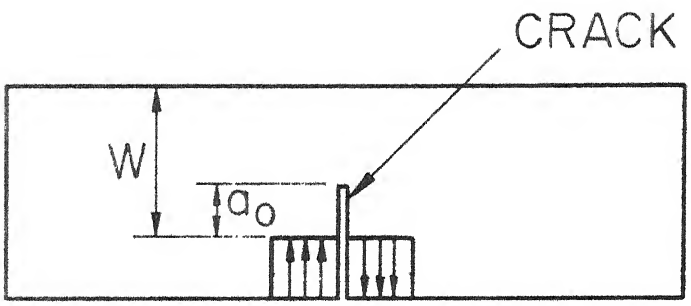

FIG. 5 LOADING CONDITION OF SPECIMEN IN MODE II

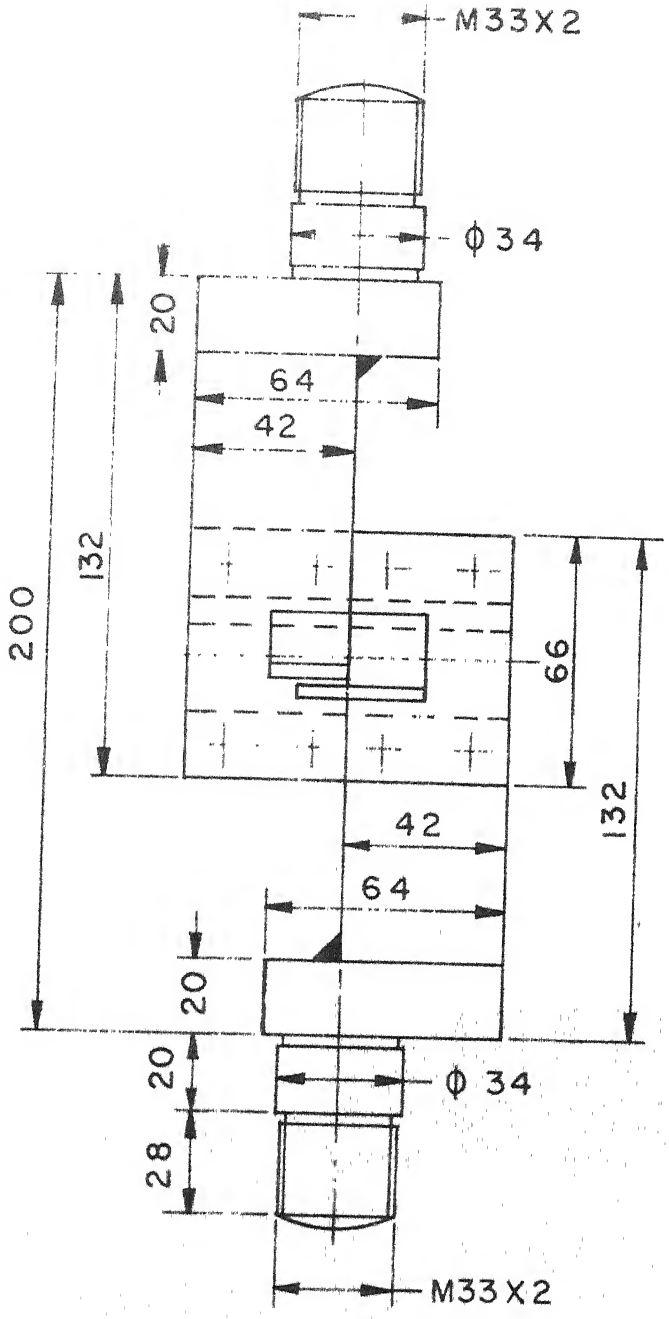

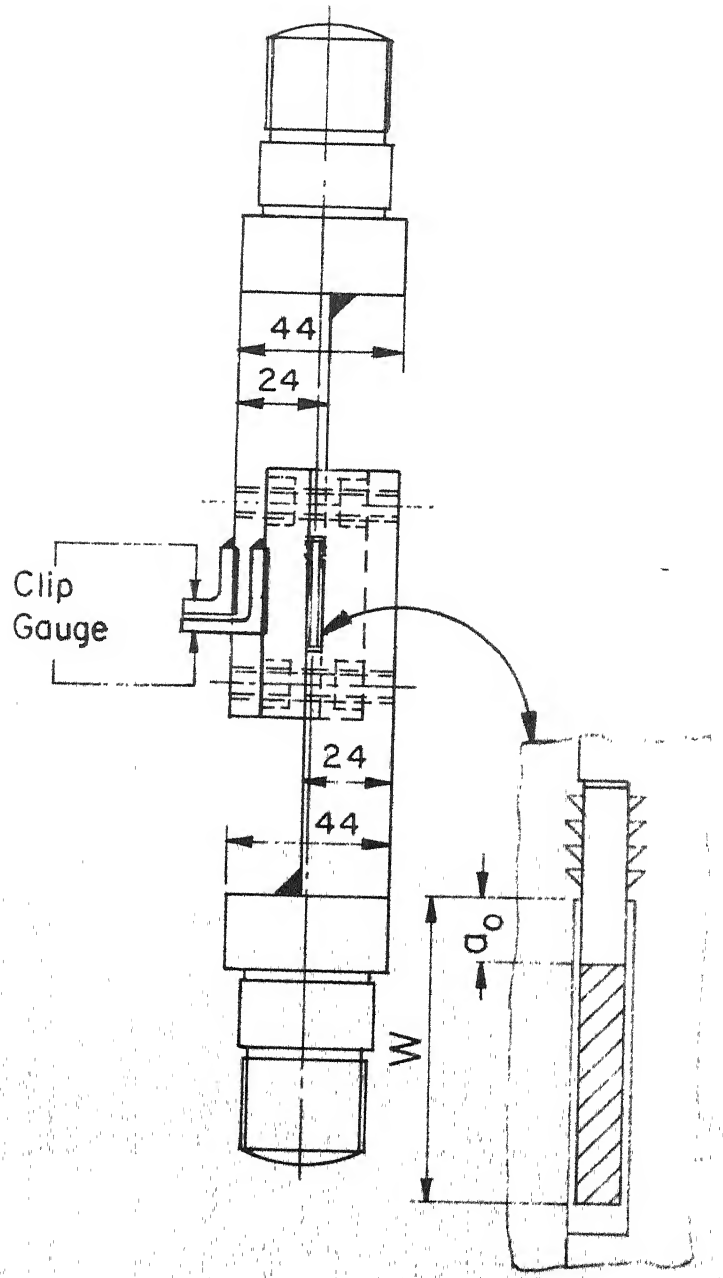

Specimen clamping arrangement

FIG. 6 DESIGN OF LOADING FIXTURE FOR TESTS IN MODE II

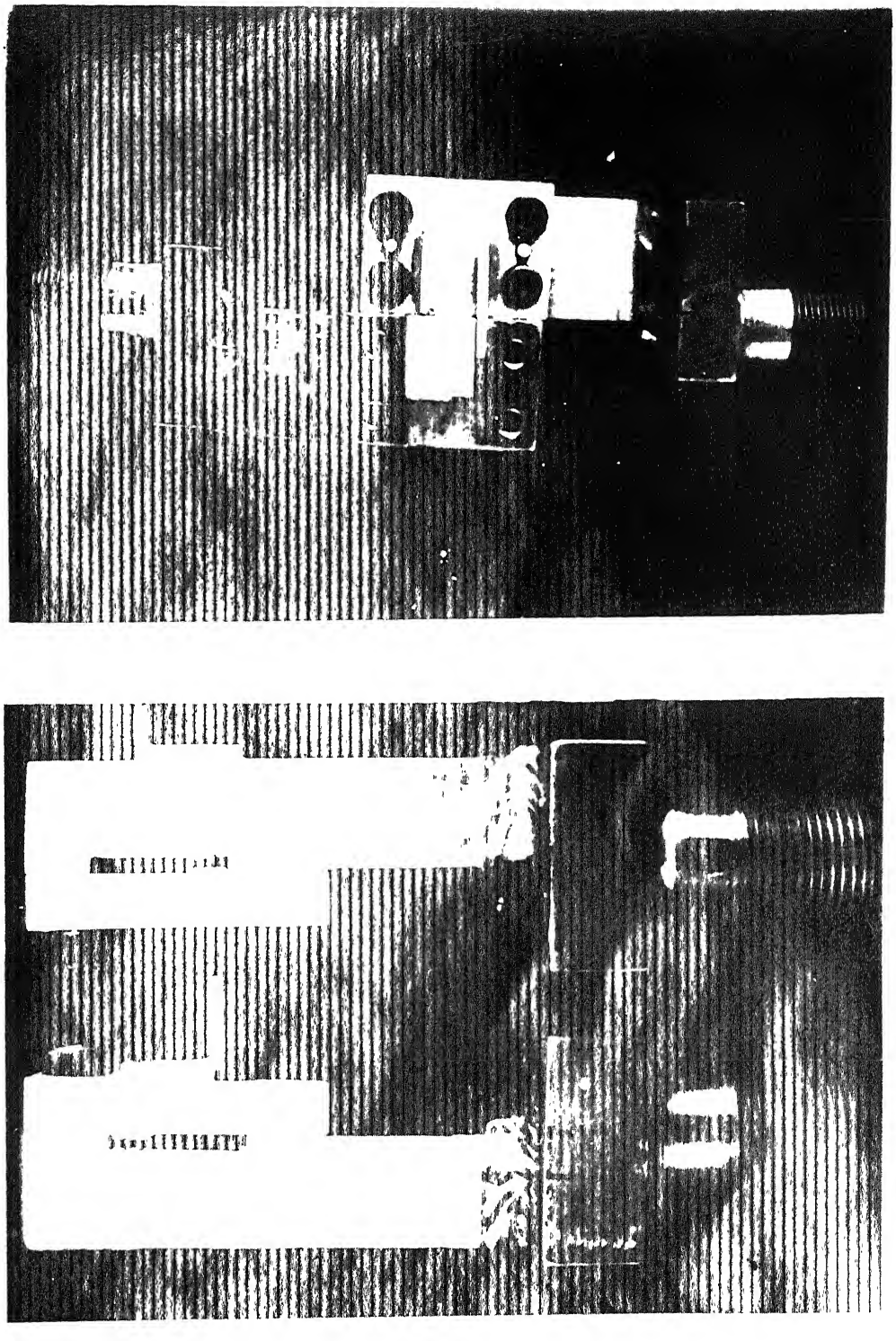

FIG. 7 PHOTOGRAPHS OF FIXTURE FOR TESTS IN MODE II

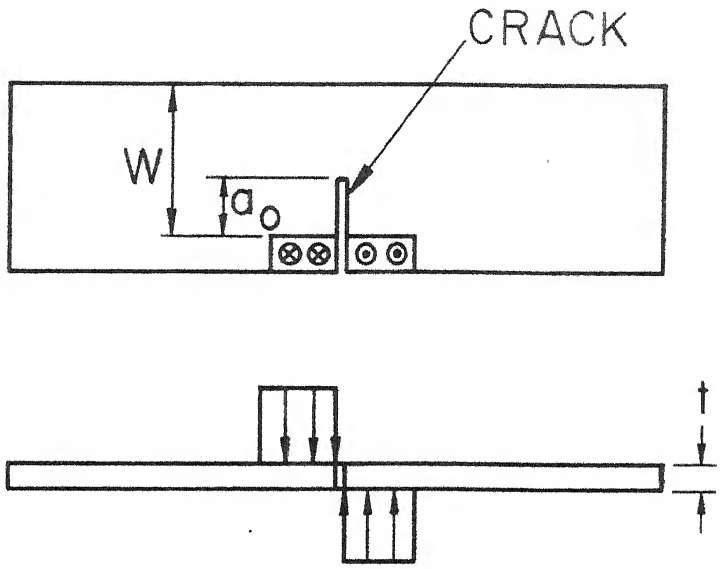

FIG. 8 LOADING CONDITION OF SPECIMEN IN MODE III

as close as possible to the crack mouth. One of the two identical parts of the (fixture used for loading in Mode III is shown in schematically in Fig. 9. Photograph of the fixture is shown in Fig. 10. Two aluminium strips, one on each of the two parts are bonded to the fixture. The clip gauge described later is slipped on these strips to measure the differential movement of the two parts which is taken to be the out-of-plane deflection of the crack lips.

2.1.5 Crack-opening Displacement Gauge (Clip Gauge)

The crack mouth opening displacement is measured using a clip gauge schematically shown in Fig. 11. The gauge consists of two 1.2 mm thick and 63 mm long strips of high speed steel. The strips were actually cut from a hacksaw blade made of high speed steel. The strips are clamped 6 mm apart at one end through an aluminium spacer. Four electrical resistance strain gauges (120) were bonded on the two strips near the clamped end. Output of the strain gauges is calibrated to give displacement at the free end or mouth of the clip gauge. The free end is slipped on the strips bonded to the specimen for measuring crack opening displacement as will be described later.

2.1.6 Heating and Cooling Jackets

Besides room temperature (25.5 ^{o}C) tests, the tests have been carried out at temperatures - 1.1, 43.3 and 60 ^{o}C (30, 110 and 140 ^{o}F respectively). To obtain

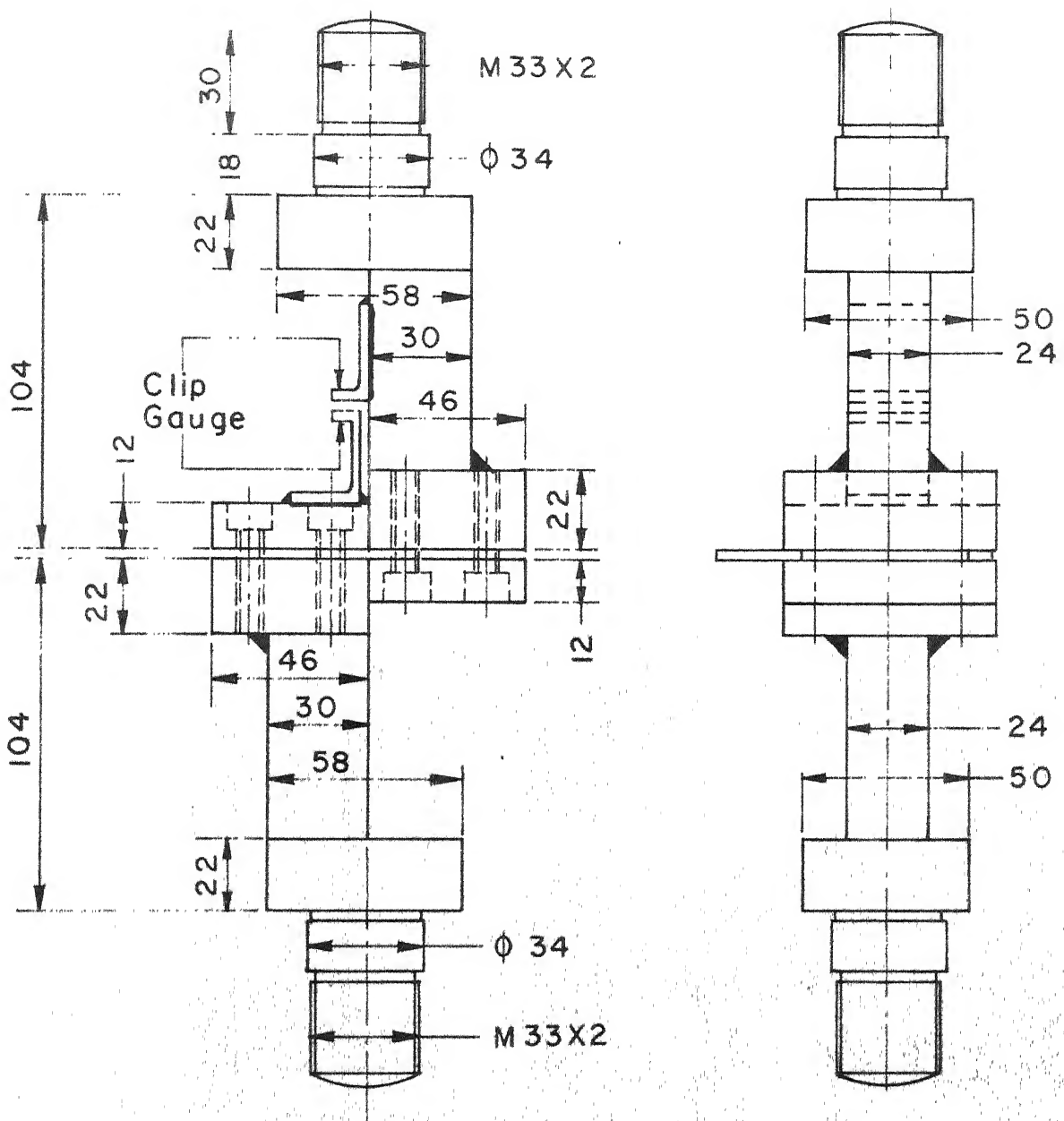

G. 9 DESIGN OF FIXTURE FOR TESTS IN MODE

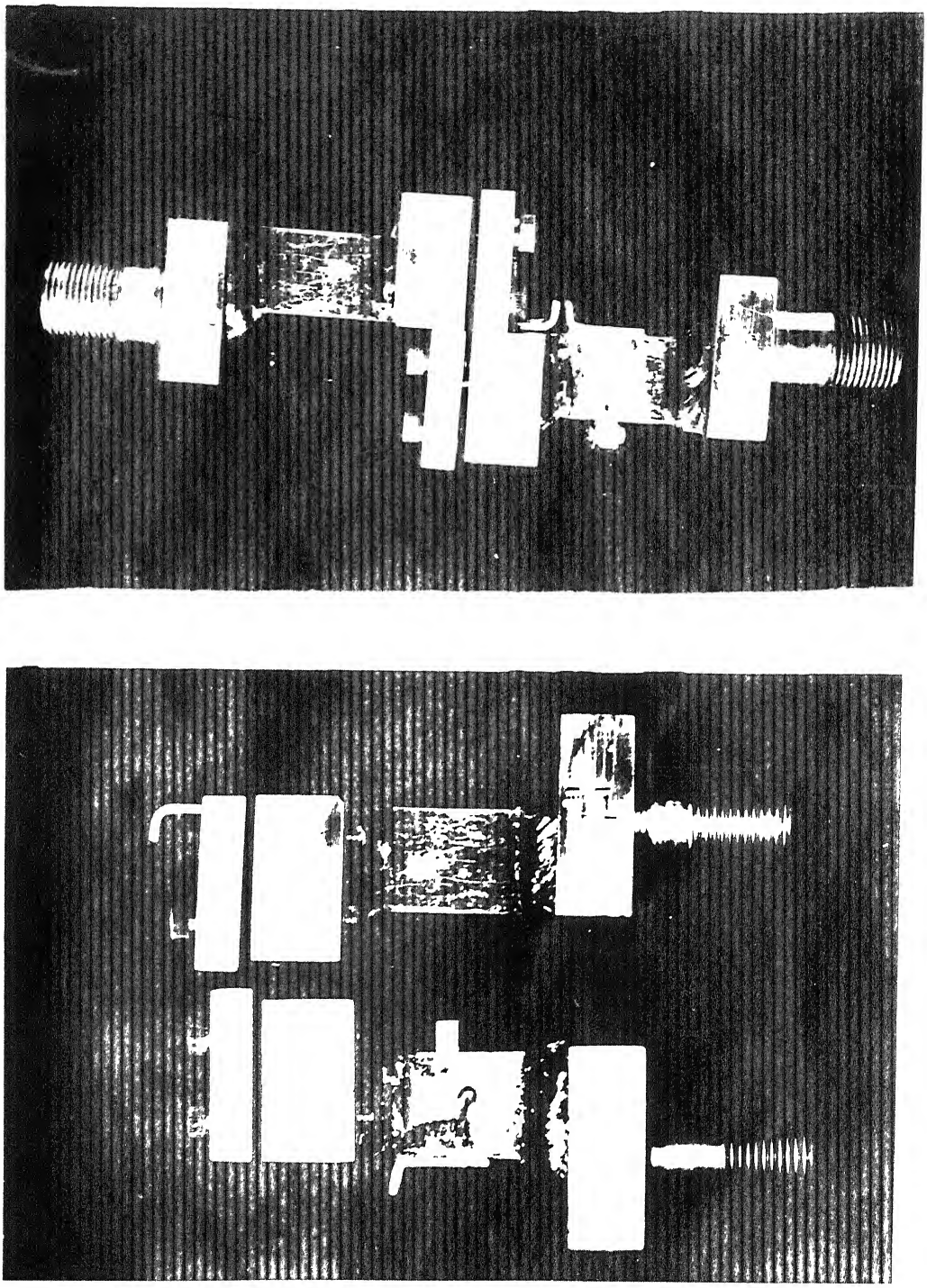

FIG. 10 PHOTOGRAPHS OF FIXTURE FOR TESTS IN MODE III

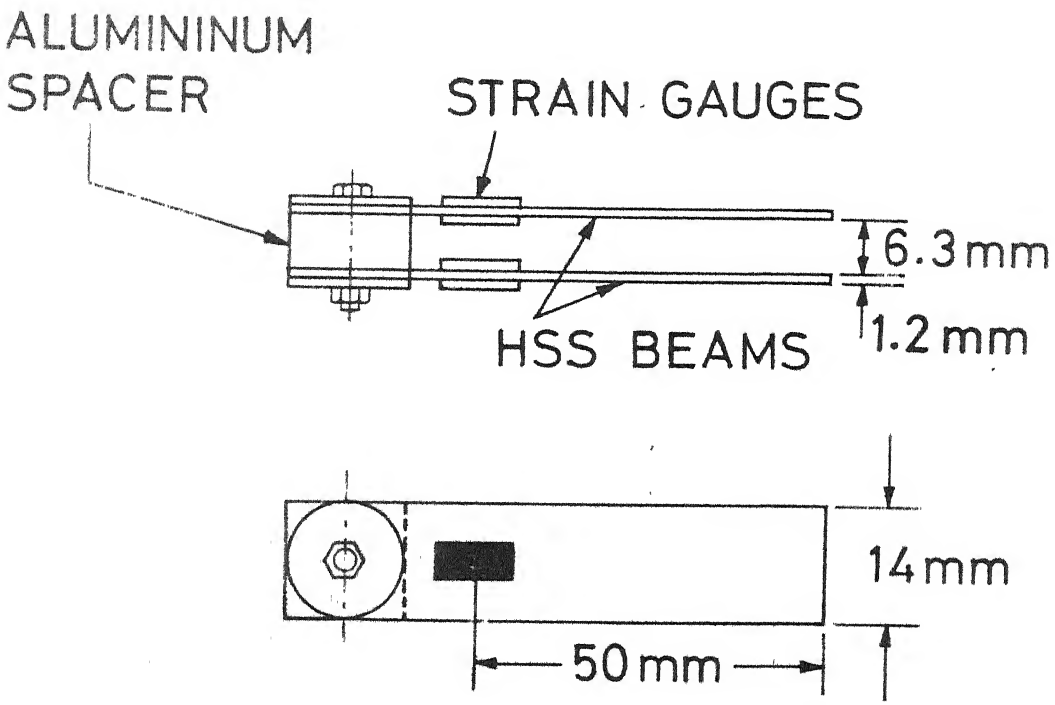

FIG. 11 SCHEMATIC DIAGRAM OF CLIP GAUGE

different test temperatures, two cylindrical jackets, one heating and one cooling were fabricated. The internal dimensions of both the jackets are such that the jackets can be slipped from the top of the testing system and will completely enclose the area between the mild steel plates which support the top and bottom clamps. Thus a temperature controlled test chamber is formed.

The heating jacket is made of a 3 mm thick copper sheet rolled to a circular cylinder and brazed at the seam. An electrical heating element of 1000 W is placed on the outer surface of the cylinder. A 20 mm thick glass wool insulation is provided on the heating element to minimize the heat loss to the outside atmosphere. The rate of heating is controlled by controlling the electrical current in the heating element. To attain the required test temperature, the maximum current is first passed through the heating element so that rapid heating of the chamber takes place. When the thermometer shows the chamber temperature about 10 ^{o}C lower than the required temperature, the power input to the heating element is reduced to a nominal value. The experience has shown that the steady state is attained in about 4 - 5 minutes. A minor adjustment is sometimes needed to attain the exact test temperature. It is found that the chamber temperature can thus be maintained to a nearly constant values for a sufficient length of time to complete the test. The tests at 43.3 and 60 ^{o}C have been

conducted using the heating jacket. A thermometer is inserted in the chamber through a hole in the top plate of the machine and it indicates the test temperature on a circular dial outside the chamber. The sensing element of the thermometer is placed in close vicinity (about 6 mm) of the specimen.

The cooling jacket is essentially an annular jacket made of thin (0.5 mm thick) galvanized iron sheet. The annular space is about 60 mm wide and is filled with ice mixed with 5% common salt. In this manner the required temperature of - 1.1 ^{o}C (30 ^{o}F) is obtained in the test chamber in about 20 minutes. The chamber temperature could be easily maintained at -1.1 ^{o}C for sufficiently long time to conduct the test. The heat loss through the outside surface is minimized by providing a layer of insulation. Figure 12 shows the photograph of heating and cooling jackets.

2.1.7 Calibration of Load Cell and Clip Gauge Output

The output of the amplifier connected to load cell employed in the testing system was calibrated by performing a tension test on a calibrated mild steel tension specimen. A 5.5 mm (width 22.5) thick mild steel tension specimen was first calibrated through a tension test on Instron. The specimen strain was measured by the electrical resistance strain gauge bonded to the specimen.

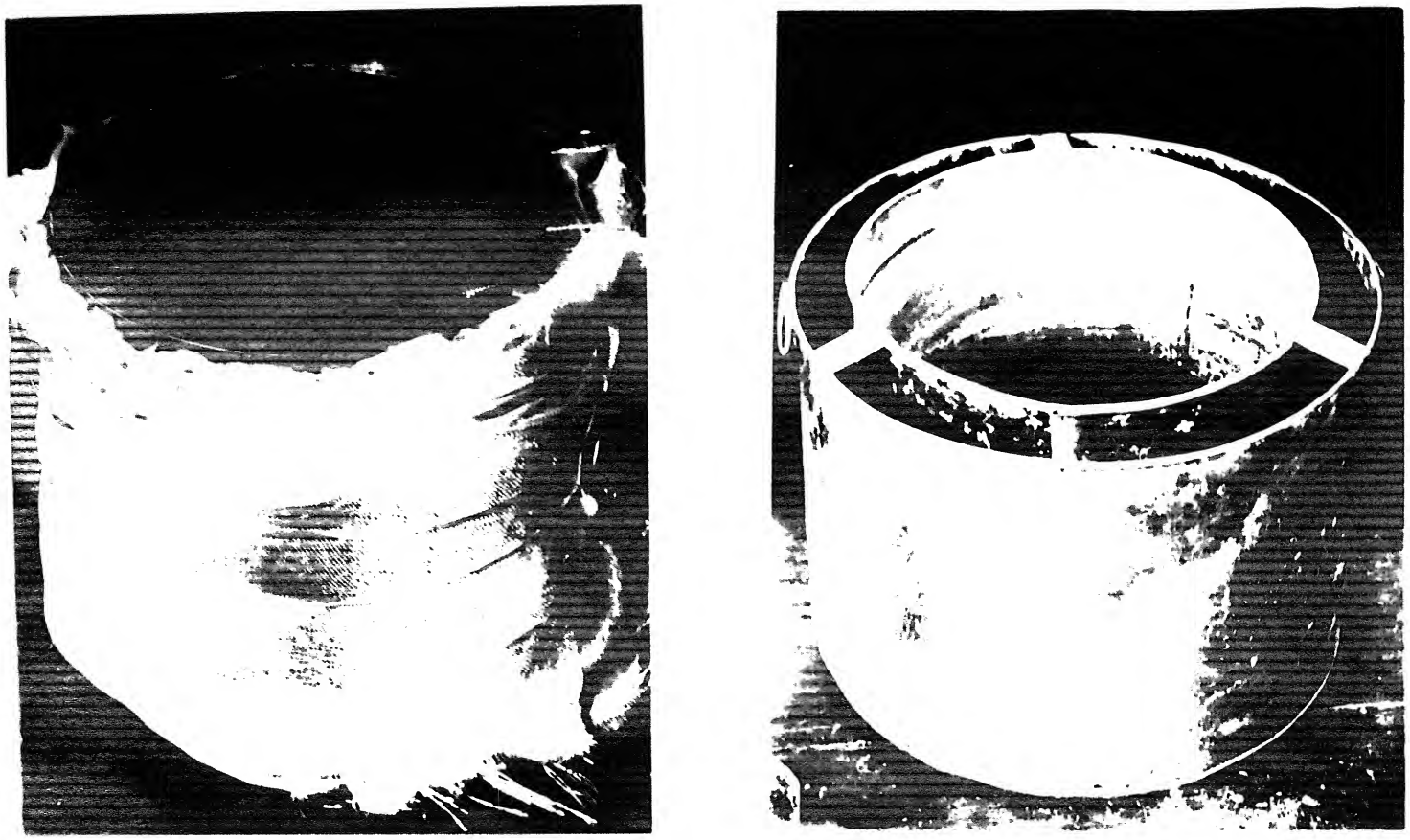

(a) (b)

FIG. 12 PHOTOGRAPH SHOWING (a) HEATING JACKET (b) COOLING JACKET

The load on the specimen was measured through the load cell which was calibrated by standard weights before starting the tension test. The specimen was loaded upto a maximum stress of 96.88 MPa which is well within the elastic limit of the material. The record of load as a function of strain during this tension test should a linear variation. This calibrated tension specimen was used to perform a tension test on the testing system used for the present investigations. Output of the amplifier connected to the load cell was related to the load on the sample through the measured strain and the load strain record during the tension test in the Instron. The amplification factor of the amplifier was so adjusted that the full scale reading (100 division corresponds to 1000 Kg). A plot of amplfier output against the measured strain in Fig. 13 shows a linear relationship between the two. The elastic modulus calculated from the test was found to be 204.4 GPa.

The amplifier recording the output of the clip gauge was calibrated by subjecting the clip gauge to known opening. The displacement to the clip gauge was applied at 4.5 mm from the free end because for the measurement of COD during the fracture toughness tests the clip gauge is slipped by the same distance on the strips bonded to the specimens for this purpose. The displacement was applied and measured by a vernier calipper having a least count of 0.02 mm. While applying the displacement sufficient care was exercised to see that the point of

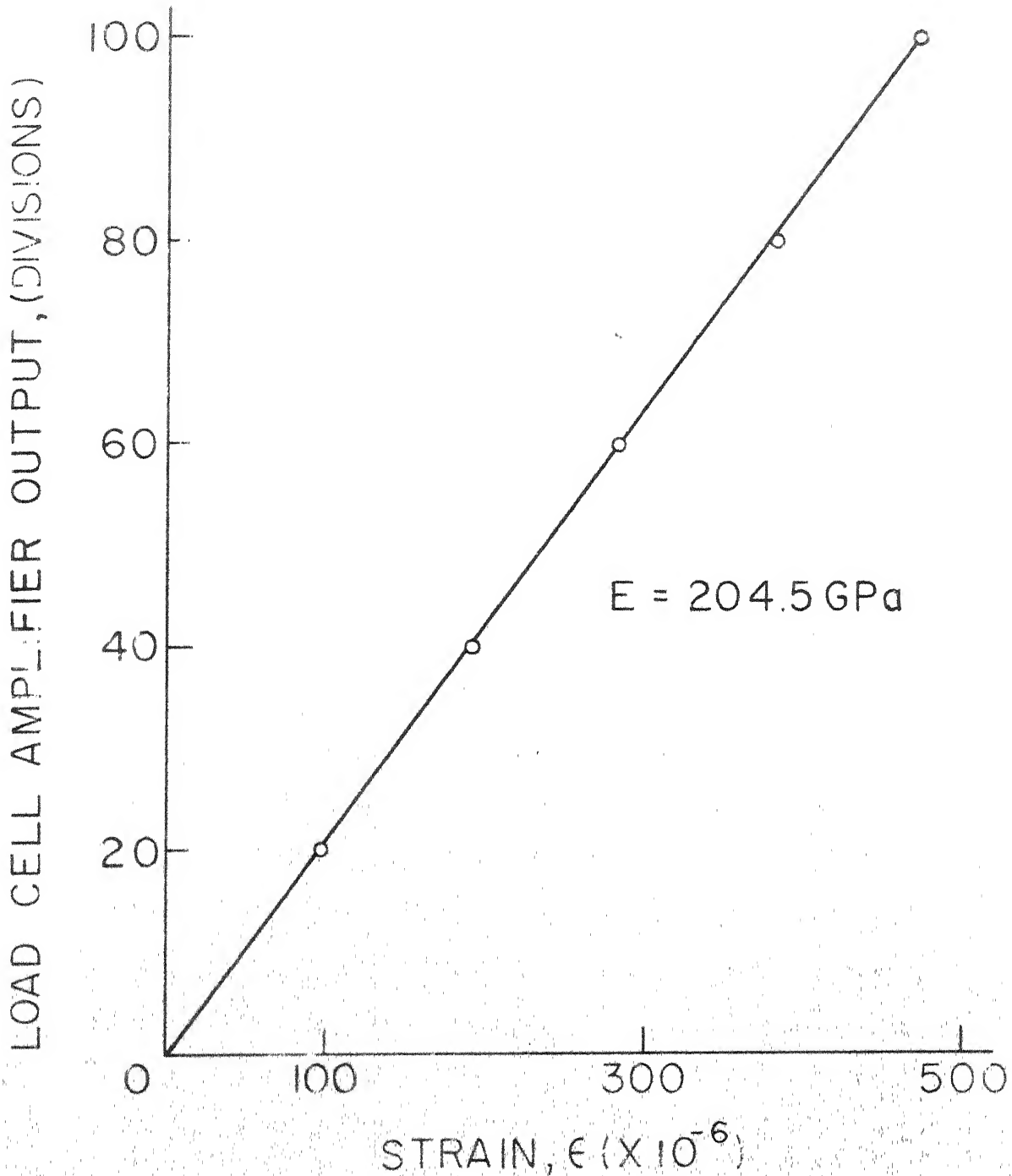

FIG. 13 CALIBRATION CURVE FOR LOAD CELL OUTPUT

deflection on the clip gauge does not shift. The amplifier output plotted against clip gauge opening in Fig. 14 shows a linear variation. Each amplifier division corresponds to 0.029 mm of clip gauge opening.

2.2 MATERIAL PREPARATION

The present investigations have been performed on short-glass-fibre-mat reinforced epoxy composites. The composite material plates were fabricated in the laboratory using chopped strand mat of glass fibres having a weight of 0.6 Kg/m^2 and an average fibre length of 50 mm. The matrix material was generally an epoxy which is commercially designated LY 553 and is recommended for structural applications. However, tests have also been performed on some other grades of epoxy.

Composite material plates were cast between two 20 mm thick mild steel mould plates lined with mylar sheets, and separated by brass washers which control the thickness of the plate being cast. Chopped strand mat was first cut into pieces of required size. The pieces were placed on the lower mould plate one by one. A small amount of the resin, mixed with the hardener, was spread on the lower mould plate and on the top of each mat piece. The resin was spread on the mat piece by rubber roller to further enhance impregnation. The plates were cured at room temperature for nearly 10 days before specimens were cut and tested.

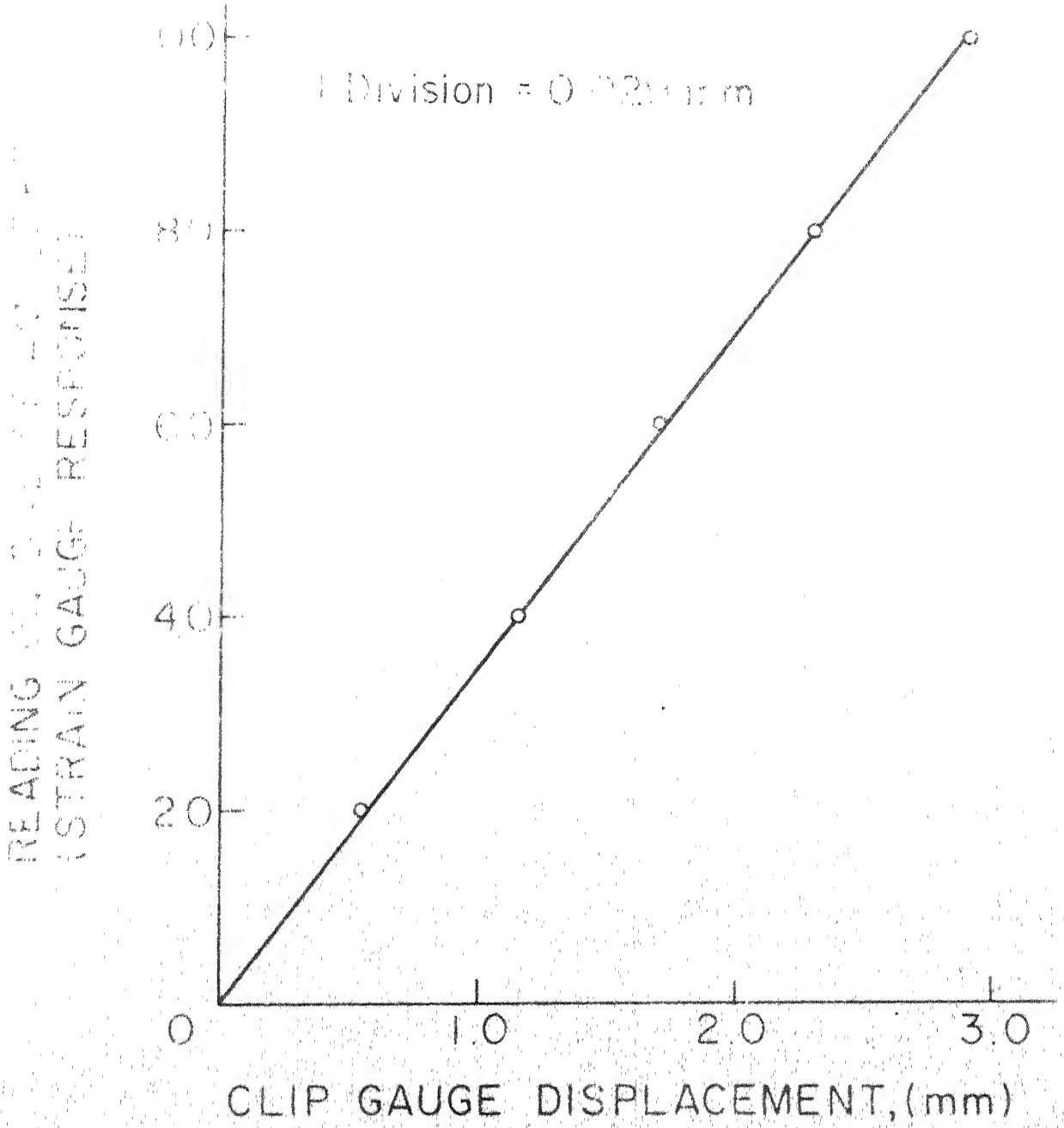

FIG. 14 CALIBRATION CURVE FOR CLIP GAUGE OUTPUT

Volume fraction of fibres was varied by placing different number of layers in the plate of equal thickness. The volume fractions were 20%, 28%, 36% and 52% as established through burn out tests on small samples from different plates. Plates with five different thicknesses (i.e. 1.35, 2.0, 2.5, 3.4 and 3.8 mm) were cast by keeping the fibre volume fraction fixed at 36%.

For purpose of characterization of matrix material some plates of different matrix material were cast in a closed mould.

Rectangular specimens were cut by a diamond impregnated wheel cooled by running water. Most of the tests in Mode I were conducted on 25.4 mm wide and 160 mm long single-edge-notched (SEN) tension specimens shown in Fig. 15. The influence of specimen width on the fracture properties was investigated through tests on additional specimens having widths 19, 30 and 38 mm. In each case the length between the grips was atleast 3 times the specimen width. The specimens for tests in Mode II and Mode III are also single notched specimen with the dimensions shown in Fig. 16.

The cracks in the specimens tested in Mode I were machined to different lengths using a 0.2 mm thick cutter. To measure the crack opening displacement (COD), two small strips of composite material (scrap) were bonded to the specimen close to the top and bottom edges

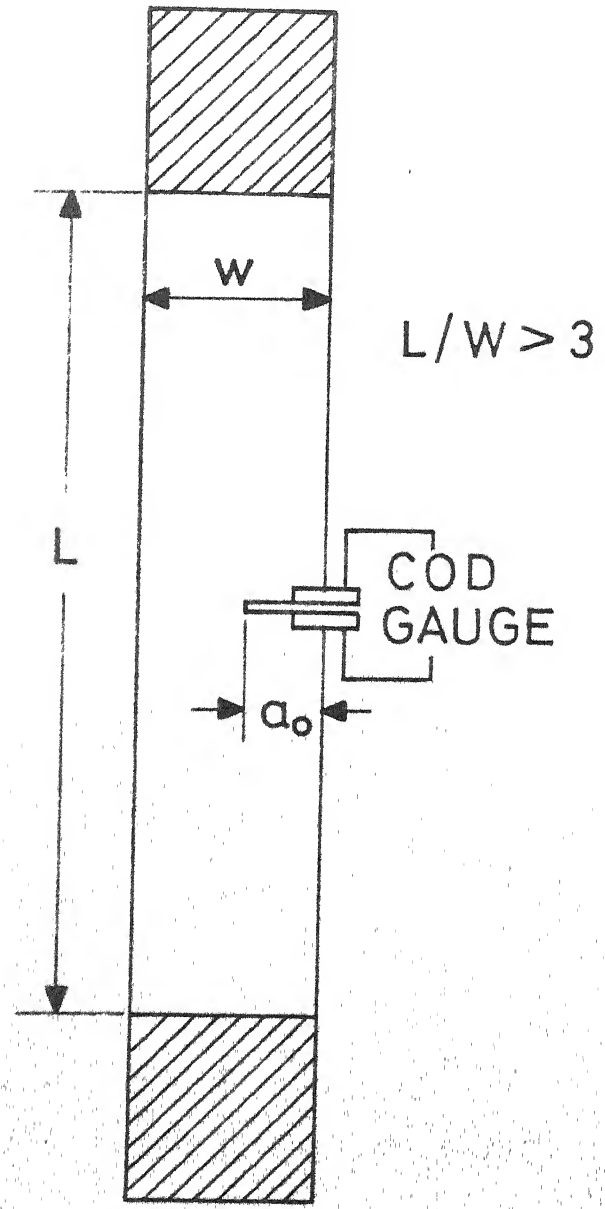

FIG.15 SINGLE EDGED NOTCHED SPECIMEN FOR TESTS IN MODE I

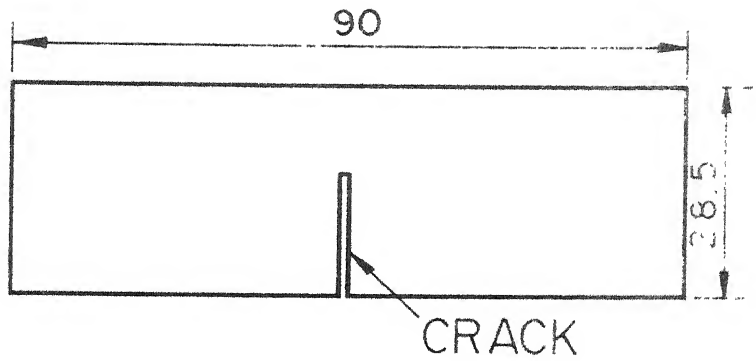

(a) MODE II SPECIMEN
(t = 3.2 mm)

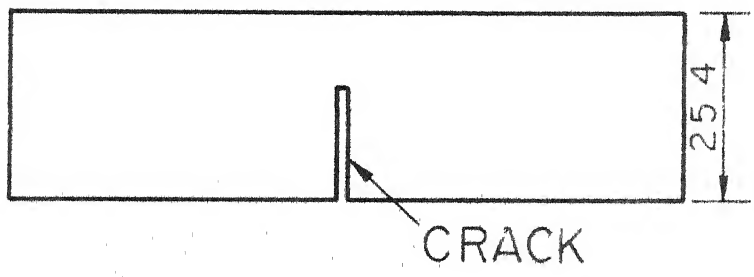

(b) MODE III SPECIMEN
(t = 3.4 mm)

FIG. 16 GEOMETRY OF SPECIMENS FOR TESTS IN MODE II AND MODE III

of the crack. During bonding a piece of mylar sheet was placed in the crack to avoid entry of the adhesive in the crack. The clip gauge described earlier was slipped on these strips for measuring the crack opening displacement.

The specimens tested in Mode II and Mode III require deeper crack to be machined because part of the specimen containing crack is clamped. Therefore, the cutter which was used to machine the cracks in the specimens tested in Mode I could not be used for Modes II and III specimens and a larger diameter cutter have to be used. The cracks were machined to require length using a 0.3 mm thick milling cutter and the crack tip (about 0.5 mm) was finished manually using a 0.15 mm thick razor blade (saw teeth cut on blade). The crack opening displacement in Mode II and Mode III are determined from the differential movement of the two parts of the respective fixtures in each case and no other arrangement need be made on the specimen.

CHAPTER 3

RESULTS AND DISCUSSION ON TESTS IN MODE I

3.1 MATERIAL AND TEST VARIABLES

The fracture toughness tests in Mode I are performed using a single edged notched (SEN) tension specimens as described in Chapter 2 and shown in Fig. 15. The specimen length is selected such that the length between grips is always at least 3 times the specimen width. The reinforcement is always short E - glass fibre mat and the matrix material LY 553 except for the specimens which are tested to study the influence of matrix material on the fracture toughness. The influence of following material and test parameters has been studied:

i. Initial Crack Length (a_o):

Keeping the specimen width constant at 25.4 mm the initial crack length has been varied between 3 and 12 mm. For a fibre volume fraction of 36 percent specimens with eight different crack lengths namely, 3, 4, 5, 6, 7, 8, 10 and 12 mm have been tested, whereas for the remaining volume fractions, crack lengths are 4, 6, 8, 10 and 12 mm.

ii. Fibre Volume Fraction (V_f):

Specimens with four different fibre volume fractions, namely 20, 28, 36 and 52 percent have been tested.

The initial crack lengths have been indicated in point i.

iii. Specimen Thickness (t):

Keeping the fibre volume fraction at 36 percent, five different specimen thickness namely 1.35, 2.0, 2.5, 3.4 and 3.8 mm have been used. The crack length for different thickness is kept constant at 6 mm.

iv. Specimen Width (W):

Keeping the fibre volume fraction at 36 percent the 4 different specimen width namely 19, 25.4, 30 and 38 mm have been used. The initial crack length has been changed to keep the ratio of initial crack length to specimen width (a_o/W) a constant at 0.315.

v. Test Temperature (T):

Besides tests at room temperature, 25.5 °C (78° F), the fracture toughness tests have also been performed at -1.1, 43.3 and 60 °C (30, 110 and 140 °F respectively). The fibre volume fraction is 36 percent and initial crack lengths 4, 6, 8 and 10 mm.

vi. Matrix Material:

Three different grades of epoxy resins namely LY 553, LY 556 and CY 230 have been used. In addition the tests have been performed on specimens in which the matrix material has been modified by addition of dibutyl - phathalate by different percentages, namely 1.5, 2.5 and

5 percent. The fibre volume fraction is 36 percent for the LY 556 matrix and 52 percent for CY 230 and for CY 230 modified by dibutyl - phathalate. With LY 553 as the matrix the results are available for four different fibre volume fraction as already indicated. With LY 556 as the matrix material the tests have been performed at room temperature 25.5 ^{o}C.

Four to five specimens have been tested with all the parameters constant. Thus the results described in this chapter are derived from tests on a total of about 350 specimens.

3.2 ANALYSIS PROCEDURE AND INFLUENCE OF CRACK LENGTH

The notched tension specimens have been tested in the testing system described in Chapter 2. In each test the crack mouth opening displacement has been recorded at increasing load. The load displacement records have been analysed in accordance with the procedures recommended in ASTM-E 399 - 71. The stress intensity factor K_I is calculated by using the following relation

$$K_I = \frac{P\, a^{1/2}}{t\, W} \qquad (1)$$

where Y = Calibration factor and is given as follows:

$$Y = 1.99 - 0.41\,(a/W) + 18.70\,(a/W)^2 - 38.40(a/W)^3 + 53.85\,(a/W)^4$$

P = applied load

a = crack length

W = specimen width

t = specimen thickness

The load versus crack mouth opening displacement (COD) curves for the composite with fibre volume fraction of 36 percent are shown in Fig. 17 for different crack lengths. Five specimen were tested at each initial crack length and the load versus COD curves plotted. In each case a typical curve, generally lying in the middle of the curves for five specimens, has been selected and shown in Fig. 17. The load versus COD curves are initially linear but deviate progressively from linearity as the damage at the crack tip progresses. The nonlinear nature of the curves in Fig. 17 suggests that a considerable amount of damage occurs at the crack tip prior to the final unstable fracture. Progress of the damage ahead of the crack tip is illustrated in Fig. 18 through photographs of a specimen subjected to different loads. The damage occurs due to debonding of the fibres from the matrix and the matrix cracking. There is a damage zone ahead of the crack tip analogous to the plastic zone in metallic materials. The crack tip damage is neither colinear nor coplaner with the original crack. Although there are a number of microcracks in the damage zone, and their number increases with the growth of damage zone, the progress of damage zone is not a crack extension in the

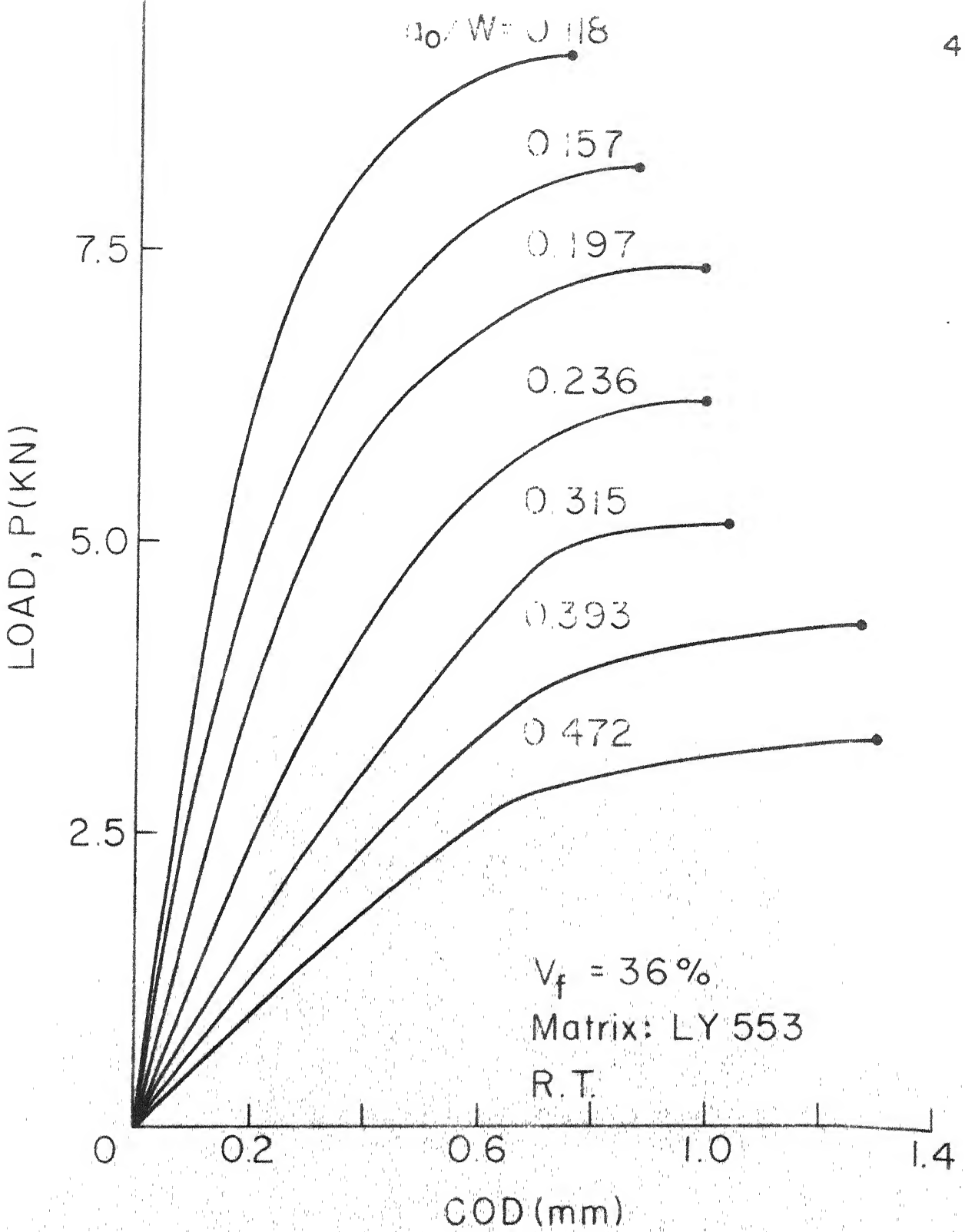

FIG.17 LOAD VERSUS COD CURVES FOR DIFFERENT INITIAL CRACK LENGTHS (V_f = 36%)

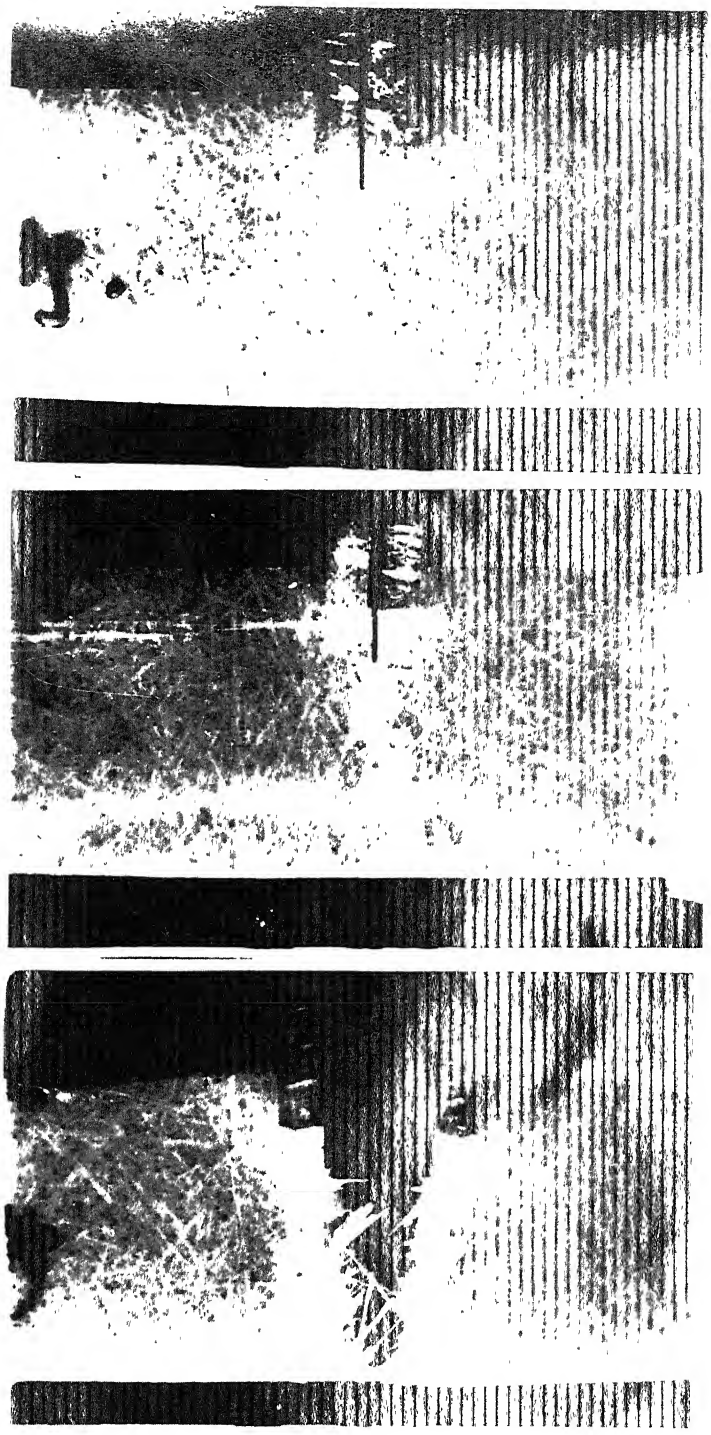

FIG. 18 PHOTOGRAPHS OF A SPECIMEN SHOWING THE PROGRESS OF DAMAGE AHEAD OF CRACK TIP AT INCREASING LOADS

conventional sense. However, the crack tip damage does increase the compliance of the specimen as a crack extension does in metallic materials.

For the purpose of analysis the damage growth at the crack tip can be modelled as a self similar crack extension through compliance matching as suggested by Gaggar and Broutman [24] for short fibrous composites and also used by Morris and Hahn [15] for graphite/epoxy laminates. In this method a crack length estimation curve is first obtained. The crack length estimation curve is a compliance curve based on COD and is obtained from the load versus COD curves. The compliance is calculated from the initial linear portion of the load versus COD curves and plotted against the corresponding initial crack length (or $\frac{a_o}{W}$). The crack length estimation curve for V_f = 36% is shown in Fig. 19. To estimate the effective instantaneous crack length during a fracture toughness test, the instantaneous compliance (based on COD) is calculated from load versus COD graph. The method of obtaining the compliance is illustrated in Fig. 20. In this procedure a straight line is drawn from the origin to a point on the load COD curve and the compliance is taken to be the reciprocal of the slope of this line. Corresponding to this compliance, the effective crack length is obtained from the crack length estimation curve (Fig. 19). Corresponding to the load at which the compliance is obtained, the stress intensity factor is obtained using Eq. (1) in which 'a' is taken as the effective crack length. This

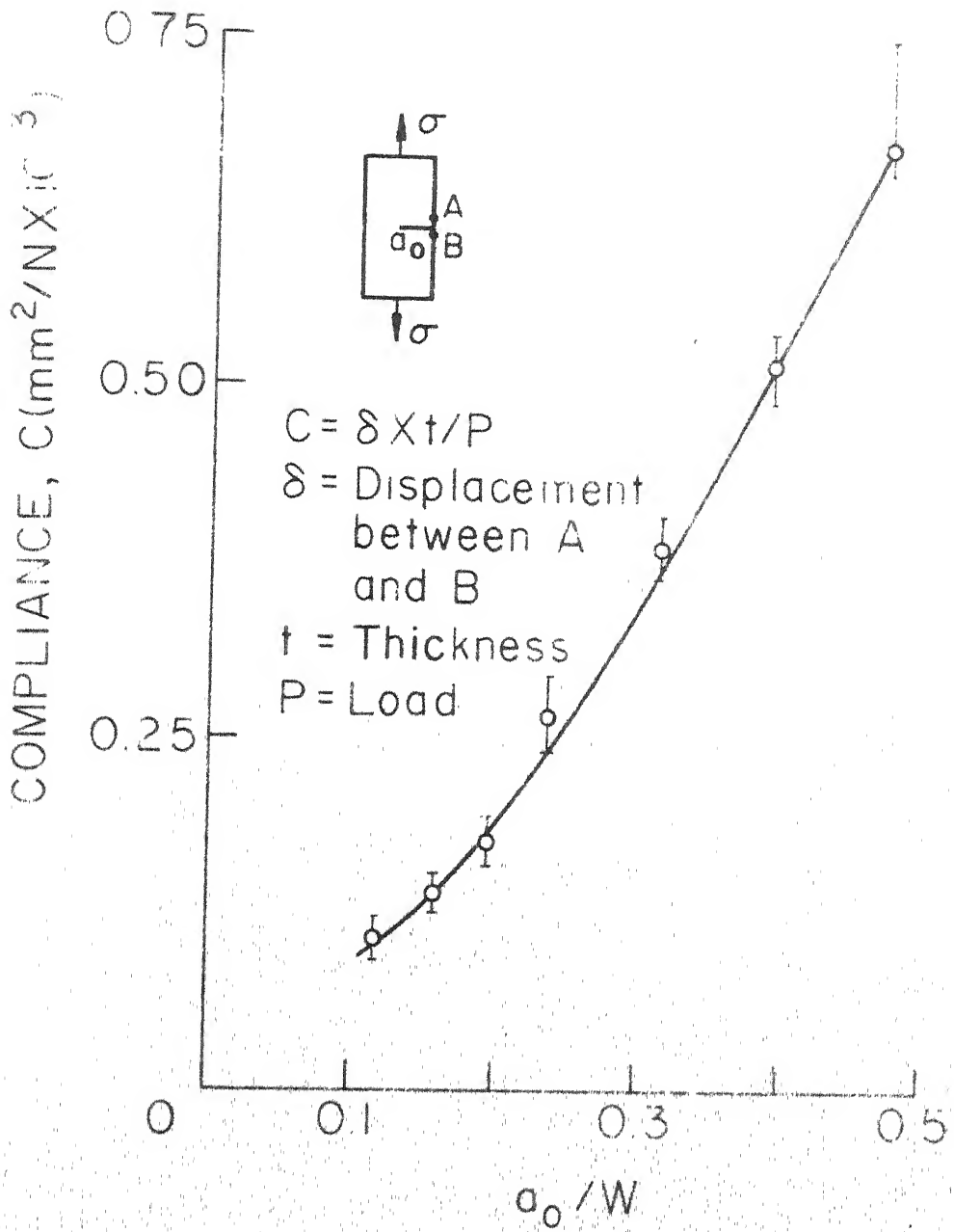

FIG 19 CRACK LENGTH ESTIMATION CURVE FOR V_f = 36 %

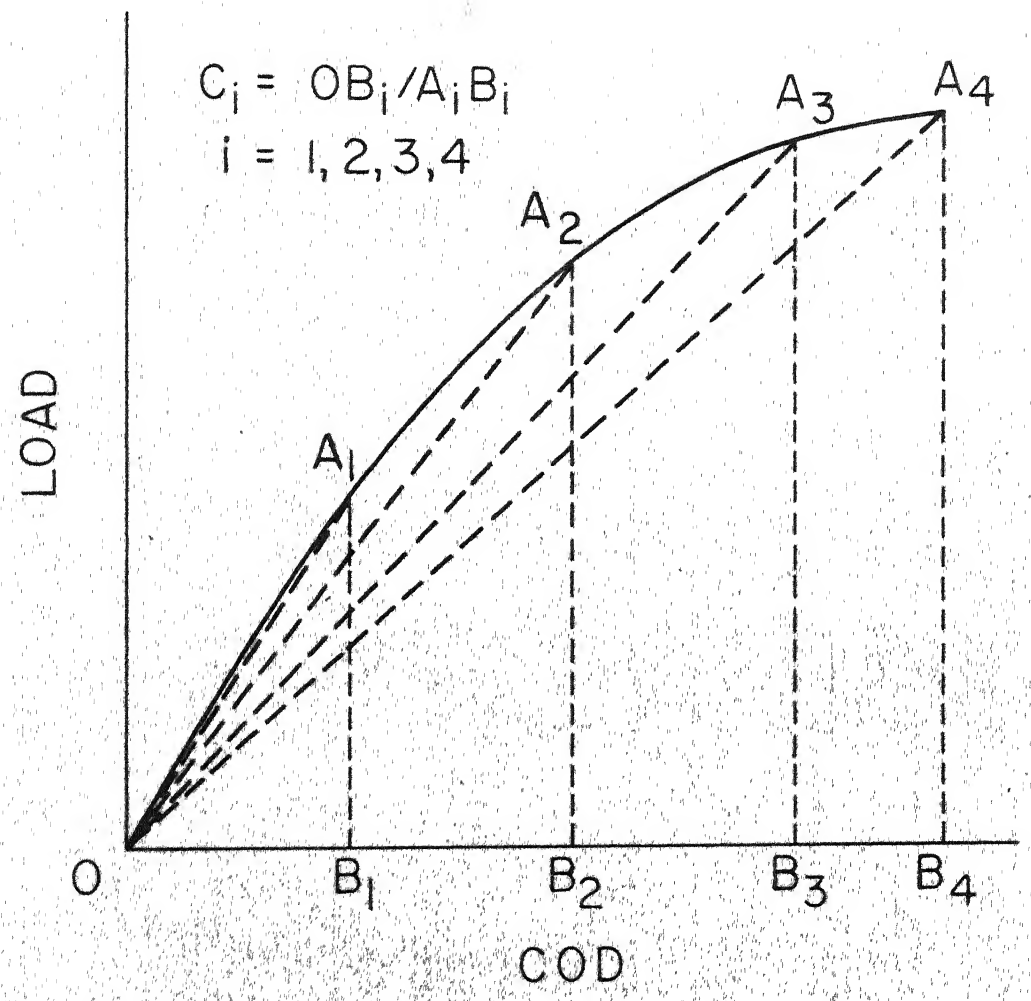

FIG. 20 ILLUSTRATION OF THE METHOD EMPLOYED FOR OBTAINING COMPLIANC AT DIFFERENT COD

value of stress intensity factor is called the instantaneous crack growth resistance and denoted by K_R. The K_R values are obtained for increasing load upto fracture. The plot of K_R against effective crack length is the crack growth resistance curve (R - curve).

The R-curves for different initial crack length are shown in Fig. 21. It may be mentioned that although the load COD curves are obtained for the initial crack lengths upto 12 mm, the R - curves can be obtained only upto the initial crack length of 8 mm. For an initial crack length of more than 8 mm, the effective crack length during loading becomes larger than 12 mm and thus, cannot be estimated from the crack length estimation curve.

From the design point of view it is necessary to know the point of instability, that is, the point where crack propogates in an unstable manner. The point of instability is established by plotting the stress intensity factor against the crack length for different values of constant load, on the same graph in which the resistance curves are plotted. The values of constant load are chosen (usually near the fracture load) such that one of the K_I curves is tangent to the R - curve. The point of tangency defines the point of instability and the value of K_R at this point is K_R instability. The method is illustrated in Fig. 22 for an initial crack length of 4 mm. The $K_{R(ins)}$ is plotted against initial crack length in Fig. 23. This

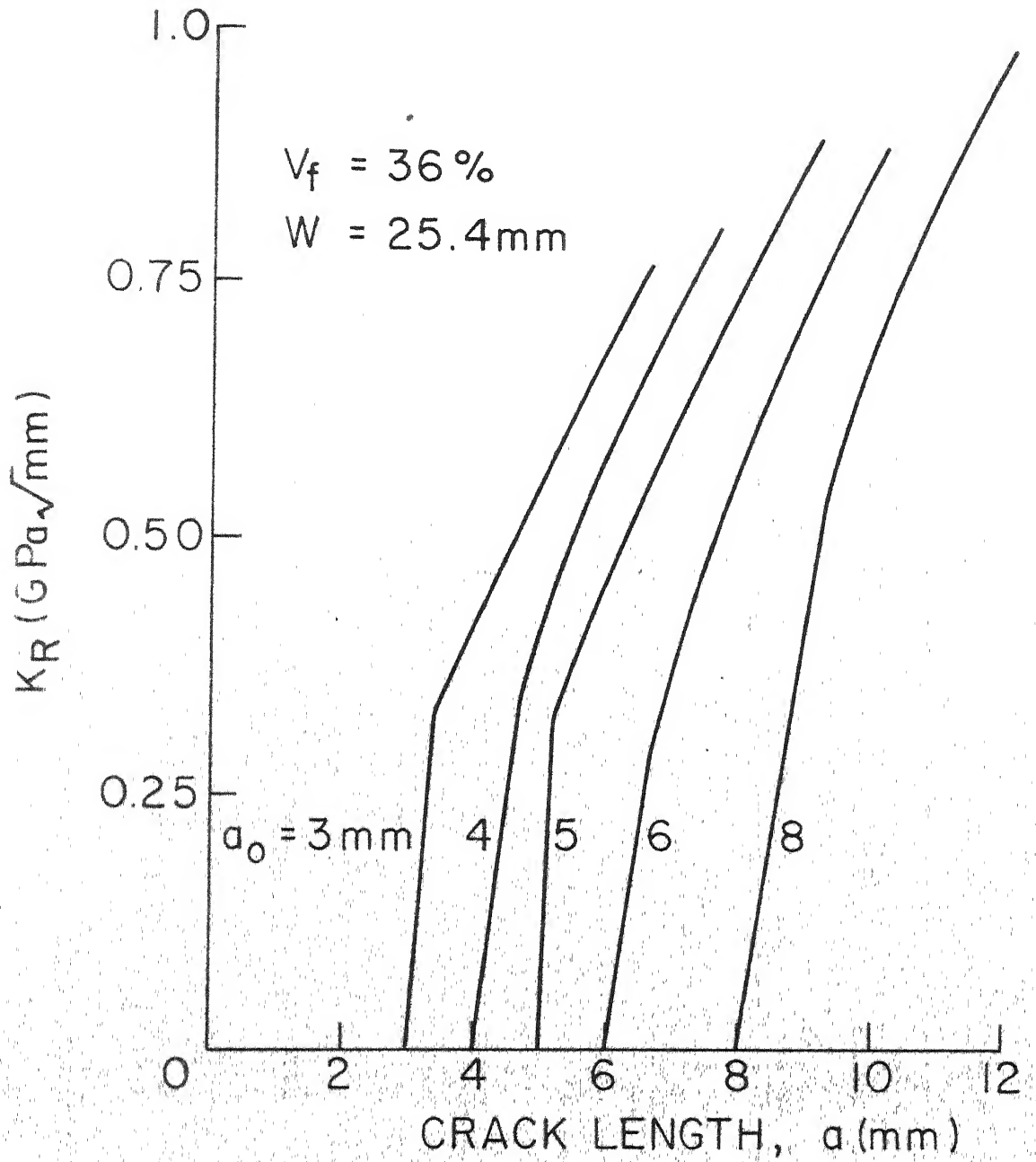

FIG. 21 R-CURVES FOR V_f = 36%

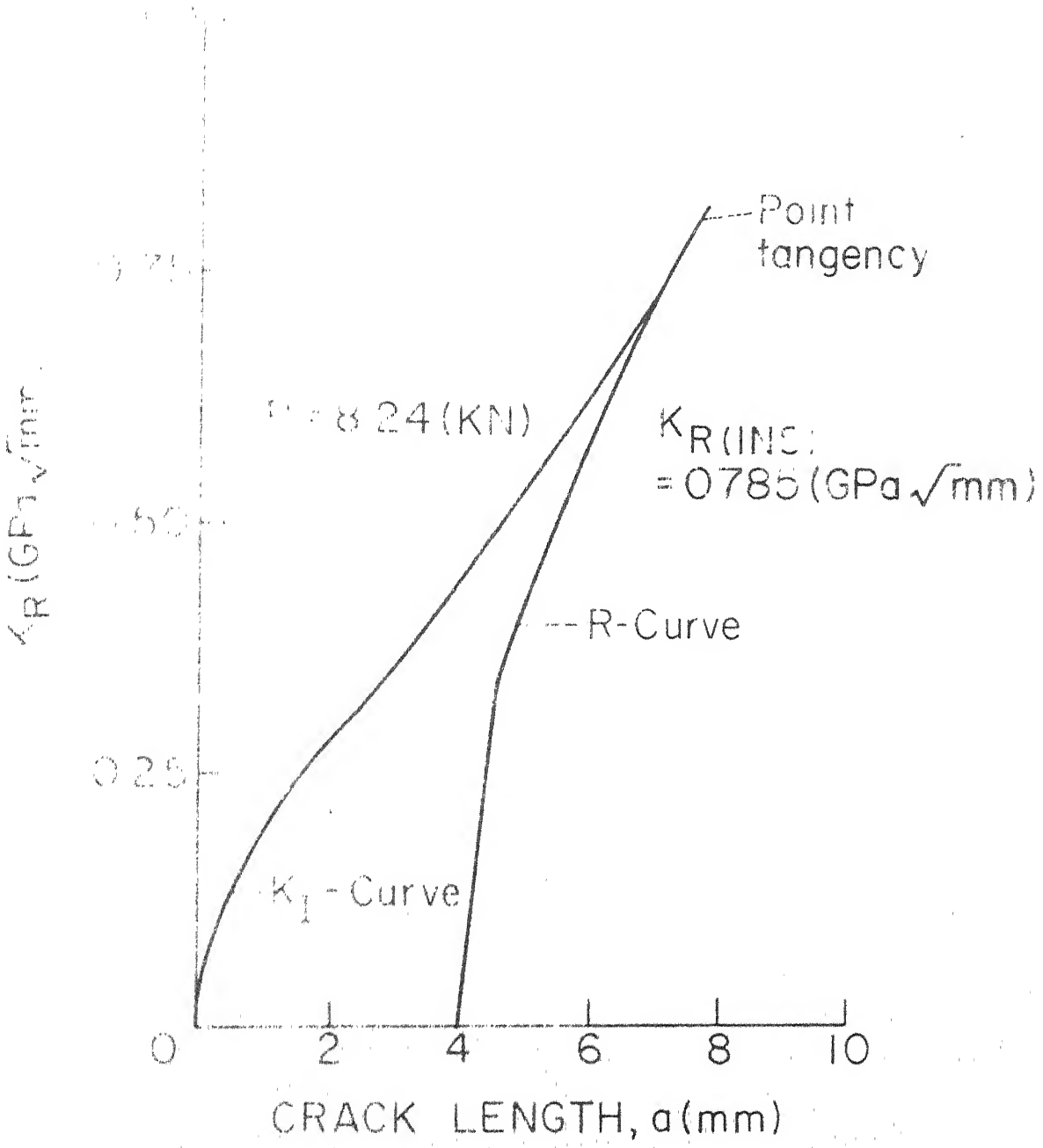

FIG 22 ILLUSTRATION OF THE METHOD EMPLOYED FOR OBTAINING $K_{R(INS)}$

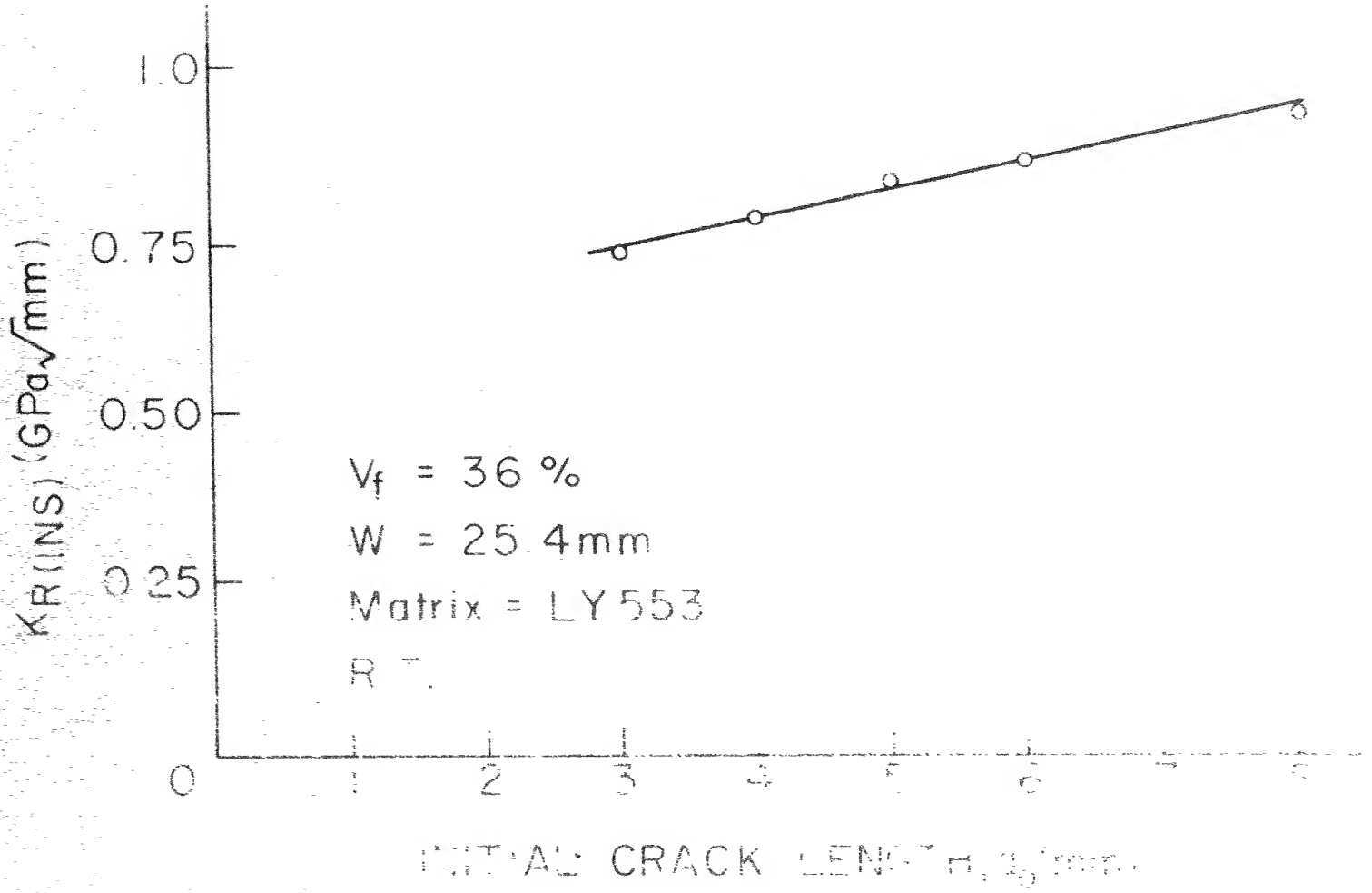

FIG. 23 VARIATION OF $K_{R(INS)}$ WITH INITIAL CRACK LENGTH (V_f = 36%)

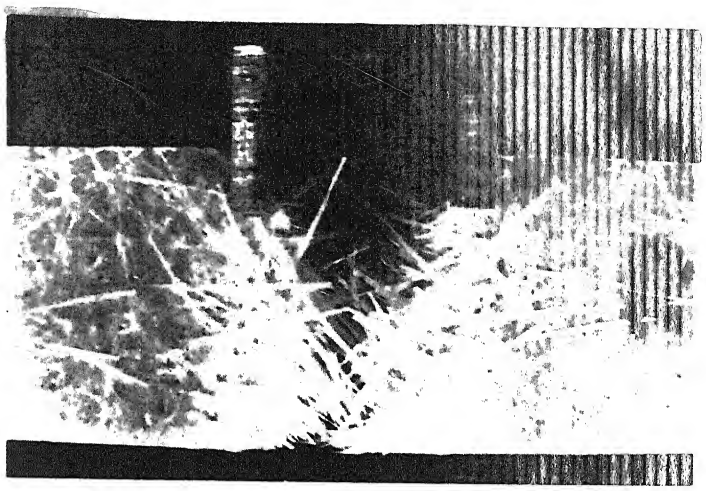

$a_0 = 4\,mm$

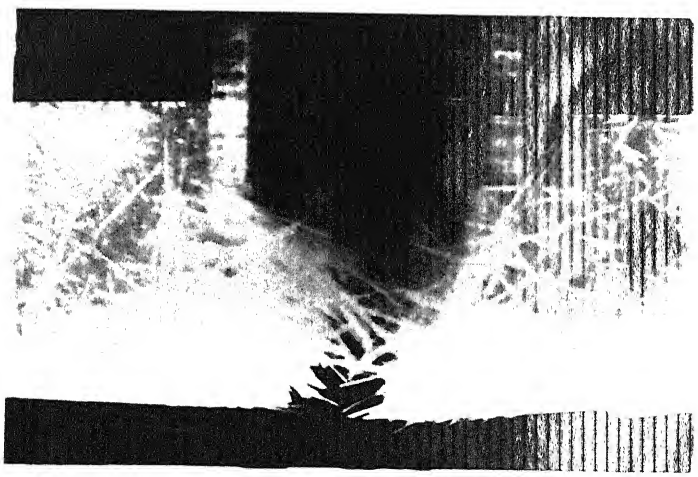

$a_0 = 8\,mm$

FIG. 24 PHOTOGRAPHS OF FRACTURE SPECIMENS SHOWING DAMAGE ZONE AHEAD OF CRACK TIP AT INITIAL CRACK LENGTHS OF 4 AND 8 mm

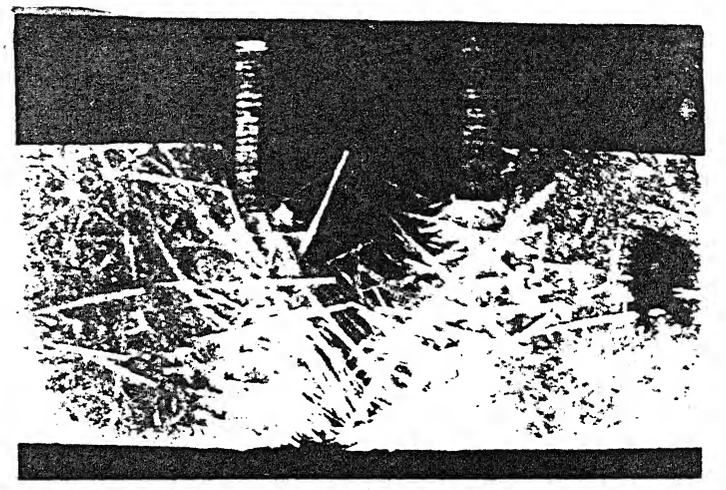

$a_0 = 4\,mm$

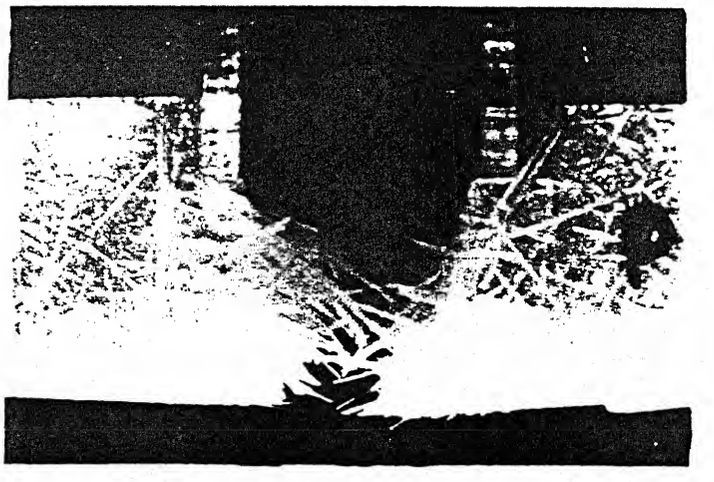

$a_0 = 8\,mm$

FIG. 24 PHOTOGRAPHS OF FRACTURE SPECIMENS SHOWING DAMAGE ZONE AHEAD OF CRACK TIP AT INITIAL CRACK LENGTHS OF 4 AND 8 mm

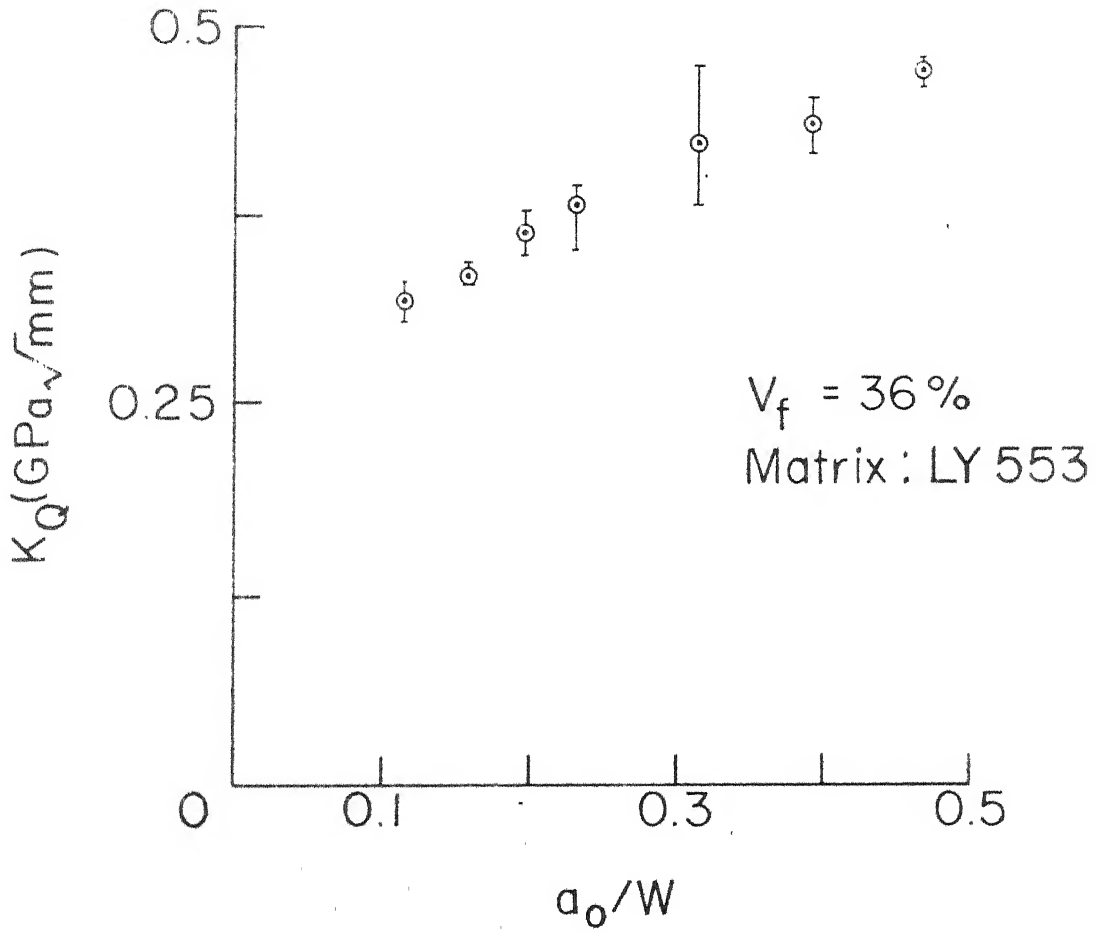

FIG. 26 VARIATION OF CANDIDATE STRESS INTENSITY FACTOR WITH INITIAL CRACK LENGTH (V_f = 36%)

The K_Q increases with crack length as was observed by Gaggar and Broutman [26] for epoxy and polyester composites.

The procedures adopted for fracture toughness test and the data analysis have been illustrated in this section. The same procedures have been adopted for studying influence of different variables on fracture properties as will be discussed in the following paragraphs.

3.3 EFFECT OF FIBRE VOLUME FRACTION

In addition to the tests on specimens with a fibre volume fraction of 36%, the tests have been conducted for three other V_f, namely 20, 28 and 52%. Elastic modulus, shear modulus, Poisson's ratio, ultimate tensile strength and ultimate elongation of the composites are given in Table 1. The load versus COD curves, crack lengths estimation curves and K_R curves were obtained in a manner illustrated earlier for V_f = 36 percent. The load versus COD curves for different V_f are shown in Figs. 27 to 29 and the crack length estimation curves in Fig. 30. As the fibre volume fraction increases from 20 to 36 percent the compliance for equal initial crack length decreases because the material becomes stiffer with increase in fibre concentration. The K_R, curves for different V_f shown in Figs. 31 - 33 and similar in nature to the K_R curves for V_f = 36 percent shown in Fig. 2.1.

TABLE 1 : Average Room Temperature Properties of Composite Material (Matrix: LY 553)

V_f Percent	Elastic Modulus E_c GPa	Shear Modulus G GPa	Poisson's Ratio	Ultimate Tensile (Composite C_u MPa	Percentage Elongation
20	7.55	2.93	0.287	113.95	2.1
28	10.30	4.09	0.260	134.37	1.76
36	12.75	5.12	0.245	190.60	1.64
52	17.16	6.92	0.240	208.52	2.2

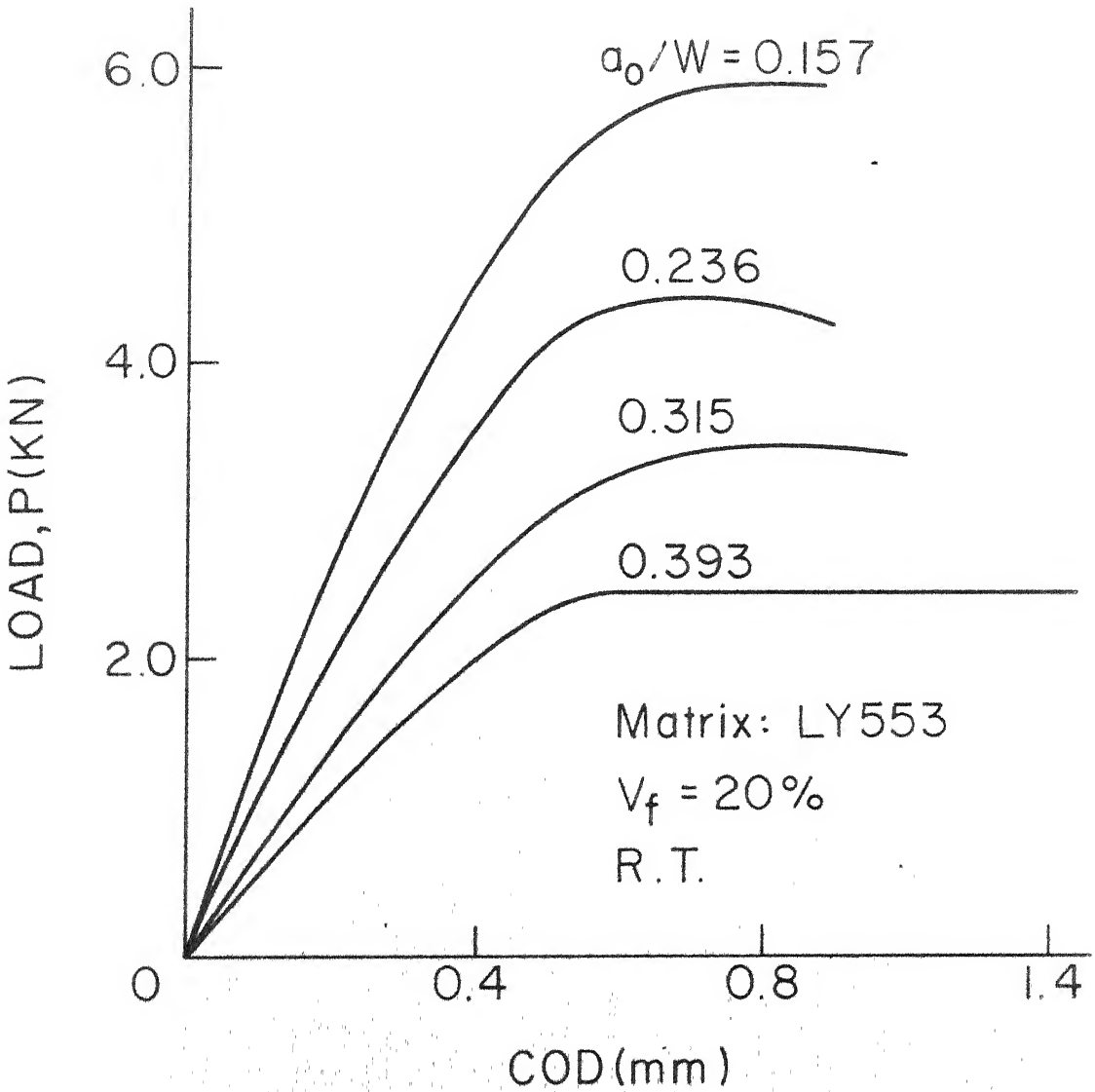

FIG. 27 LOAD VERSUS COD CURVES FOR DIFFERENT INITIAL CRACK LENGTH (V_f = 20 %)

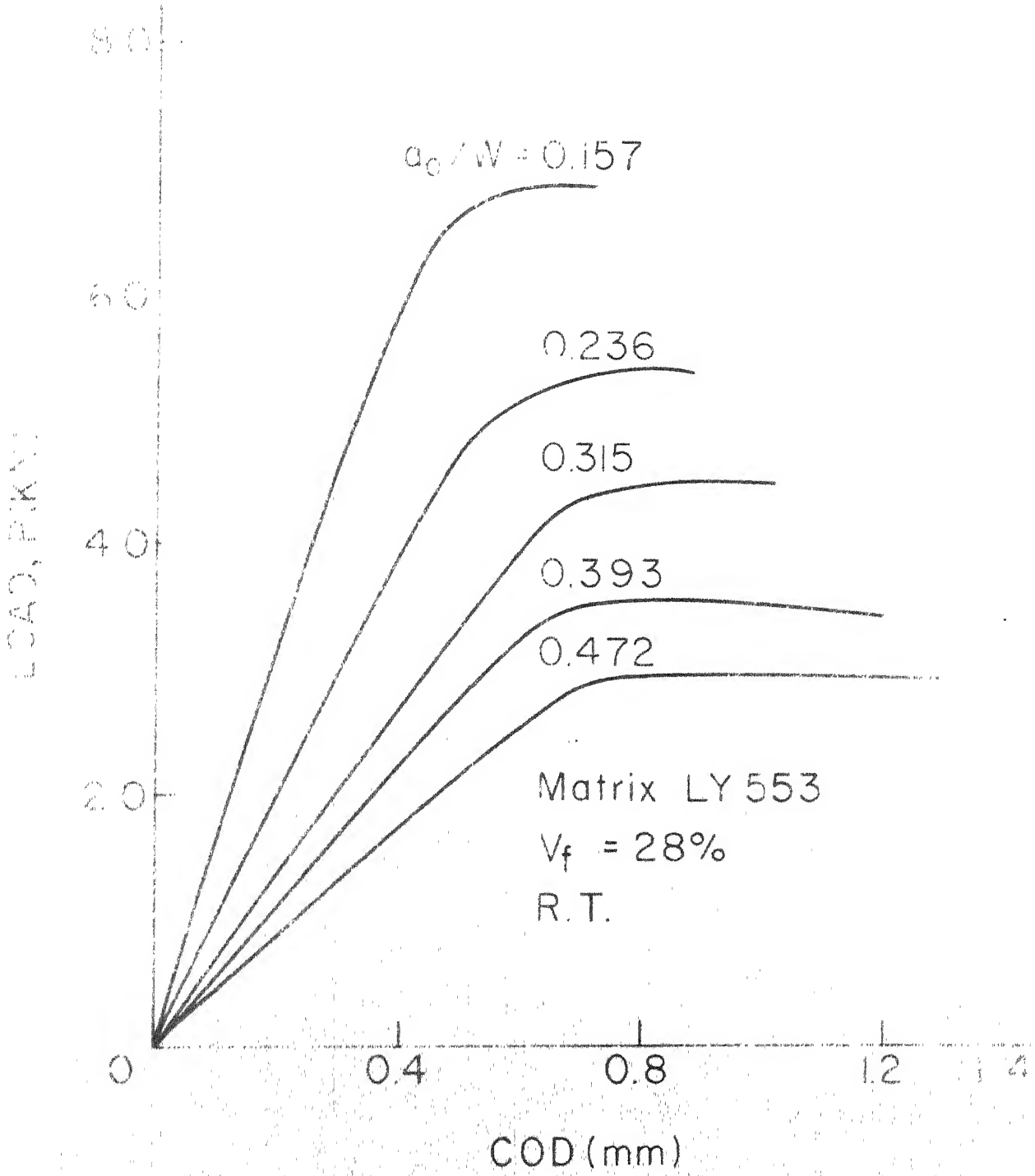

FIG 28 LOAD VERSUS COD CURVES FOR DIFFERENT INITIAL CRACK LENGTH (V_f = 28%)

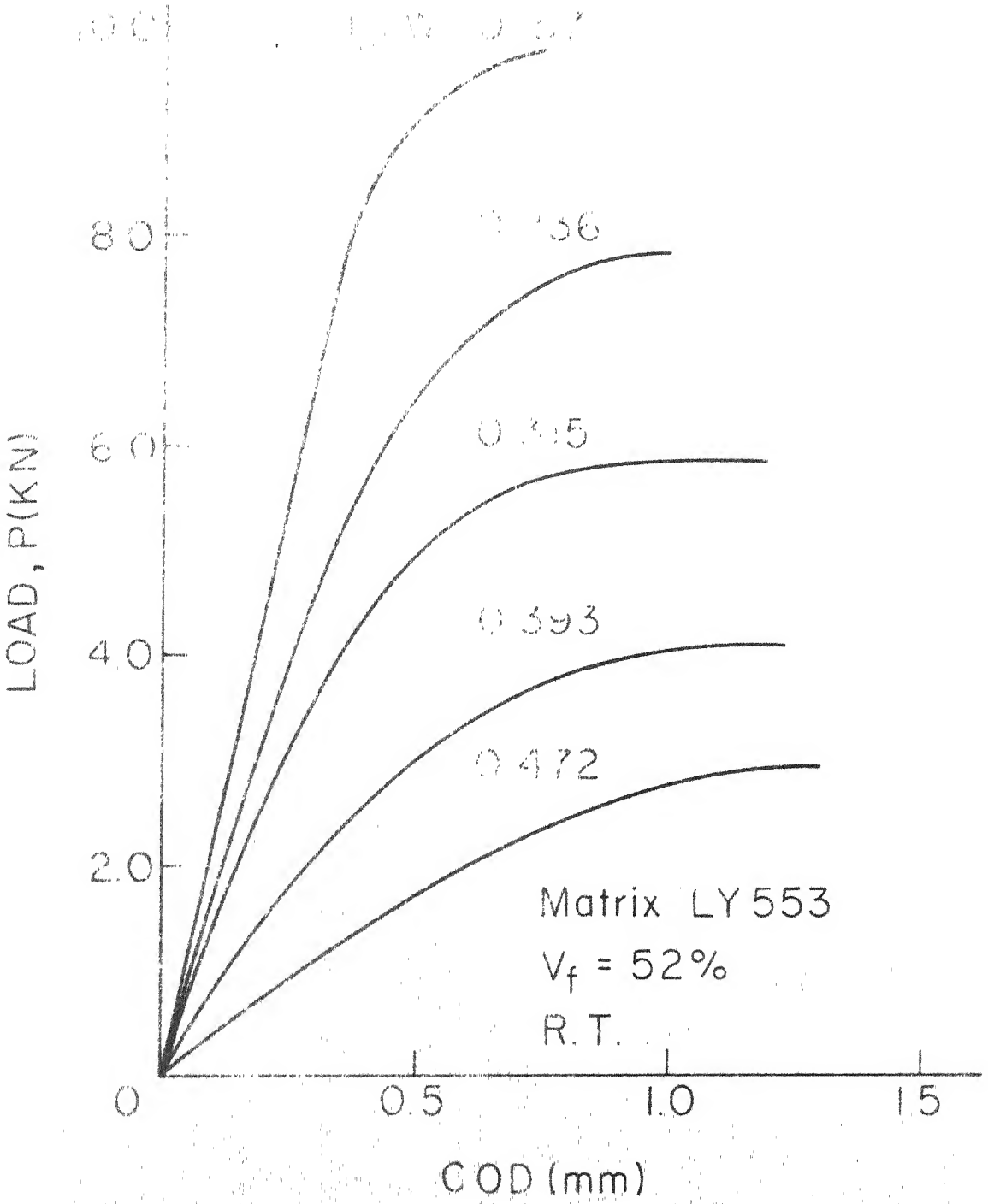

FIG. 29 LOAD VERSUS COD CURVES FOR DIFFERENT INITIAL CRACK LENGTH (V_f = 52 %)

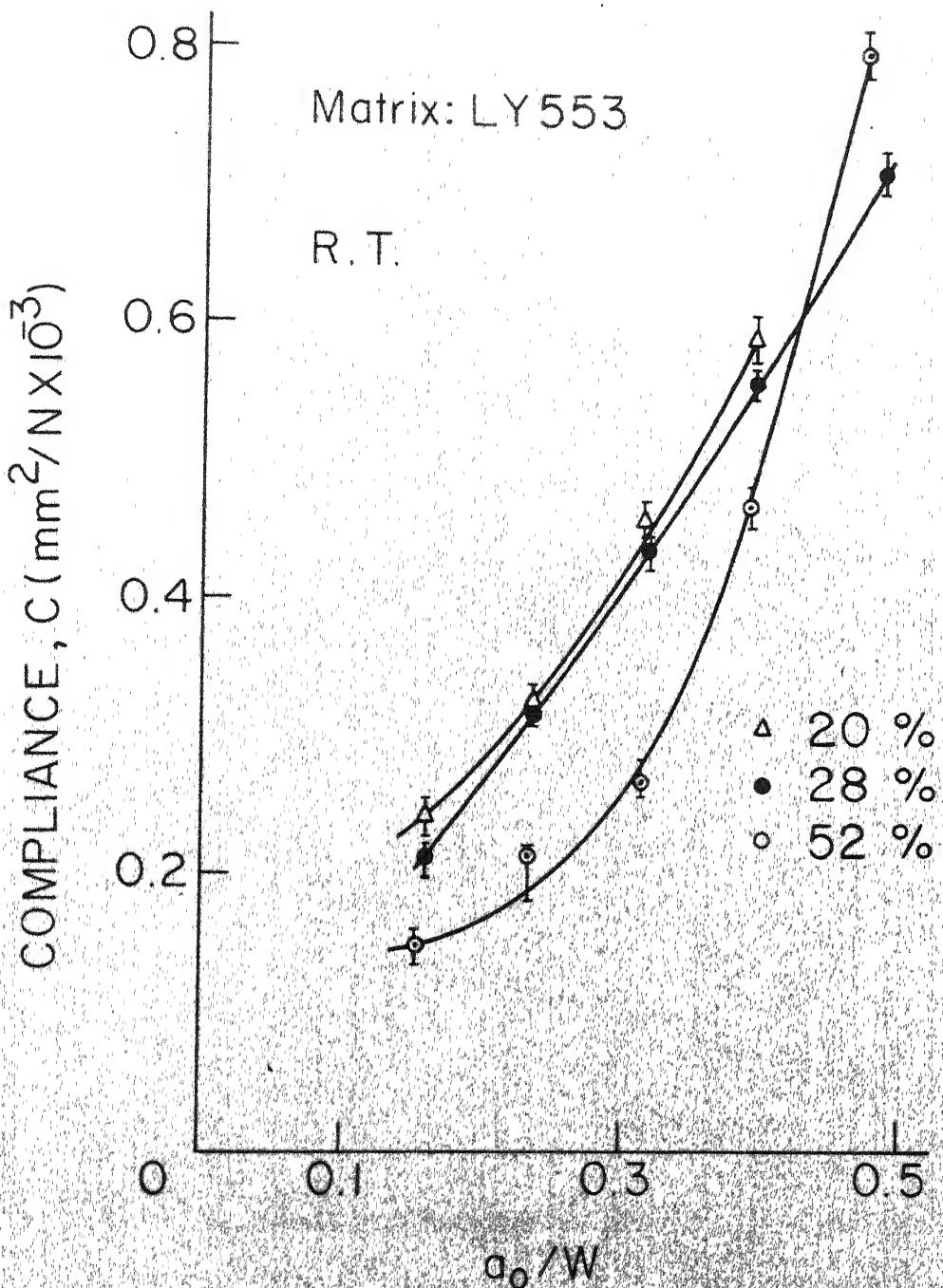

FIG. 30 CRACK LENGTH ESTIMATION CURVES FOR DIFFERENT V_f

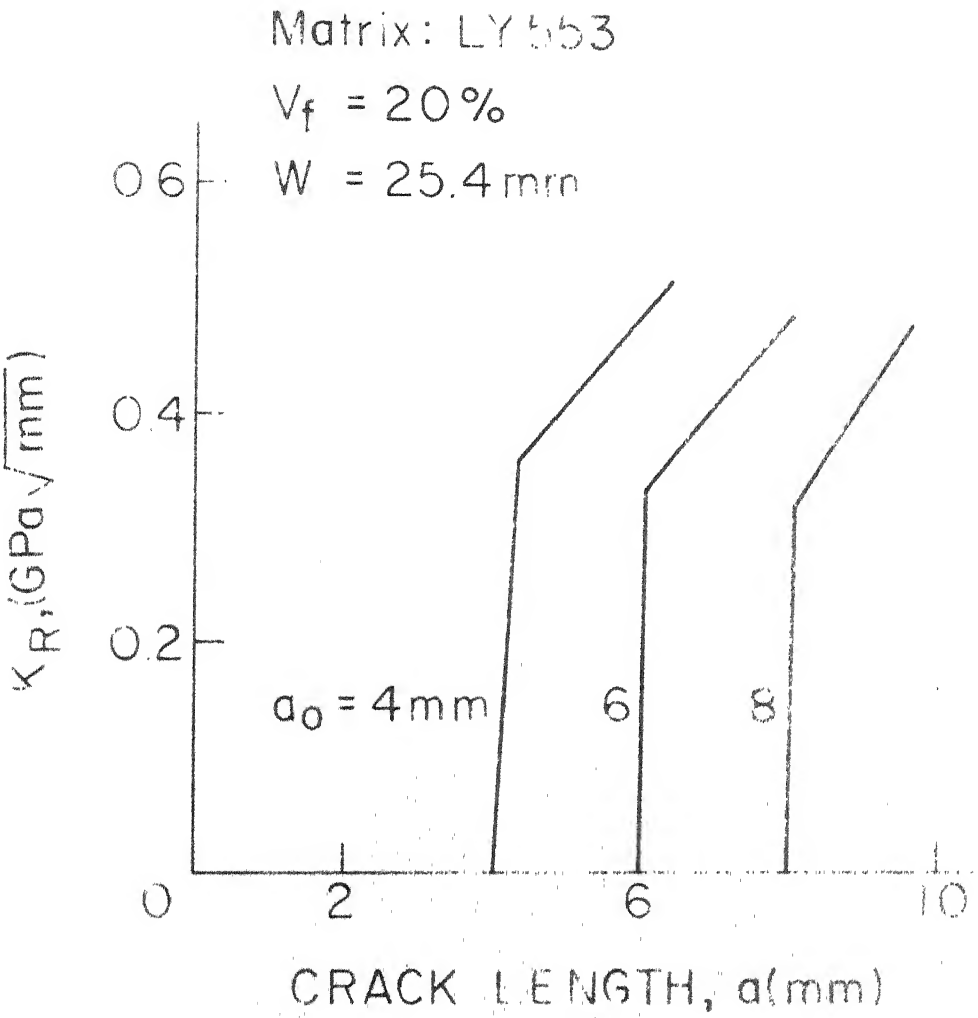

FIG. 31 R-CURVES FOR V_f = 20%

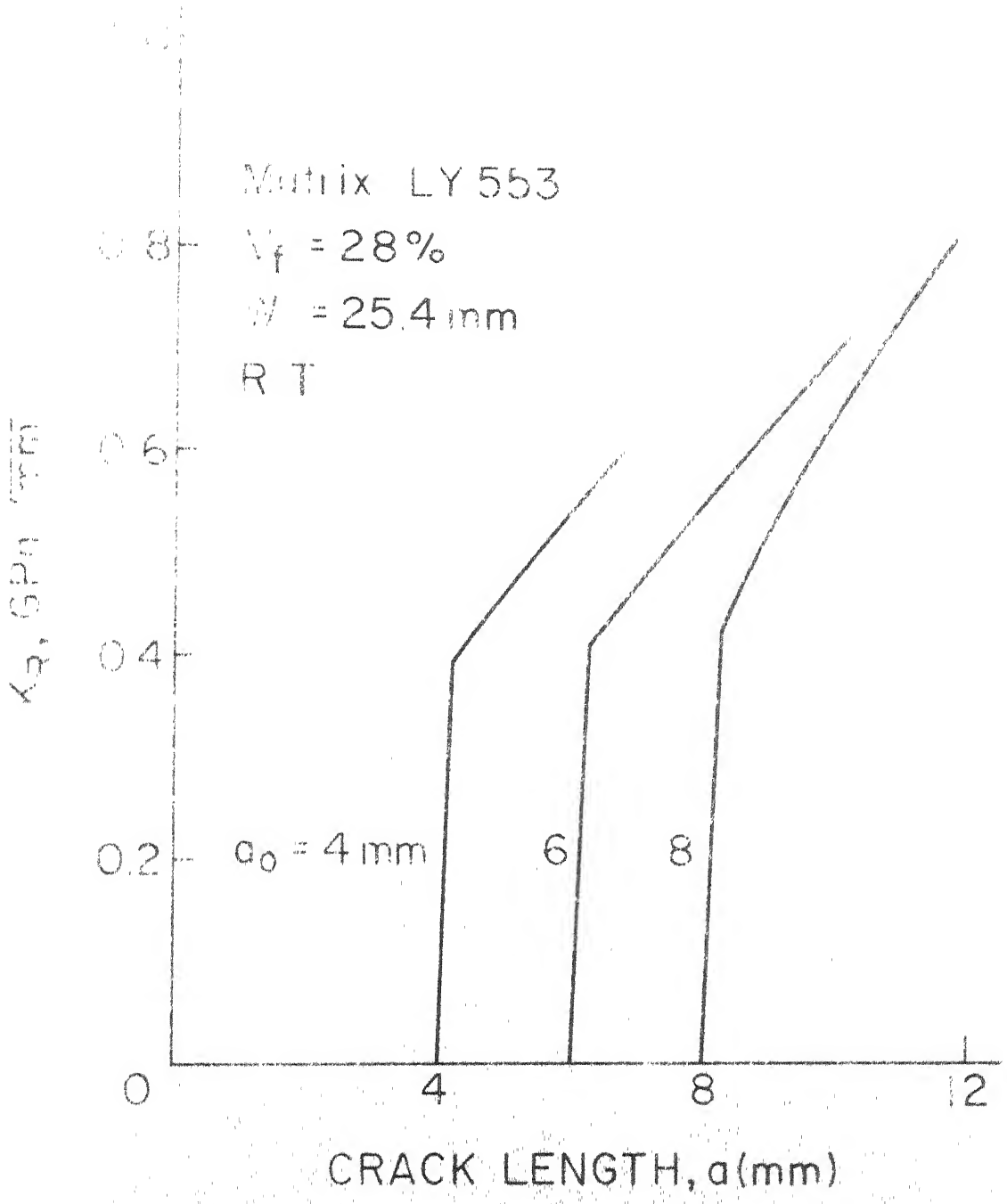

FIG. 32 R-CURVES FOR V_f = 28%

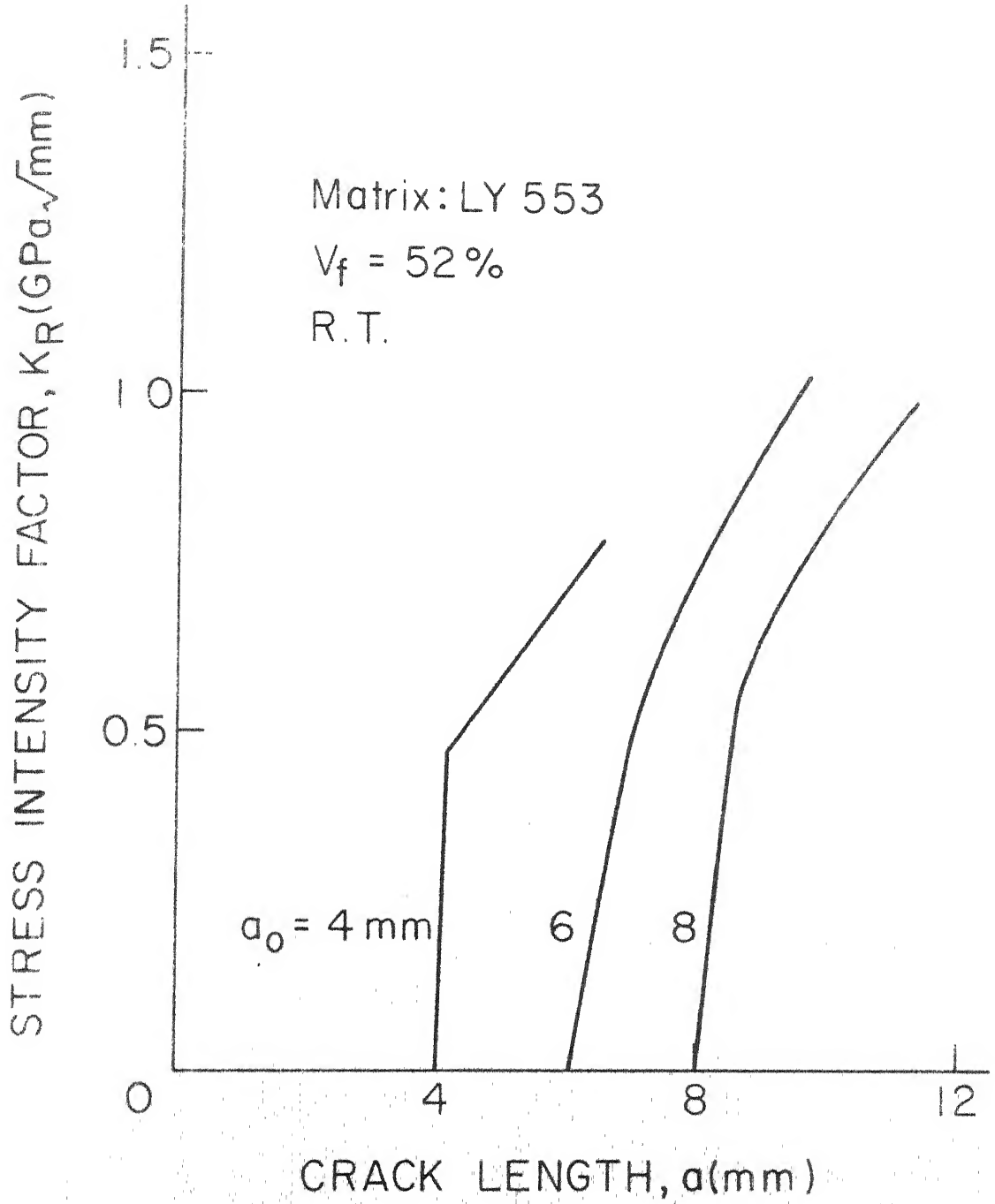

FIG. 33 R - CURVES FOR V_f = 52%

The stress intensity factors at instability, $K_{R(ins)}$, are given in Table 2 and plotted in Fig. 34 against initial crack length for different fibre volume fractions. It is observed that, for each fibre volume fraction, the $K_{R(ins)}$ increases with an increase in initial crack length. This confirms the earlier observation that the $K_{R(ins)}$ does depend upon the initial crack length. For V_f = 20% the increase in $K_{R(ins)}$ is small compared to that at V_f = 28% and 36%. This is because at V_f = 20% there is a limited availability of the fibres for debonding which is primarily responsible for the energy absorbed (fracture toughness) in the composite material . Therefore, initial crack length influences the amount of debonding to a smaller extent. The $K_{R(ins)}$ is plotted against V_f for different initial crack lengths in Fig. 35. The $K_{R(ins)}$ first increases with V_f and then shows a slight drop as V_f changes from 36% to 52%. This drop in fracture toughness is due to the fact that the composite is very stiff at fibre volume fraction of 52% and consequently COD is small. Another reason may be that at V_f = 52% the quality of the composite may not be as good as that at lower fibre volume fraction.

The variation of candidate stress intensity factor K_Q with fibre volume fraction is shown in Fig. 36 for different crack lengths. The dandidate stress intensity factor increases with fibre volume fraction as should be expected.

TABLE 2 : Stress Intensity Factors at Instability, $K_{R(ins)}$
(Mode I, Matrix: LY 553, Room Temperature)

Initial Crack Length a_o, (mm)	$K_{R(ins)}$, (GPa $\sqrt{mm}$)			
	V_f (Percent)			
	20	28	36	52
3	-	-	0.716	-
4	0.441	0.539	0.765	0.755
5	-	-	0.804	-
6	0.451	0.637	0.853	0.922
7	-	-	0.892	-
8	0.480	0.686	0.931	0.892

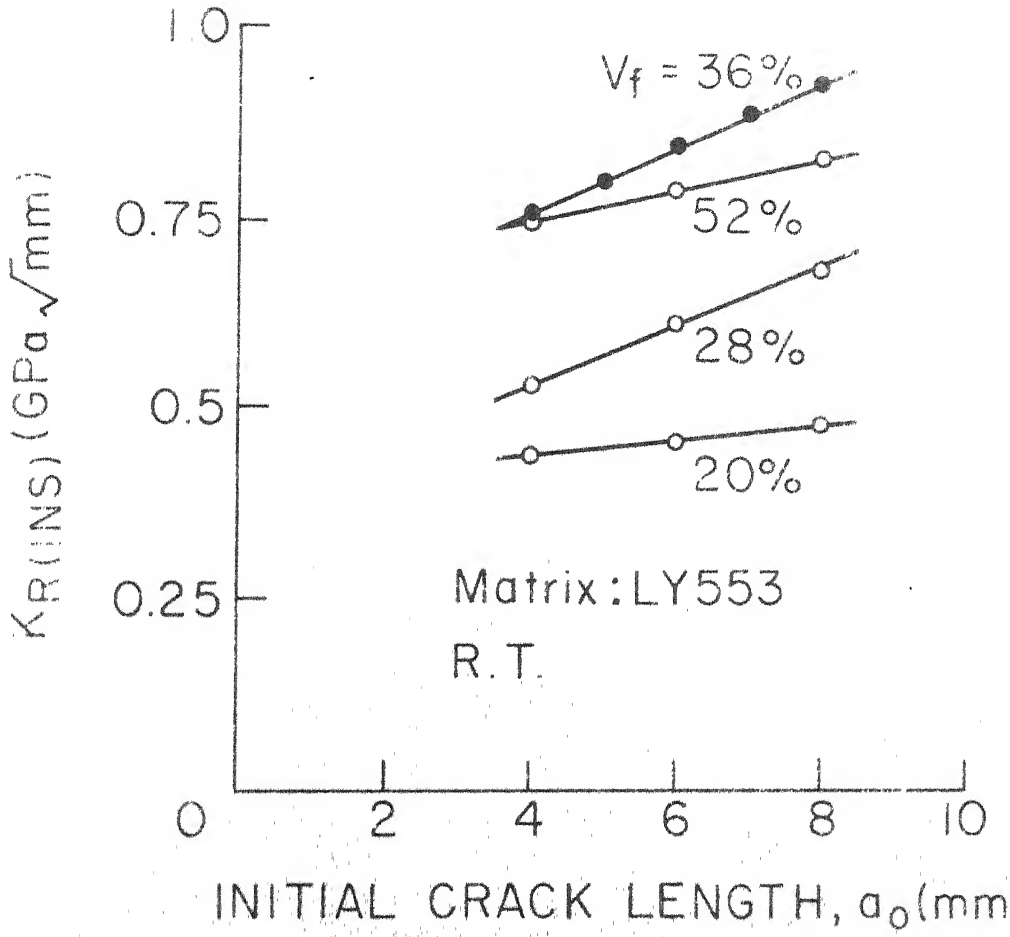

FIG. 34 VARIATION OF $K_{R(INS)}$ WITH INITIAL CRACK LENGTH

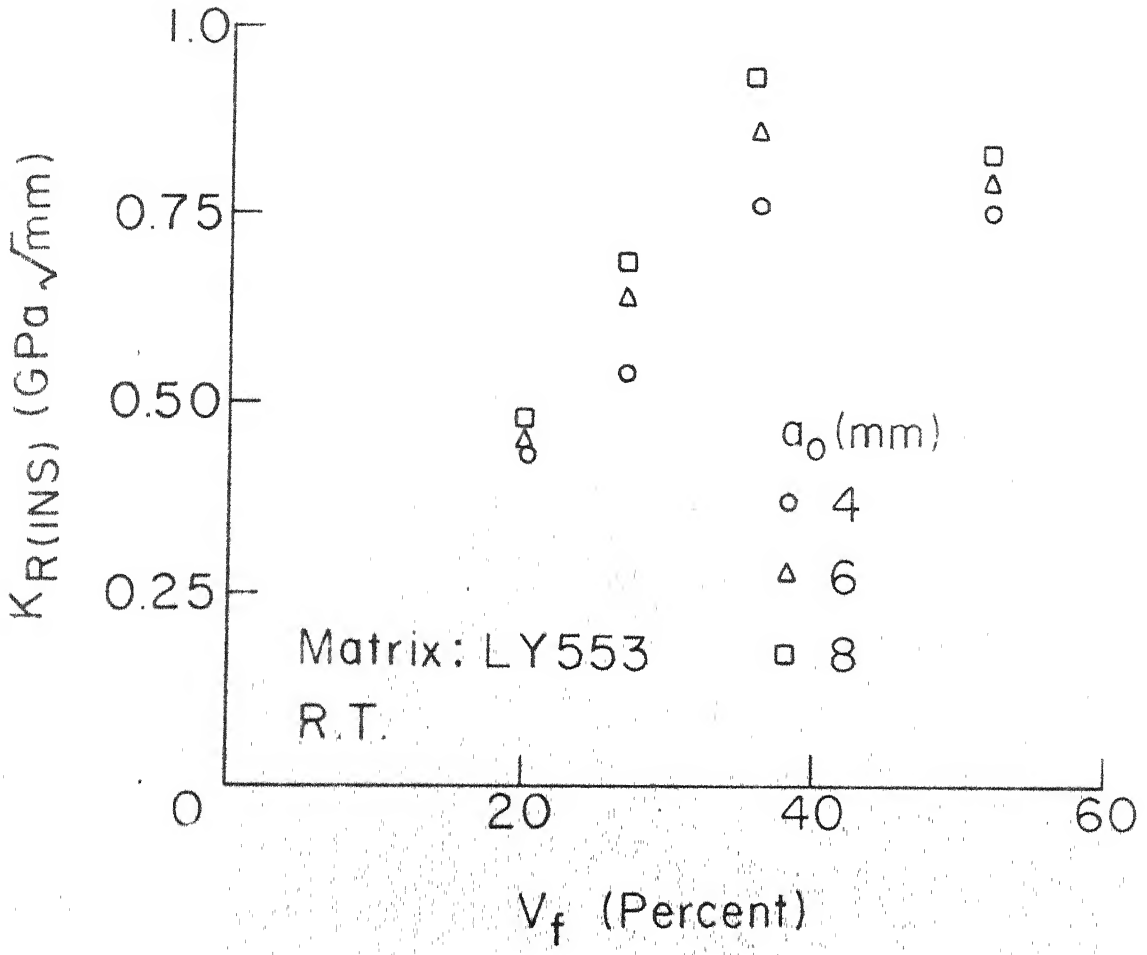

FIG. 35 VARIATION OF $K_{R(INS)}$ WITH VOLUME FRACTION OF FIBRES

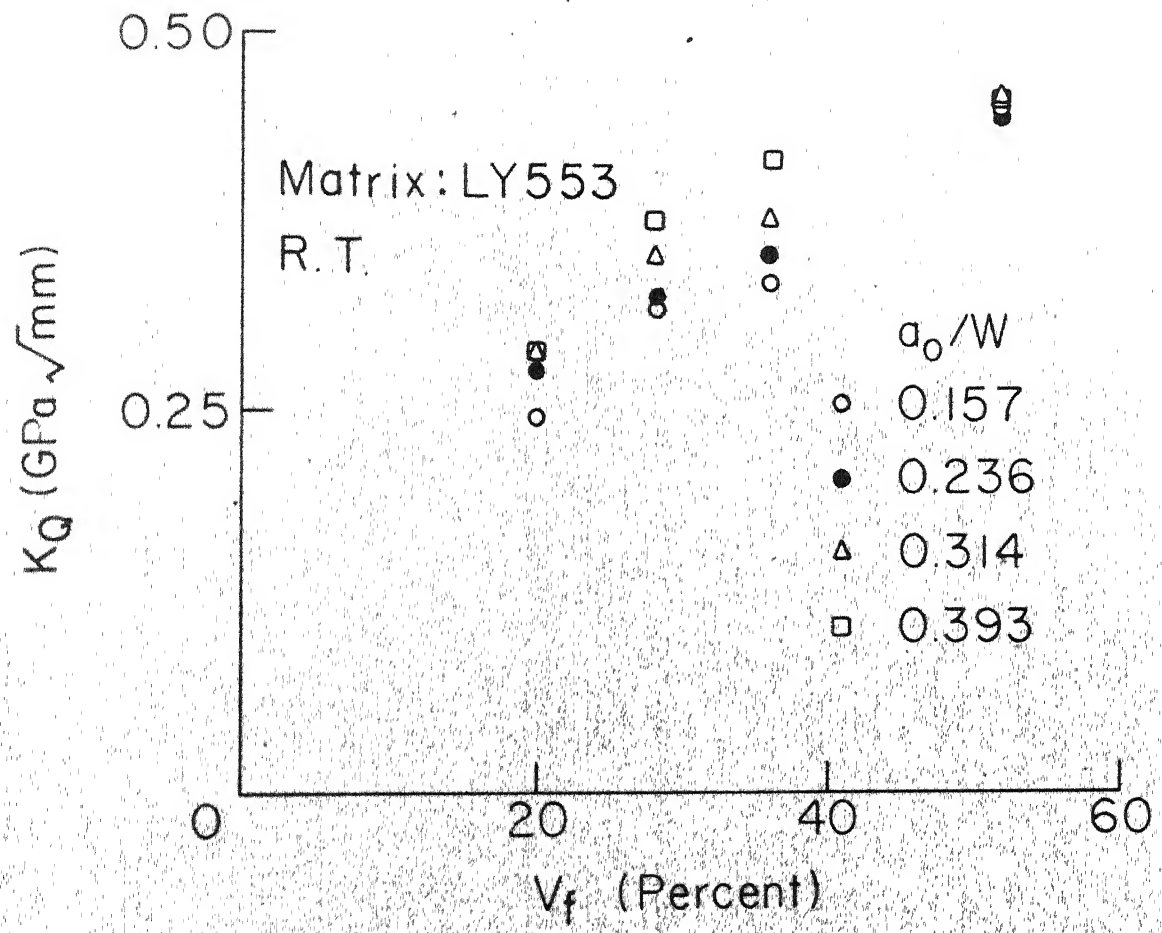

FIG. 36 VARIATION OF K_Q WITH VOLUME FRACTION OF FIBRES

Whitney and Nuismer [9] have proposed two criteria to predict notched strength of the composite laminate. For sharp cracks both the criteria are independent of material properties. The point stress criterion predicts the notched strength as

$$\frac{\sigma_N}{\sigma_o} = \sqrt{1 - p_1^2} \qquad (3)$$

where σ_N = notched strength

σ_o = unnotched strength

$p_1 = \frac{a_o}{a_o + d_o}$, a_o being the initial crack length and d_o the characteristic distance.

The average stress criterion predicts the notched strength as

$$\frac{\sigma_N}{\sigma_o} = \sqrt{\frac{1 - p_2}{1 + p_2}} \qquad (4)$$

where $p_2 = \frac{a_o}{a_o + c_o}$, c_o being another characteristic distance.

In their original paper Whitney and Nuismer [9] proposed the characteristic lengths $d_o = 0.04$ inch and $c_o = 0.15$ inch. The present results have also been compared with the Whitney - Nuismer criteria in Fig. 37. The characteristic distanceshave been rounded off to $d_o = 1$ mm and $c_o = 4$ mm. The results for different fibre volume fractions have been plotted on the same graph. The results show a reasonable agreement with both of the Whitney Nuismer criteria.

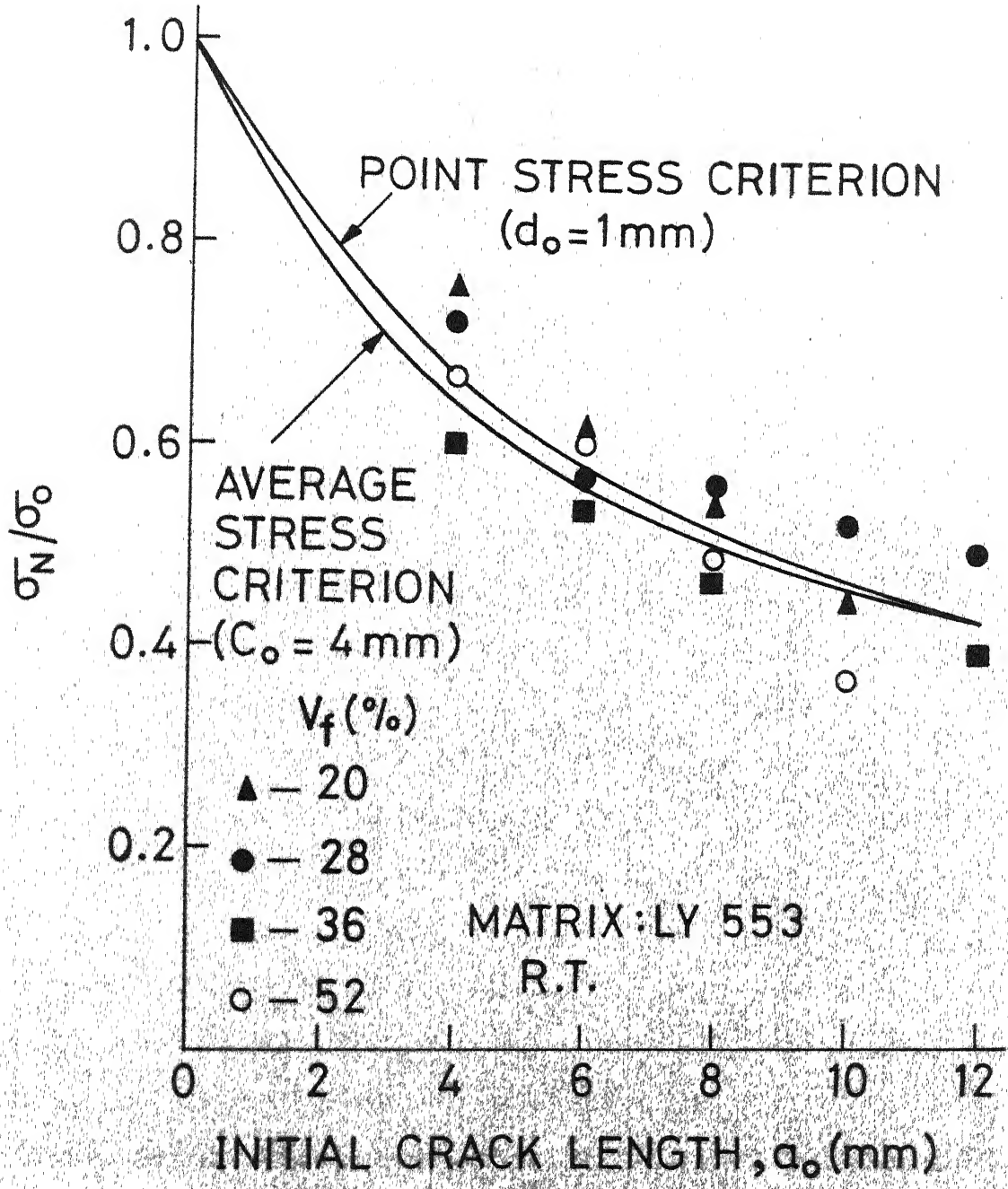

FIG. 37 VARIATION OF NORMALISED NOTCHED
STRENGTH WITH INITIAL CRACK LENG

3.4 EFFECT OF SPECIMEN THICKNESS

The load versus COD curves for specimens with different thickness are shown in Fig. 38. The volume fraction for all specimens is 36% and the initial crack length is 6 mm ($\frac{a_o}{W}$ = 0.236). Initial slope of the load versus COD curve increases as the specimen thickness increases. However, if the load per unit thickness (load divided by thickness) is plotted against COD, the initial portion of all the load versus COD curves will generally overlap. The COD at fracture shown in Fig. 39 increases as the specimen thickness increases, which indicates that the energy absorbed (fracture toughness) of the short fibre composites increases as the thickness increases. In metals, the effect of thickness on fracture toughness is just the opposite, because an increase in thickness causes the failure to change from plane stress mode to plane strain mode and consequently resulting in the lower fracture toughness. In the short fibre composites, the primary mechanisms of energy absorption are fibre debonding and pull out. As the thickness increases, in addition to the two primary mechanisms of energy absorbed, the interaction between fibres (particularly the different layers of fibre mat) also increases, thereby increasing the fracture toughness. However, the influence of this interaction is not very pronounced. The variation of the candidate stress intensity factor, K_Q, with specimen thickness is shown in Fig. 40. The K_Q also shows a slight increase with increasing specimen thickness.

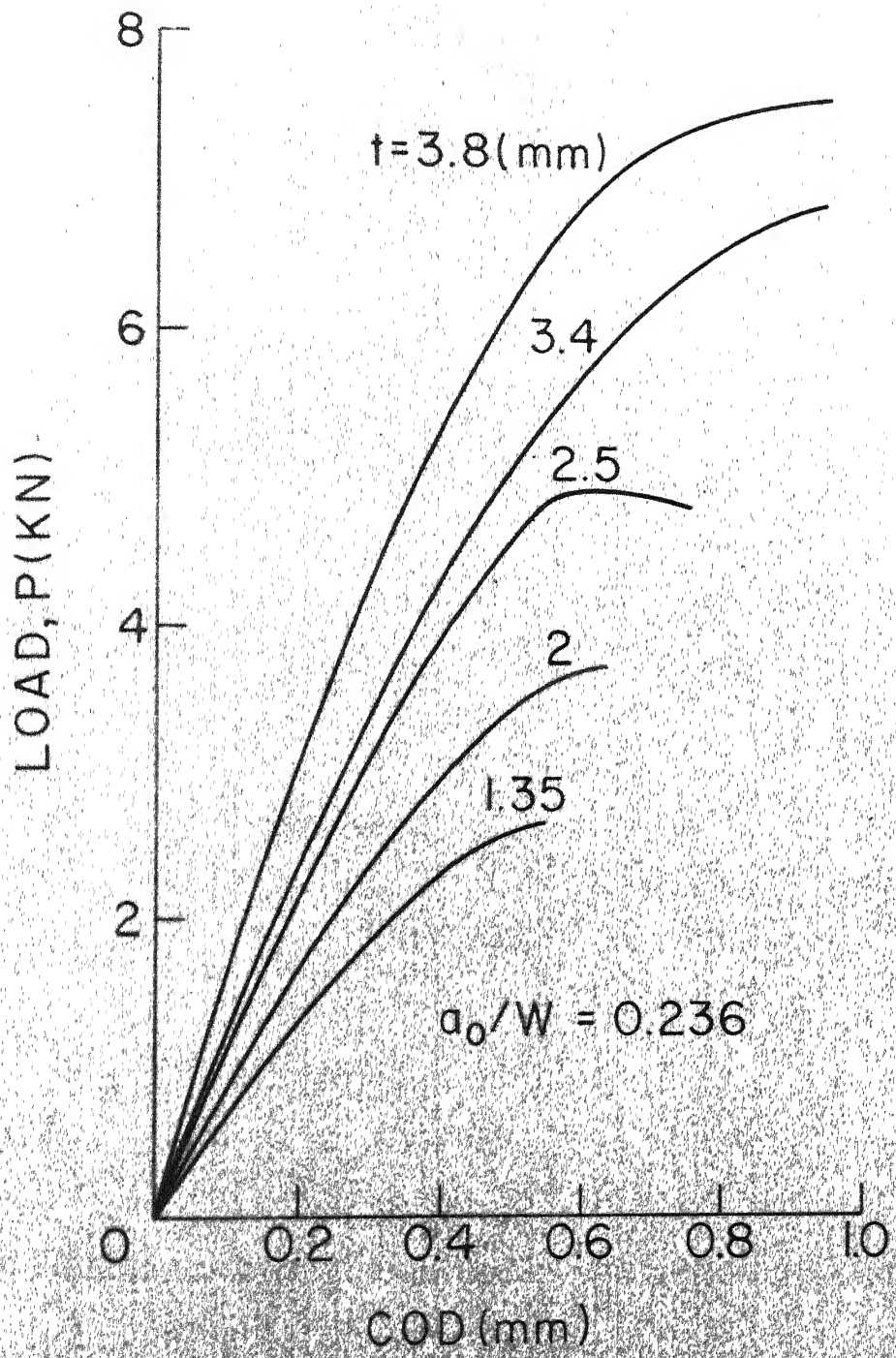

FIG. 38 LOAD VERSUS COD CURVES FOR DIFFERENT SPECIMEN THICKNESS

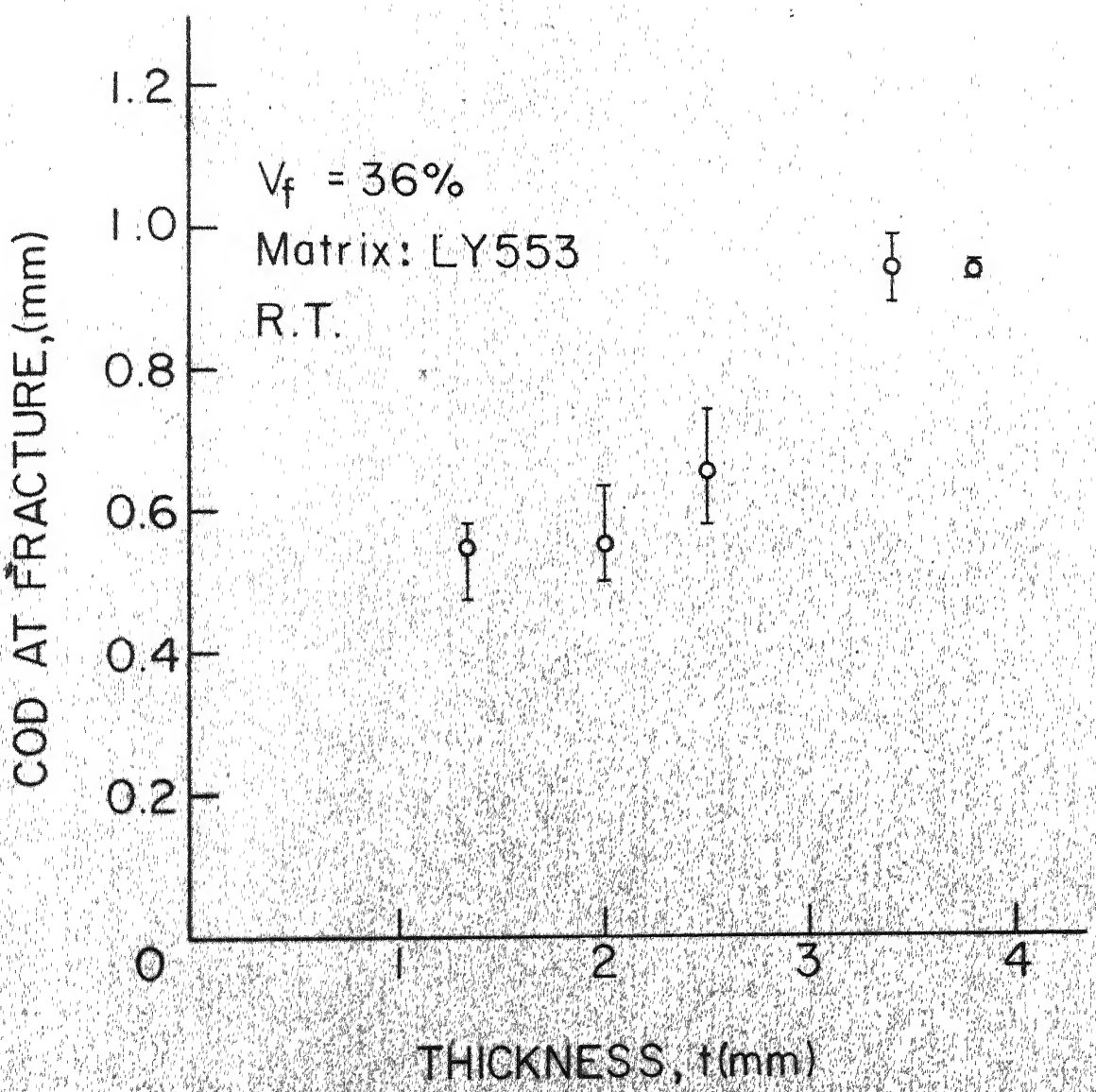

FIG. 39 VARIATION OF COD AT FRACTURE WITH SPECIMEN THICKNESS

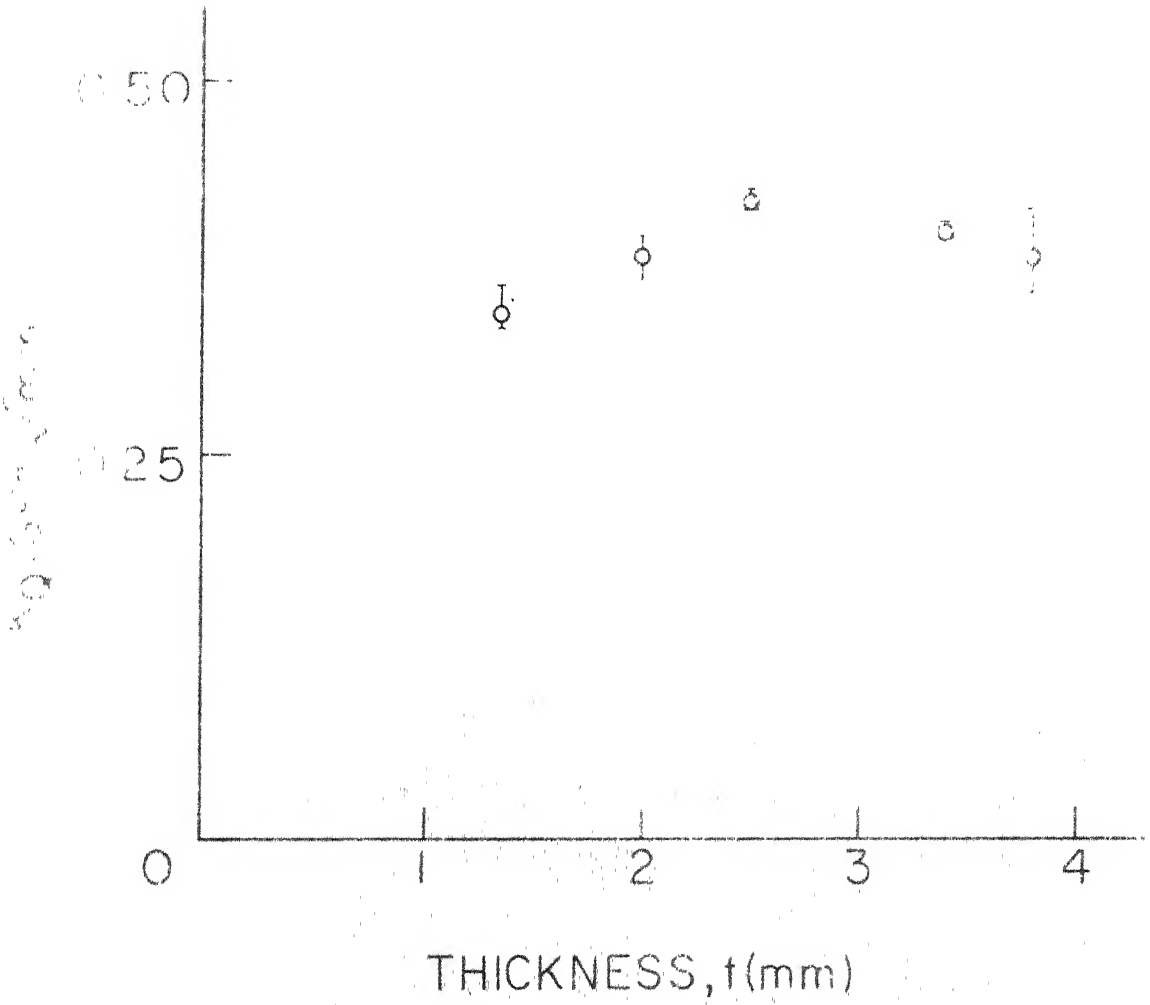

FIG.40 VARIATION OF K_Q WITH SPECIMEN THICKNESS

3.5 EFFECT OF SPECIMEN WIDTH

The effect of specimen width on fracture properties has been studied by conducting tests on specimens with four different widths (19, 25.4, 30 and 38 mm). In each case, the ratio of initial crack length to specimen width was kept at 0.315 and V_f at 36%. The specimen length was also increased so that the length between the grips is at least three times the specimen width. The variation of notched strength with width is shown in Fig. 41. The notched strength decreases as the specimen width increases. The decrease in notched strength occurs because the ratio $\frac{a_o}{W}$ being constant the initial crack length is increasing with increase in width.

The experimental notched strength is in agreement with the prediction of Whitney - Nuismer point stress criterion (Eq. 3). The load versus COD curves for different width are similar to the ones shown in Fig. 17 and are not being presented. The candidate stress intensity factor is plotted against width in Fig. 42. The K_Q also decreases as the specimen width increases.

3.6 EFFECT OF TEST TEMPERATURE

The load versus crack mouth opening displacement (COD) curves are shown in Figs. 43 - 45 for different temperatures and crack lengths. The corresponding curves for room temperature tests have been presented and discussed in the preceding sections. Although the general nature of the

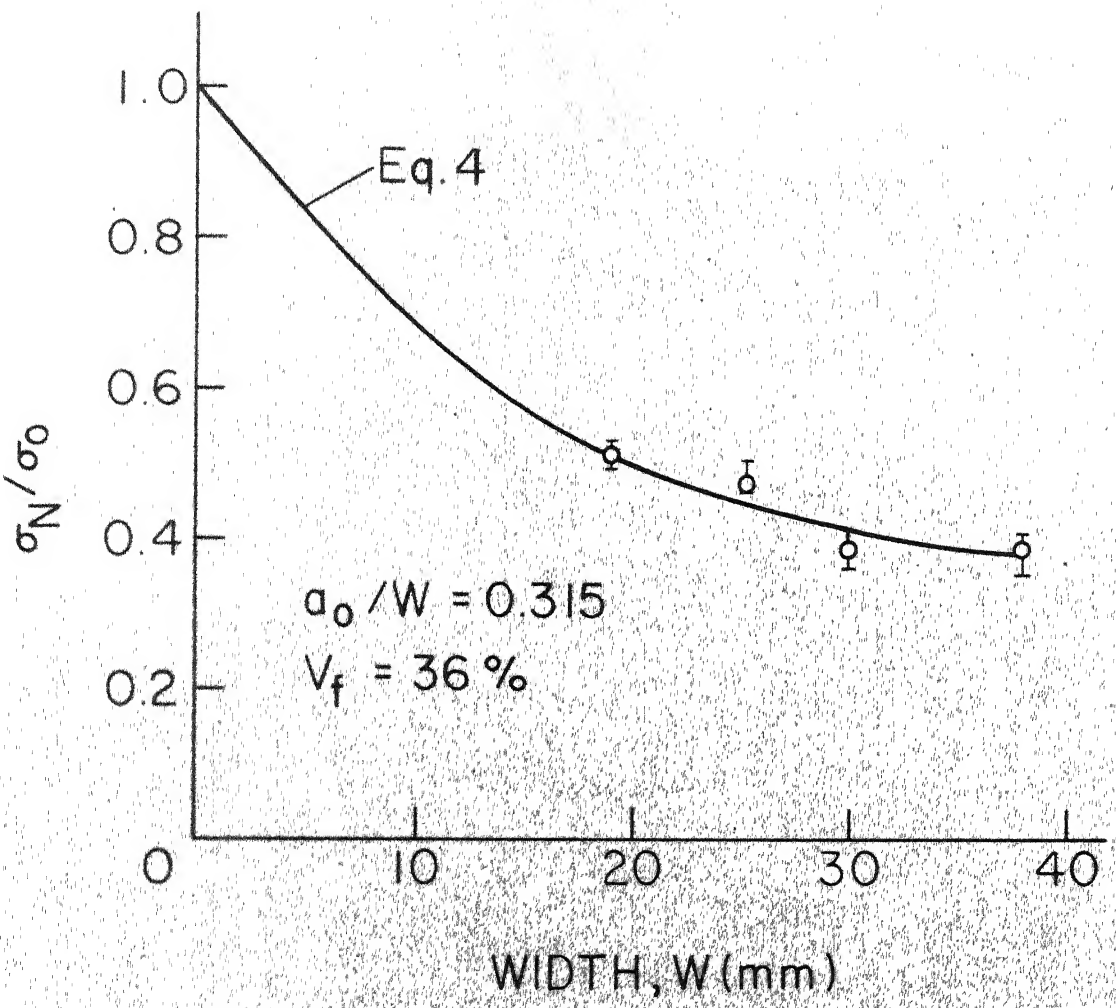

FIG. 41 VARIATION OF NORMALISED NOTCHED STRENGTH WITH SPECIMEN WIDTH, W ($a_0/W = 0.315$)

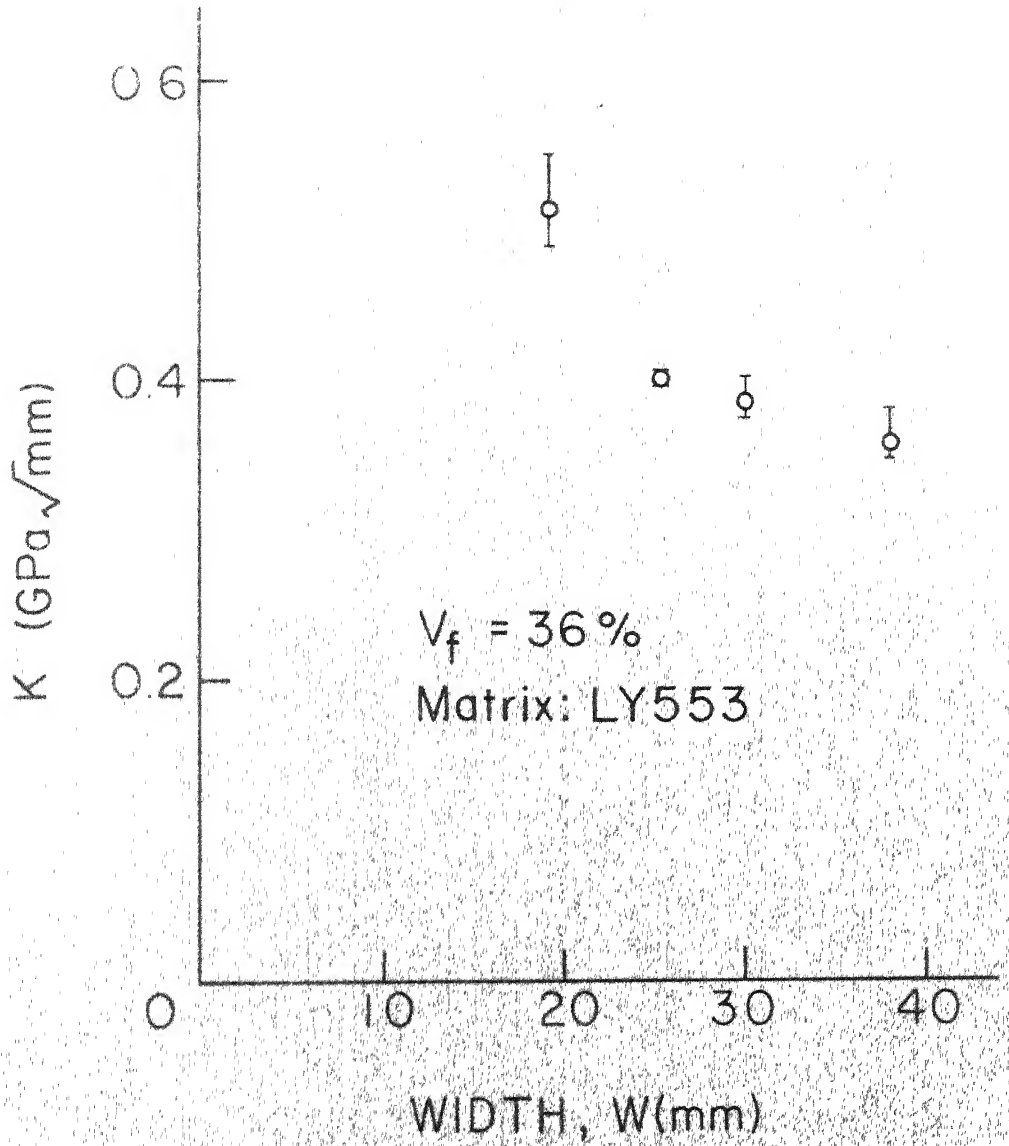

FIG. 42 VARIATION OF K_Q WITH SPECIMEN WIDTH

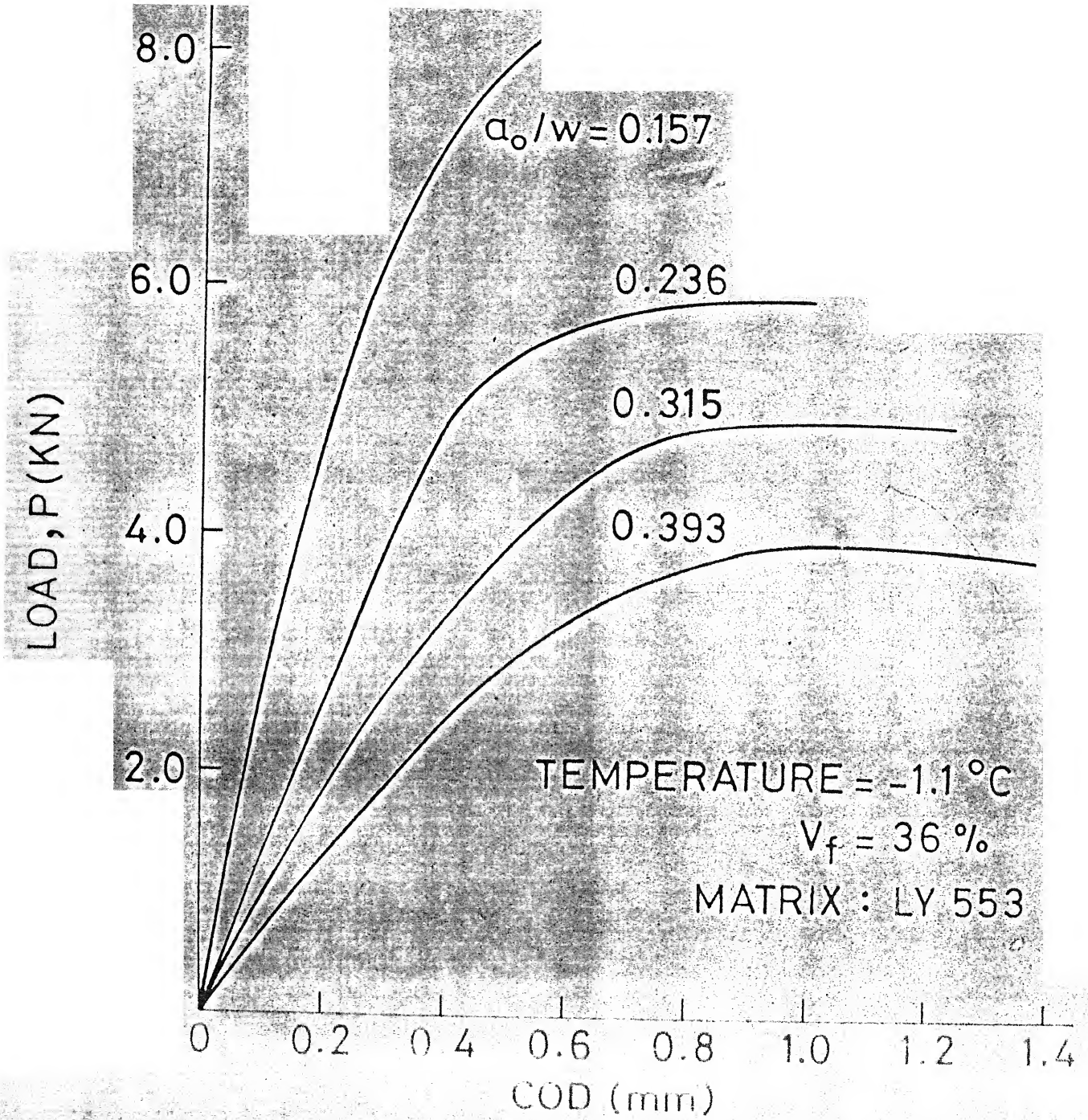

FIG -13 LOAD VERSUS COD CURVES FOR DIFFERENT INITIAL CRACK LENGTH (TEST TEMPERATURE -1.1 °C)

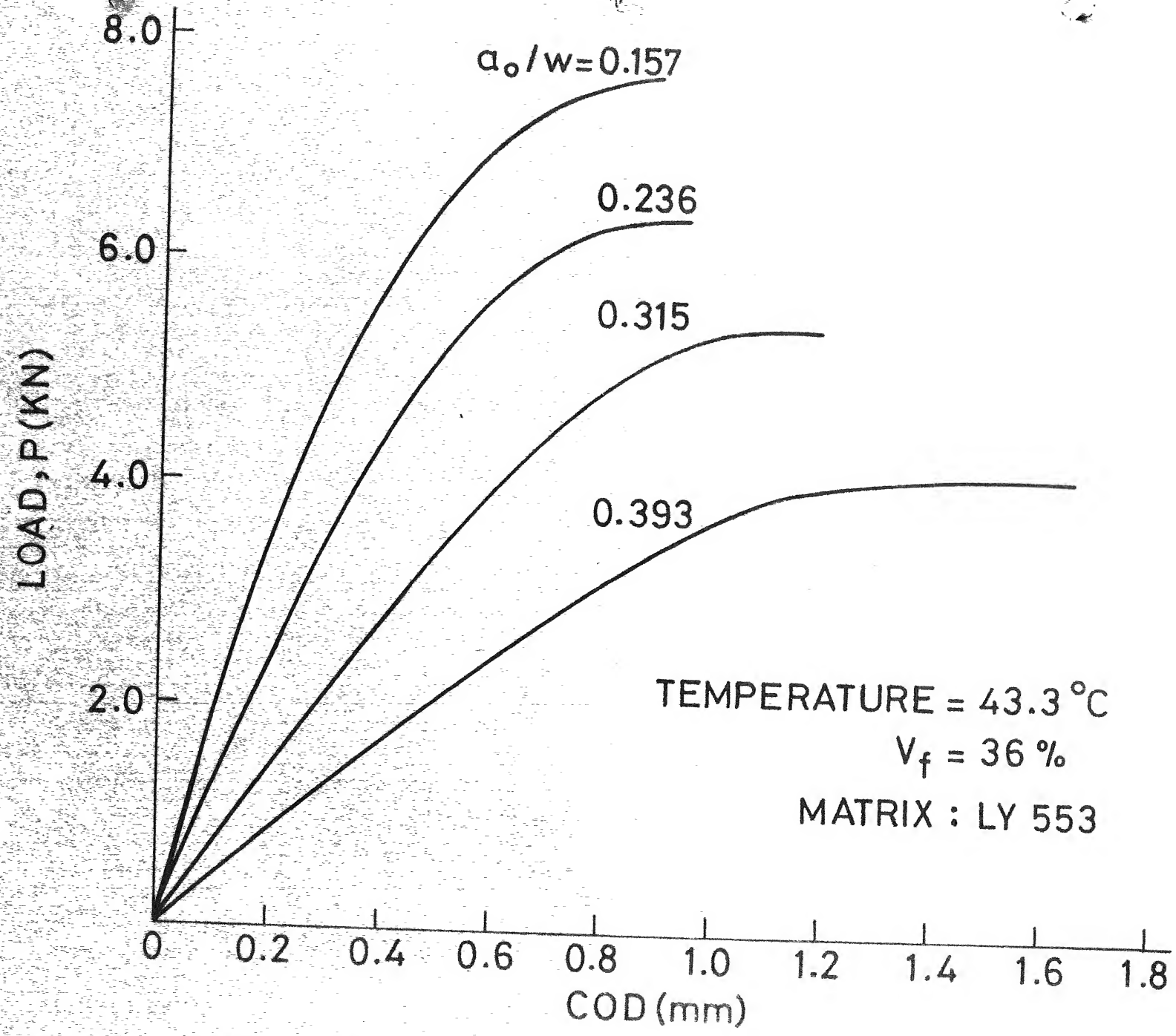

FIG 44 LOAD VERSUS COD CURVES FOR DIFFERENT INITIAL CRACK LENGTH (TEST TEMPERATURE = 43.3°C)

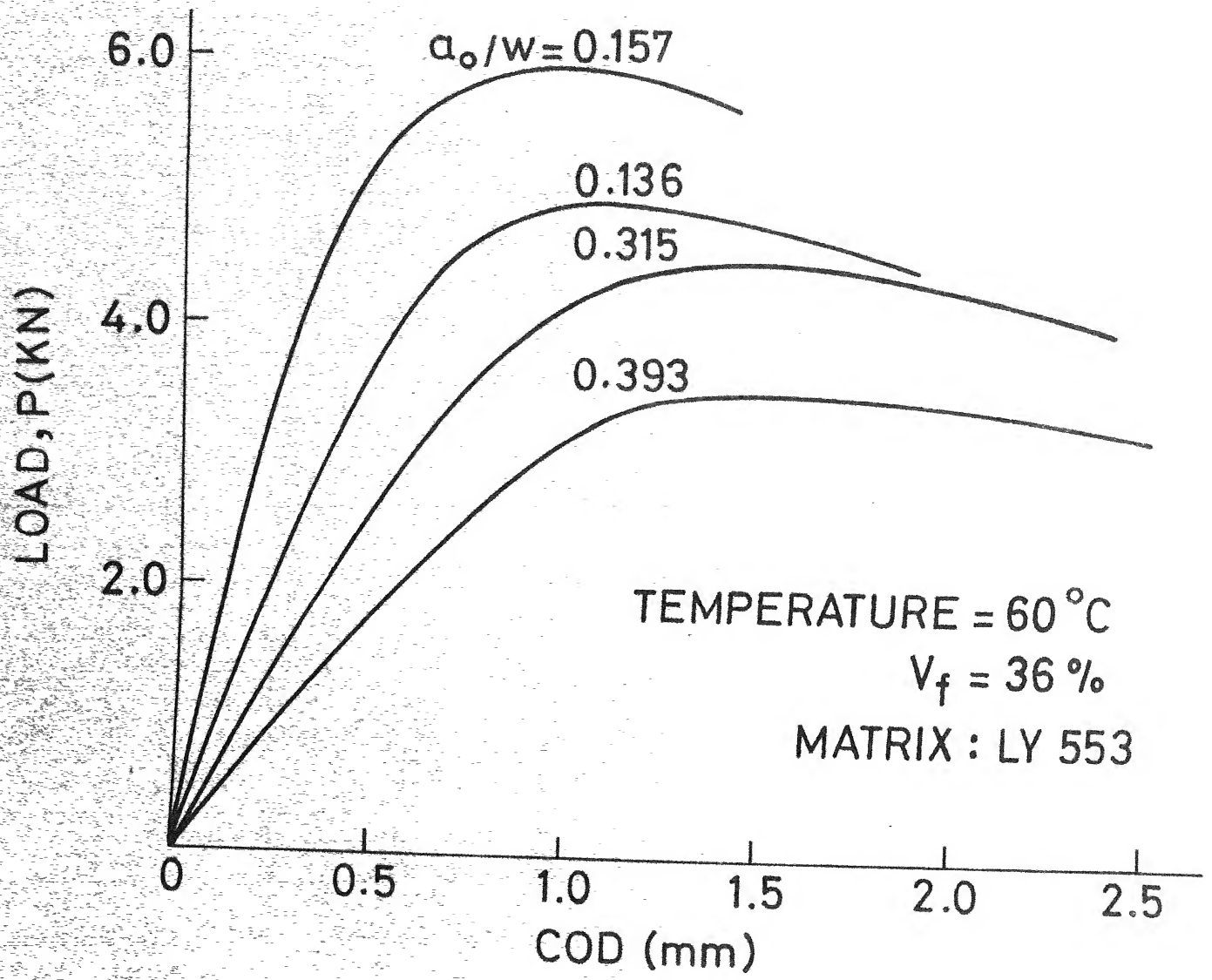

FIG. 45 LOAD VERSUS COD CURVES FOR DIFFERENT INITIAL CRACK LENGTH (TEST TEMPERATURE = 60 °C)

curves is same at different temperatures, their initial slope, the load at fracture (notched strength) and COD at fracture are different for a constant initial crack length. The crack length estimation curves which are obtained from the compliance based on the COD, are shown in Fig. 46 for different temperatures. The crack length estimation curves become higher as the temperature increases because the material becomes softer. These curves have been later used to obtain the effective crack length required to plot the resistance curve (R - curves). The compliance (based on COD) is plotted against temperature in Fig. 47 for different initial crack lengths. The compliance increases as the temperature increases. It is observed that, for a small initial crack length, the increase in compliance in the entire range of temperature is small. As the initial crack length increases the increase in compliance becomes significantly greater as shown in Fig. 48. For a constant temperature the initial compliance (with no damage ahead of the crack tip) should be expected to increase with increase in crack length for geometrical reasons. As the crack length increases, the crack mouth opening displacement and hence the compliance increases non-linearly. As the temperature increases the plastic matrix becomes soft and the effect of initial crack length becomes pronounced.

The COD at fracture has been plotted against temperature for different crack lengths in Fig. 49. The COD at fracture increase as the test temperature increases

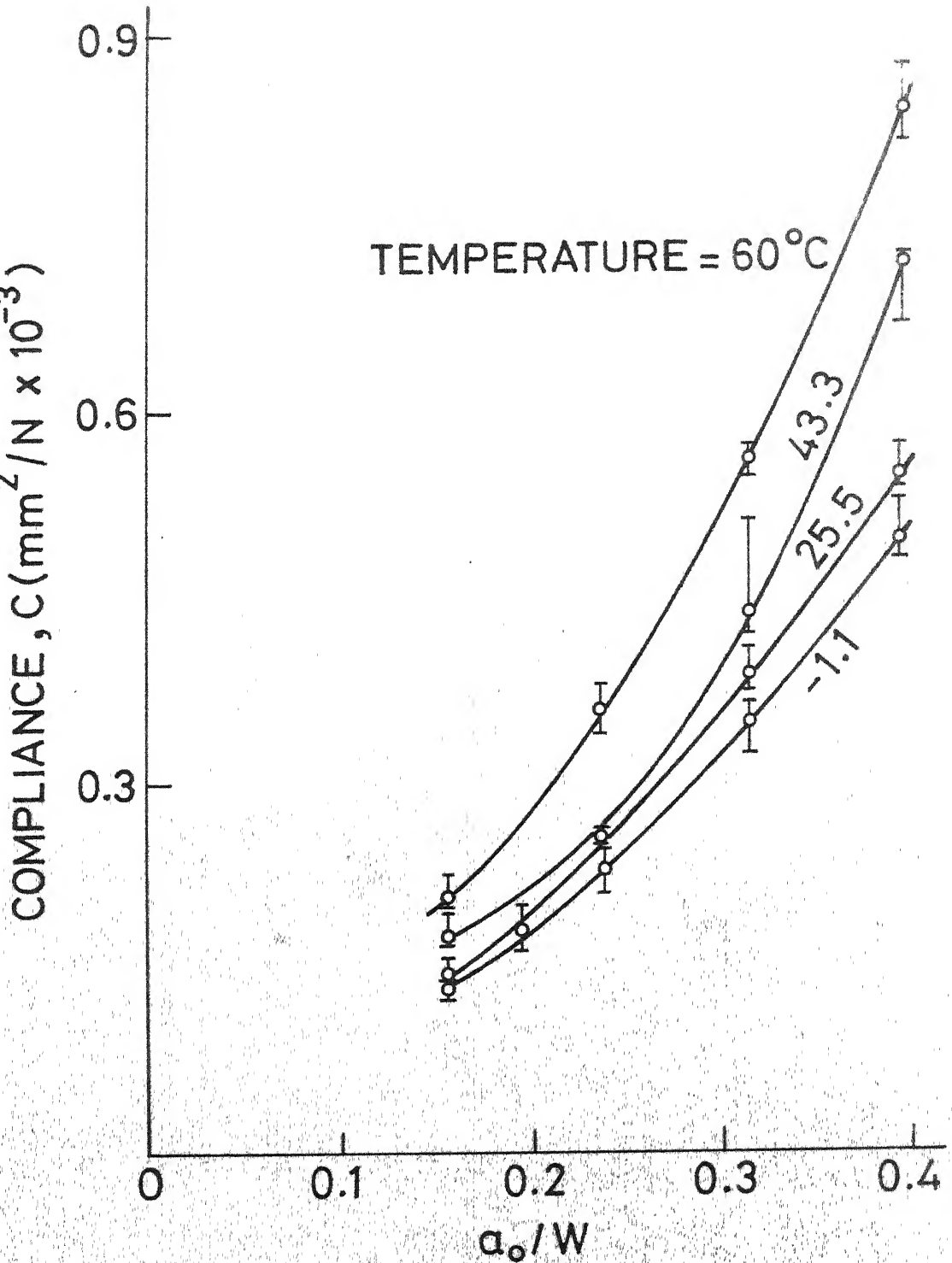

FIG. 46 CRACK LENGTH ESTIMATION CURVES

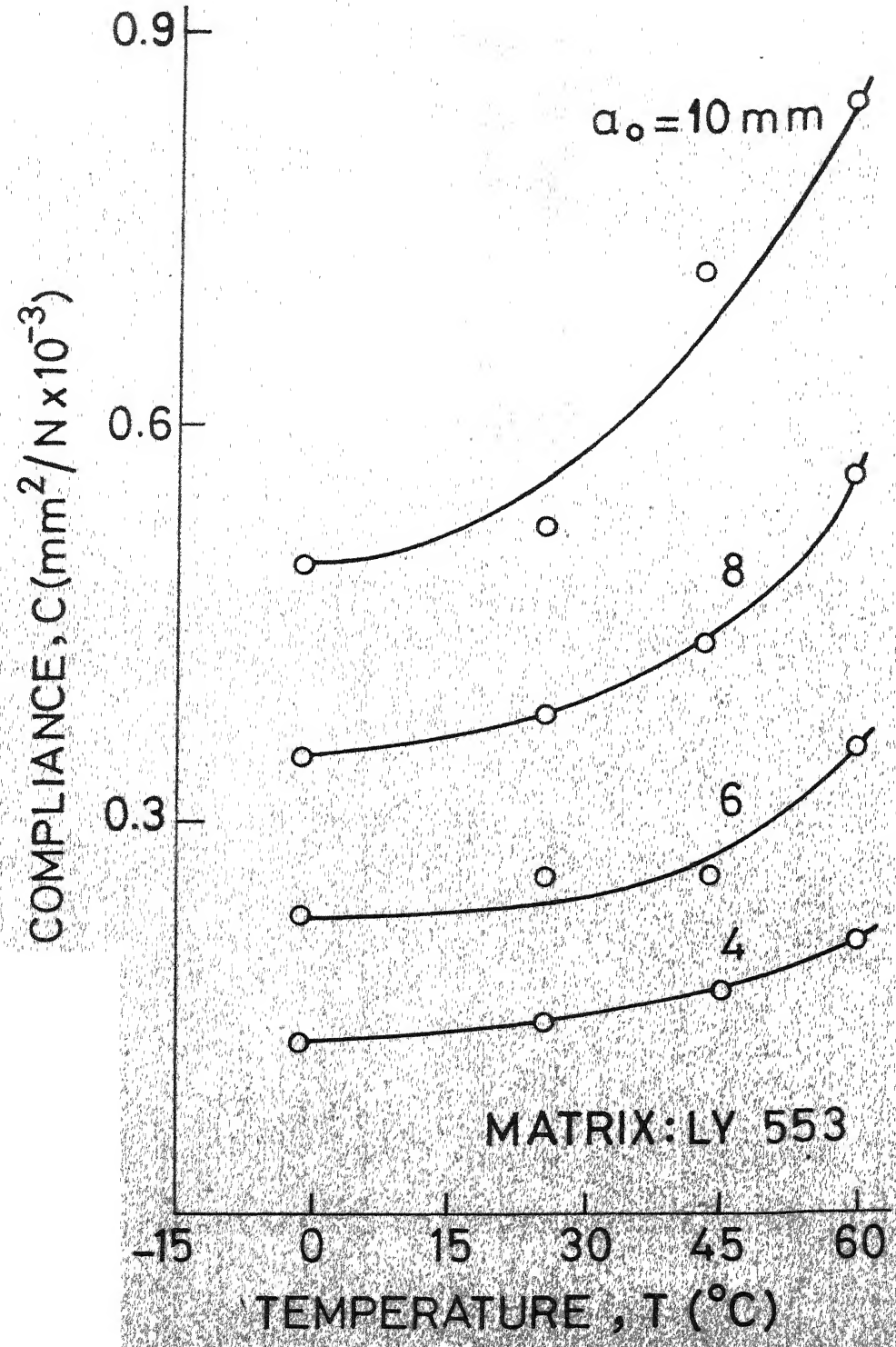

VARIATION OF COMPLIANCE WITH TEMPERATURE

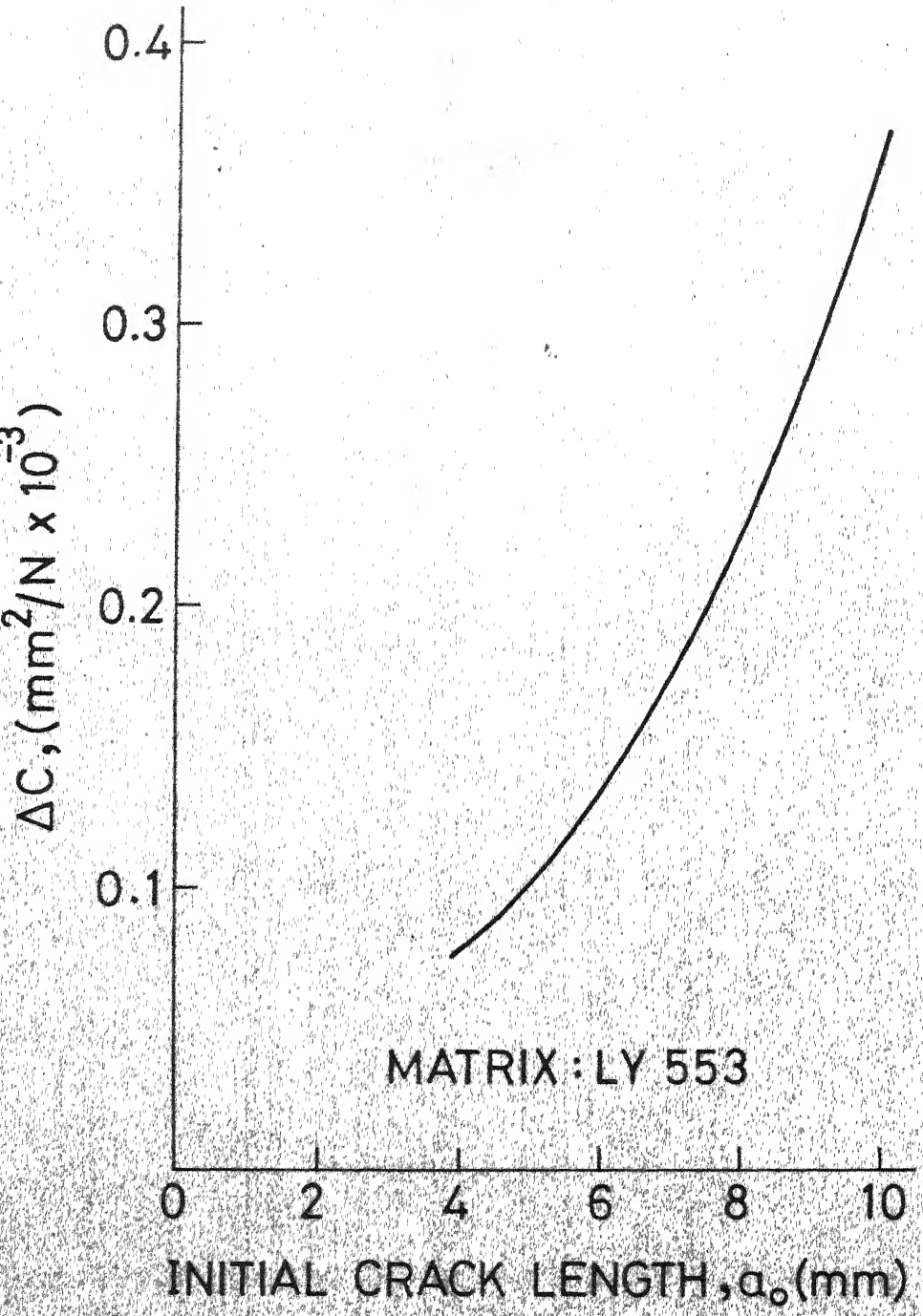

FIG. 48 VARIATION OF COMPLIANCE CHANGE WITH INITIAL CRACK LENGTH

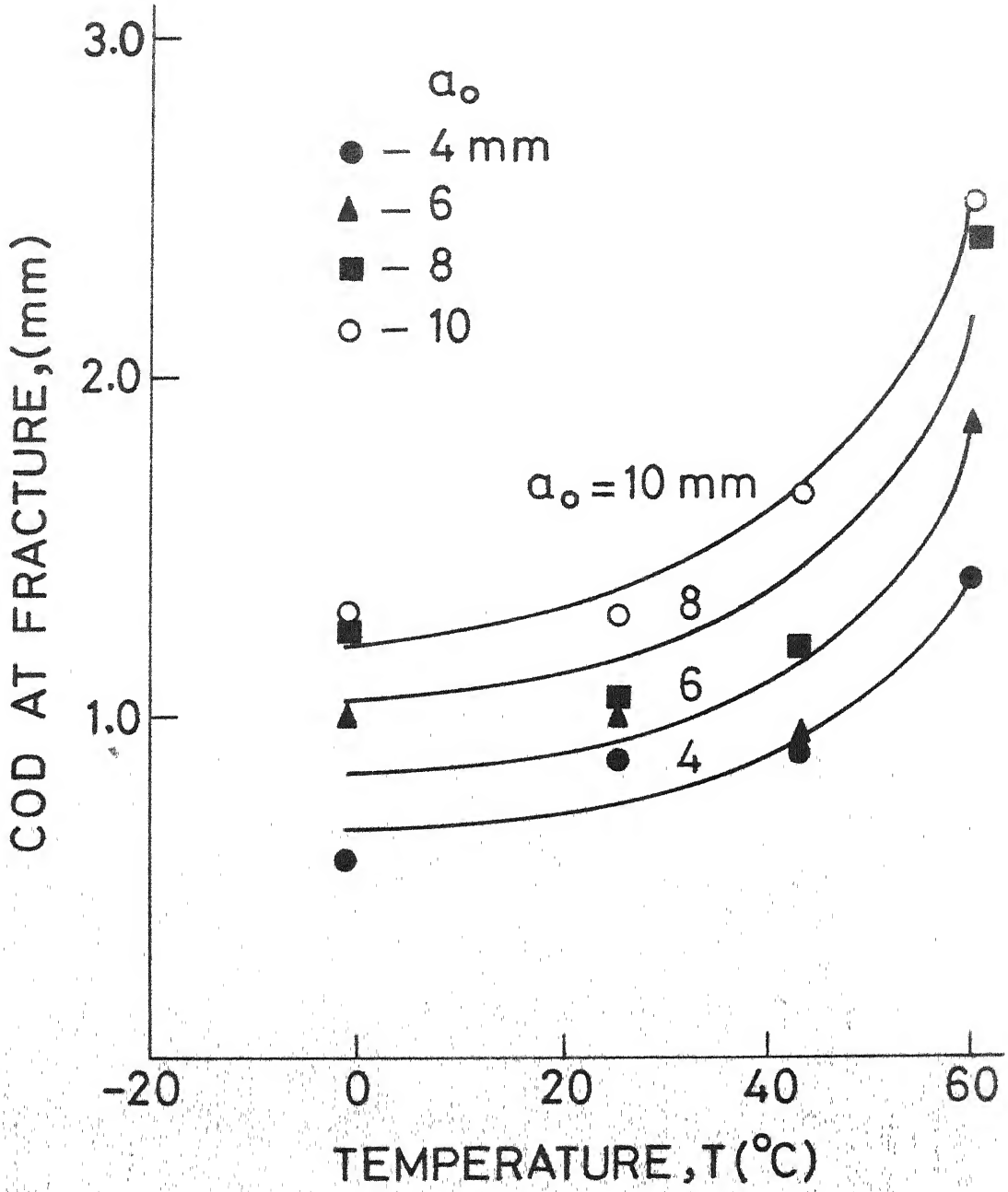

FIG. 49 VARIATION OF COD AT FRACTURE WITH TEMPERATURE

as would be expected. Like compliance, the COD at fracture also shows a greater change with initial crack length at higher temperature (60 °C) than at lower temperature. Also the increase in COD at fracture for an initial crack length of 10 mm is larger than that for a 4 mm crack.

The crack growth resistance curves (R - curves) at different temperatures are shown in Figs. 50 - 52. The room temperature R - curves have been presented earlier. The stress intensity factors at instability, ($K_{R(ins)}$), are given in Table 3 and plotted against initial crack length in Fig. 53 for different temperatures. At temperatures -1.1 and 25.5 °C, the $K_{R(ins)}$ increases with increase in initial crack length, whereas at temperatures 43.3 and 60 °C, the $K_{R(ins)}$ is practically independent of initial crack length. This difference can be attributed to different mechanisms causing failure. It has been observed during the tests that at - 1.1 and 25.5 °C the failure occurs by growth of damage ahead of the crack tip symmetric about the plane of initial crack. However, overall fracture is not a low energy absorbing brittle fracture because the energy is absorbed in fibre pullout and debonding. The increase in $K_{R(ins)}$ occurs due to increased debonding at larger initial crack lengths. At temperature 60 °C the damage occurs at approximately 45° to the load axis as shown in Fig. 54. Thus the overall fracture is a ductile fracture and insensitive to the initial crack lengths. This fact will be further discussed through the influence of crack length on notched strength at different temperatures.

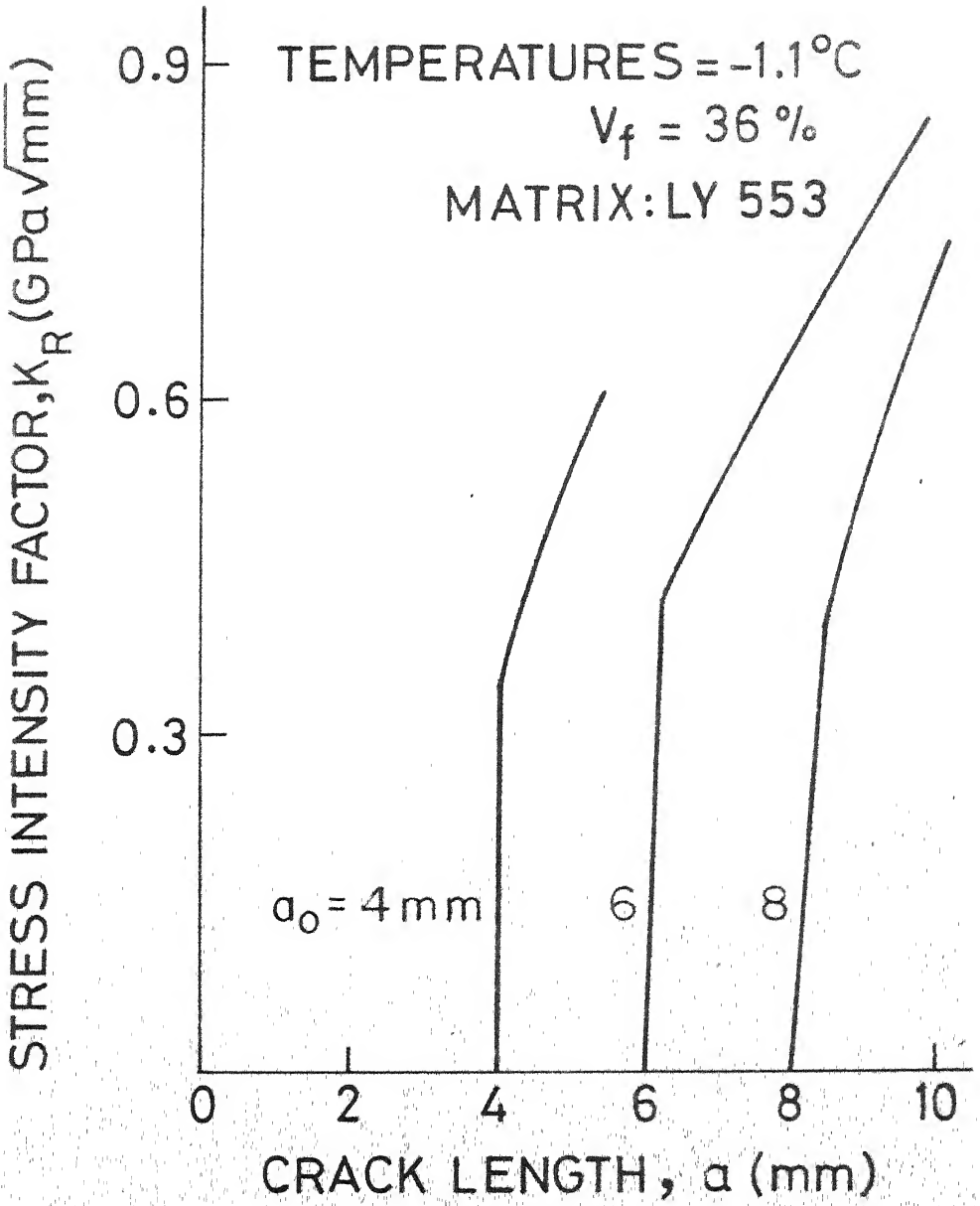

FIG. 50 R-CURVES AT TEST TEMPERATURE OF -1.1°C

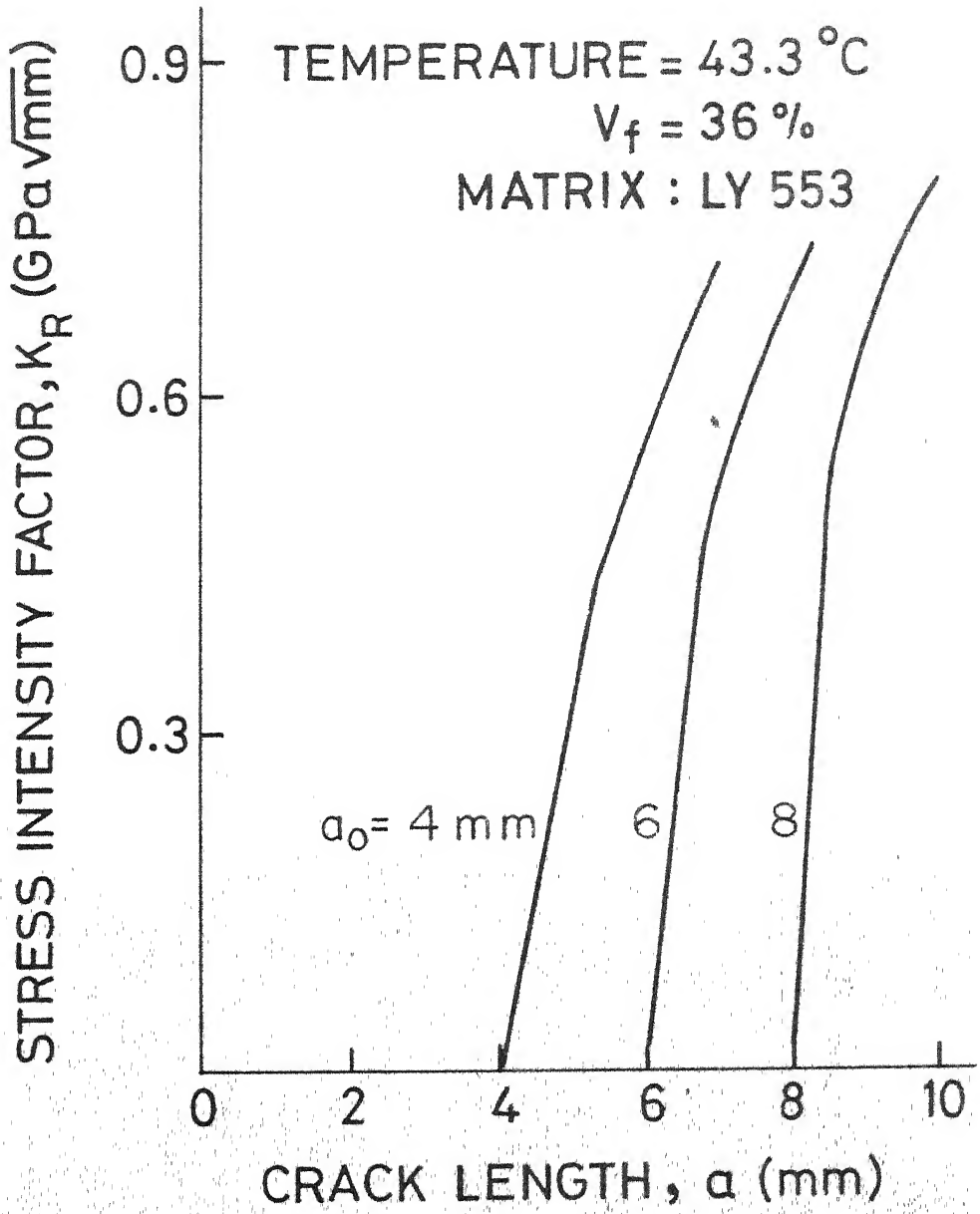

FIG. 51 R-CURVES AT TEST TEMPERATURE OF 43.3 °C

TABLE 3 : Stress Intensity Factors at Instability

$K_{R(ins)}$ (Mode I, V_f = 36%, Matrix: LY 553)

Initial Crack Length a_o, (mm)	$K_{R(ins)}$, (GPa $\sqrt{mm}$)			
	Temperature, (^oC)			
	-1.1	25.5	43.3	60
4	0.608	0.765	0.695	0.588
6	0.706	0.853	0.706	0.618
8	0.706	0.931	0.735	0.618

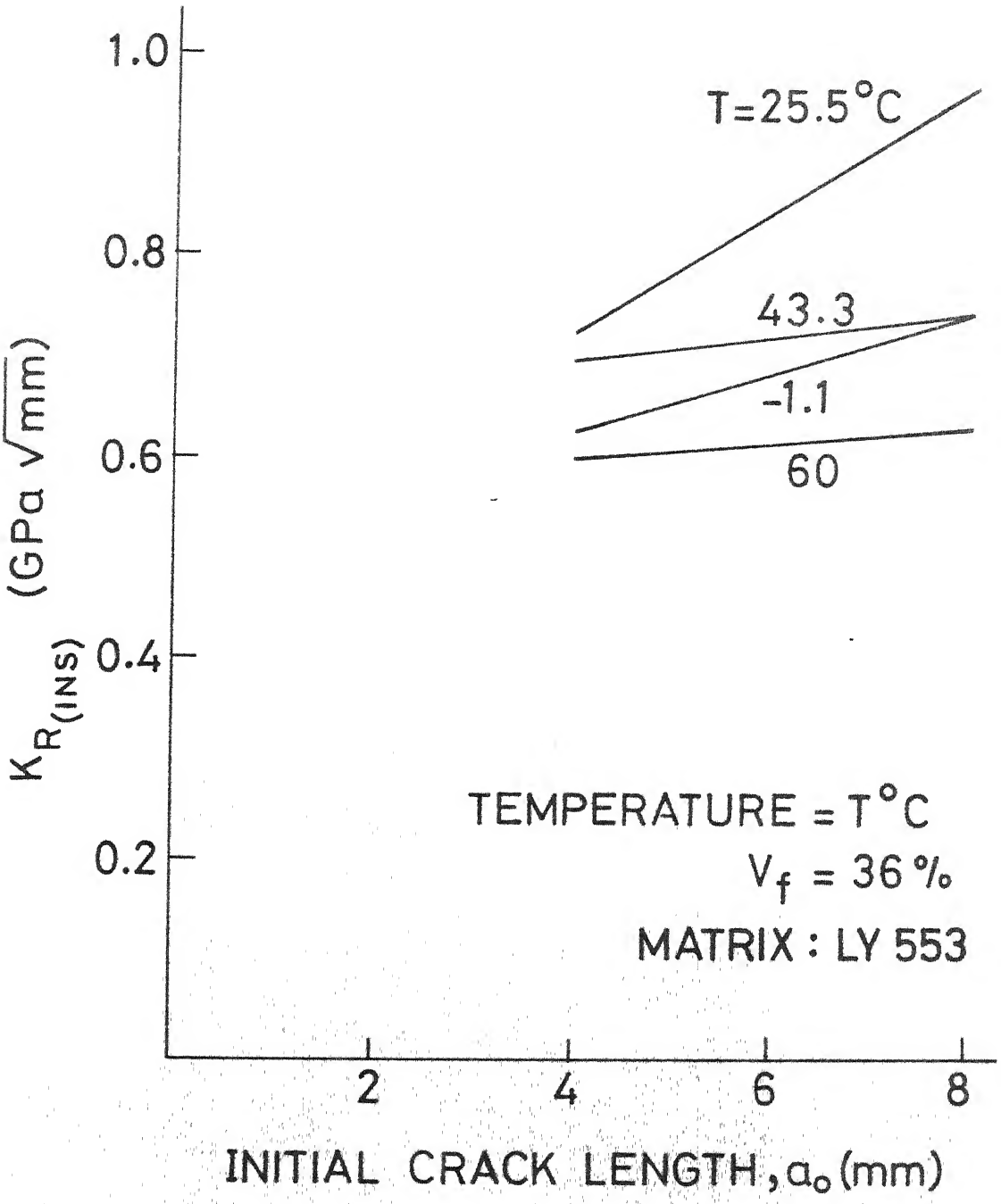

FIG. 53 VARIATION OF $K_{R(INS)}$ WITH INITIAL CRACK LENGTH

T = −1.1 °C

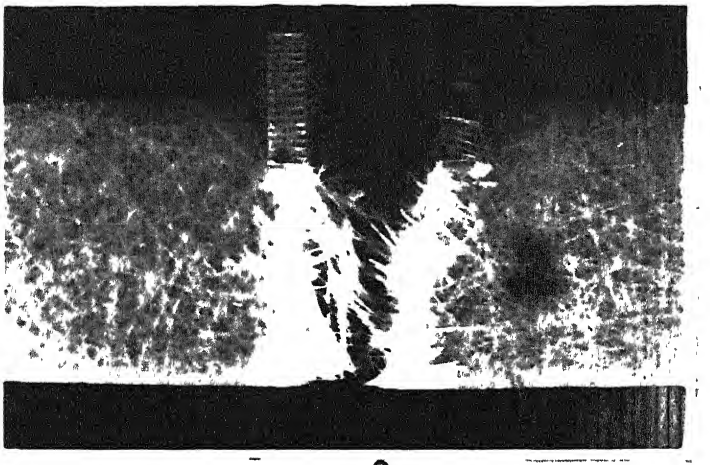

T = 43.3 °C

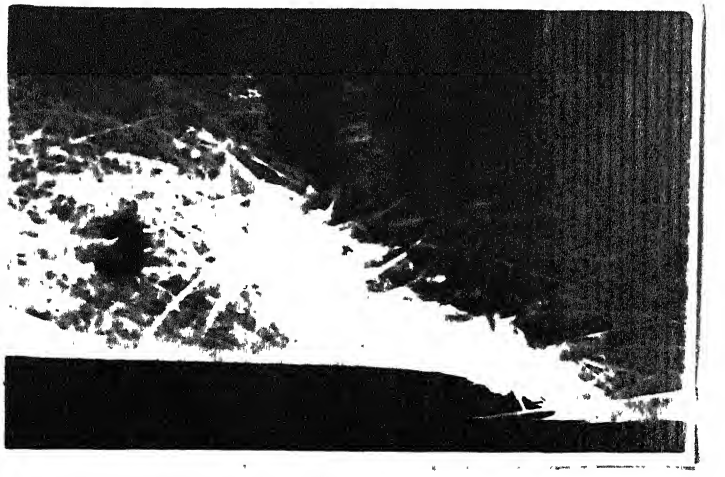

T = 60 °C

G.54 PHOTOGRAPHS OF SPECIMENS SHOWING FRACTURE AT DIFFERENT TEST TEMPERATURES

The $K_{R(ins)}$ is plotted against temperature for different crack lengths in Fig. 55. This shows that initially the fracture toughness of the material increases as the temperature increases. However, as the temperature is increased beyond the room temperature the fracture toughness again decreases because of the deterioration of the matrix. The crack growth resistance K_R has been plotted against effective crack extension ($\Delta a = a - a_o$) in Figs. 56 - 58 for different temperatures. They also do not indicate if the crack growth resistance is independent of initial crack length.

The resistance to fracture of the composite material can be better understood through the crack toughness performance in terms of $K_{R(ins)} / \sigma_o$ where σ_o is the un-notched strength. This ratio is a measure related to critical flow size. The larger this ratio is, the better the resistance to fracture. The ratio $K_{R(ins)} / \sigma_o$ is plotted as a function of test temperature for different initial crack lengths in Fig. 59. The resistance to fracture increases as the test temperature increases. It is also observed that the crack toughness performance parameter $(K_{R(ins)} / \sigma_o)$ is less sensitive to initial crack lengths than the $K_{R(ins)}$ is.

The normalised notched strength is plotted against initial crack length in Fig. 60 for different temperatures. The normalised notched strength curves become higher as the

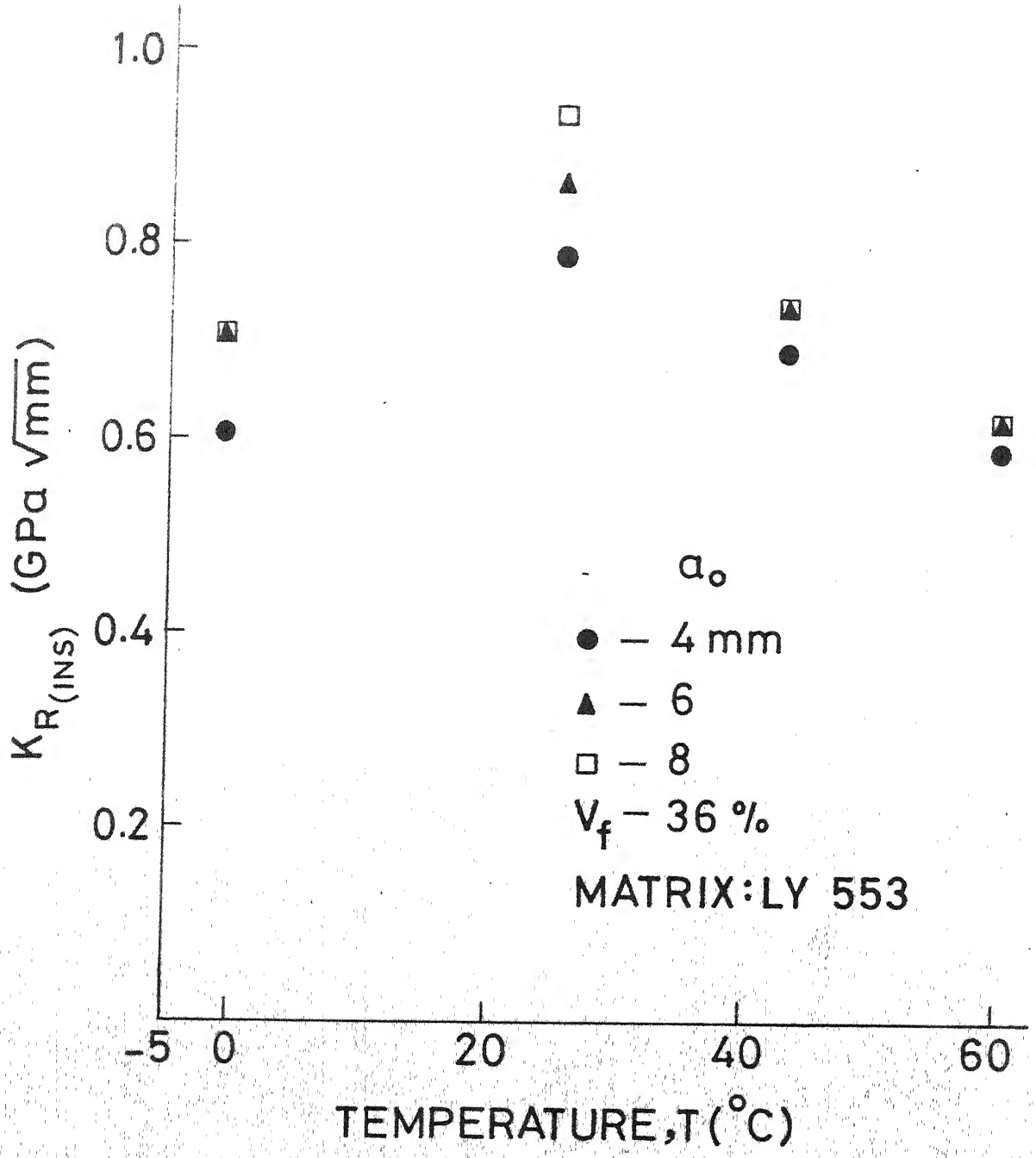

FIG. 55 VARIATION OF $K_{R(INS)}$ WITH TEST TEMPERATURE

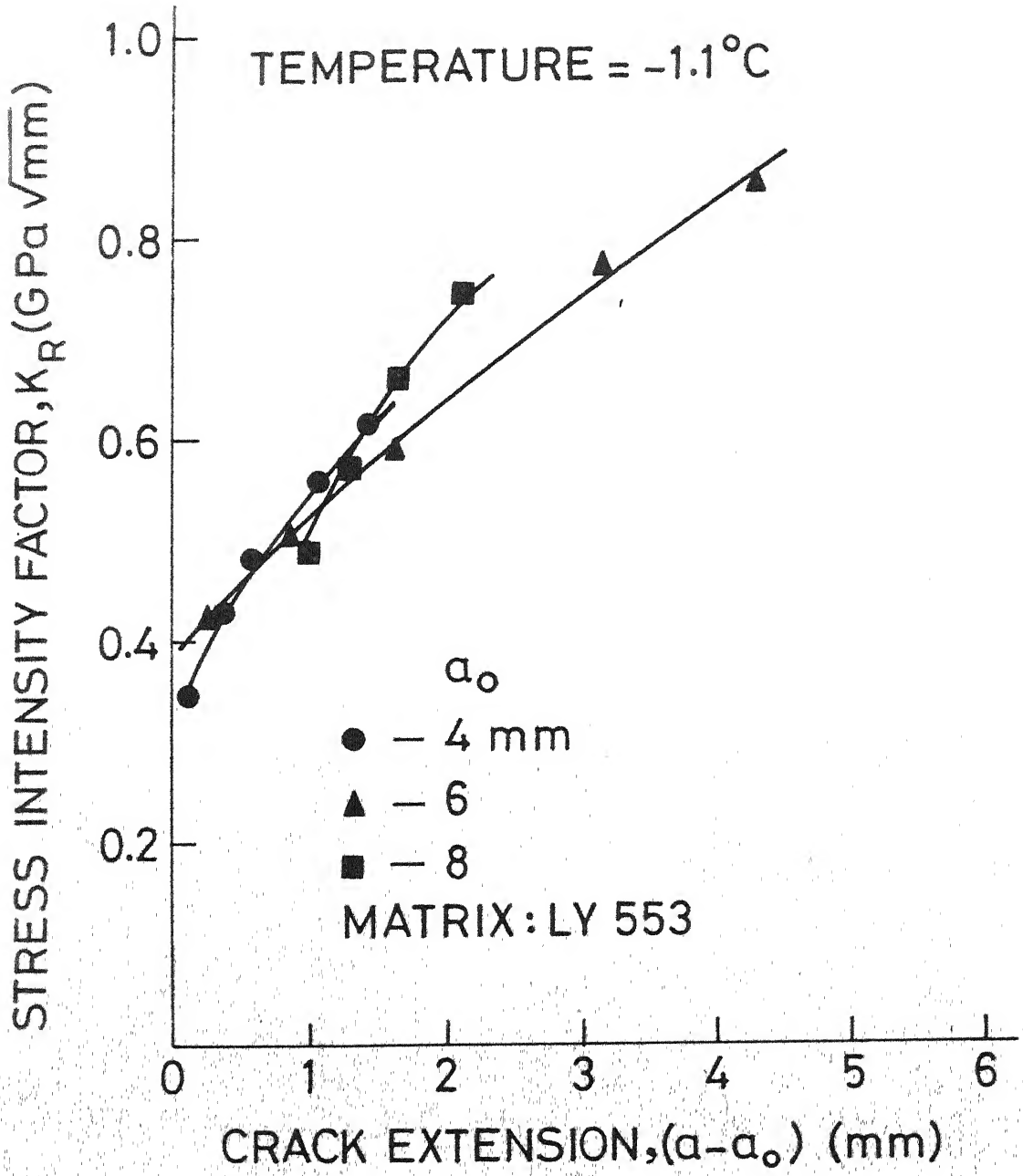

FIG. 56 VARIATION OF CRACK GROWTH RESISTANCE WITH CRACK EXTENSION AT TEST TEMPERATURE OF -1.1°C

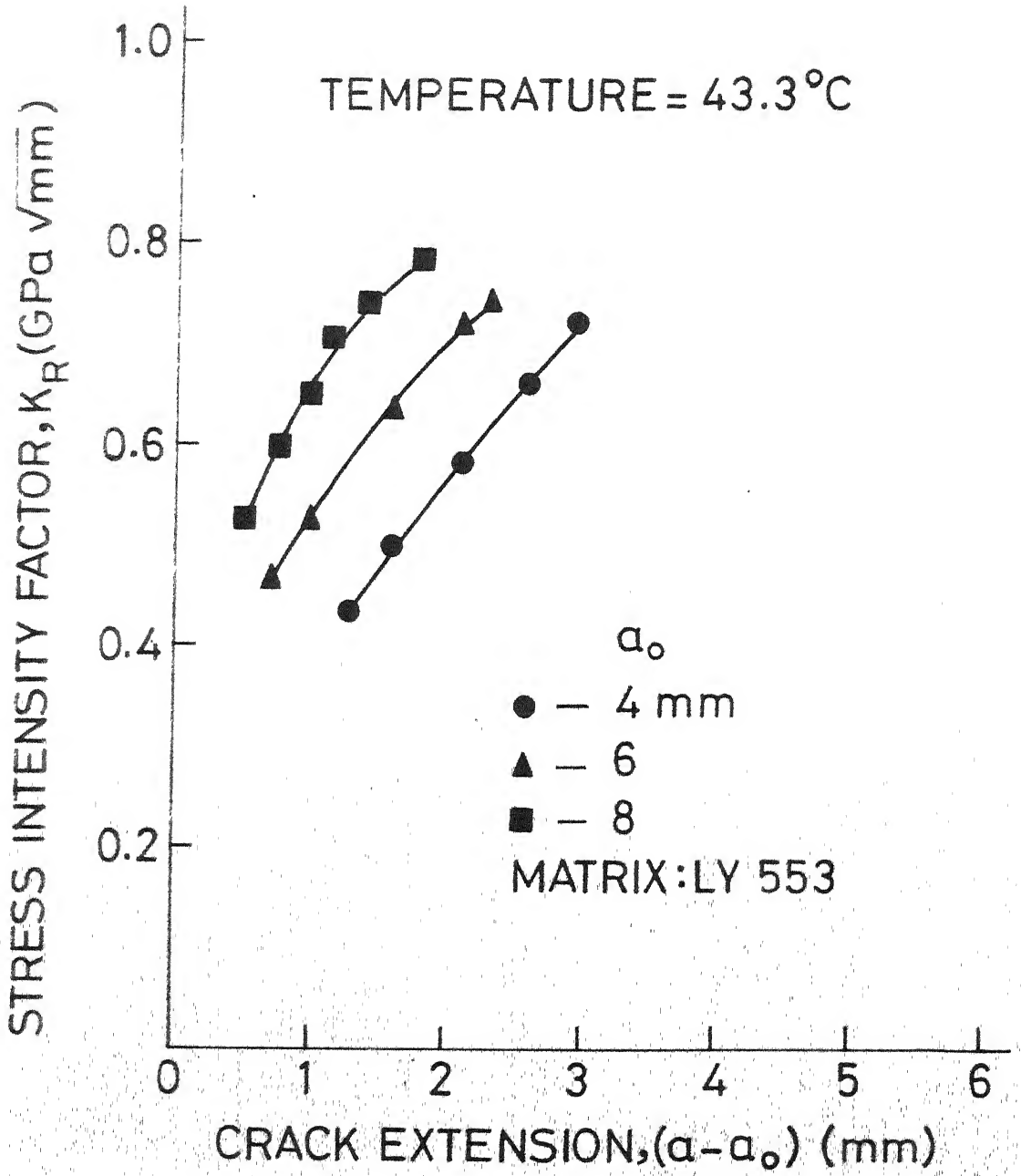

FIG. 57 VARIATION OF CRACK GROWTH RESISTANCE WITH CRACK EXTENSION AT TEST TEMPERATURE OF 43.3 °C

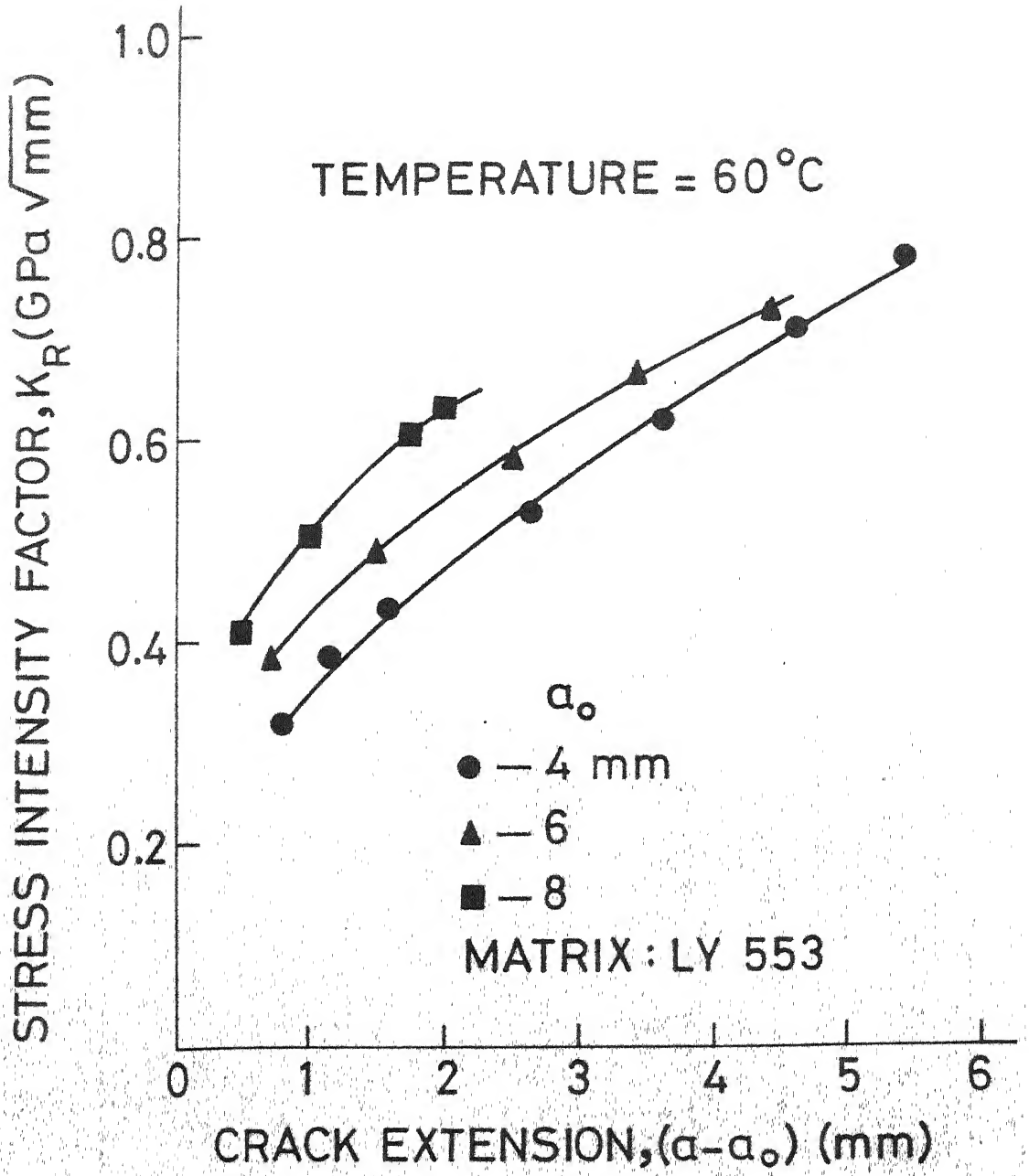

FIG. 58 VARIATION OF CRACK GROWTH RESISTANCE WITH CRACK EXTENSION AT TEST TEMPERATURE OF 60 °C

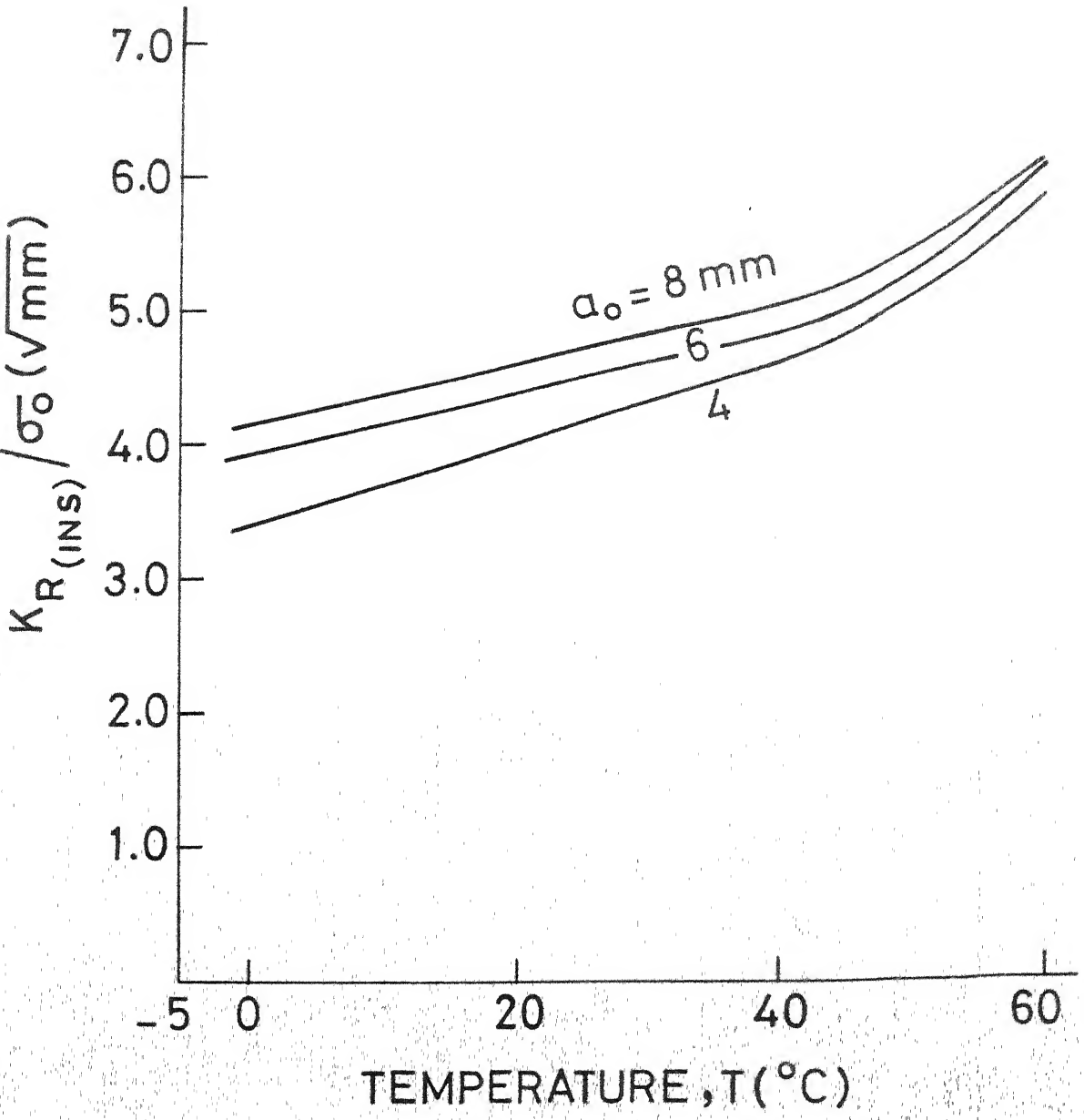

FIG. 59 VARIATION OF CRACK TOUGHNESS PERFORMANCE ($K_{R(INS)}/\overline{\sigma_o}$) WITH TEST TEMPERATURE

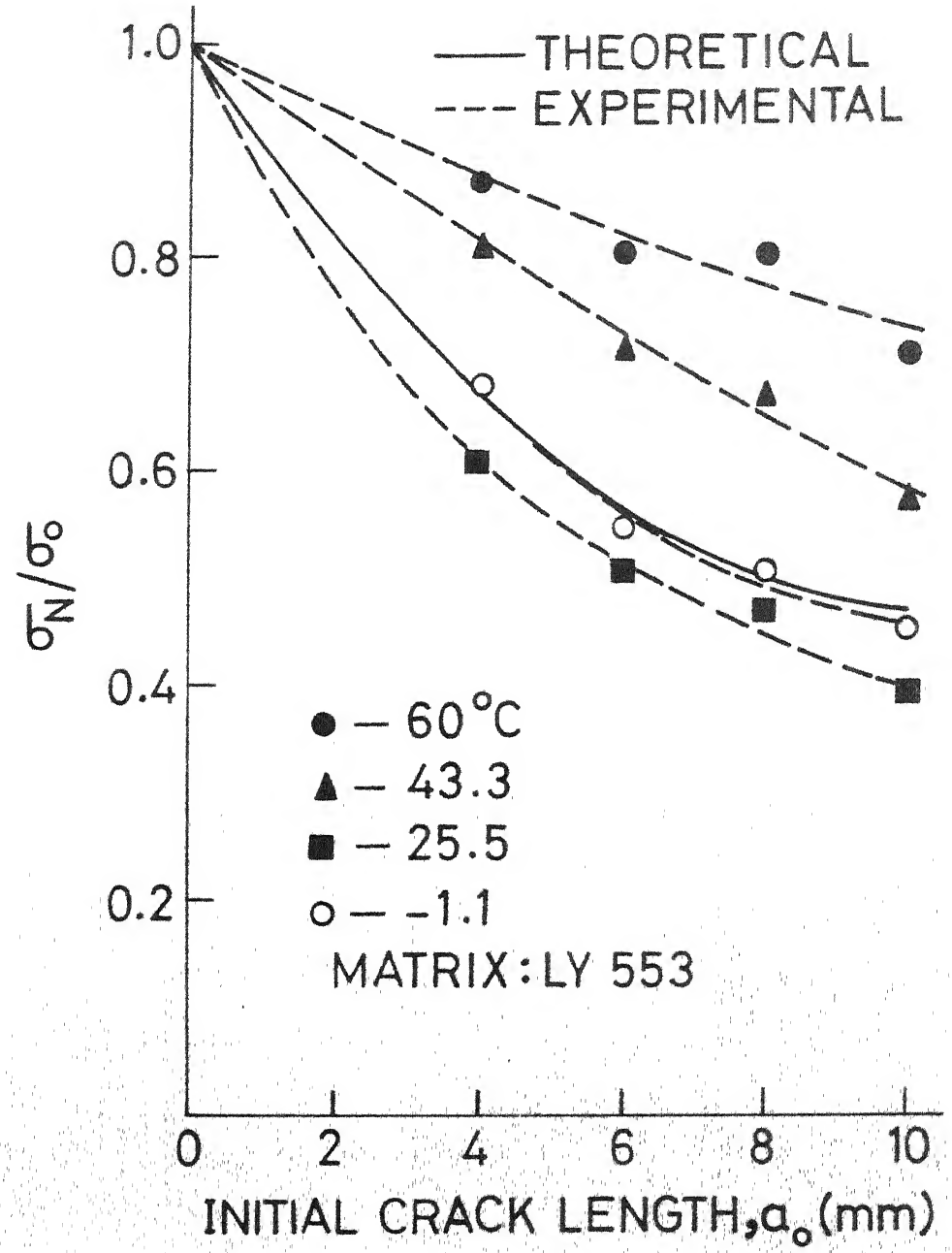

FIG. 60 VARIATION OF NORMALISED NOTCHED STRENGTH WITH INITIAL CRACK LENGTH

temperature increases indicating that the notched sensitivity of the composite is considerably reduced at elevated temperatures. Also shown in the Fig. 60 is a theoretical notched strength curve representing point stress criterion proposed by Whitney - Nuismer [8, 9] . The theoretical normalised notched strength is independent of temperature. It is observed that at room temperature and at - 1.1 ^{o}C the theoretical predictions agree reasonably well with the experimental results. However, as the notch sensitivity of the composite decreases at elevated temperature, the experimental notched strengths are significantly higher than the theoretically predicted. This indicates that the criteria such as those of Whitney - Nuismer [8, 9] predicting notched strength of the composite should be applied with caution. They may be applied only when the material is notch sensitive.

3.7 EFFECT OF MATRIX

The effect of matrix properties on fracture toughness has been studied through tests on the composites prepared by using different grades of epoxy as matrix material. The different epoxies used are Araldite LY 553, LY 556 and CY 230. In addition, CY 230 has been modified by adding 1.5, 2.5 and 5.0 percent dibutyl-phathalate, which reduces the viscosity of uncured matrix material. The stress strain curves for different matrix material and composites are shown in Figs. 61, 62 and 63, average tensile properties given in Table 4. The Araldite LY 556 is very viscous at

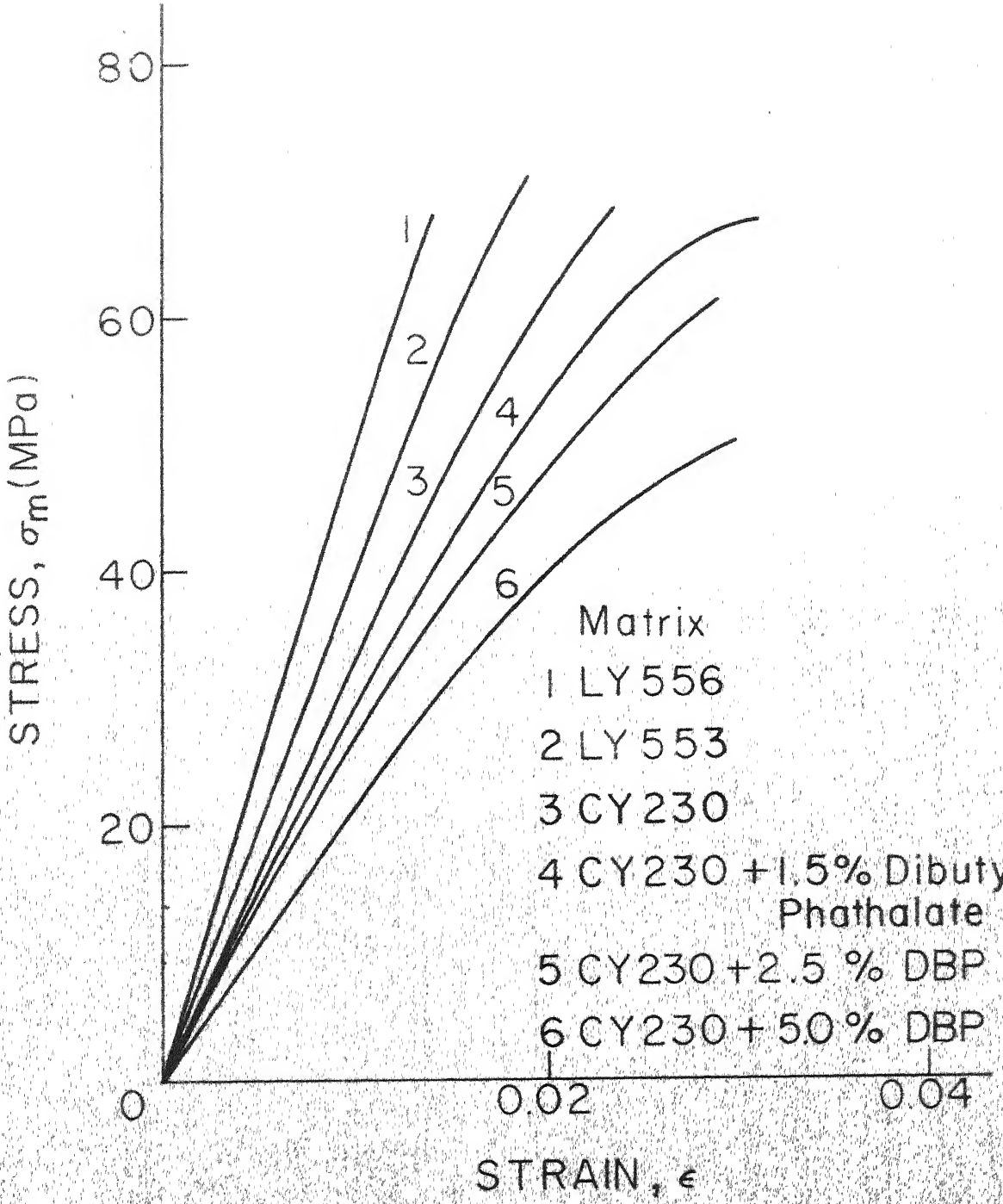

ESS STRAIN CURVES FOR
ERENT MATRIX MATERIALS

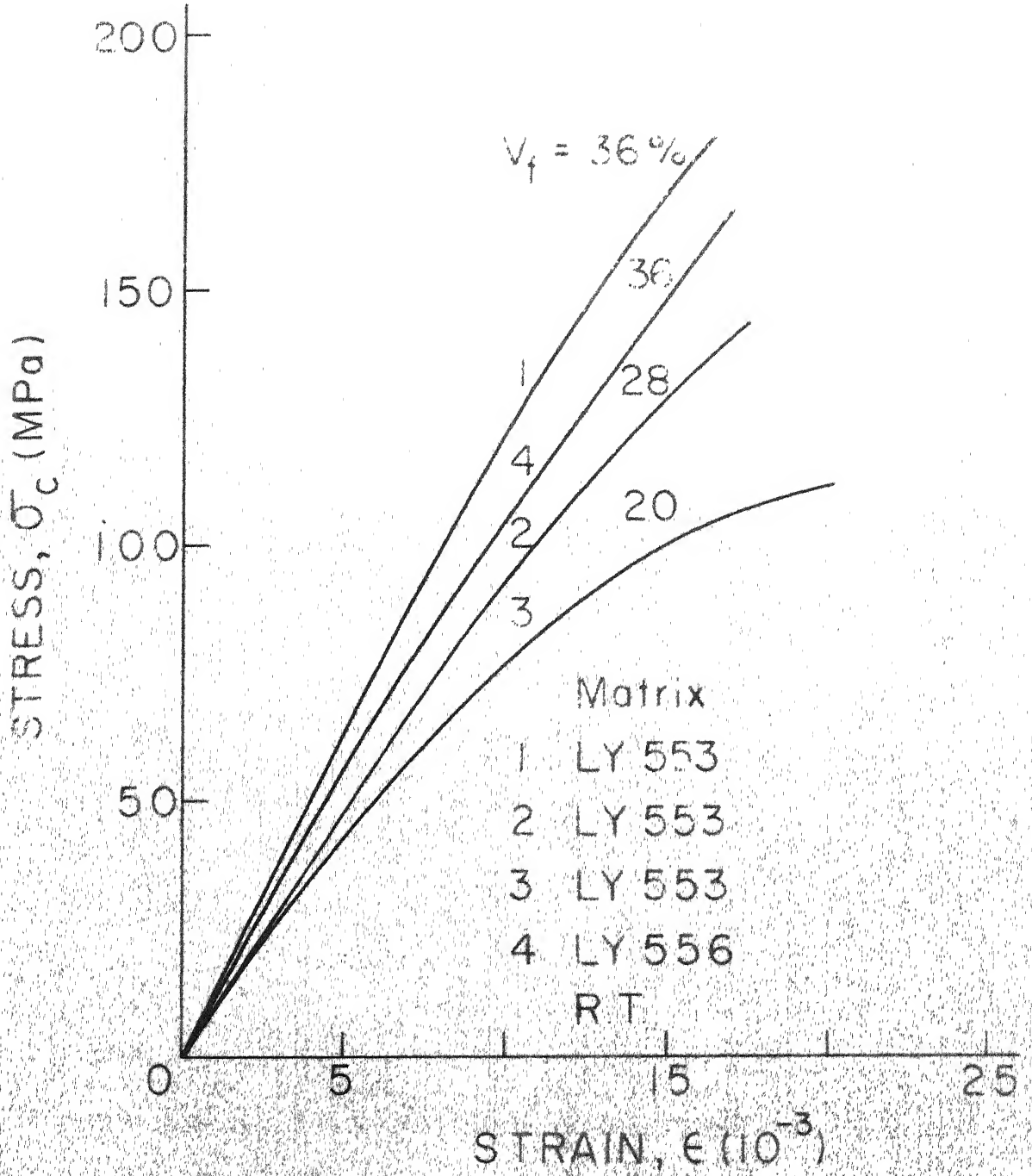

FIG 62 STRESS AND STRAIN CURVES FOR COMPOSITES USING DIFFERENT MATRIX MATERIALS (V_f = 20, 28 AND 36 %)

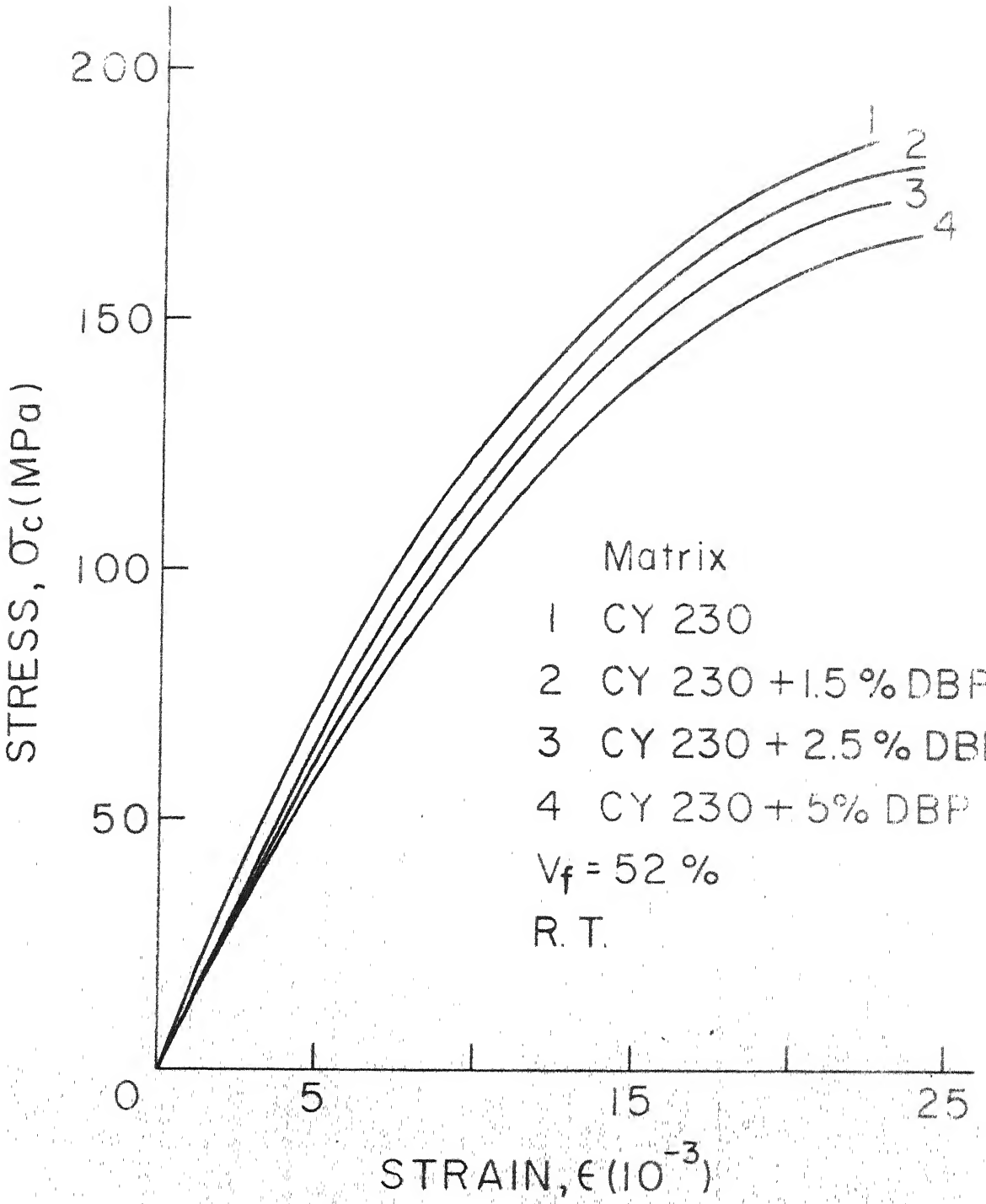

FIG. 63 STRESS AND STRAIN CURVES FOR COMPOSITES USING DIFFERENT MATRIX MATERIALS (V_f = 52 %)

TABLE 4 : Tensile Properties of Matrix and Composite

Matrix Material	Matrix Properties			V_f	Composite Properties		
	Em GPa	mu MPa	Percentage Elongation		E_c GPa	cu MPa	Percentage Elongation
LY 556	5.101	68.12	1.40	36	12.380	165.2	1.70
LY 553	4.080	70.85	1.88	36	12.750	190.60	1.64
LY 553	-	-	-	52	17.160	208.52	2.20
CY 230	3.330	68.50	2.33	52	14.710	184.70	2.26
CY 230 + DBP*(1.5%)	3.065	67.44	3.08	52	13.830	180.20	2.40
CY 230 + DBP*(2.5%)	2.786	61.29	2.90	52	12.940	173.50	2.30
CY 230 + DBP* (5%)	2.118	50.34	3.00	52	11.870	166.47	2.40

* Dibutyl - Phathalate

room temperature compared to other grades of epoxies so that the composite with this matrix material could be prepared with fibre volume fraction of only 36 percent. With other grades of epoxy it was practical to prepare composites having fibre volume fraction of 52 percent.

The load versus COD curves of composites made from different matrix material are shown in Figs. 64 - 68. The general nature of load versus COD curves is same for all the composites with different matrix material. The crack length estimation curves for the composites with CY 230 and modified CY 230 as matrix material are shown in Fig. 69 and that for the composite with LY 556 as the matrix is shown in Fig. 70. It is observed that the crack length estimation curves for the composite with CY 230 as the matrix material are not significantly influenced by the addition of dibutylphathalate in the matrix.

The R - curves for composites with different matrix material are shown in Figs. 71 - 75. The crack growth resistance, K_R, for the composites with different matrix material are plotted against crack extension in Figs. 76 - 80. It is observed that the crack growth resistance for the composite with the LY 556 as the matrix material is independent of the initial crack length (Fig. 76), whereas that for the composites with CY 230 and modified CY 230 as matrix material depends upon the initial crack length (Figs. 77 - 80). The difference in behaviour can be attributed to the fact that LY 556 is comparatively stiff and

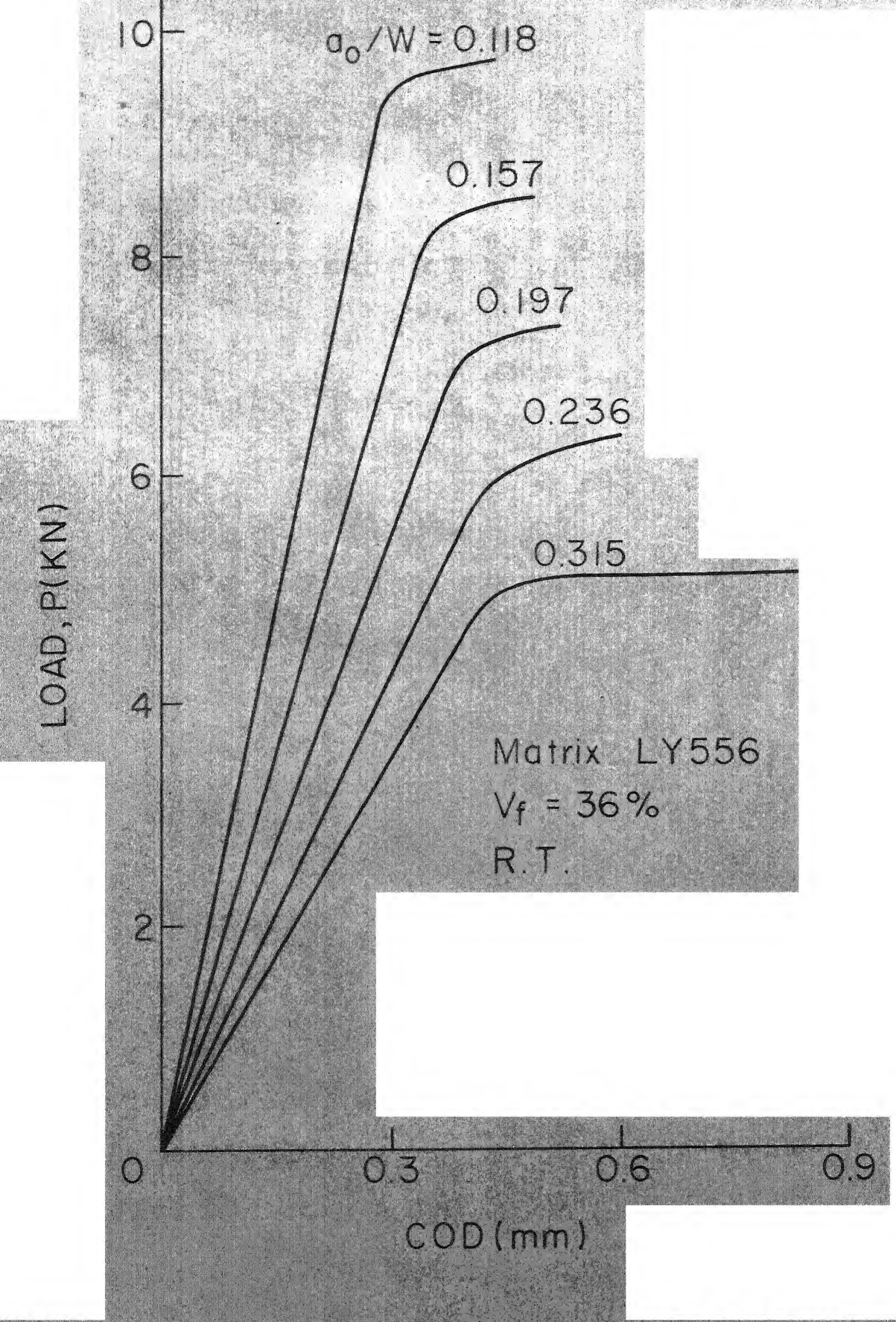

FIG. 64 LOAD VERSUS COD CURVES FOR DIFFERENT INITIAL CRACK LENGTH (MATRIX LY 556, V_f = 36%)

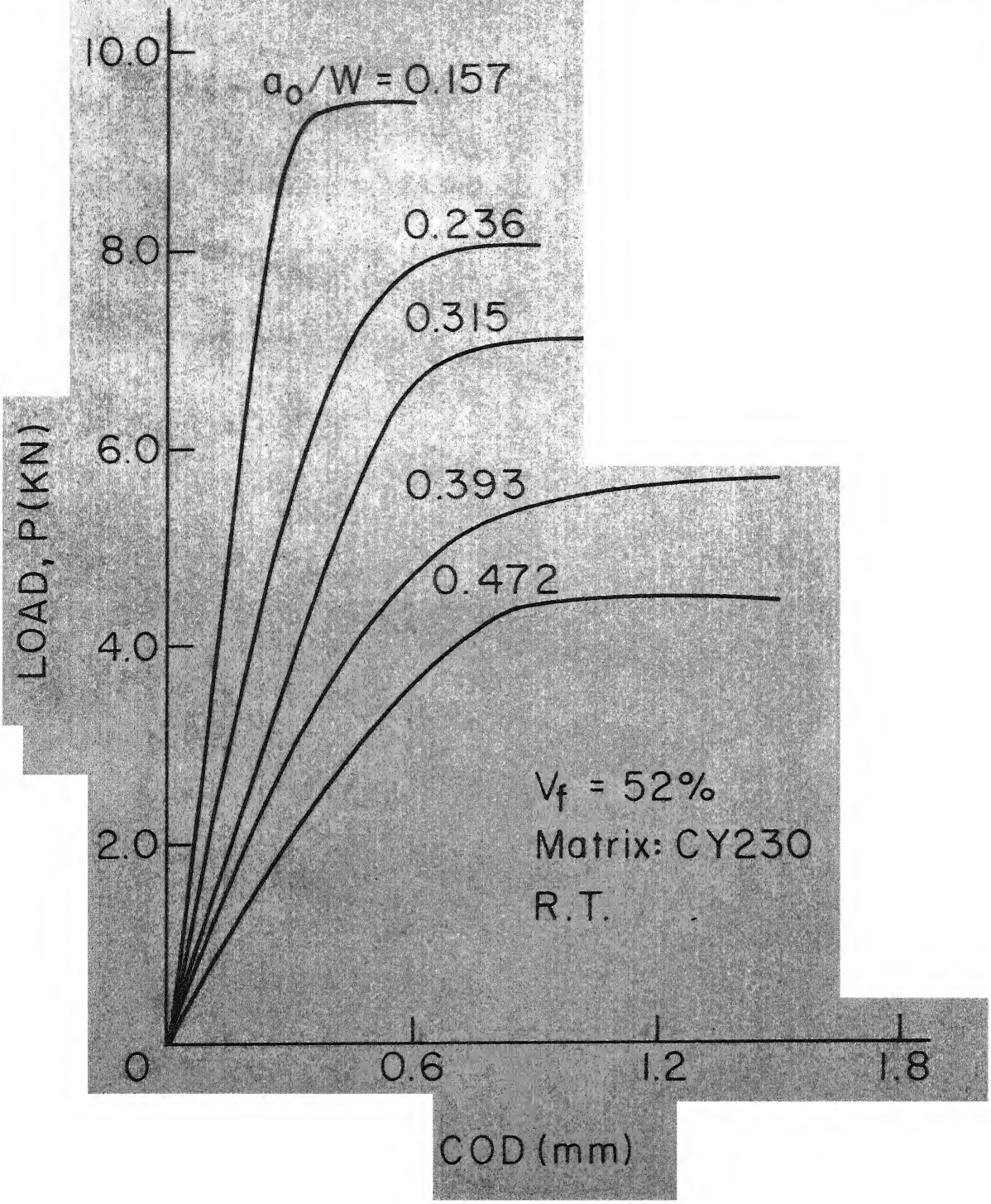

FIG. 65 LOAD VERSUS COD CURVES FOR DIFFERENT INITIAL CRACK LENGTH (MATRIX: CY 230, V_f = 52 %)

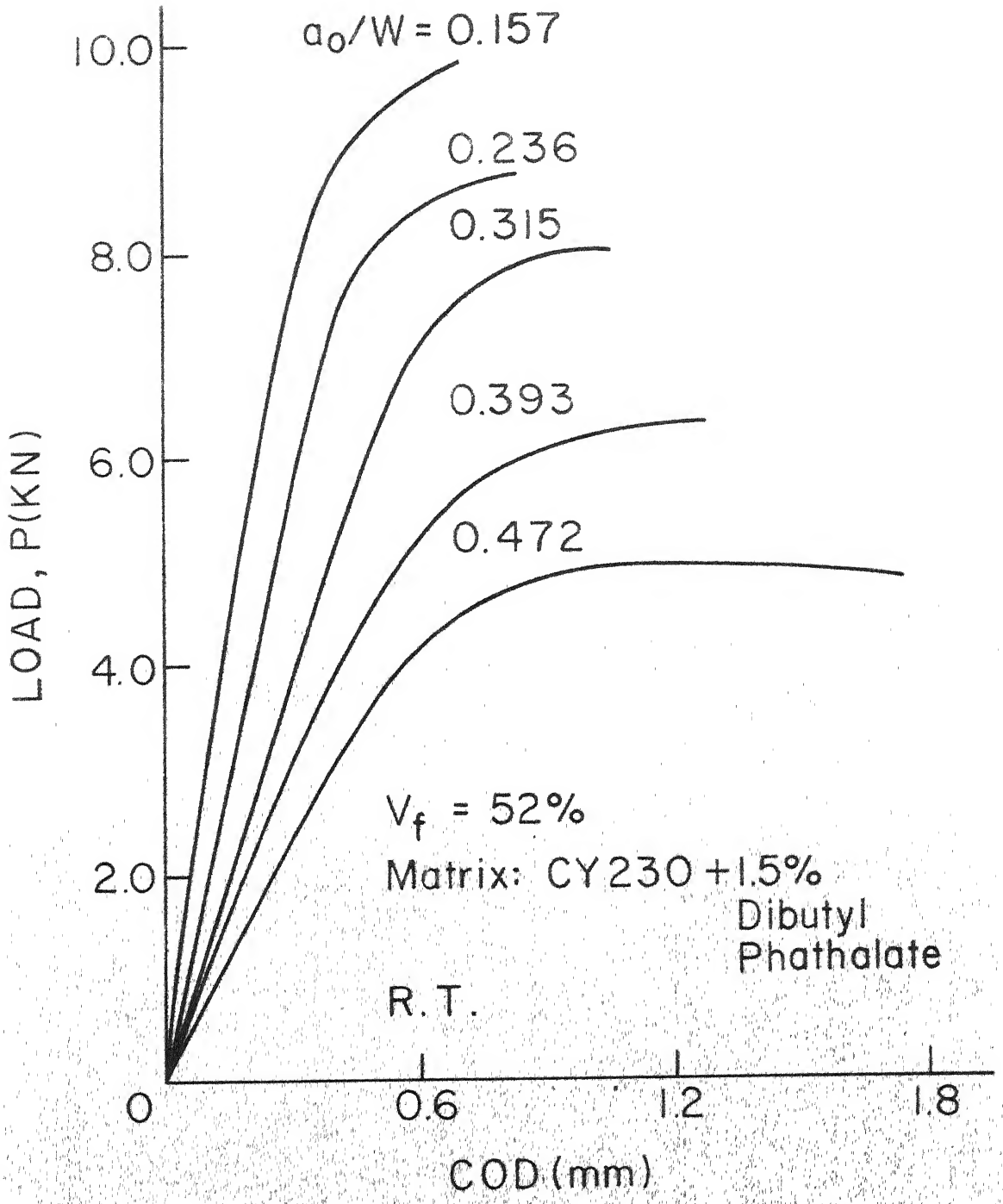

FIG. 66 LOAD VERSUS COD CURVES FOR DIFFERENT INITIAL CRACK LENGTH (MATRIX CY 230 + 1.5% DIBUTYL PHATHALATE, V_f = 52%)

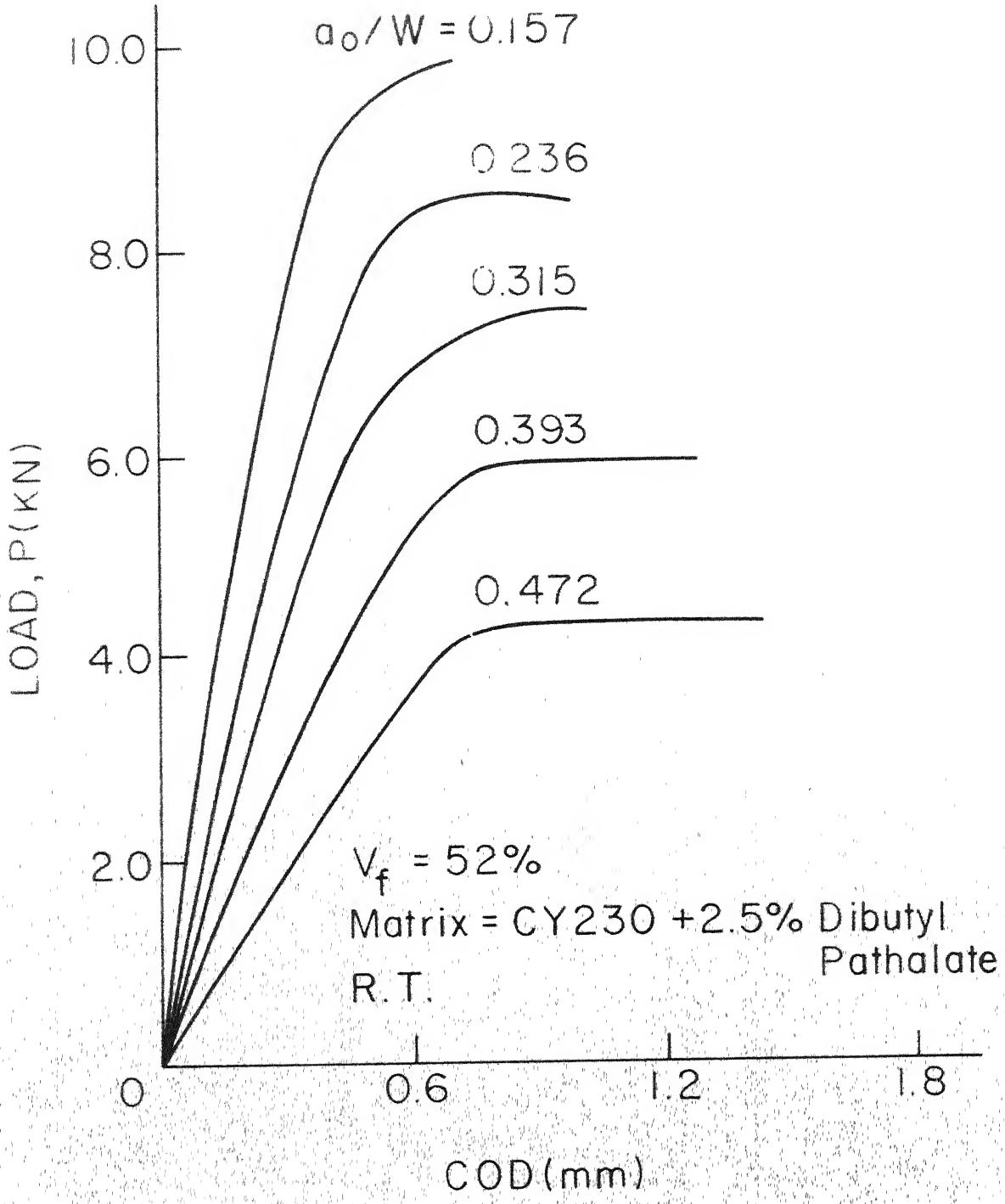

FIG.67 LOAD VERSUS COD CURVES FOR DIFFERENT INITIAL CRACK LENGTH (MATRIX CY230 +2.5% DIBUTYL PHATHALATE, V_f = 52%)

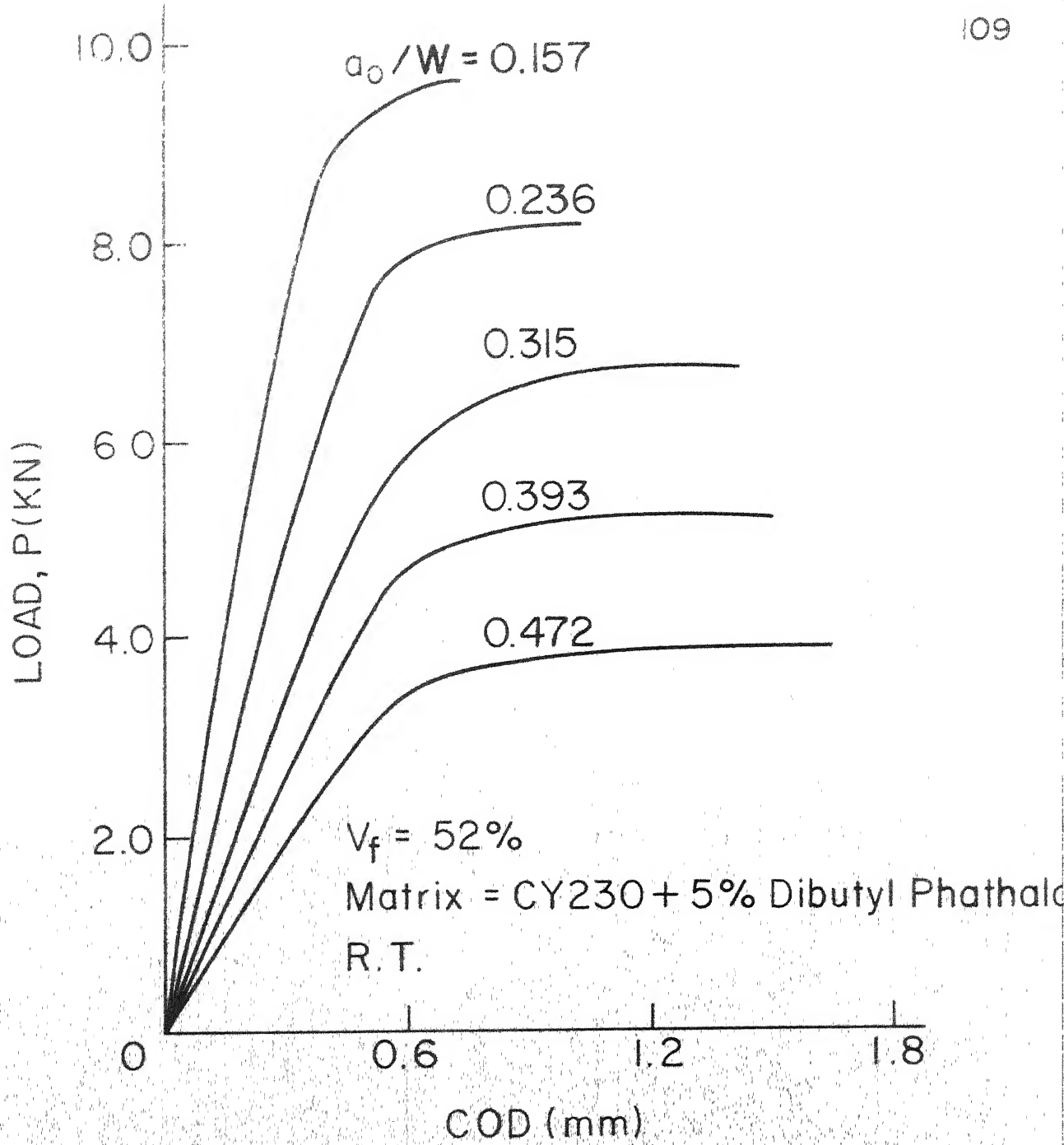

FIG. 68 LOAD VERSUS COD CURVES FOR DIFFERENT INITIAL CRACK LENGTH (MATRIX CY 230 + 5% DIBUTYL-PHATHALATE, V_f = 52%)

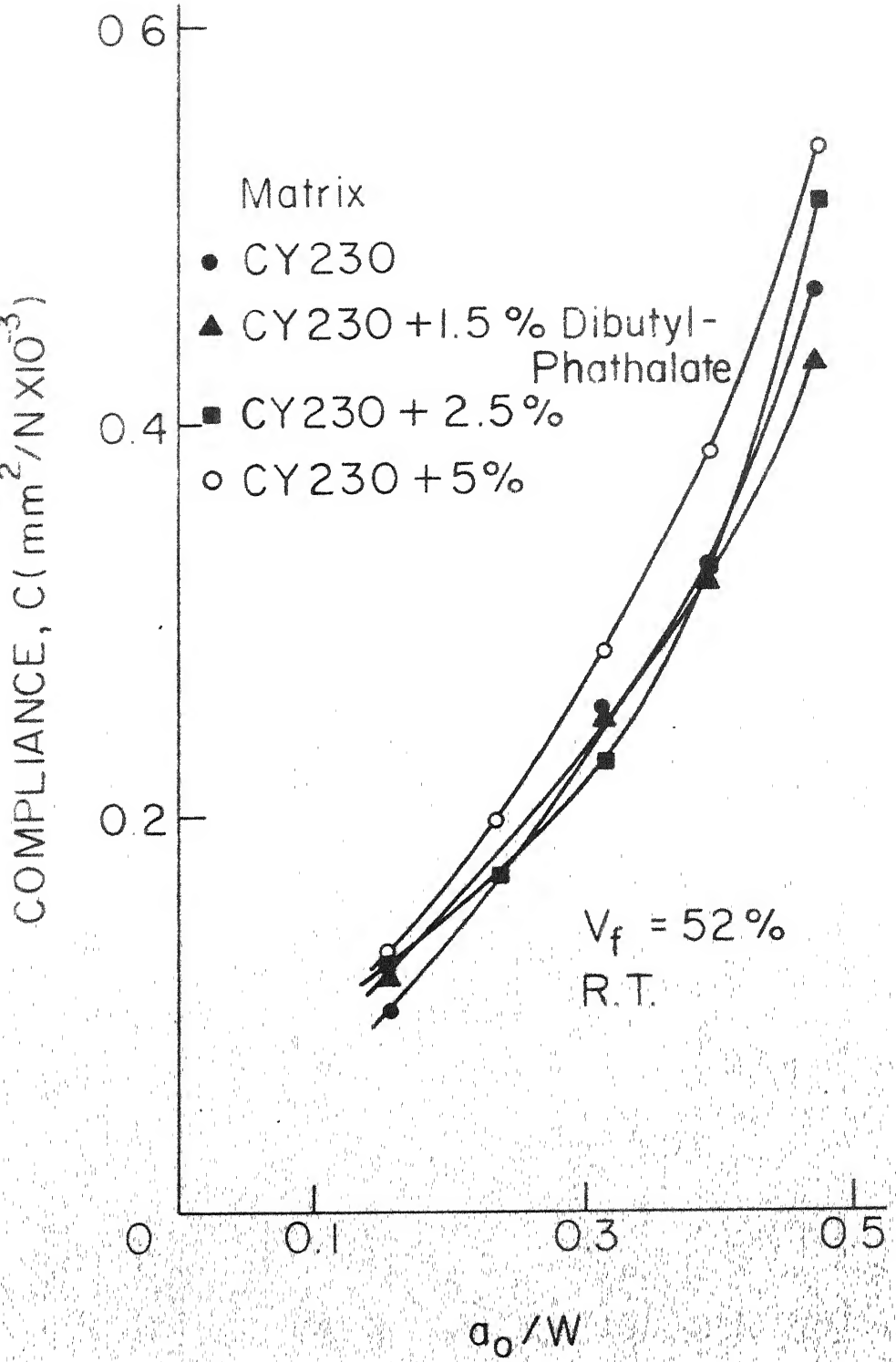

FIG 69 CRACK LENGTH ESTIMATION CURVES FOR COMPOSITES WITH CY230 AND MODIFIED CY230 AS MATRIX MATERIALS

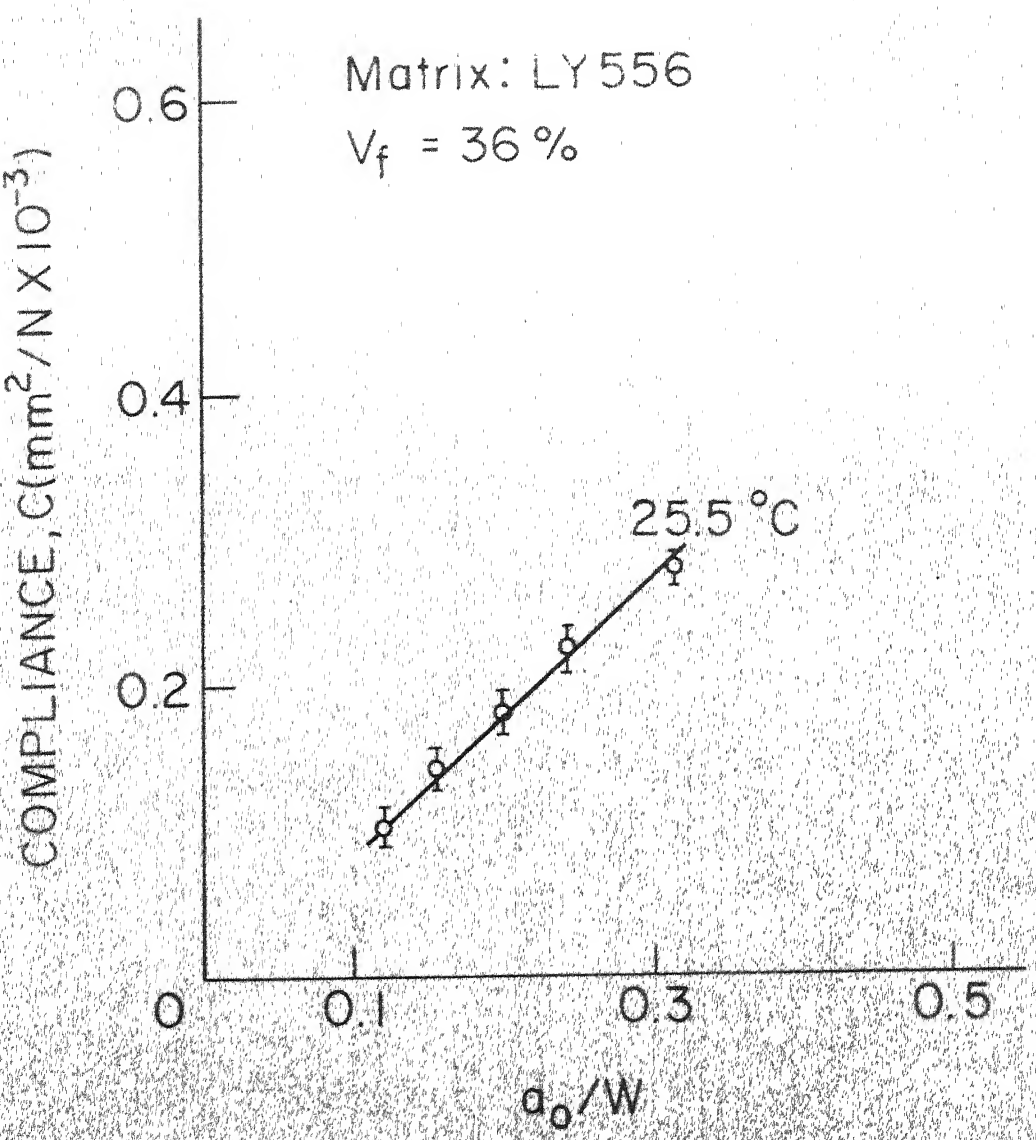

FIG.70 CRACK LENGTH ESTIMATION CURVE FOR COMPOSITE WITH LY556 AS MATRIX

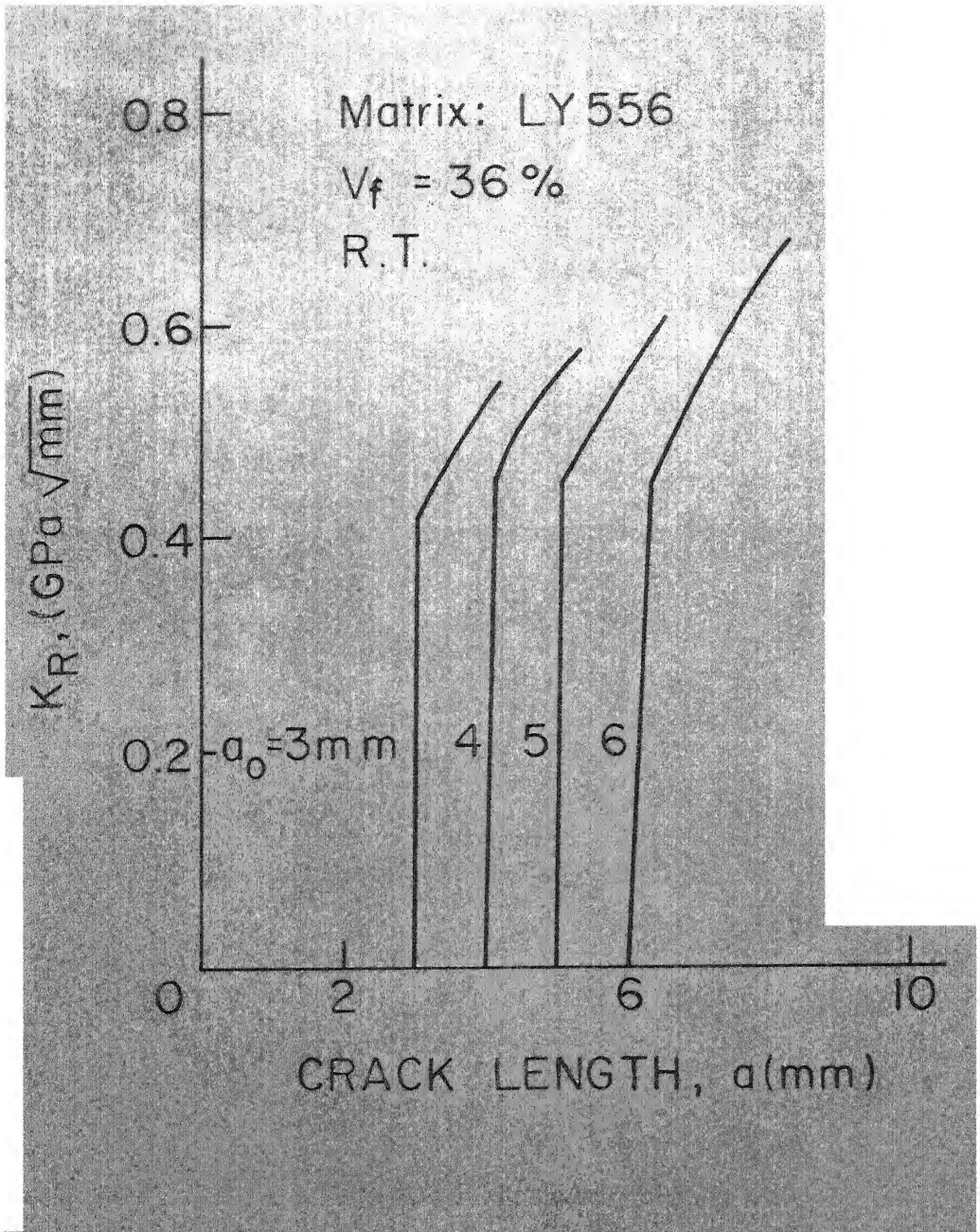

FIG. 71 R-CURVES FOR COMPOSITE WITH LY556 AS MATRIX (V_f = 36%)

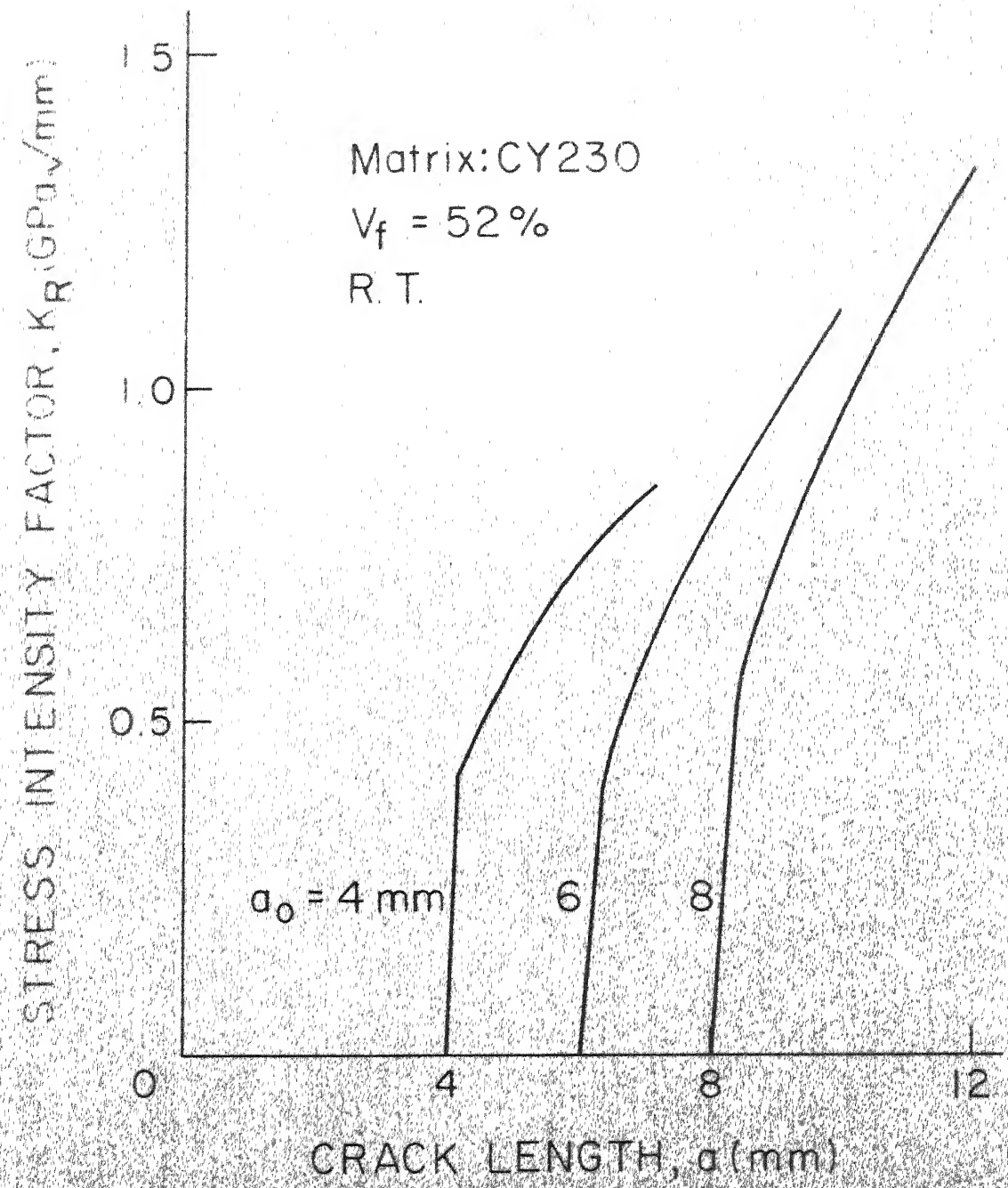

FIG. 72 R-CURVES FOR COMPOSITE WITH CY230 AS MATRIX (V_f = 52%)

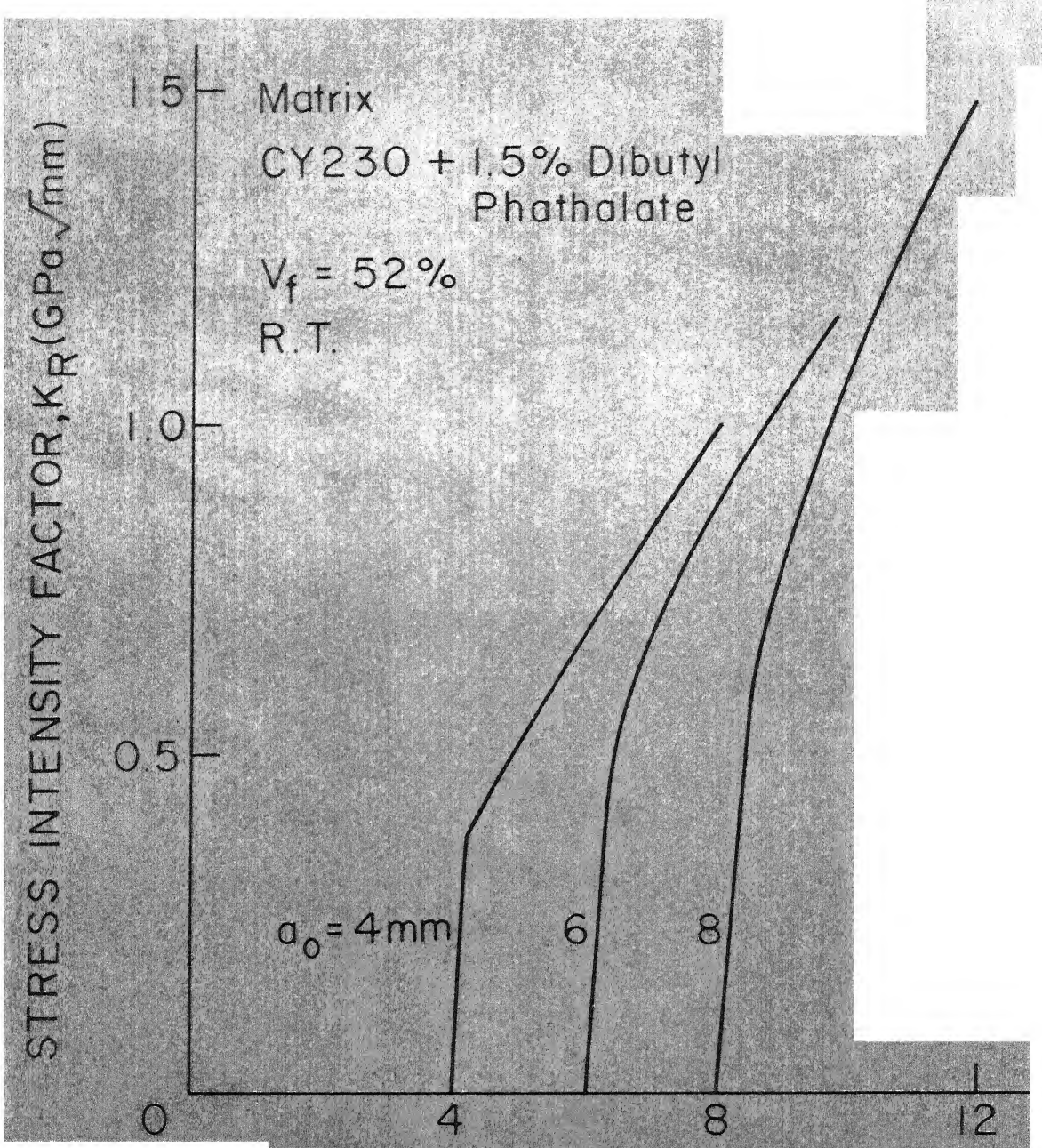

FIG. 73 R-CURVES FOR COMPOSITE WITH CY230 + 1.5% DIBUTYL-PHATHALATE AS MATRIX (V_f = 52%)

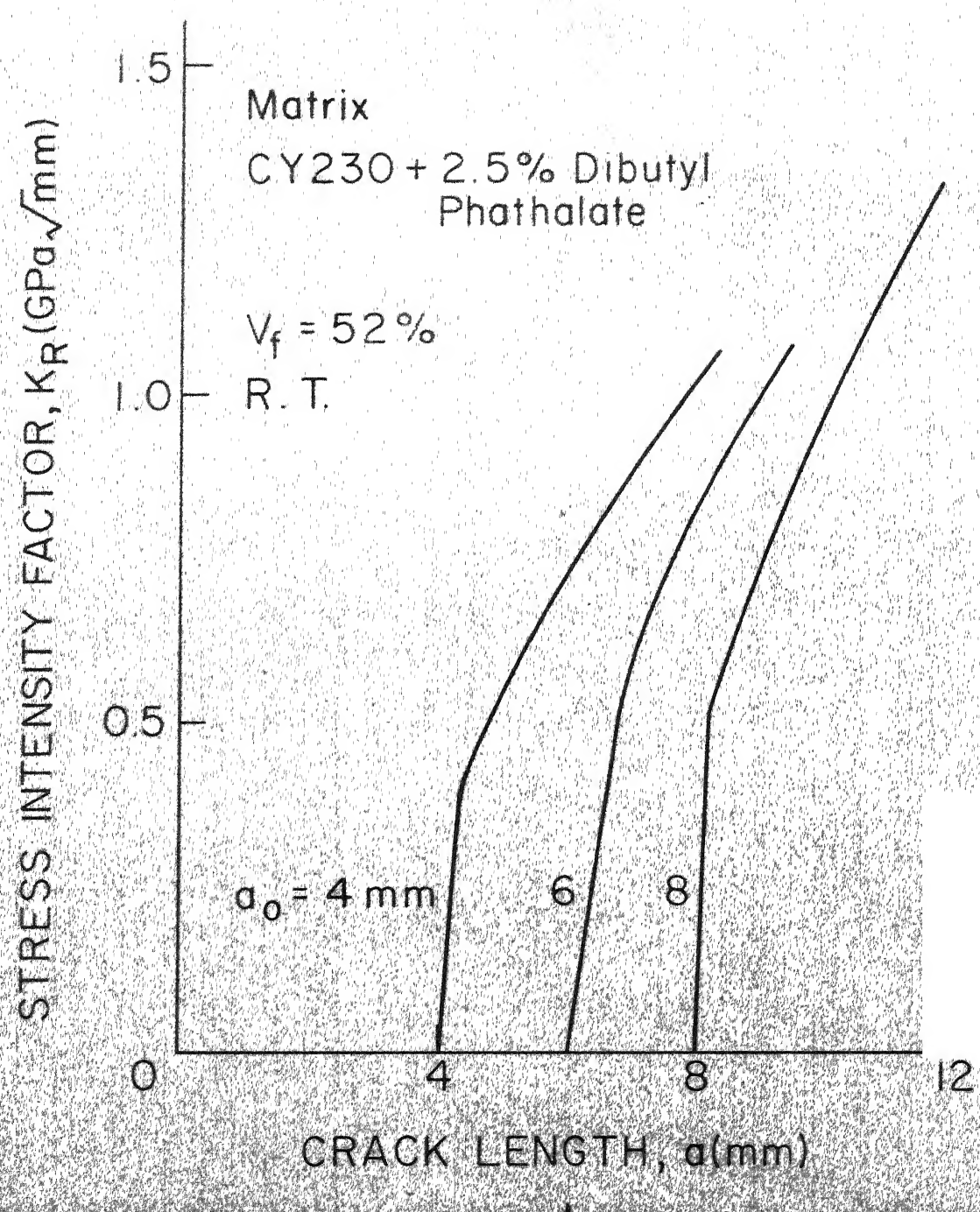

FIG. 74 R-CURVES FOR COMPOSITE WITH CY230 + 2.5% DIBUTYL-PHATHALATE AS MATRIX (V_f = 52%)

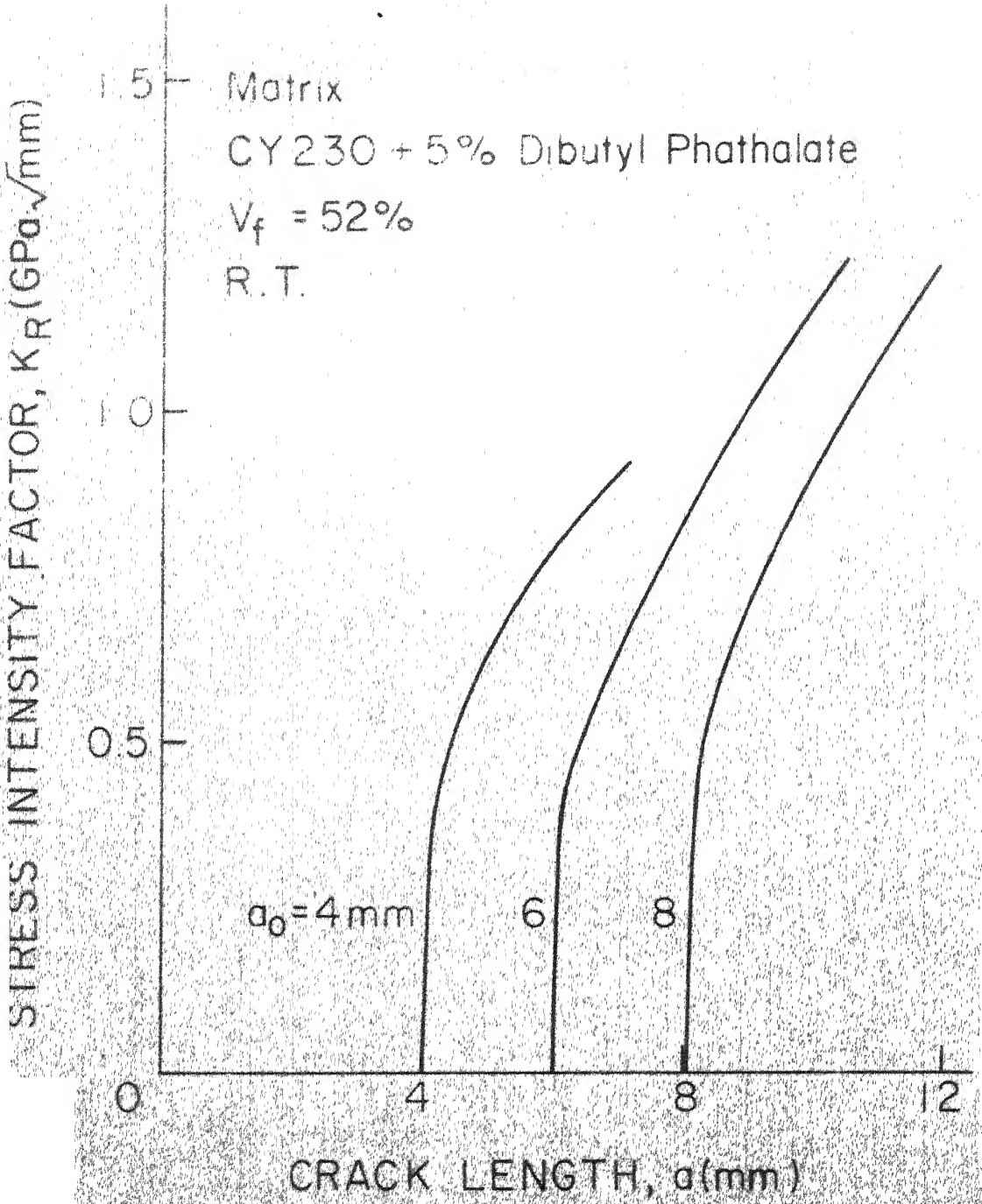

.75 R-CURVES FOR COMPOSITE WITH CY 230 + 5% DIBUTYL-PHATHALATE AS MATRIX (V_f = 52%)

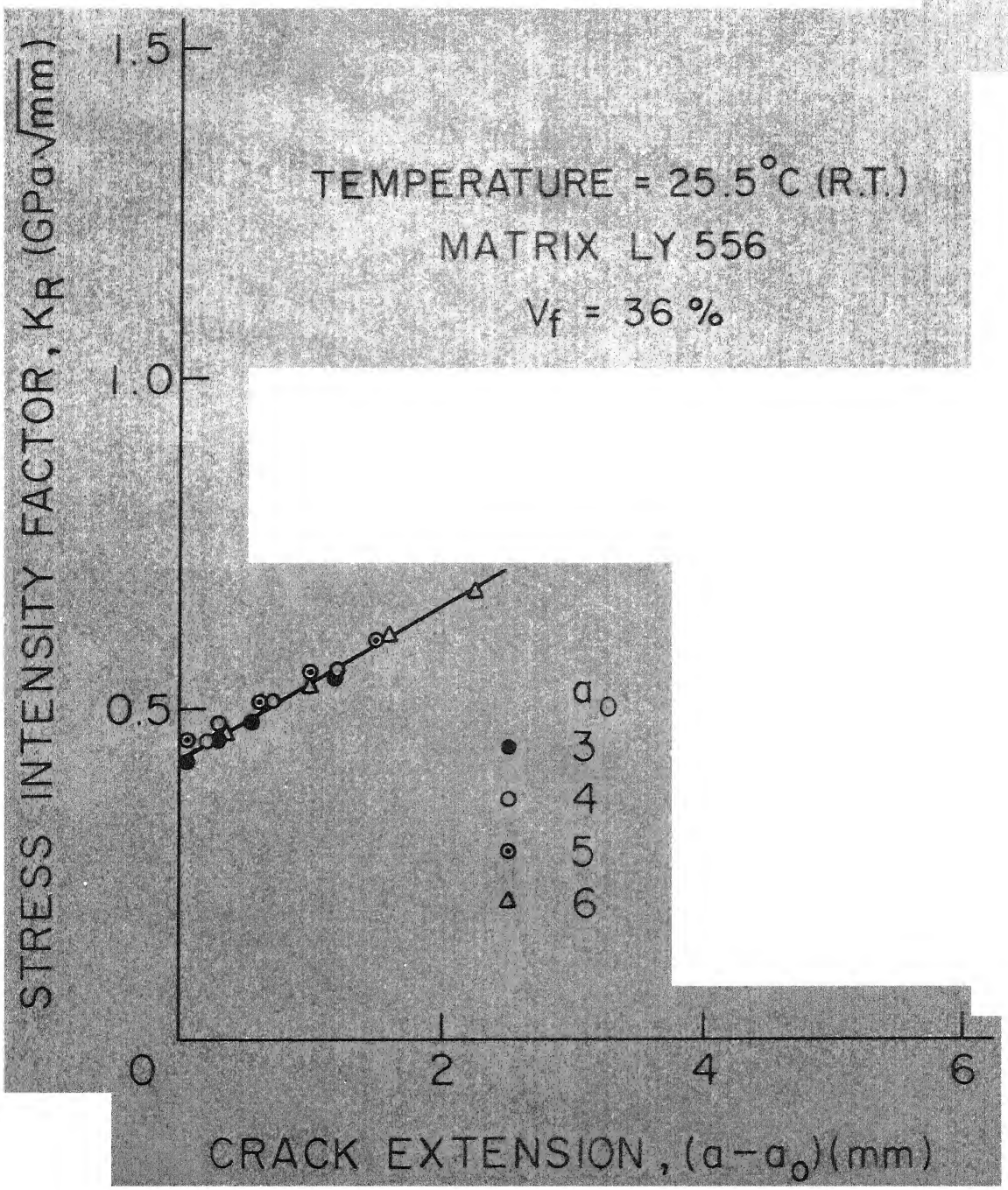

FIG. 76 VARIATION OF CRACK GROWTH RESISTANCE WITH CRACK EXTENSION (MATRIX: LY 556, V_f = 36%)

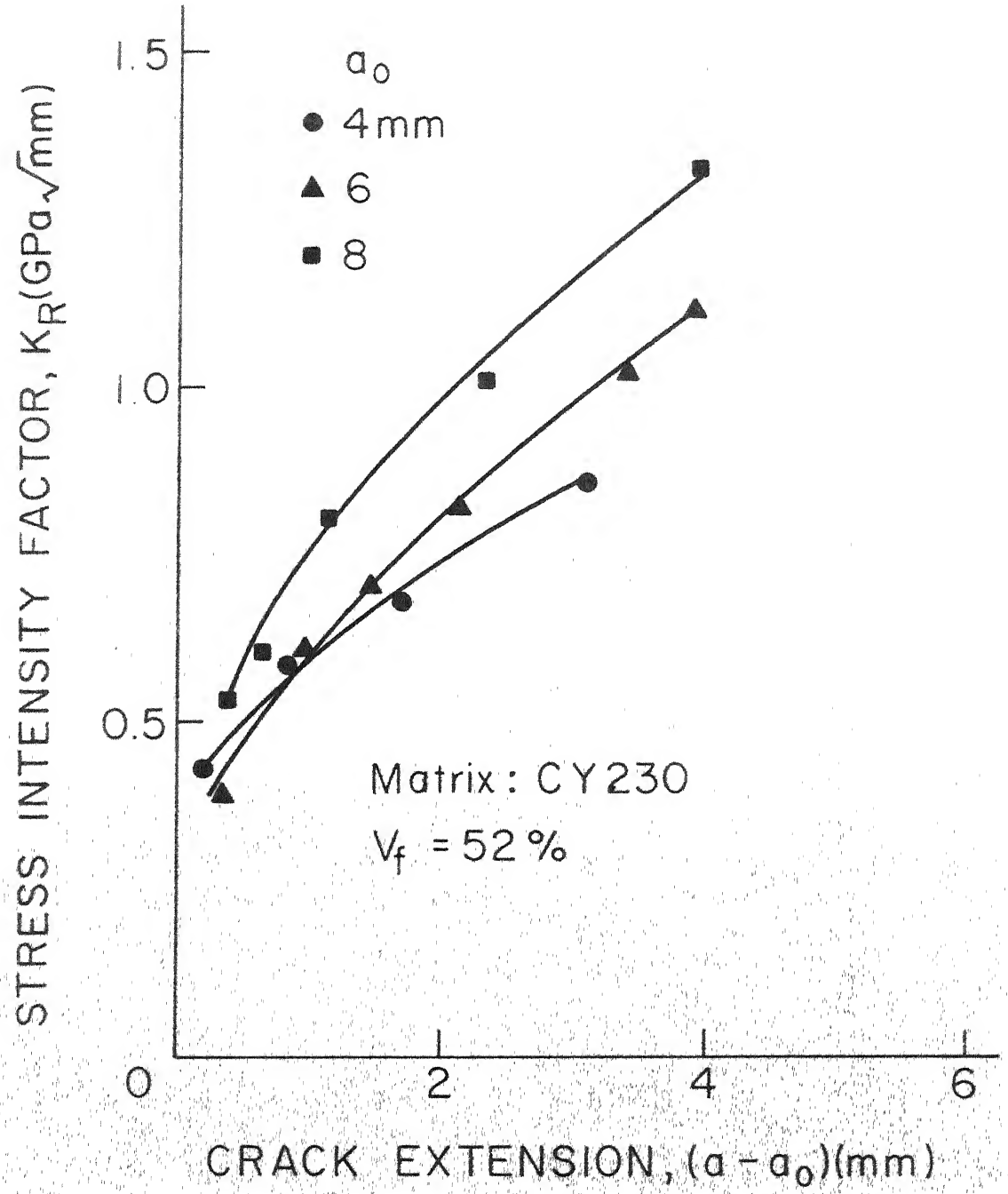

FIG. 77 VARIATION OF CRACK GROWTH RESISTANCE WITH CRACK EXTENSION (MATRIX CY230, V_f = 52 %)

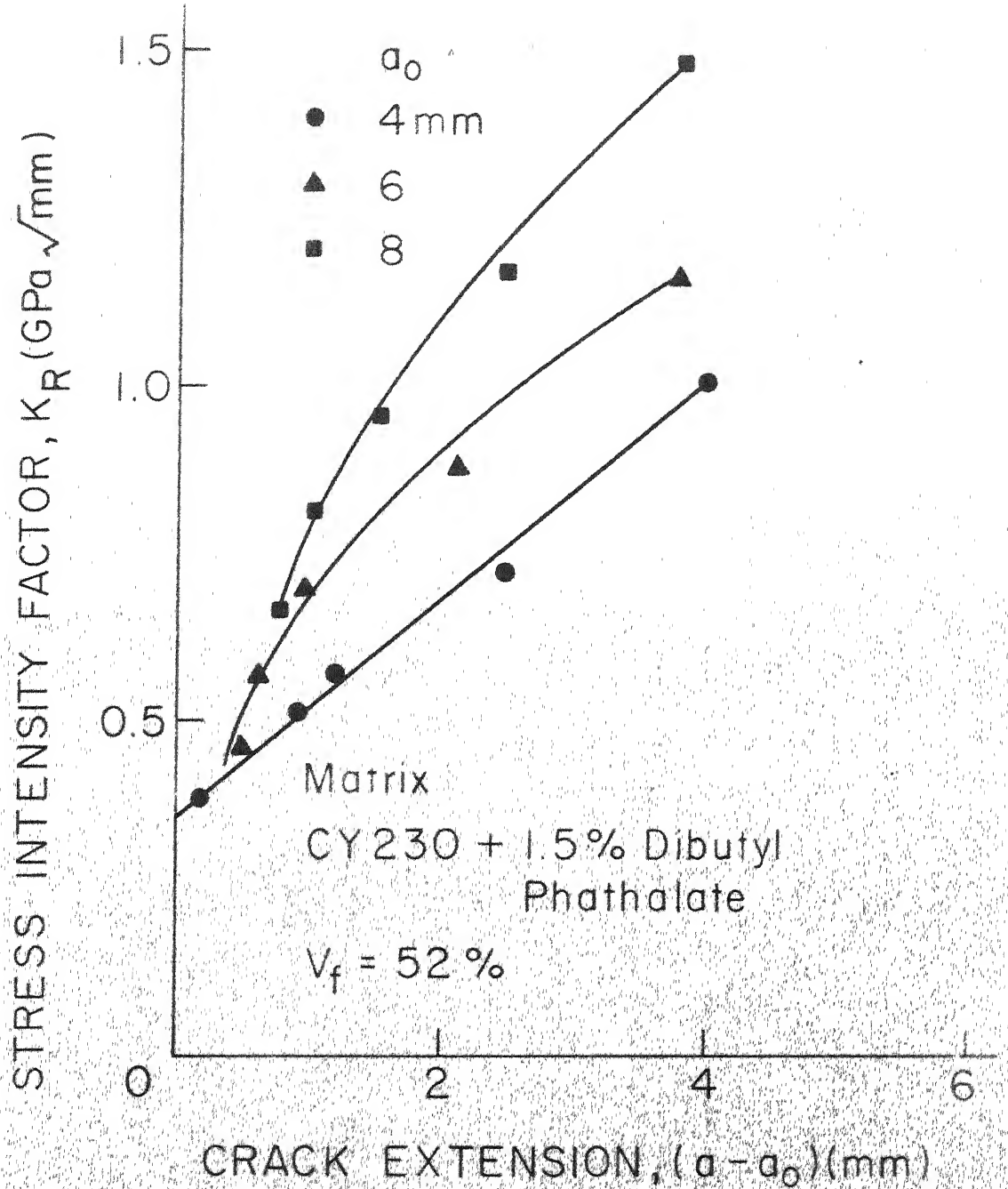

FIG. 78 VARIATION OF CRACK GROWTH RESISTANCE WITH CRACK EXTENSION (MATRIX CY230 + 1.5% DIBUTYL-PHATHALATE, V_f = 52%)

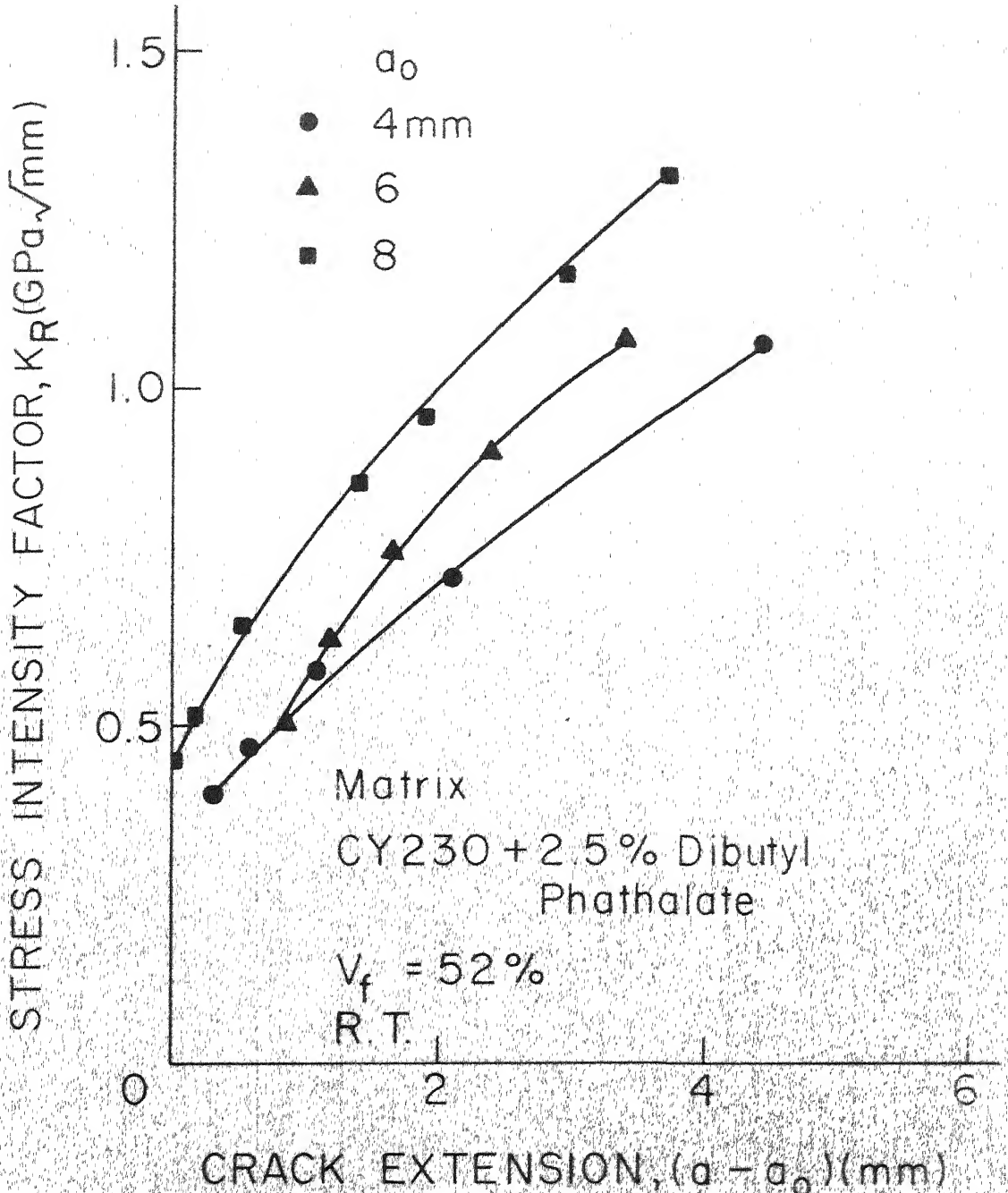

IG.79 VARIATION OF CRACK GROWTH RESISTANCE WITH CRACK EXTEN (MATRIX: CY 230 + 2.5% DIBUTYL PHATHALATE, V_f = 52%)

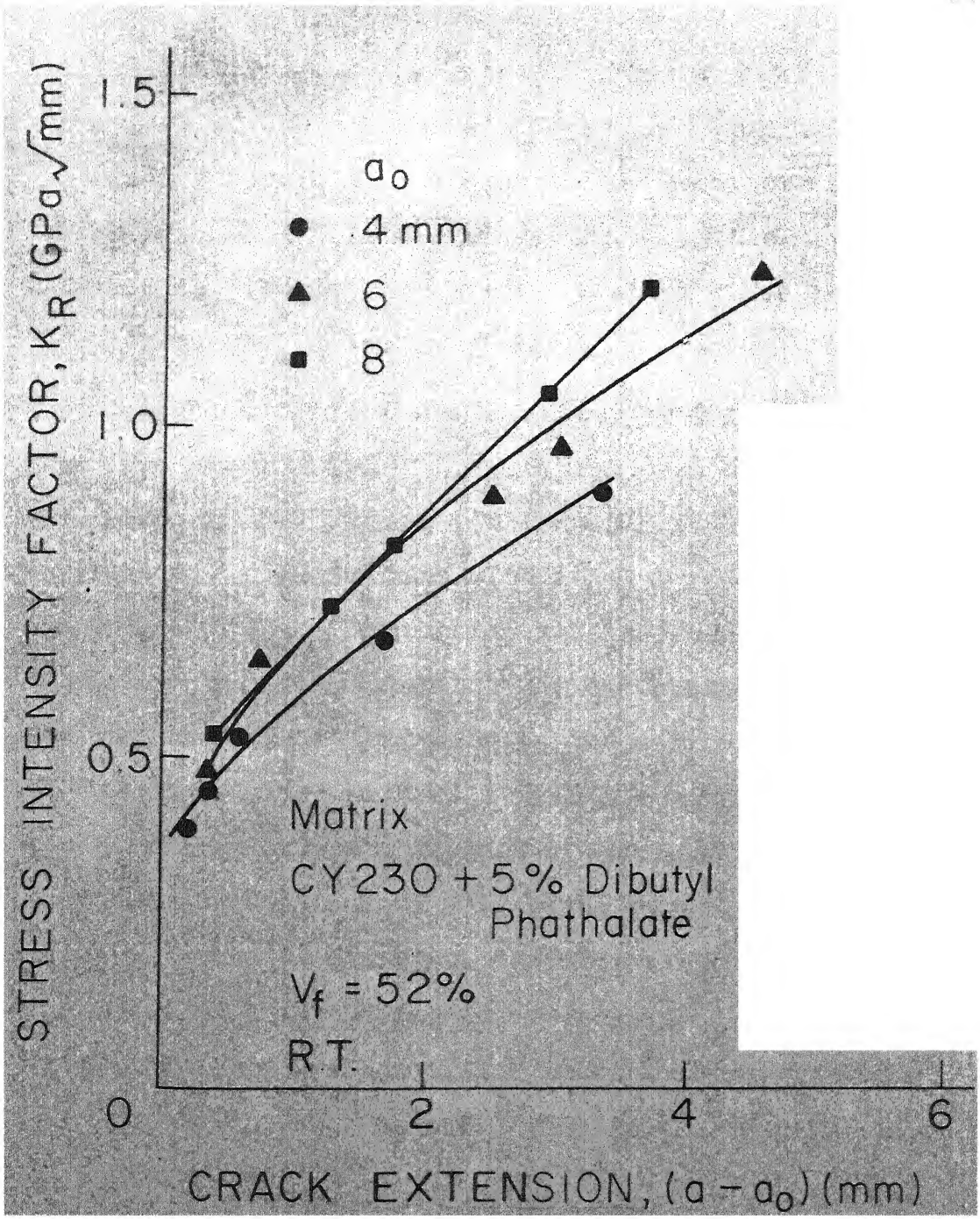

FIG. 80 VARIATION OF CRACK GROWTH RESISTANCE WITH CRACK EXTENSION (MATRIX CY230 + 5% DIBUTYL-PHATHALATE, V_f = 52%)

brittle material as indicated in Table 4 and Fig. 61. The behaviour of composites with CY 230 and modified CY 230 as the matrix material is closer to the behaviour of the composites with LY 553 as the matrix in which the crack growth resistance does depend upon the initial crack length as has been discussed in Section 3.2.

The stress intensity factor at instability, $K_{R(ins)}$, for composites with LY 553 and LY 556 as the matrix materials are given in Table 5 and plotted in Fig. 81. For both composites $K_{R(ins)}$ increases with initial crack length, although the value of $K_{R(ins)}$ and also its increase with the initial crack length are smaller for the composites with LY 556 as the matrix material compared to the corresponding values for the composites with LY 553 as the matrix material. The stress intensity factor at instability, $K_{R(ins)}$, for composites LY 553 and CY 230 as the matrix materials (V_f = 52 percent) are given in Table 6 and plotted in Fig. 82. For these composites also the $K_{R(ins)}$ increases with increasing crack length. For the composites with CY 230 as the matrix material the increase appears to be quite sharp.

The stress intensity factor at instability, $K_{R(ins)}$, is plotted against elastic modulus of the matrix and composite in Figs. 83 and 84. It is observed that the highest value of $K_{R(ins)}$ is obtained for the composite having CY 230 + 1.5 percent dibutyl-phathalate as the matrix material. The composites having CY 230 as the matrix

TABLE 5 : Stress Intensity Factor at Instability, $K_{R(ins)}$ (Mode I, V_f = 36%, Matrix, LY 553, LY 556)

Initial Crack Length a_o, (mm)	$K_{R(ins)}$, (GPa $\sqrt{mm}$)	
	Matrix	
	LY 553	LY 556
3	0.716	0.510
4	0.765	0.529
5	0.804	0.559
6	0.853	0.588
7	0.892	-
8	0.931	-

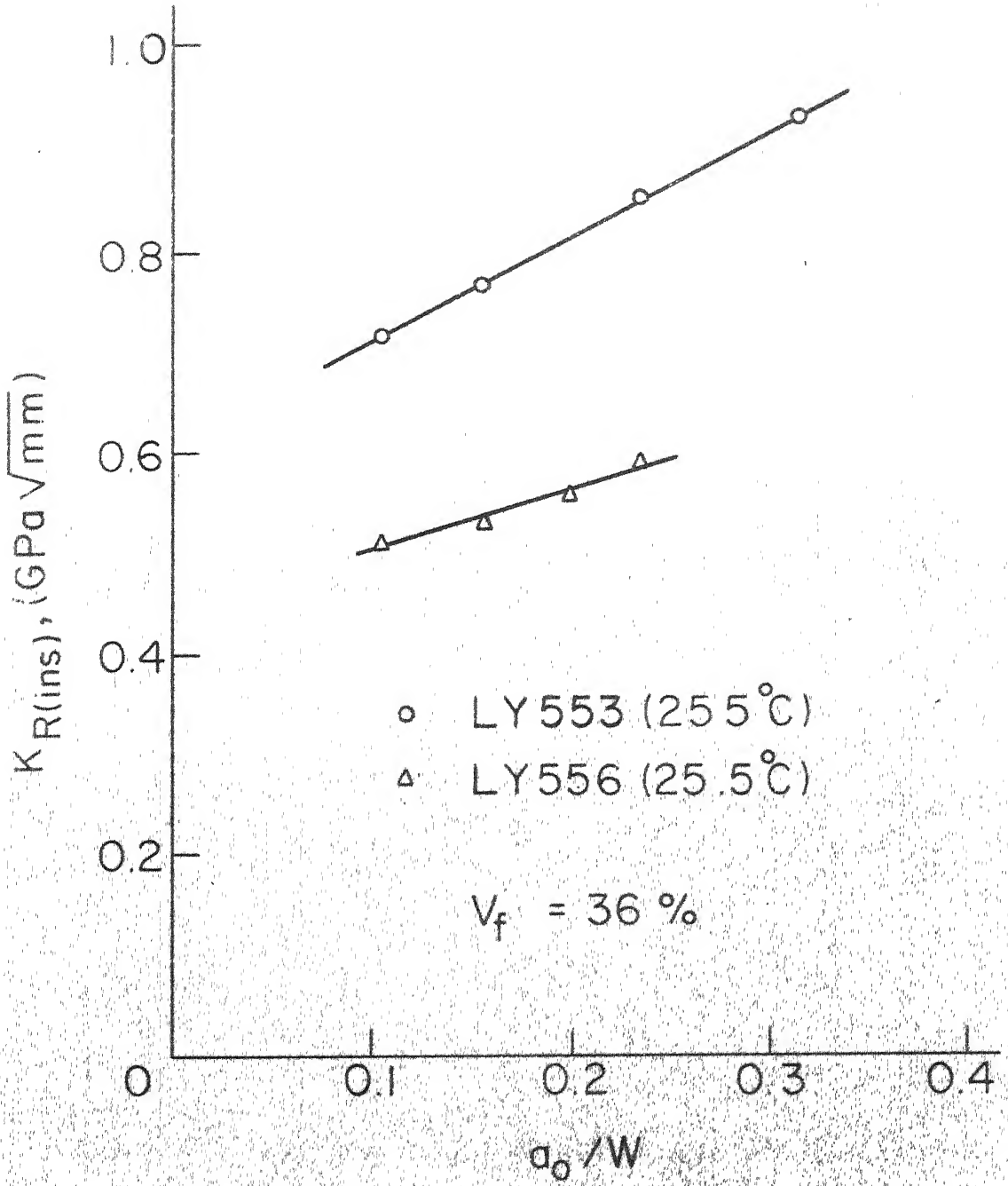

FIG. 81 VARIATION OF $K_{R(INS)}$ WITH INITIAL CRACK LENGTH (MATRIX LY 553, LY 556, V_f = 36 %)

TABLE 6 : Stress Intensity Factors at Instability, $K_{R(ins)}$ (Mode I, V_f = 52%, Matrix: LY 553, CY 230 and Modified CY 230).

Initial Crack Length a_o, (mm)	$K_{R(ins)}$, (GPa $\sqrt{mm}$)				
	Matrix				
	LY 553	CY 230	CY 230 + DBP*(1.5%)	CY 230 + DBP*(2.5%)	CY 230 + DBP*(5%)
4	0.755	0.833	0.981	0.882	0.833
6	0.922	1.030	1.128	1.010	1.039
8	0.892	1.177	1.324	1.137	1.147

* DBP = Dibutyl Phathalate

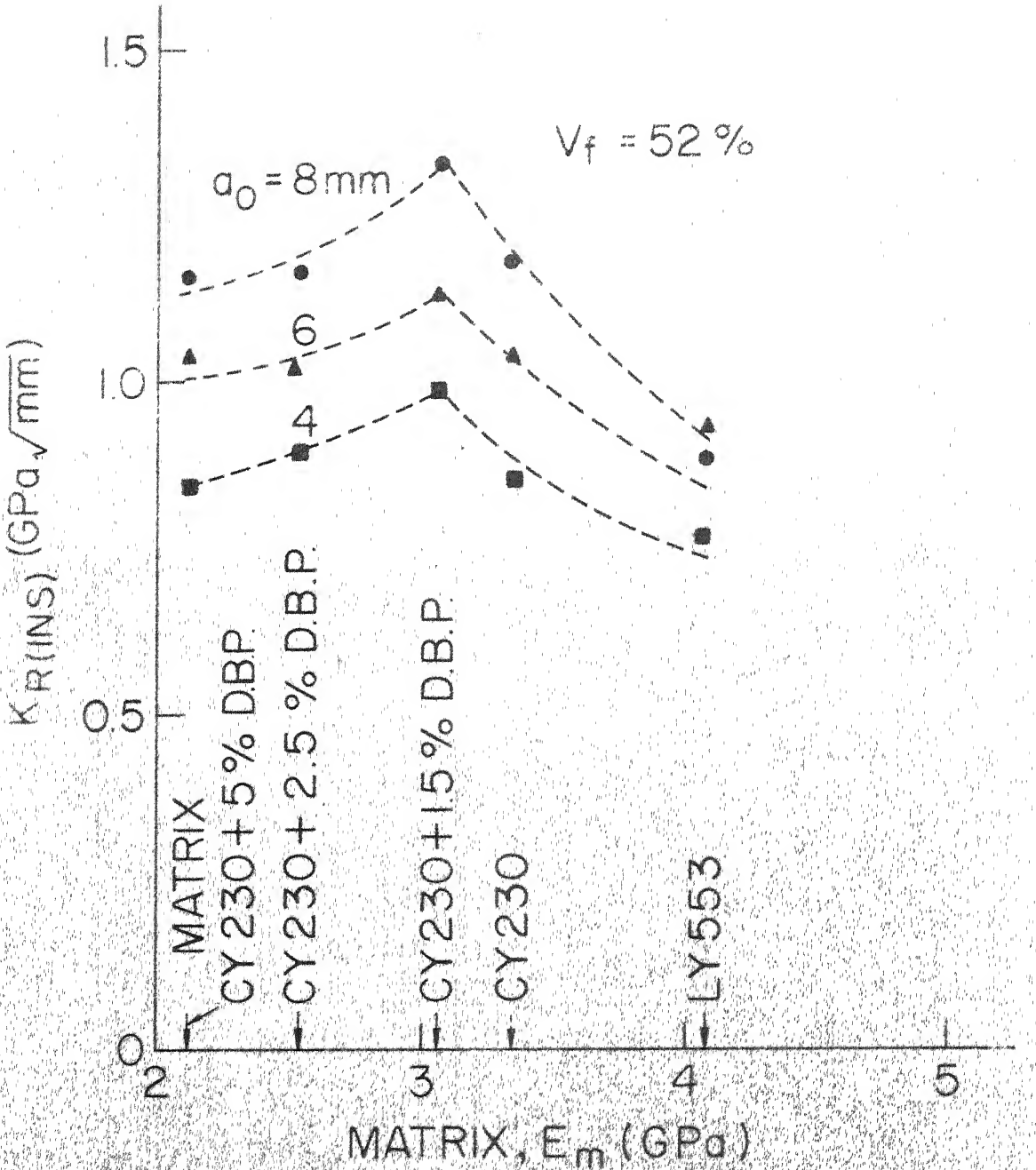

FIG 83 VARIATION OF $K_{R(INS)}$ WITH MODULUS OF MATRIX (V_f = 52 %)

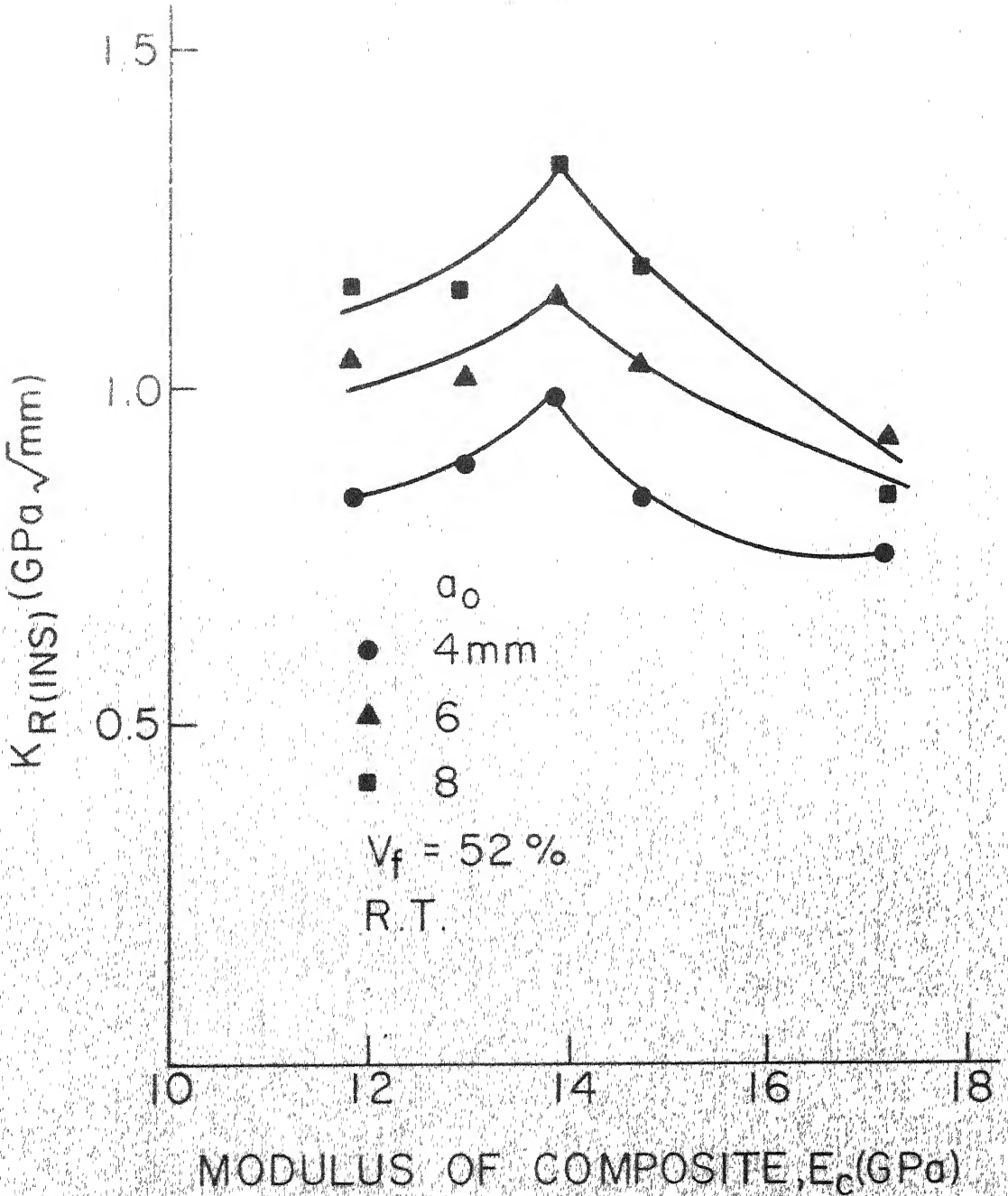

FIG. 84 VARIATION OF $K_{R(INS)}$ WITH MODULUS OF COMPOSITE (V_f = 52%)

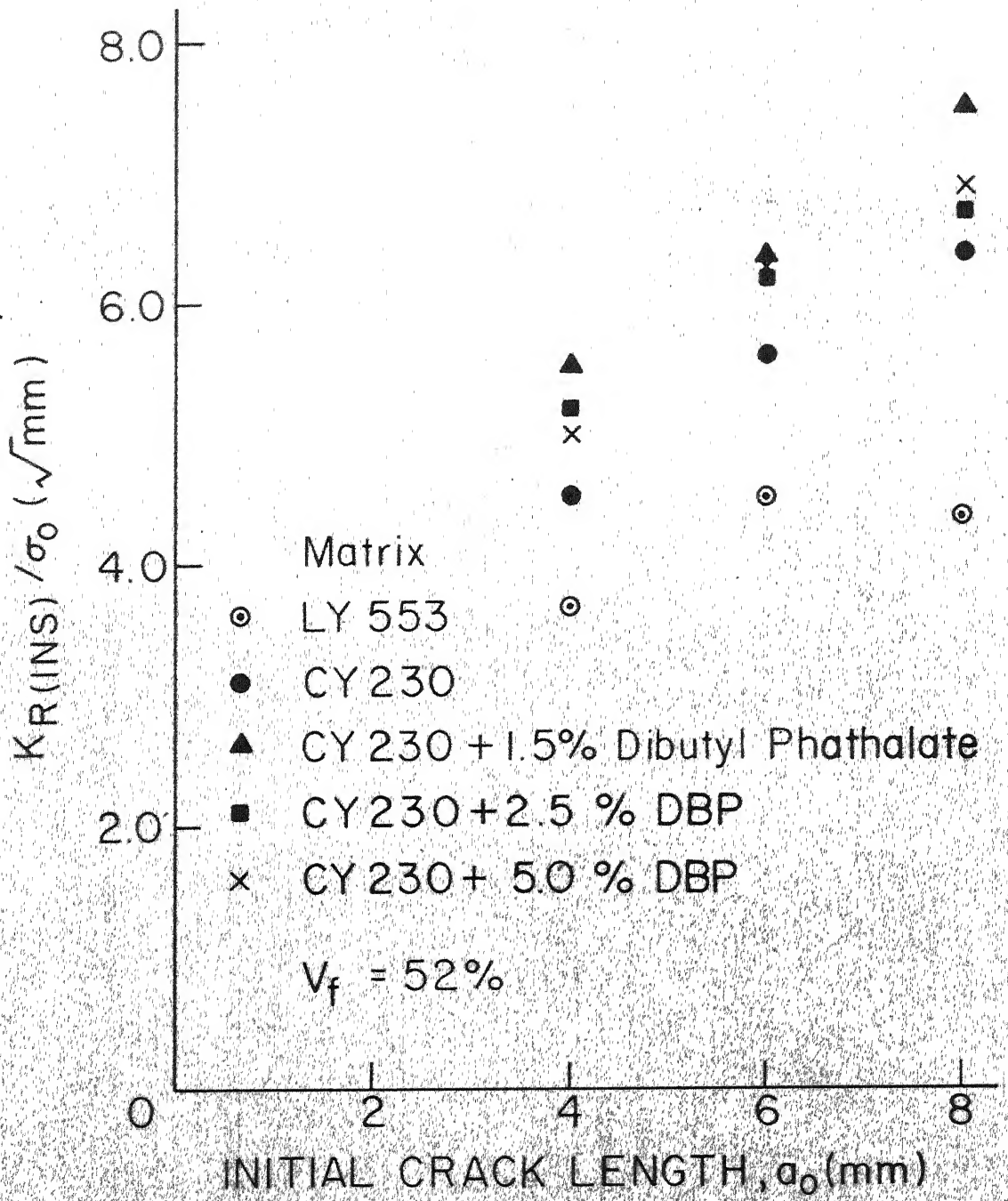

FIG. 85 VARIATION OF FRACTURE TOUGHNESS PERFORMANCE FACTOR ($K_{R(INS)}/\sigma_0$) WITH INITIAL CRACK LENGTH (V_f = 52%

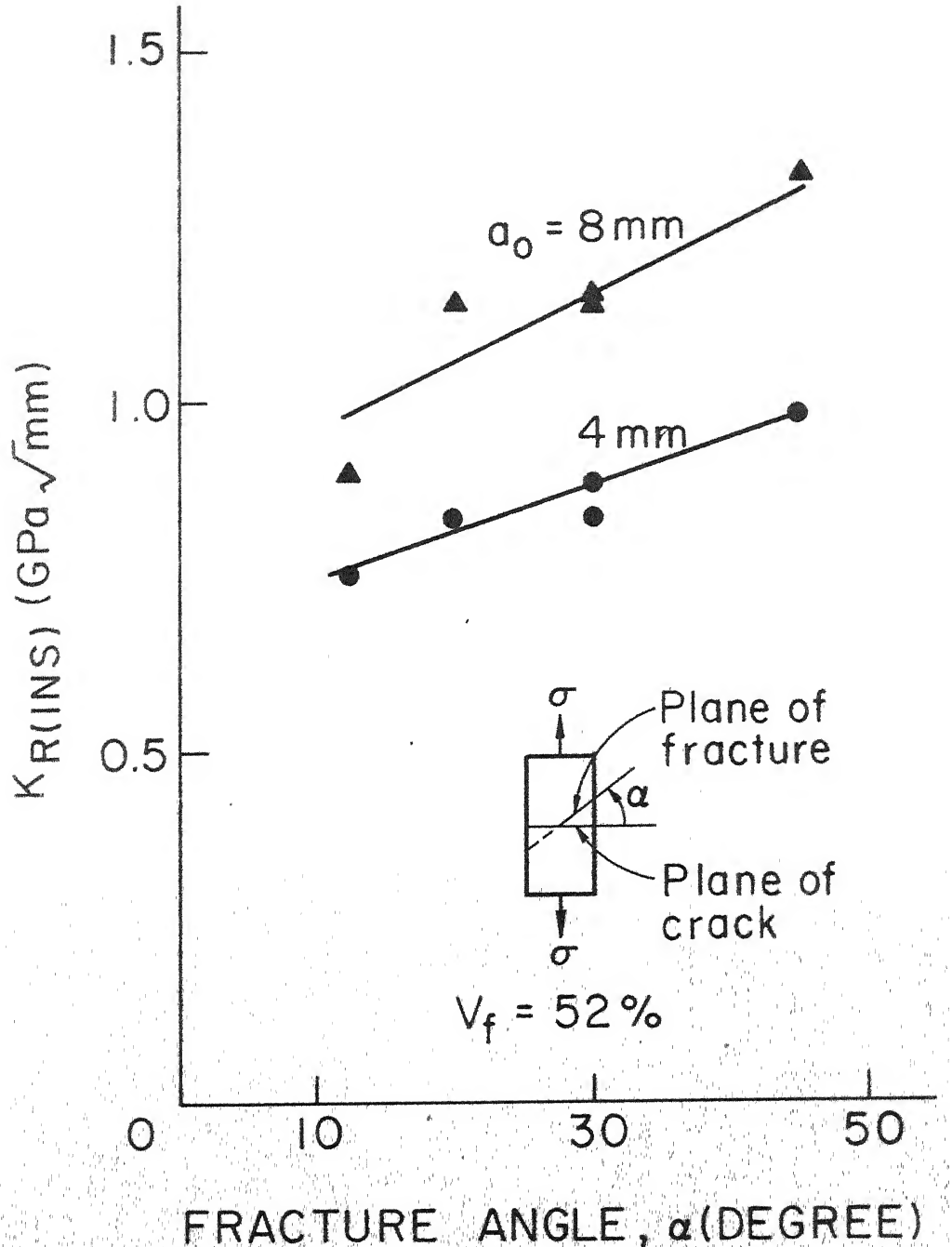

FIG. 86 VARIATION OF $K_{R(INS)}$ WITH FRACTURE ANGLE

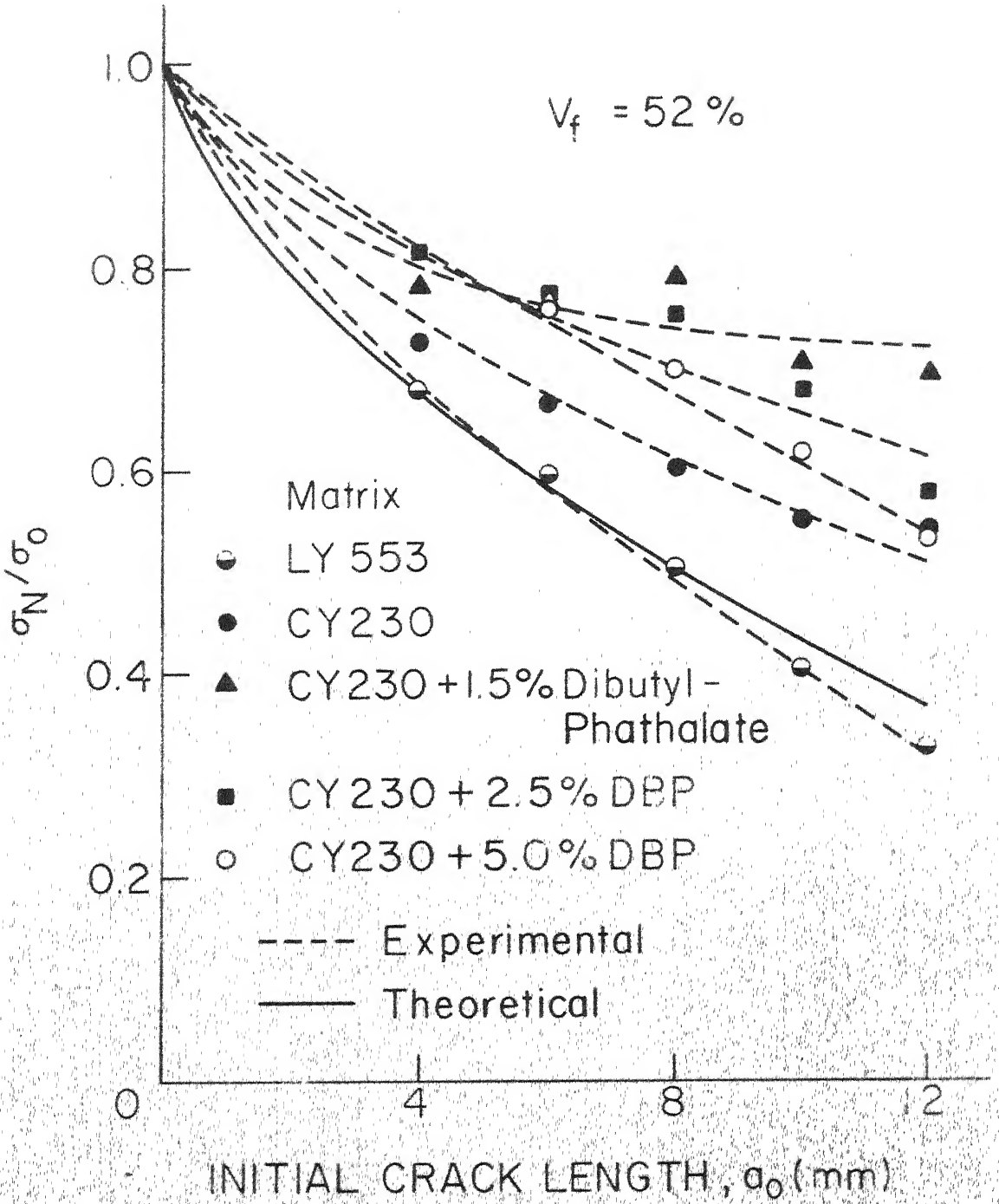

FIG. 87 VARIATION OF NORMALISED NOTCHED STRENGTH WITH INITIAL CRACK LENGTH FOR COMPOSITE WITH DIFFERENT MATRIX MATERIALS

notched strength as predicted by Whitney - Nuismer point stress criterion (Eq. 3). It is observed that for the composite having LY 553 as the matrix, theoretical values of notched strength are in good agreement. However, for the composites having CY 230 and modified as matrix material the experimental notched strength is greater than theoretically predicted. The reduced notched sensitivity of the latter composites can be attributed to the fact that the matrix material in them are more ductile and have a lower elastic modulus (Table 4).

CHAPTER 4

RESULTS AND DISCUSSION ON TESTS IN MODE II AND MODE III

4.1 INTRODUCTION

Fracture toughness tests in shear modes (Mode II and Mode III) are not important for homogeneous and isotropic materials such as metals, because in such materials the loading condition associated with the extension mode of crack propogation is most critical. However, this may not be so for fibrous composites which are generally weak in shear. It was therefore decided to investigate the fracture toughness of short fibre composites in forward shear (Mode II) and anti-plane shear (Mode III) in addition to that in extension mode (Mode I). The testing system and special loading fixtures used for the tests in Mode II and Mode III have been described in Chapter 2. The results and discussion on tests in Mode II and Mode III are described in this chapter.

4.2 CALIBRATION FACTOR FOR MODE II

Consider the single edge notched specimen shown in Fig. 88 loaded to produce forward shear at the crack tip. The Mode II stress intensity factor at the crack tip can be written in the form

$$K_{II} = X \tau \sqrt{a} \qquad (5)$$

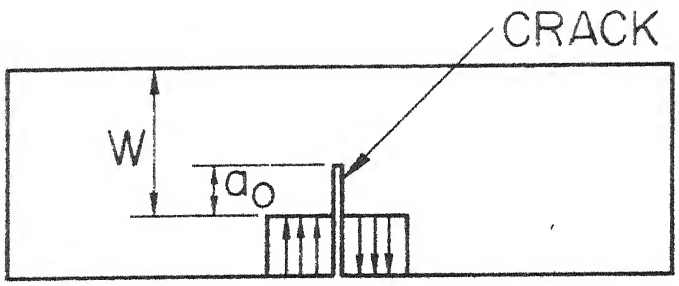

FIG.88 LOADING CONDITION OF SPECIMEN IN MODE II

where X = Mode II calibration factor,

$= \frac{S}{tW}$ = nominal shear stress,

S = applied shear force,

t = specimen thickness,

W = specimen width,

a = crack length.

The calibration factor, X, is incorporated in Eq. (5) to account for the finite width of the specimens and depends upon the ratio of crack length to specimen width ($\frac{a}{W}$). In the absence of any information concerning the nature of X, it was first obtained experimentally through compliance measurement procedure as suggested in reference [28]. In this calibration procedure a set of compliance measurement is made on the specimens with different crack lengths. The range of crack length is selected such that it covers the entire range of crack length to be used in the fracture toughness tests. Details of the procedure along with the results are described in the following paragraphs.

The shear load versus displacement (relative displacement of the crack lips in the plane of the crack) curves are shown in Fig. 89. The initial compliance obtained from these curves is plotted against ($\frac{a_o}{W}$) in Fig. 90. The nondimensionalised compliance ($\frac{E}{S}\frac{t\delta}{}$) is plotted against ($\frac{a_o}{W}$) in Fig. 91. The solid curve in Fig. 91 is the best fit curve obtained by a simple computor analysis and is given by

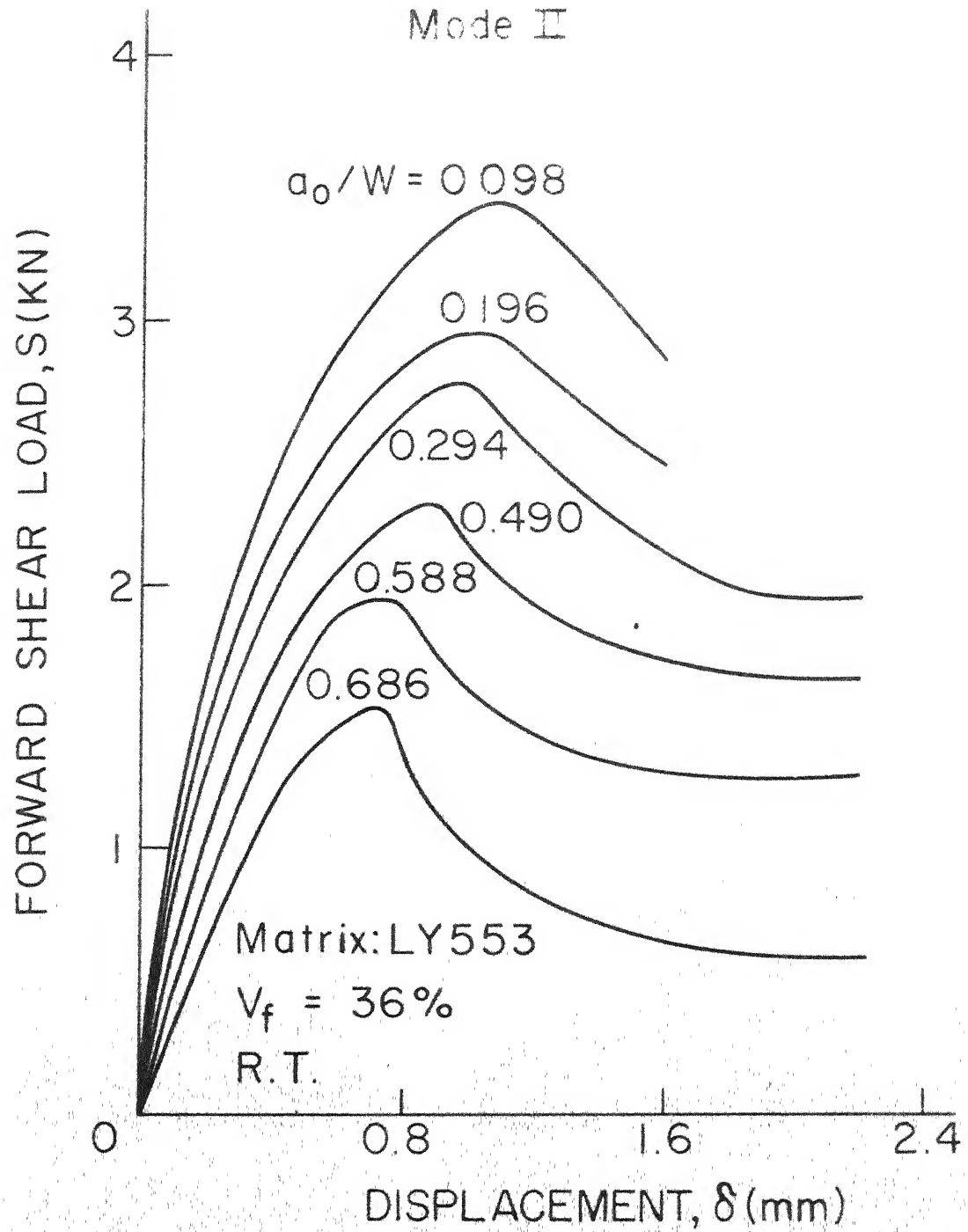

FIG. 89 LOAD VERSUS DISPLACEMENT CURVES (MODE II)

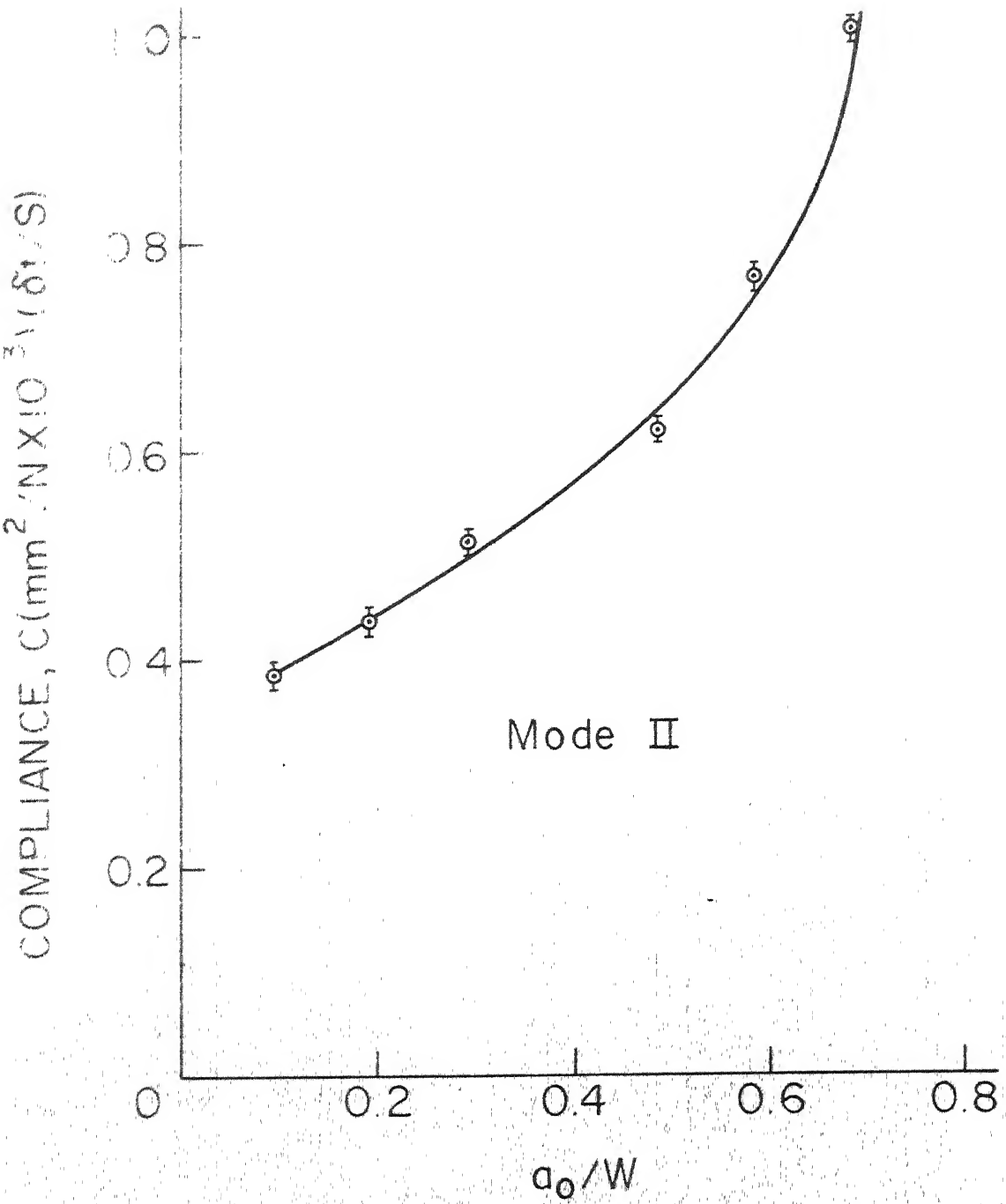

FIG. 90 COMPLIANCE CURVE FOR MODE II

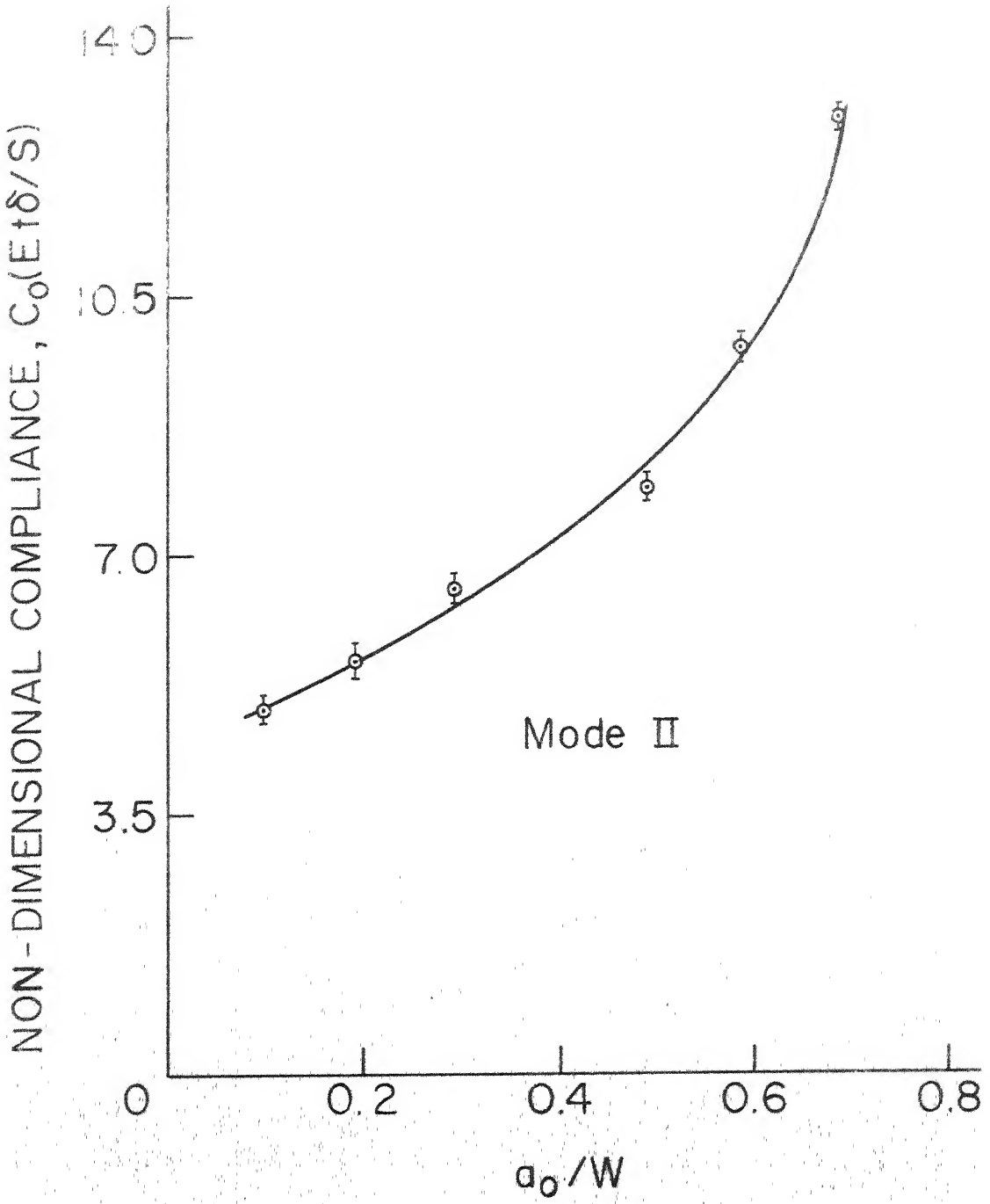

FIG. 91 VARIATION OF NON-DIMENSIONAL COMPLIANCE ($E t \delta / S$) WITH INITIAL CRACK LENGTH (MODE II)

$$\frac{E\,t\,\delta}{S} = 4.24818 + 5.8200\,(a/W) + 3.9869\,(a/W)^2 + 1.8203\,(a/W)^3 + 0.6232\,(a/W)^4 + 6.28\,(a/W)^5 \quad (6)$$

It can be easily shown [28] that

$$\frac{d\left(\frac{E\,t\,\delta}{S}\right)}{d\left(\frac{a}{W}\right)} = \frac{2\,E\,G_{II}\,t^2\,W}{S^2} \quad (7)$$

where G_{II} is the strain energy release rate for the Mode II deformation in the plane stress condition and is related to K_{II} through the following equation [29] :

$$G_{II} = \frac{K_{II}^2}{E} \quad (8)$$

Substituting Eq. (8) in Eq. (7) and rearranging the terms yields

$$K_{II} = \frac{S}{tW}\sqrt{a}\,\sqrt{\frac{1}{2}\,\frac{d\left(\frac{E\,t\,\delta}{S}\right)}{d\left(\frac{a}{W}\right)} \Big/ \frac{a}{W}} \quad (9)$$

Comparison of Eq. (9) with Eq. (5) gives

$$X = \sqrt{\frac{1}{2}\,\frac{d\left(\frac{E\,t\,\delta}{S}\right)}{d\left(\frac{a}{W}\right)} \Big/ \frac{a}{W}} \quad (10)$$

The calibration factor, X, is obtained by evaluating the right hand side of Eq. (10) using Eq. (6). The calibration factor X, thus obtained is plotted against $\frac{a_o}{W}$ in Fig. 92. The following polynomial is the best fit to the Mode II calibration factor shown in Fig. 92.:

$$X = 6.1387 - 7.6700\,(a/W) + 4.7912\,(a/W)^2 - 1.9953\,(a/W)^3 + 3.152\,(a/W)^4 \quad (11)$$

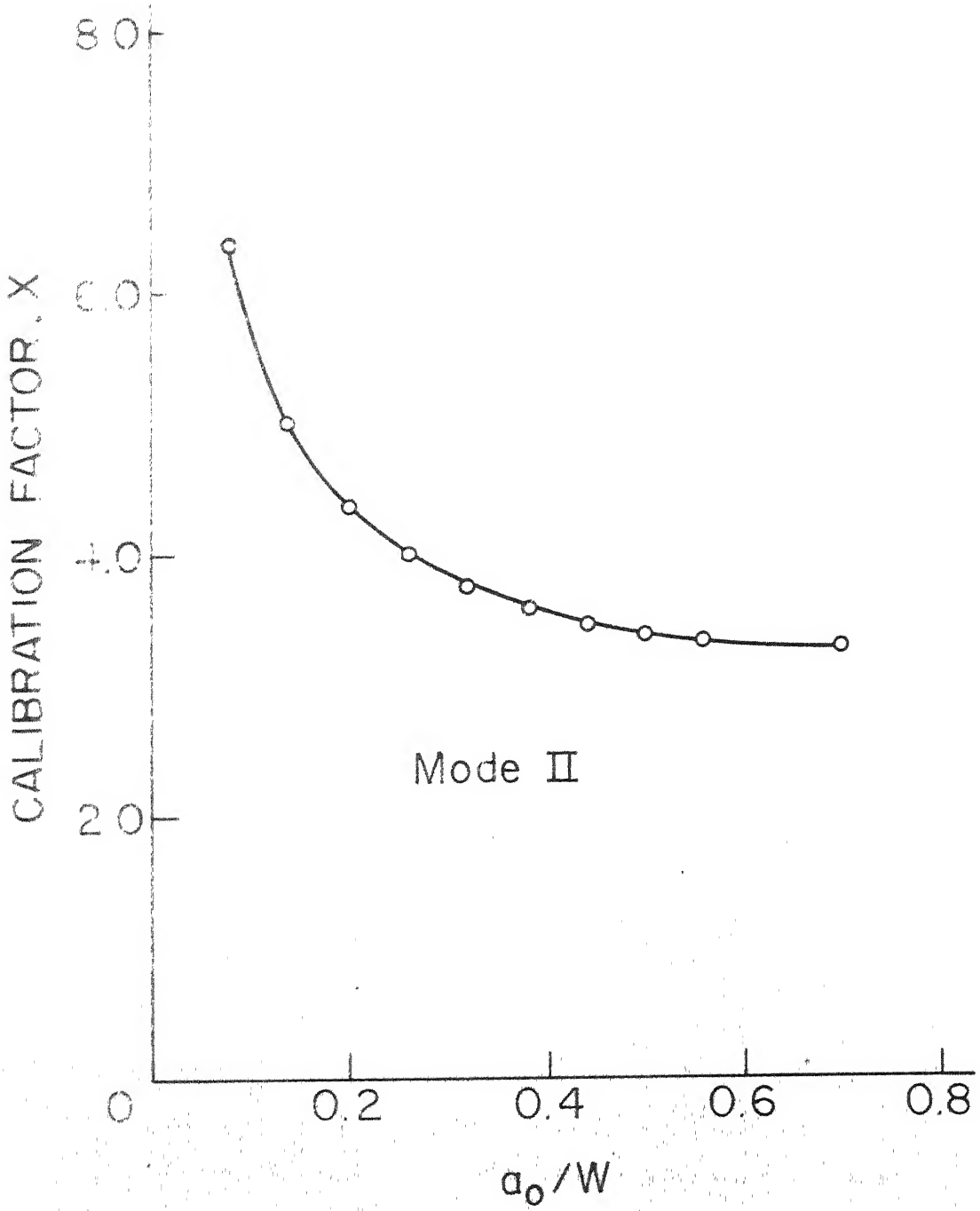

FIG. 92 . VARIATION OF CALIBRATION FACTOR, X, WITH INITIAL CRACK LENGTH (MODE II)

This calibration factor has been used to calculate K_{II} and to construct resistance curves.

4.3 CALIBRATION FACTOR FOR MODE III

Consider the single edge notched specimen shown in Fig. 93 loaded to produce out-of-plane shear at the crack tip. The Mode III stress intensity factor at the crack tip can be written as

$$K_{III} = Z \tau \sqrt{a} \qquad (12)$$

where Z = Mode III calibration factor

$\tau = \frac{F}{tW}$ = nominal shear stress

F = applied out-of-plane shear force

t = specimen thickness

W = specimen width

a = crack length.

The Mode III calibration factor, Z, like those in Modes I and II, is incorporated in Eq. (12) to account for the finite width of the specimens and depends upon the ratio of crack length to specimen width ($\frac{a}{W}$). A procedure, similar to the one used for obtaining Mode II calibration factor, X, has been used to obtain the Mode III calibration factor Z. The details follow in the following paragraphs.

The shear load versus displacement (relative displacement of the crack lips measured perpendicular to the plane of the specimen and parallel to the crack front)

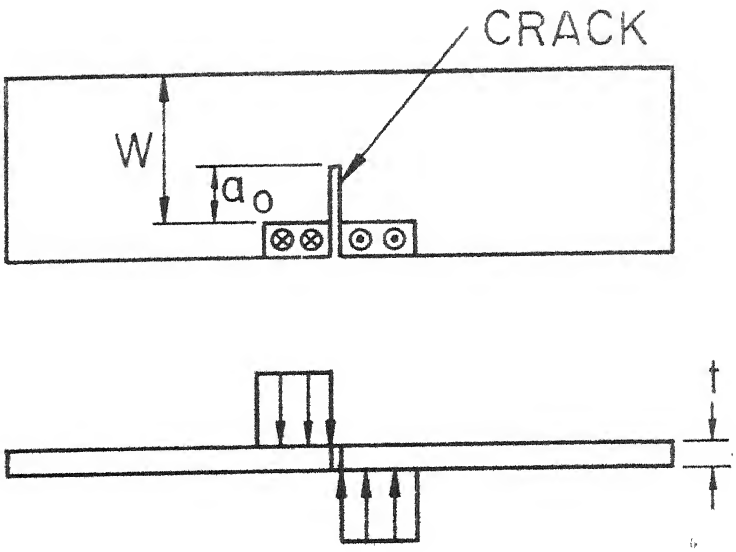

FIG. 93 LOADING CONDITION OF SPECIMEN IN MODE III

curves are shown in Fig. 94. The initial compliance obtained from these curves is plotted against ($\frac{a_o}{W}$) in Fig. 95. The non-dimensionalised compliance ($\frac{G\,t\,\delta}{F}$) is plotted against ($\frac{a_o}{W}$) in Fig. 96. The solid curve in Fig. 96 is the best fit curve obtained by a simple computer analysis and is given by

$$\frac{Gt\delta}{F} = 21.828 + 63.861\ (a/W) + 93.416\ (a/W)^2 + 91.100\ (a/W)^3 + 66.630\ (a/W)^4 + 38.986\ (a/W)^5 \qquad (13)$$

It can be easily shown [28] that

$$\frac{d\left(\frac{G\,t\,\delta}{F}\right)}{d\left(\frac{a}{W}\right)} - \frac{2\,G\,G_{III}\,t^2\,W}{F^2} \qquad (14)$$

where G_{III} is strain energy release rate for the Mode III deformation in the plane stress condition and is related to K_{III} through the following equation [29]

$$G_{III} = \frac{K_{III}^2}{2\,G} \qquad (15)$$

where G = shear modulus of composite.

Substituting Eq. (15) in Eq. (14) and rearranging the terms yields

$$K_{III} = \frac{F}{tW}\sqrt{a}\sqrt{\frac{d\left(\frac{G\,t\,\delta}{F}\right)}{d\left(\frac{a}{W}\right)} \Big/ \frac{a}{W}} \qquad (16)$$

Comparison of Eq. (16) with Eq. (12) gives

$$Z = \sqrt{\frac{d\left(\frac{G\,t\,\delta}{F}\right)}{d\left(\frac{a}{W}\right)} \Big/ \frac{a}{W}}. \qquad (17)$$

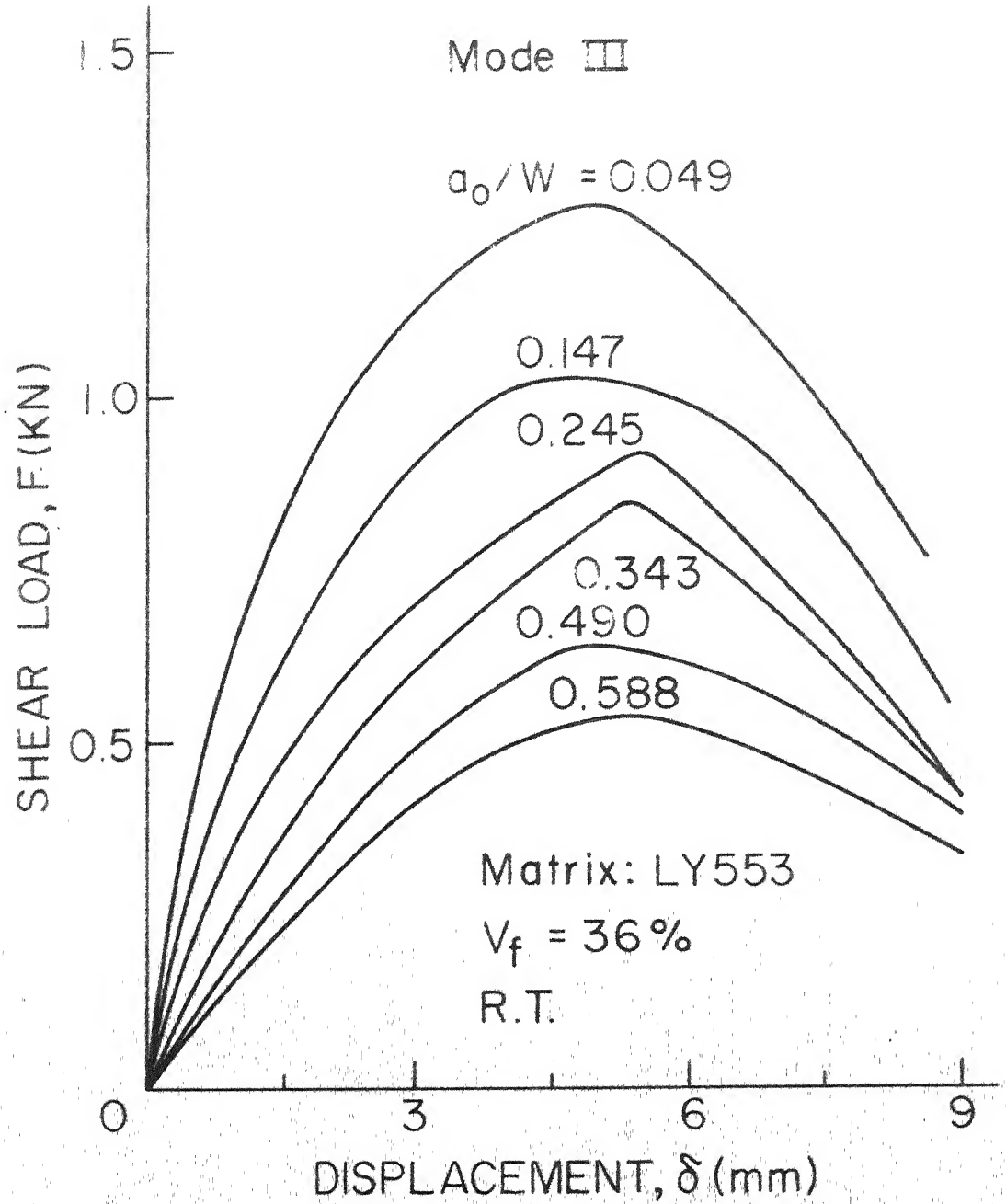

FIG.94 LOAD VERSUS DISPLACEMENT CURVES (MODE III)

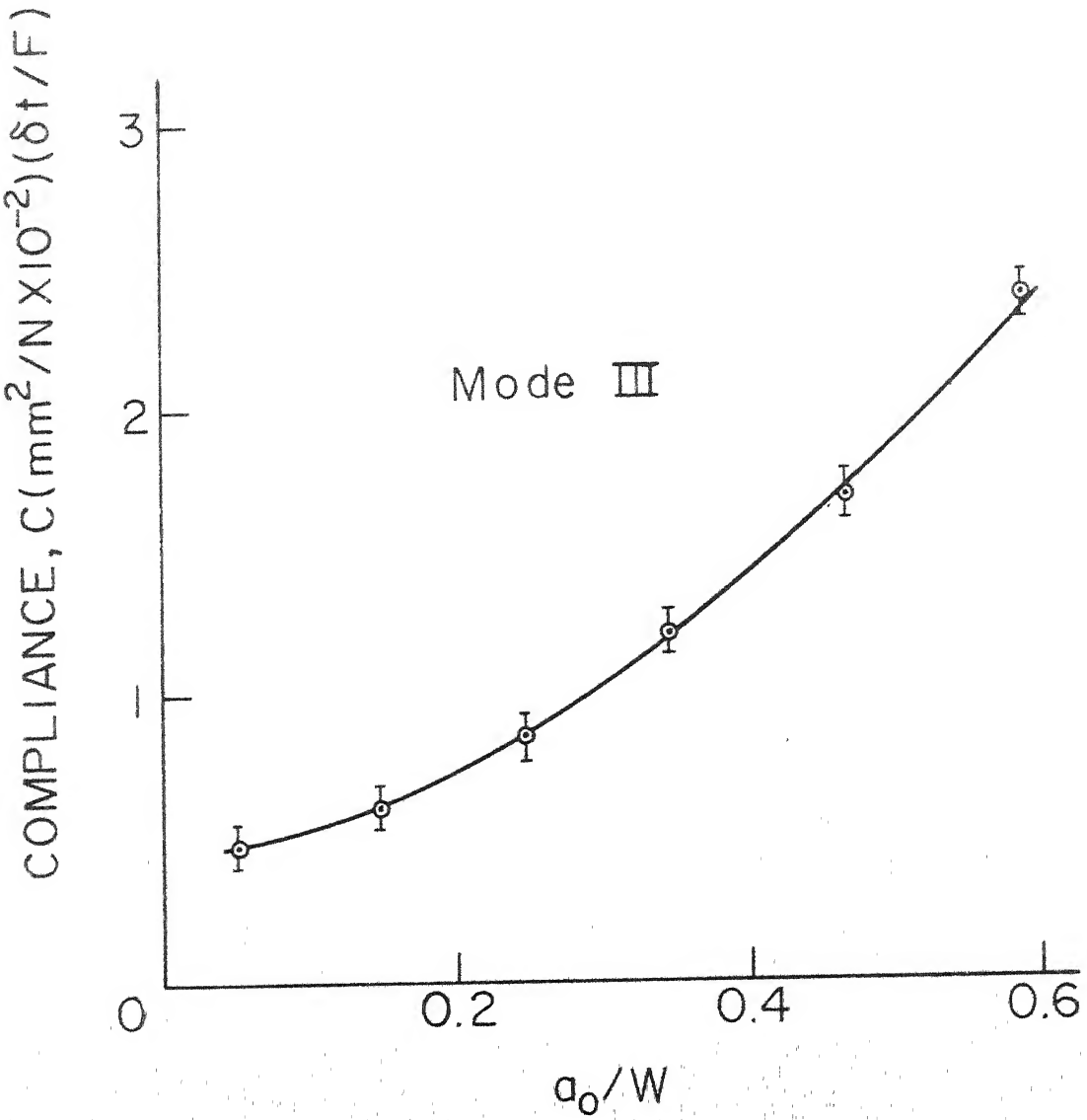

FIG. 95 COMPLIANCE CURVE FOR MODE III

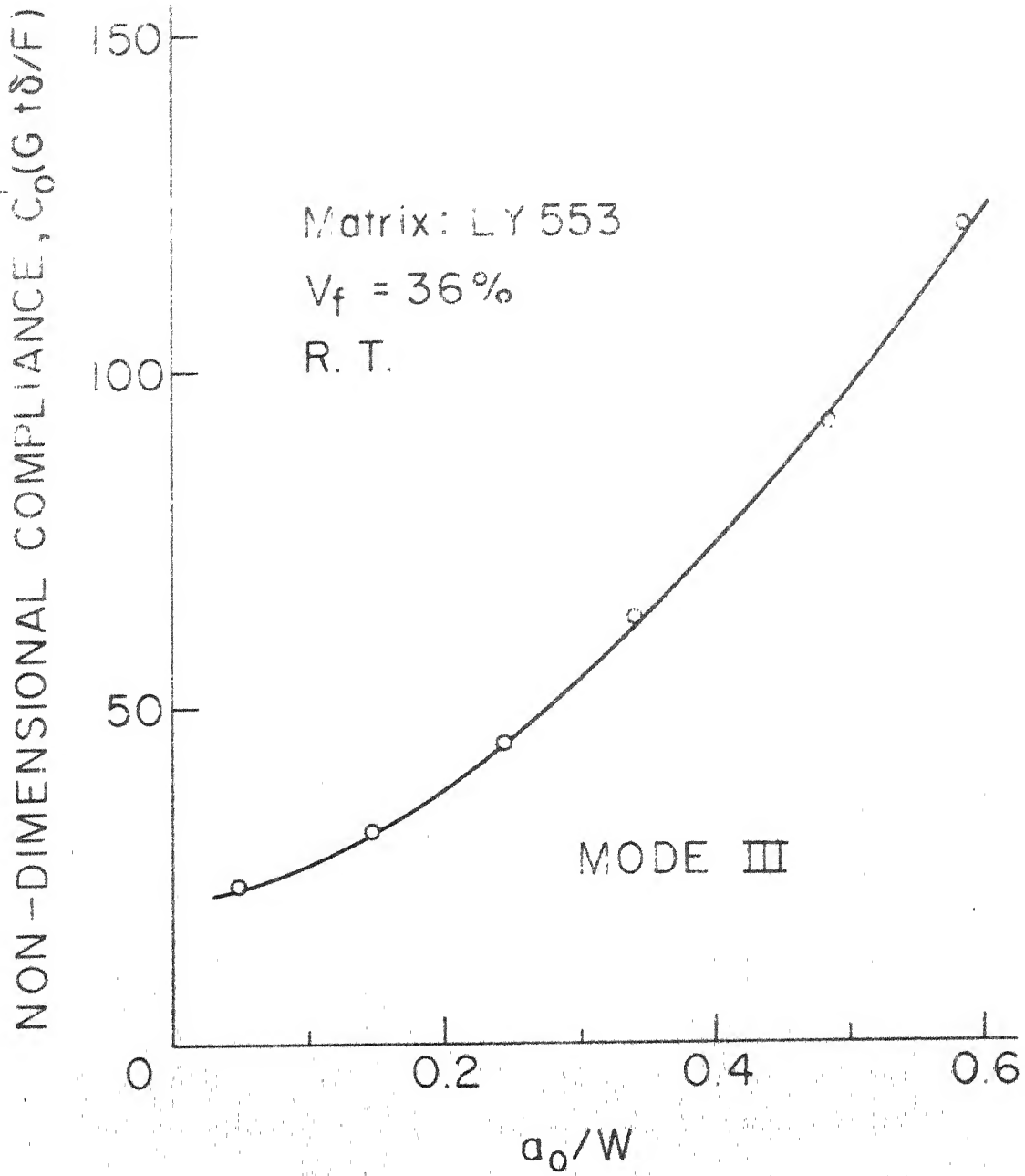

FIG. 96 VARIATION OF NON-DIMENSIONAL COMPLIANCE ($G \dagger \delta/F$) WITH INITIAL CRACK LENGTH (MODE III)

The calibration factor, Z, is obtained by evaluating the right hand side of Eq. (17) using Eq. (13). The calibration factor, Z, thus obtained is plotted against $\frac{a_o}{W}$ in Fig. 97. The following exponential curve is the best fit to the Mode III calibration factor shown in Fig. 97:

$$Z = 22.796 + 37.730\, e^{-17.586 \frac{a}{W}} \qquad (18)$$

This calibration factor has been used to calculate K_{III} and to construct resistance curves.

4.4 CRACK GROWTH RESISTANCE IN MODE II AND MODE III

Load versus displacement curves for Mode II and Mode III are shown in Figs. 89 and 94 respectively. The nature of these curves is different from that of corresponding curves for Mode I as discussed in Chapter III. In Mode I the fracture occurs at the maximum load whereas in Mode II and Mode III the load displacement curves show peak and considerable amount of damage occurs at reduced load prior to final fracture. In Mode II, first there is a sharp drop in the load beyond the peak load and then the load reduces gradually as the displacement increases. The sharp drop in load occurs due to sudden damage initiated at the crack tip. It is observed that the damage which initiates at the crack tip is not coplanar with the original crack and also does not propogate symmetrically about the plane of the crack. Typical failure paths for different initial crack length are shown through the

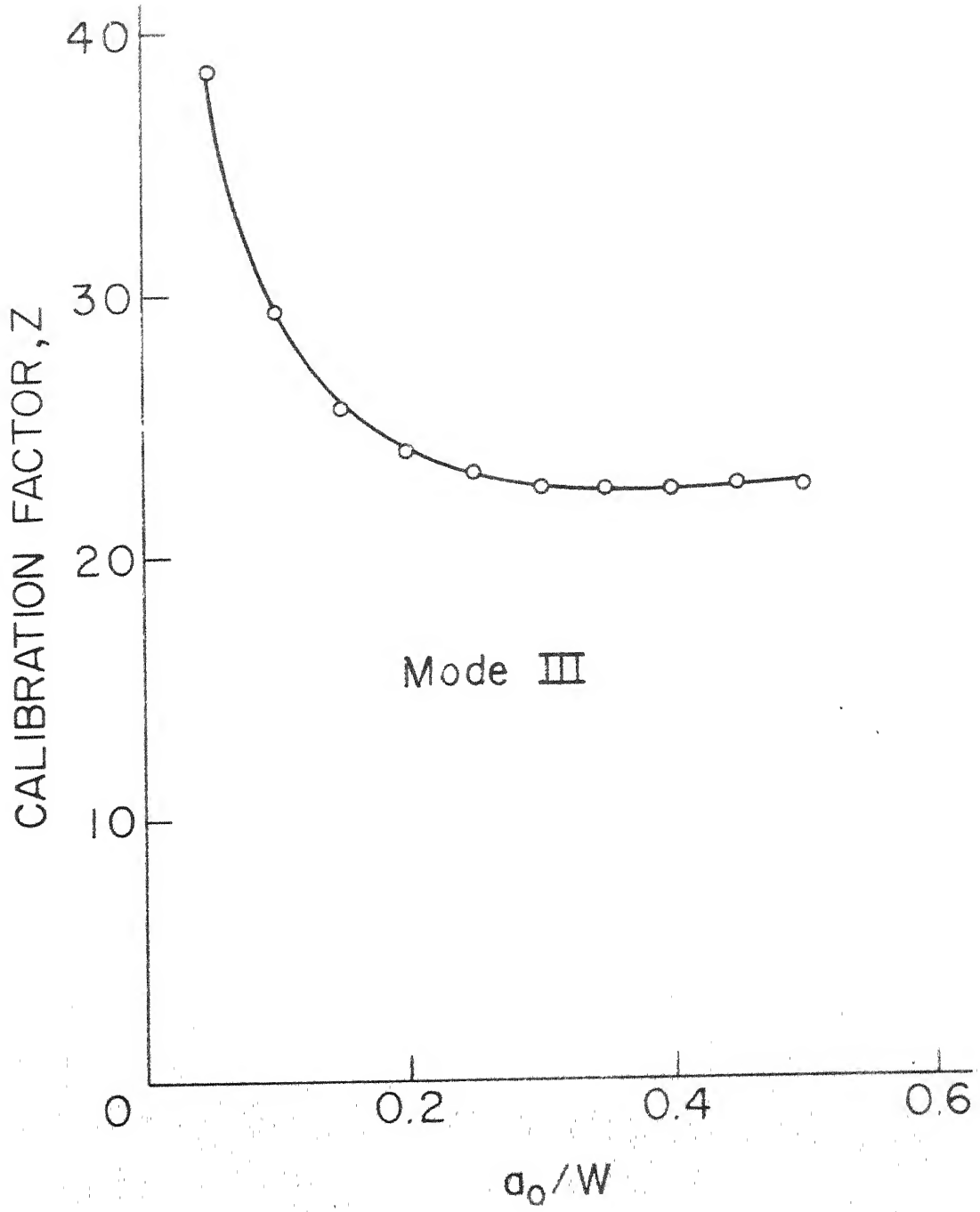

FIG. 97 VARIATION OF CALIBRATION FACTOR, Z, WITH INITIAL CRACK LENGTH (MODE III)

photograph in Fig. 98. It is also observed (Fig. 98) that there is only a very small amount of damage adjacent to the crack path resulting in lower energy absorbed. In Mode III, the reduction in load beyond the peak load is gradual and occurs due to propogation of damage. The damage occurs by debonding and fibre pull out and is generally symmetric about the plane of initial crack. Photograph of some of the specimens failed in Mode III are shown in Fig. 99.

The crack growth resistance curves (R - curves) for Mode II and Mode III are constructed for different initial crack lengths by the compliance matching procedure as illustrated for Mode I in Chapter 3. However, for Mode II and Mode III the compliance curves (Figs 90 and 95) are directly used as the crack length estimation curves. The crack growth resistance curves for Mode II and Mode III are shown in Figs. 100 and 101 respectively. The crack growth resistance at instability for Mode II ($K_{II\ R(ins)}$) and Mode III ($K_{III\ R(ins)}$) have been obtained from the R-curves through the same procedure as was adopted for Mode I in Chapter III. The $K_{II\ R(ins)}$ and $K_{III\ R(ins)}$ for different crack lengths are given in Table 7. The $K_{II\ R(ins)}$ and $K_{III\ R(ins)}$ as given in Table 7 are independent of initial crack length. This indicates that $K_{II\ R(ins)}$ and $K_{III\ R(ins)}$ may be considered material property for comparing fracture properties of composite materials. The crack growth resistance is plotted against crack extension in Figs. 102 and 103 for Mode II and Mode III respectively. It is clear

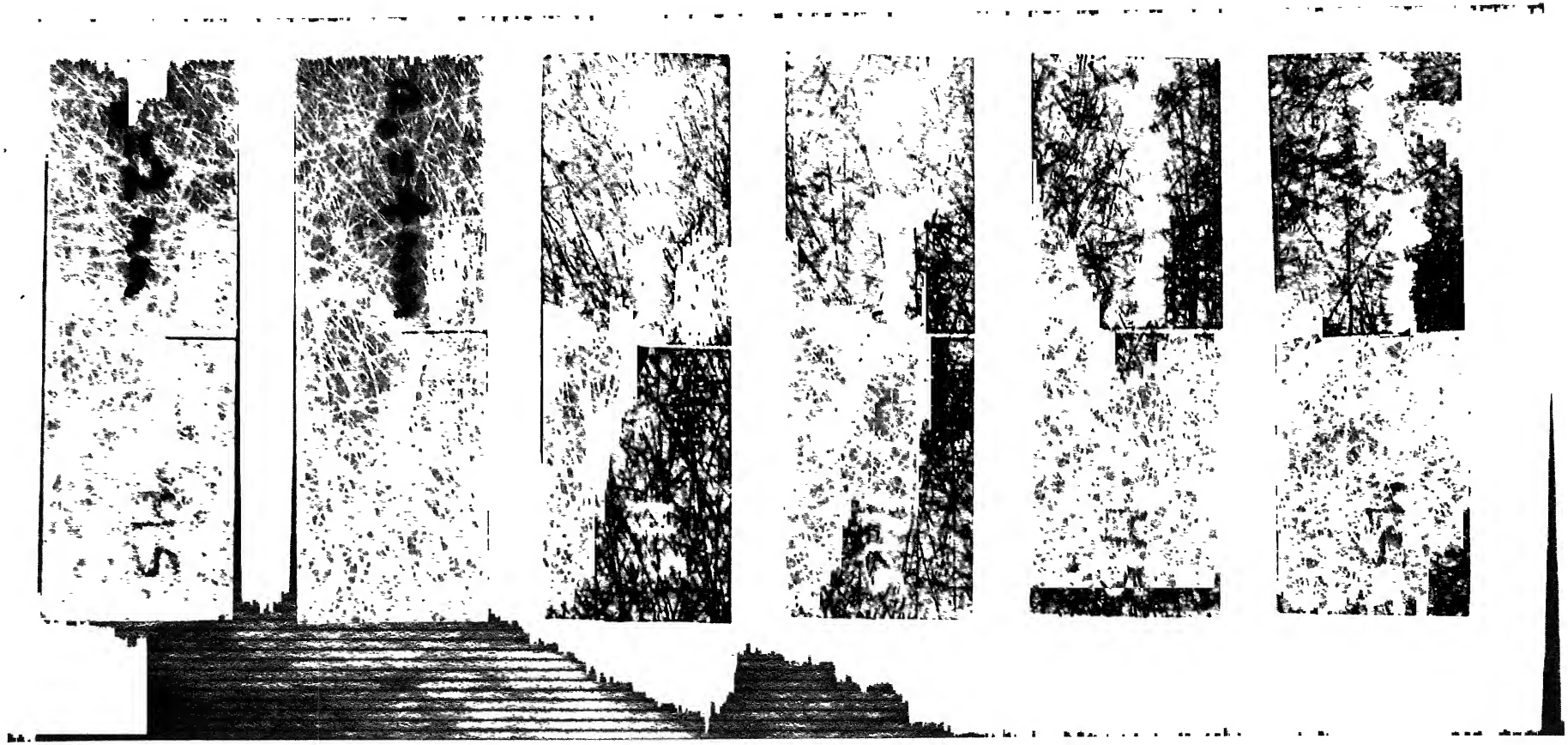

FIG. 98 PHOTOGRAPH OF SPECIMENS FAILED IN MODE II. INITIAL CRACK LENGTHS (FROM LEFT TO RIGHT) 2, 4, 6, 8, 10 AND 14mm

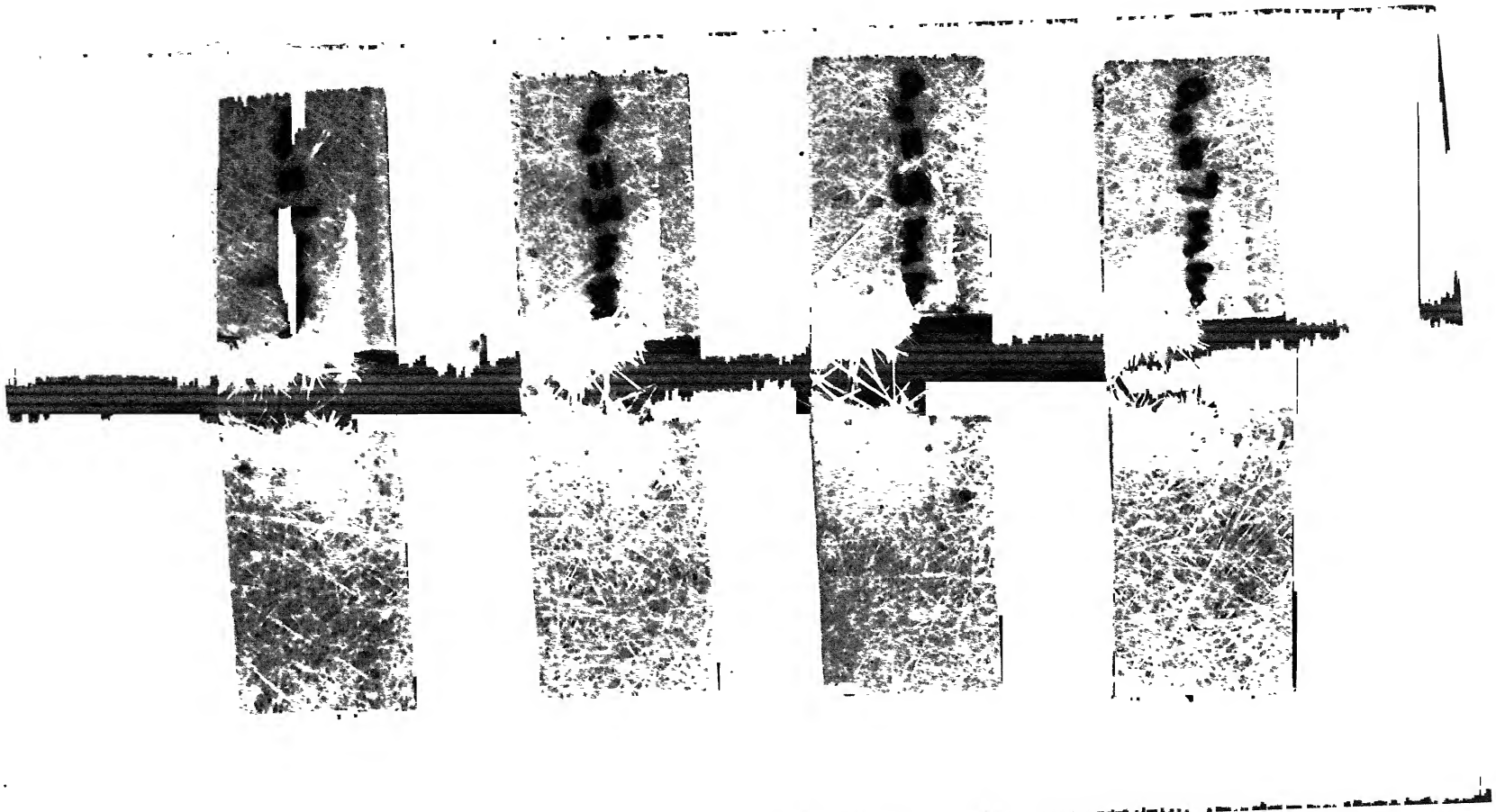

FIG. 99 PHOTOGRAPH OF SPECIMENS FAILED IN MODE III. INITIAL CRACK LENGTHS (FROM LEFT TO RIGHT) 1, 3, 5 AND 7 mm

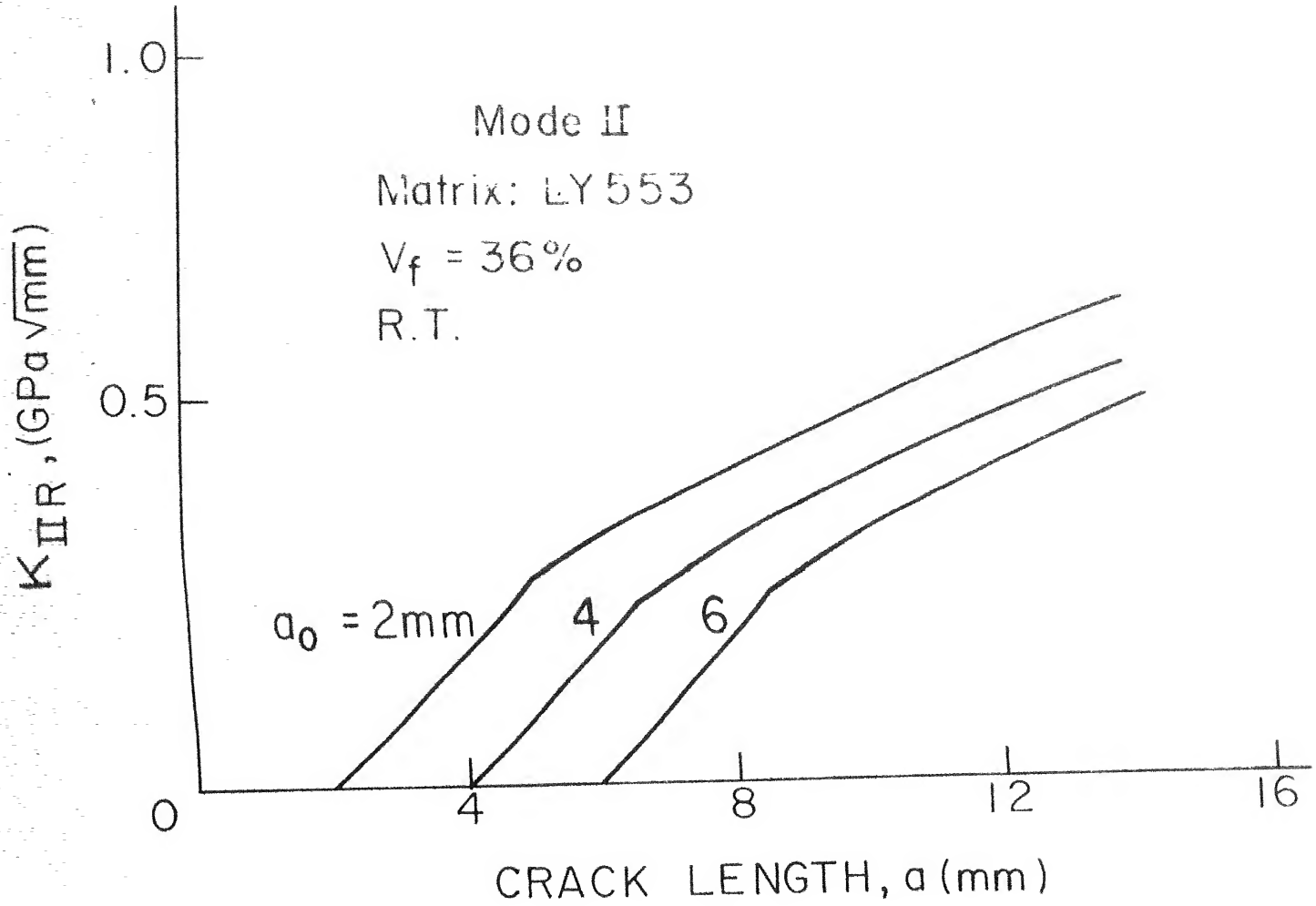

FIG. 100 R-CURVES FOR MODE II

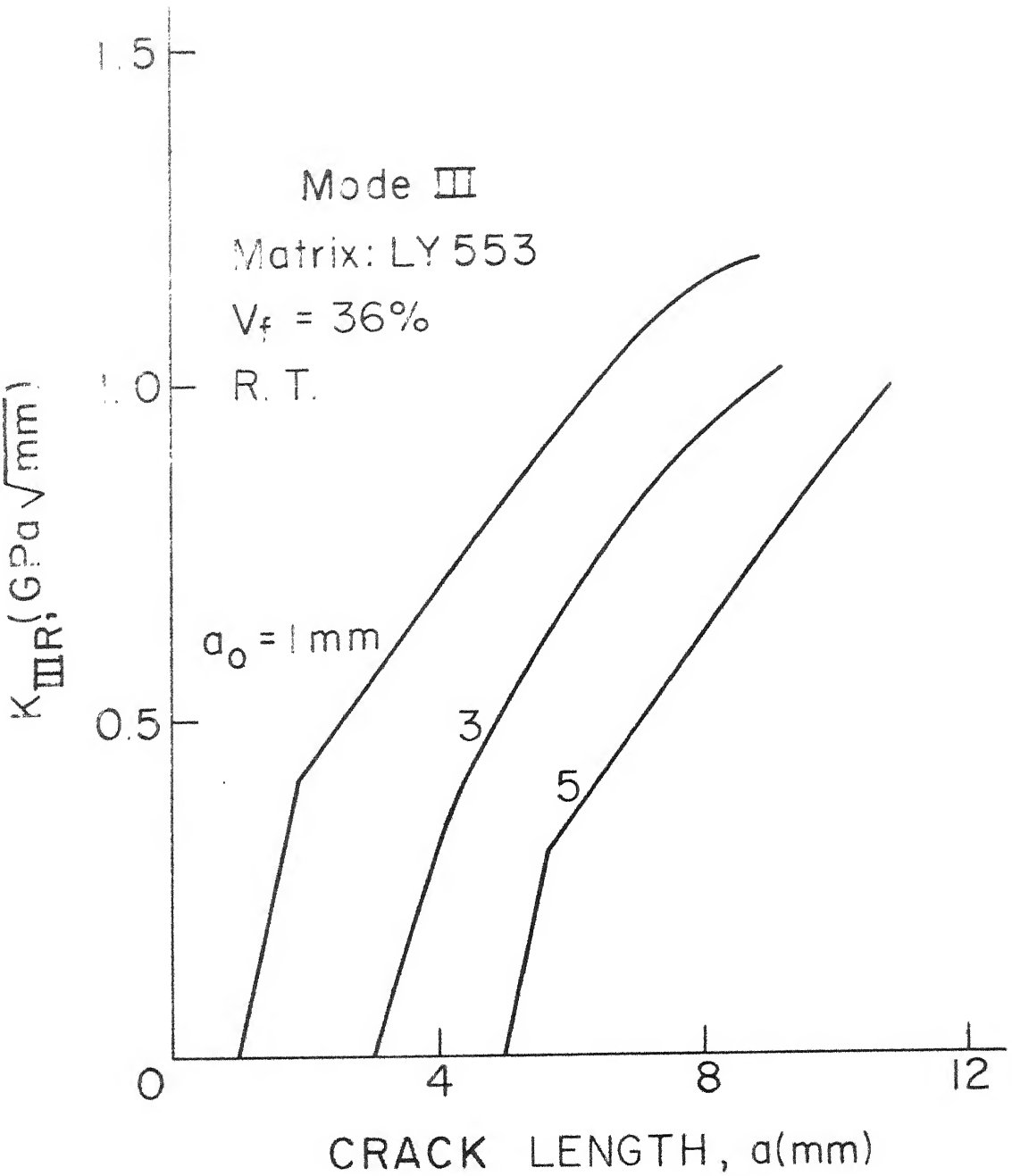

FIG. 101 R-CURVES FOR MODE III

TABLE 7 : Stress Intensity Factors at Instability, $K_{II\ R(ins)}$ for Mode II and $K_{III\ R(ins)}$ for Mode III.

Initial Crack length, a_o (mm)	$K_{II\ R(ins)}$ G Pa $\sqrt{mm}$	$K_{III\ R(ins)}$ G Pa $\sqrt{mm}$
1	-	0.990
2	0.559	-
3	-	0.961
4	0.549	-
5	-	0.971
6	0.549	-

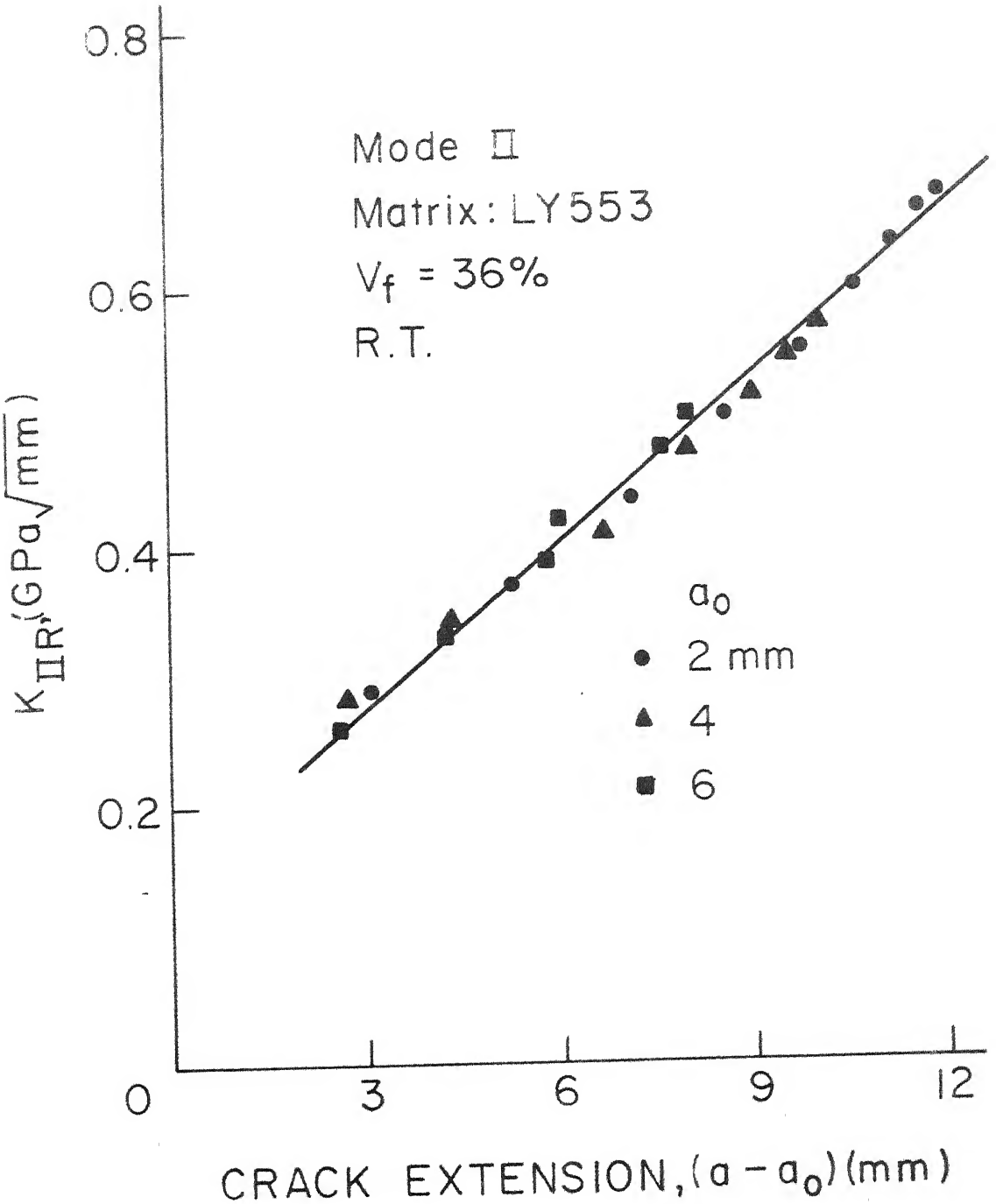

FIG. 102 VARIATION OF CRACK GROWTH RESISTANCE WITH CRACK EXTENSION (MODE II)

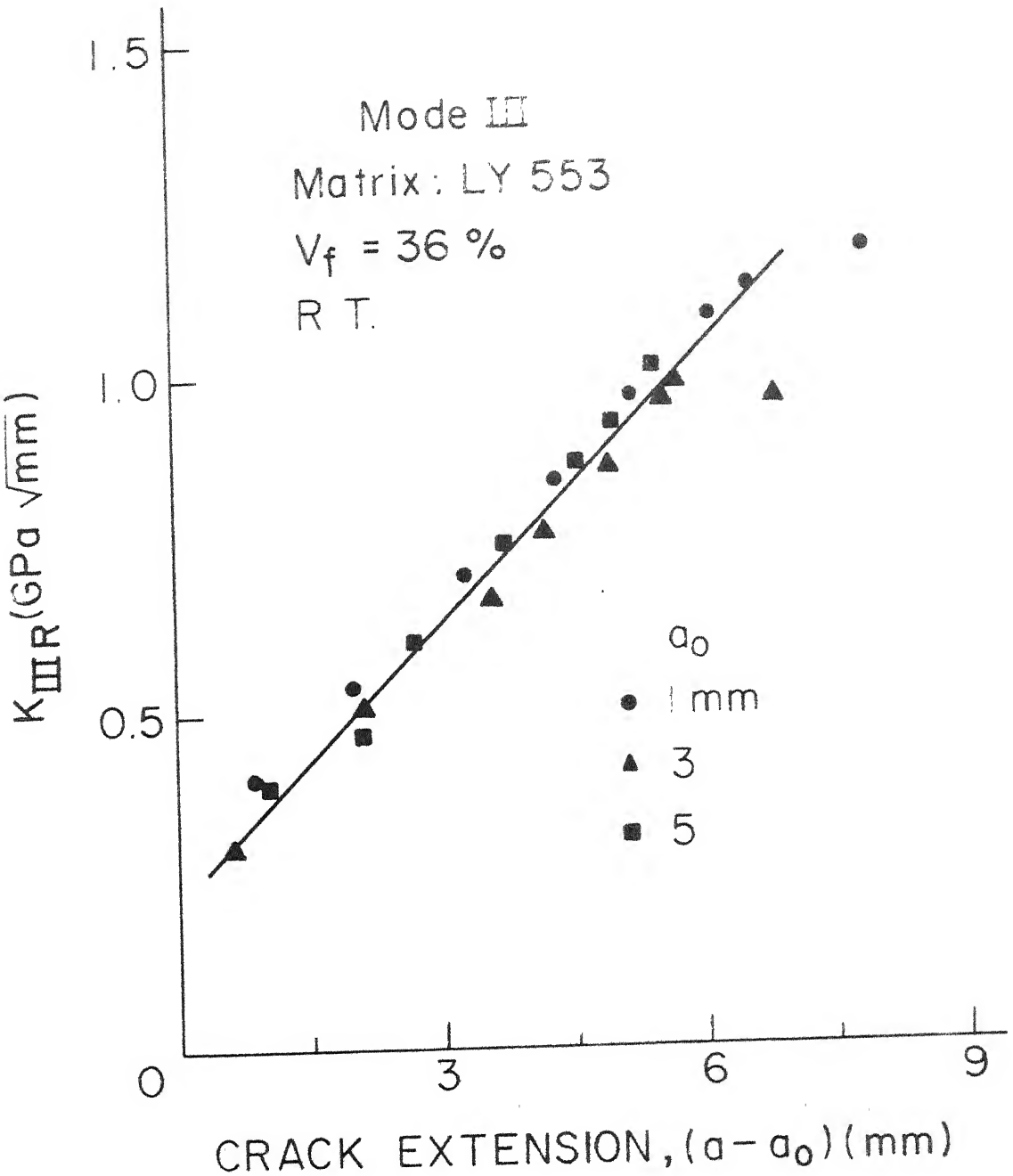

FIG 103 VARIATION OF CRACK GROWTH RESISTANCE WITH CRACK EXTENSION (MODE III)

from these figures that crack growth resistance in Mode II and Mode III is also independent of initial crack length.

The critical strain energy release rates for Mode II (G_{IIC}) and Mode III (G_{IIIC}) have been calculated using Eqs. (8) and (15) in which the stress intensity factors have been replaced by the corresponding values of $K_{II\ R(ins)}$ and $K_{III\ R(ins)}$. The values of G_{IIC} and G_{IIIC} are given in Table 8 and plotted against initial crack length in Fig. 104. Also plotted in Fig. 104 is G_{IC} which has been calculated using the following expression 29 :

$$G_{IC} = \frac{K^2_{R(ins)}}{E} \qquad (19)$$

where the value of $K_{R(ins)}$ have been given in Table 5 in Chapter 3.

It is observed that the critical strain energy release rate is independent of initial crack length in Mode II and Mode III but not in Mode I. It is also observed that the critical strain energy release rate in Mode II is much smaller (less than half) than that in Mode I and Mode III. The lower critical strain energy release rate in Mode II can be attributed to the fact that only a very small amount of debonding is observed to occur. During fracture in Mode I and Mode III the higher strain energy release rates are obtained due to greater amount of debonding and fibre pull out.

TABLE 8 : Strain Energy Release Rates for Mode I, Mode II and Mode III

Initial Crack length a_o (mm)	G_{IC} (N-mm/mm^2)	G_{IIC} (N-mm/mm^2)	G_{IIIC} (N-mm/mm^2)
1	-	-	95.0
2	-	24.5	-
3	47.2	-	90.0
4	45.9	23.6	-
5	50.8	-	92.0
6	57.0	23.6	-
7	62.4	-	-
8	67.9	-	-

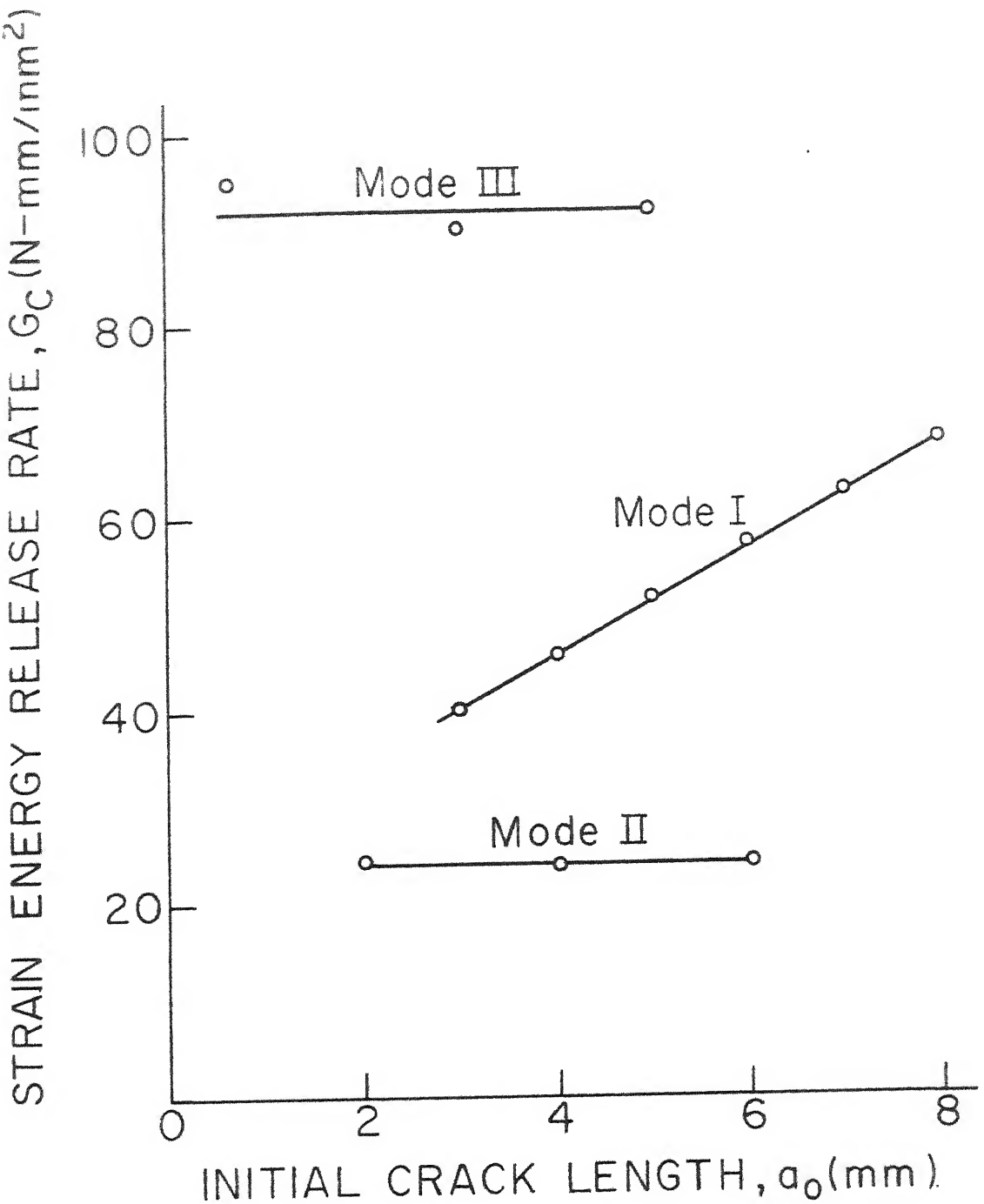

FIG. 104 VARIATION OF STRAIN ENERGY RELEASE RATE WITH INITIAL CRACK LENGTH FOR DIFFERENT MODES OF LOADING

CHAPTER 5

CONCLUSIONS AND SCOPE FOR FUTURE WORK

5.1 CONCLUSIONS

Fracture behaviour of short glass fibre composites has been investigated in extension Mode (Mode I), forward shear Mode (Mode II), and out-of-plane shear (Mode III). Based on the results the following conclusions can be drawn:

1. In short fibre composites a considerable amount of damage occurs at the crack tip prior to final unstable fracture. Although there are number of micro-cracks in the damage zone, the progress of damage zone is not a crack extension in the conventional sense. However, the crack tip damage does increase the compliance as crack extension does in the metallic materials.

2. The crack growth resistance curves (R - curves) for short fibre composites can be constructed by obtaining effective crack length through a compliance matching procedure.

3. The crack growth resistance at instability in Mode I, $K_{R(ins)}$, increases with the initial crack length, for different fibre volume fractions and test temperatures. This dependence of $K_{R(ins)}$ on

the initial crack length indicates that it is uncertain if $K_{R(ins)}$ can be regarded as a material property for short fibre composites

4. The notched strength of the composites has been found to be in agreement with the theoretical prediction of Whitney - Nuismer criteria. When the matrix material is brittle (e.g. LY 553 at room temperature and - 1.1 ^{o}C). However, the composites exhibit a much reduced notch sensitivity when the matrix material is ductile (e.g. LY 553 at elevated temperature, CY 230 and modified CY 230).

5. The candidate stress intensity factor shows a slight increase with the specimen thickness whereas it decreases with increase in specimen width.

6. The failure modes of composites strongly depend upon the test temperature. At room temperature and at - 1.1 ^{o}C the fracture is generally brittle with low energy absorption, whereas the fracture at 43.3 and 60 ^{o}C is ductile.

7. The stress intensity factor at instability, $K_{R(ins)}$, depends upon the elastic modulus of matrix material. Variation of $K_{R(ins)}$ with matrix modulus shows a peak. For a value of matrix modulus higher than that at peak, adhesion between the matrix and the

fibres is so good that the fibres break in the fracture plane and very little fibre pull out takes place. At matrix less than that at peak, the adhesion is poor so that the fibre pull outs are accompanied by low energy absorption.

8. The load displacement curves for Mode II and Mode III show peak (unlike the load COD curves for Mode I which increase monotonically) and a considerable amount of damage occurs at reduced load prior to final fracture.

9. In Mode II and Mode III the stress intensity factors at instability $K_{IIR(ins)}$ and $K_{IIIR(ins)}$, are independent of initial crack length, indicating that they may be material properties. Also, the critical strain energy release rate is independent of initial crack length, for Mode II and Mode III but not for Mode I critical strain energy release rate.

10. The critical strain energy release rate in Mode II is less than half of that in Mode I and Mode III. This can be attributed to the fact that only a very small amount of debonding occurs during fracture in Mode II. Thus the fracture toughness tests in Mode II are quite important for composite materials.

5.2 SUGGESTED FUTURE RESEARCH WORK

It is suggested that further investigations be carried out to study the fracture properties of composite materials:

1. Fibre length is an important parameter affecting the properties of short fibre composites. Its influence on fracture toughness should be investigated.

2. Influence of such environmental variables as moisture, saline water, acids and oils should be investigated.

3. Fracture toughness of composites containing high modulus fibres (graphite and kevalar) should be studied.

4. It is not yet evident if the R - curve approach is a good approach to characterize fracture toughness of composite materials. Other approaches should be explored.

5. Effort should be made to correlate internal damage to the fracture toughness.

6. Preliminary results of the present work indicate that Mode II may represent the severe most loading condition for short fibre composites. Extensive studies should be performed to establish this.

7. Effect of hybridization on fracture properties of fibre composites should be studied. In addition to fibres, metal foils may be introduced to increase the fracture toughness.

8. Efforts should be simultaneously directed to apply the fracture mechanics approach to continuous fibre composites.

REFERENCES

1. G.C. Sih, P.D. Hilton, R. Badaliance, P.S. Shenberger, and G. Villarreal, "Fracture Mechanics for Fibrous Composites", Analysis of the Test Method for High Modulus Fibers and Composites, ASTM STP 521, American Society for Testing and Materials, Philadelphia, Pa, 1973, pp. 98 - 132.

2. C. Zweben, "Fracture Mechanics and Composites Materials: A Critical Analysis", Analysis of the Test for High Modulus Fibres and Composites, ASTM STP 521, American Society for Testing and Materials, Philadelphia, Pa, 1973, pp. 65 - 97.

3. S.N. Atluri and Albert S. Kobayashi and Machihiko Nakagaki, "Applications of an Assumed Displacement Hybrid Finite Element Procedure to Two Dimensional Problems in Fracture Mechanics", AIAA/ASME/SAE 15th Structures, Structural Dynamics and Materials Conference Las Vegas, Nevada, April 17 - 19, 1974.

4. S.N. Atluri, A.S. Kobayashi and M. Nakagaki, "A Finite Element Program for Fracture Mechanics Analysis of Composite Material," Fracture Mechanics of Composite, ASTM STP 593, American Society for Testing and Materials, Philadelphia, Pa, 1975, pp. 86 - 98.

5. P.W.R. Beaumont, "A Fracture Mechanics Approach to Failure in Fibrous Composites", J. Adhesion, Vol. 6, 197[illegible], pp. 107 - 137.

6. J.F. Mandell, S.S. Wang, and F.J. Mc Garry, "The Extension of Crack Tip Damage Zones in Fibre Reinforced Plastic Laminates," Journal of Composite Materials, Vol. 9, No. 2, 1975, pp. 266.

7. E.M. Wu, "Strength and Fracture of Composites", in L.J. Broutman, Ed., Fracture and Fatigue, Academic Press 1974.

8. J.M. Whitney and R.J. Nuismer, "Stress Fracture Criteria for Laminated Composites Containing Stress Concentration", Journal of Composite Materials, 8(2), 253, 1974.

9. R.J. Nuismer and J.M. Whitney, "Uniaxial Failure of Composite Laminates Containing Stress Concentration", in Fracture Mechanics of Composites, ASTM STP 593, American Society for Testing and Materials, Philadelphia, Pa, 1975, pp. 117 - 142.

10. R.J. Nuismer and J.D. Labor, "Applications of the Average Stress Failure Criterion: Part I Tension", Journal of Composite Materials, Vol. 12, July 1978, p. 238

11. R.J. Nuismer and J.D. Labor, "Applications of the Average Stress Failure Criterion: Part II - Compression" Journal of Composite Materials, Vol. 13, January 1979, p. 49.

12. H.F. Brinson and Y.T. Yeow, "Experimental Study of the Fracture Behaviour of Laminated Graphite-Epoxy Composites", In Composite Materials: Testing and Design (Fourth Conference), ASTM STP 617, American Society for Testing and Materials, Philadelphia, Pa., 1977, pp. 18 - 38.

13. Y.T. Yeow, D.H. Morris and H.F. Brinson, "The Fracture Behaviour of Graphite/Epoxy Laminates", Experimental Mechanics, Vol. 19, No. 9, January 1979, pp. 1 - 8.

14. D.H. Morris and H.T. Hahn, "Mixed Mode Fracture of Graphite/Epoxy Composites: Fracture Strength", Journal of Composite Materials, Vol. 11, April 1977.

15. D.H. Morris and H.T. Hahn, "Fracture Resistance Characterization of Graphite/Epoxy Composites," in Composite Materials Testing and Design (Fourth Conference), ASTM STP 617, American Society for Testing and Materials, Philadelphia, Pa., 1977, pp. 5 - 17.

16. I.M. Daniel, "Strain and Failure of Graphite/Epoxy Plates with Cracks", Experimental Mechanics, Vol. 18, No. 7, July 1978, pp. 246 - 252.

17. I.M. Daniel, "The Behaviour of Uniaxially Loaded Graphite/Epoxy Plates with Holes", Presented at Second International Conference on Composite Materials, ICCM/II, Toronto, Canada, April 16 - 20, 1978.

18. I.M. Daniel, "Deformation and Failure of Composite Laminates with Cracks in Biaxial Stress Fields", Presented at Sixth International Conference on Experimental Stress Analysis, Munich, West Germany, September 18 - 22, 1978.

19. J.D. Barret and R.O. Foschi, "Mode II Stress - Intensity Factors for Cracked Wood Beams", Engineering Fracture Mechanics, Vol. 9, 1977, pp. 371 - 378.

20. A.R. Bunsell, "The Nature of Crack Growth in Composite Materials," Proceedings of First USA - USSR Symposium on Fracture of Composite Materials, Riga, USSR September 4, 1978, pp. 349.

21. M.F. Kanninen, E.F. Rybicki and H.F. Brinson, "A Critical Look at Current Applications of Fracture Mechanics to the Failure of Fibre Reinforced Composites," COMPOSITES, Vol. 8, January 1977, pp. 17 - 22.

22. S.K. Gaggar and L.J. Broutman, "The Development of a Damage Zone at the Tip of a Crack in a Glass Fibre Reinforced Polyester Resin", International Journal of Fracture, 10, 1974.

23. S.K. Gaggar and L.J. Broutman, "Effect of Crack Tip Damage on Fracture of Random Fibre Composites", Materials Science and Engineering, Vol. 21, 1975, pp. 177 - 183.

24. S.K. Gaggar and L.J. Broutman, "Crack Growth Resistance of Random Fibre Composites", J. Composite Materials, Vol. 9, 1975.

25. S.K. Gaggar and L.J. Broutman, "Crack Propogation Resistance of Random Fibre Composites", in R.D. Deanin and A.M. Crugnola, Eds., Toughness and Brittleness of Plastics, American Chemical Society, 1976, pp. 335 - 366.

26. S.K. Gaggar and L.J. Broutman, "Strength and Fracture Properties of Random Fibre Polyester Composites". Fibre Science and Technology (9), 1976.

27. S.K. Gaggar and L.J. Broutman, "Fracture Toughness of Random Glass Fibre Epoxy Composites: An Experimental Investigation, "Flaw Growth and Fracture, ASTM STP 631, American Society for Testing and Materials, Philadelphia, Pa, 1977, pp. 310 - 330.

28. A.S. Kobayashi, Editor, "Experimental Technique in Fracture Mechanics", Society for Experimental Stress Analysis, Westport, Connecticut, 1973.

29. H. Liebowitz, Editor, "Fracture. An Advanced Treatise, Vol. 2, Mathematical Fundamentals", Academic Press, Newyork - London, 1968.